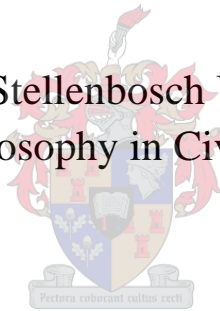


The Role of Cracks and Chlorides in Corrosion of Reinforced Strain Hardening Cement-Based Composite (R/SHCC)

Suvash Chandra Paul

A Thesis Submitted to the Stellenbosch University for the Degree of
Doctor of Philosophy in Civil Engineering



Supervisor: Prof. Dr. Eng. Gideon P.A.G van Zijl

Date: December 2015

Declaration

I, the undersigned, hereby declare that the work contained in this thesis report is my own original work and that I have not previously in its entirety or in part submitted it at any university for a degree.

Signature: _____

Date: _____

Abstract

By using various kinds of fibre-reinforced concrete (FRC), new dimensions of structural performance have been developed. Strain-hardening cement-based composite (SHCC) is a branch of these FRCs and show remarkably improved mechanical and durability performance. FRCs provide ductility and through fibre-bridging show remarkable strain hardening behaviour of up to 3% and in some cases, beyond 5% tensile strain for SHCC with especially-graded fine sand (particle size less than 0.3 mm). SHCC forms multiple fine cracks that are closely spaced together when subjected to tensile or flexural loads. This behaviour is a key feature of the material's ability to potentially reduce the ingress rates of harmful substances such as water, oxygen and chlorides which are the key ingredients that cause corrosion of steel in reinforced SHCC (R/SHCC). This dissertation reports on a research study where the fibre-controlled crack widths and spacings are investigated to determine if these fine cracks delay or prevent chloride-induced corrosion in R/SHCC. Therefore, the main aim of this research was to determine a relationship between the crack width distribution, cover depth, chloride level and corrosion.

The mechanical characteristics of the SHCC and reference mortar specimens are reported on where the material's behaviour in compression, direct tension and flexural load are discussed. For the purpose of this research work, quite a large number of different types of SHCC and mortar specimens such as cubes, cylinders, small prisms and beams were tested to determine the mechanical properties. The crack widths and crack distribution under uni-axial tension and flexural testing were measured on the surfaces of the specimens made with both reinforced and un-reinforced SHCC. In the case of corrosion testing, a total of about 100 beam specimens of R/SHCC having two different sand types, two different reinforcing bar layouts and three different cover depths, were cracked and exposed to a 3.5% NaCl solution (by wt of water) representing sea water. The copper/copper-sulphate half-cell was used to record the corrosion potential in the specimens periodically in order to indicate changes in the corrosion process. The Coulostatic method (as part of the polarization resistance technique) was also used to measure the corrosion rate of steel bars inside SHCC. Little corrosion damage was seen in the specimens after about 2 years of testing. A relationship between the cracks, cover depths, chloride content and corrosion rate was then documented for the SHCC material used in this research work.

The chloride ion content in SHCC and mortar specimens was determined by means of X-ray fluorescence (XRF) and chemical analysis. The presence of chloride in concrete can be in the form of free chloride and bound chloride. Therefore, XRF was mainly used to determine the total chloride (free plus bound) content at different depths of the specimens while chemical testing was performed for both total and free chloride. A link was established between these recorded values and the rate of corrosion of the steel reinforcement. The chloride diffusion coefficient of un-reinforced SHCC and mortar was also determined by doing rapid chloride migration testing. Steady-state chloride penetration profiling by means of capillary and ponding suction was also done in finely-cracked SHCC specimens. It was found that the

ingress of chloride ions in an average crack width of about 50 μm occurred up to full crack height of 60 to 80 mm in under an hour of exposure. Some other durability tests such as freeze-thaw attack, capillary water absorption and electrical resistivity of SHCC and mortar were also investigated.

Finally, it was found that in cracked R/SHCC specimens in the early stage of testing, a higher change (from passive to active) in corrosion potential reading could be observed due to the electro-chemical reaction. Nevertheless for this higher potential value, no major corrosion damage can be seen in the specimen in the early stage of testing. A 25 mm cover depth was found to be an approximate threshold for chloride penetration in this specific mix of SHCC material. In addition to corrosion potential and rate readings, actual corrosion-induced pitting depth and area, mass loss and loss of tensile resistance were measured after removal of the steel from the specimens at the end of the tests.

Based on the detailed experimental results obtained from this research work, empirical formulas are proposed to predict the corroded depths and loss of steel force due to pitting and mass loss. A number of recommendations are made for the corrosion rate measurement methodology used here of how to improve the variations in experimental and actual results. Some observations and suggestions are also proposed based on the mechanical and durability tests performed in SHCC. In the final conclusions, some approaches are suggested for future studies on durability of SHCC, which could help researchers in increasing their knowledge of SHCC properties and which may lead to the optimal use of SHCC in a sustainable way. The use of SHCC may be feasible in the protection of concrete structures from severe chloride-induced corrosion or in delaying such corrosion.

Acknowledgements

Many people have contributed to this thesis in various ways. First of all, I would like to acknowledge the incredible input made by my supervisor, Professor Gideon P.A.G van Zijl of the Stellenbosch University, for giving me the chance to work with him and for his valuable discussions and support through all stages of this work. He also gave me the opportunity for establishing contact with leading researchers in our research field in many parts of the world, enabling me to share in their profound knowledge. He provided guidance and many inspiring inputs during my research for which I am very grateful.

At different stages of my work, I had very valuable advice from Professor Koichi Kobayashi of the Gifu University, Dr. Faiz Shaikh of the Curtin University, Professor Viktor Mechtcherine of the Technical University Dresden and Professor Folker Wittmann of the Aedificat Institute Freiburg which is hereby acknowledged gratefully.

I am also grateful to Dr. Wolfram Schmidt, Dr. Andreas Rogge and Dr. Hans-Carsten Kuehne of the Federal Institute for Materials Research and Testing (BAM), in Berlin, Germany for giving me the opportunity to use their facilities for some part of this research work.

I would also like to thank all the colleagues at the Department of Civil Engineering at the Stellenbosch University for creating a pleasant working environment. The assistance by the laboratory staff of the Department of Civil Engineering at the Stellenbosch University is also gratefully acknowledged.

The South African Industry and the Technology and Human Resources for Industry Programme (THRIP) of the South African Ministry of Trade and Industry is acknowledged for financing this work. The additional financial support from the German-South African year of science for travelling and working in BAM, Germany is also greatly appreciated.

Before I finish, I wish to express my gratitude to my family in Bangladesh, and in particular to my brother Suman and sister Dipa and my mother for giving me the things that are so much more important in life than the combination of cracks, chloride, corrosion and concrete. Last but not least, I would like to thank my wife Prianka, for her patience and encouragement.

Dedication

I would like to dedicate my whole contribution to my deceased Father Dinesh Chandra Paul (1944-2007) and my Nephew Samir Paul (1982-2011), whom I feel were very important in my life.

Thesis Layout

Chapter 1: Introduction

This chapter briefly introduces and gives a description to the reader, the strain-hardening cement-based composite (SHCC) materials. This chapter also serves to state the research problem and aim, and sets the stage for the overall research presented in the dissertation.

Chapter 2: Existing Results on SHCC (A Literature Survey)

In this chapter a historic overview of SHCC and its uses are presented to the reader. This chapter concludes with an overview and example of the influencing factors on concrete durability which can be overcome by using SHCC. It also provides a detailed review of the various SHCC characteristics for concrete durability found by many researchers world-wide.

Chapter 3: Influence of Cracks and Chlorides in Concrete Structures

This chapter presents a detailed overview of the durability of a normal concrete structure. The threshold crack widths and chloride levels in a concrete structure are reported here. The current research results on various concrete durability properties are also discussed in this chapter.

Chapter 4: Reinforcement Corrosion Mechanism and Measurement Methods

The different methods of measuring corrosion potential and rate in reinforced concrete are discussed here. A Coulostatic method which was used in this research work to measure the corrosion rate is also broadly discussed in this chapter. Some recommendations from the Coulostatic method are also made which can be very important for future researchers to take into account and so avoid errors in the results.

Chapter 5: Experimental Methodology

In this chapter a detailed overview of the different materials studied in this research work, of the physical properties of materials, of the preparation of materials and of casting SHCC and mortar specimens, is given. The test setup for SHCC and mortar specimens in accordance with different guidelines and literature used in this research is described.

Chapter 6: Fresh and Mechanical Behaviour of SHCC

This chapter presents a critical analysis of the different physical and mechanical properties of SHCC and mortar matrix that are used in this research work. The research sheds light on the various compositions (fibre and aggregate content, cement content, etc.) of SHCC and their distinct features that help achieve the desired benefits in a structural application. A critical

overview is given on the tensile and flexural cracking behaviour under different strain and deformation levels of both un-reinforced and reinforced SHCC specimens. The application of acoustic emission for characterising the crack propagation in SHCC and mortar specimens under both tensile and flexural testing is also reported on in this chapter.

Chapter 7: Chloride Ingress and Reinforcement Corrosion in SHCC

The durability performance of SHCC and mortar specimens is covered in this chapter. Different types of tests, namely chloride penetration, corrosion, freeze-thaw, capillary water absorption and electrical resistivity have been performed and the results are presented graphically. The consequences of corrosion, such as pitting depths, yield force loss and mass loss in the steel bars inside SHCC and mortar specimens are also reported on.

Chapter 8: Towards Corrosion Modelling of R/SHCC

Based on the experimental results obtained in this research work, empirical relationships are described in this chapter. Some modelling such as prediction of corrosion and chloride at different cover depths, crack widths, crack spacing, loss of mass and yield force in steel bars due to corrosion is also developed from the empirical relationships described in this research work.

Chapter 9: Conclusions and Recommendations

This chapter reviews the research objectives and states the related conclusions. The overall performances of SHCC in both chloride and corrosion are compared with its crack properties (number of cracks, crack spacing, widths, etc.) and recommendations are made for further work.

List of publications

From this research a numbers of papers were written and published in local and international conferences and journals and are listed below:

International Journal papers

- (1) **Paul, SC**, Pirskawetz, S, van Zijl, GPAG & Schmidt, W 2015, ‘Acoustic Emission for Characterizing the Crack Propagation in Strain Hardening Cement-Based Composites (SHCC)’, *Cement and Concrete Research*, Vol. 69, pp. 19-24.
- (2) **Paul, SC &** van Zijl, GPAG 2014, ‘Crack Formation and Chloride Induced Corrosion in Reinforced Strain Hardening Cement-Based Composite (R/SHCC)’, *Journal of Advanced Concrete Technology*, Vol. 12, pp. 340-351.
- (3) **Paul, SC &** van Zijl, GPAG 2013, ‘Mechanically Induced Cracking Behaviour in Fine and Coarse Sand Strain Hardening Cement Based Composites (SHCC) at Different Load Levels’, *Journal of Advanced Concrete Technology*, Vol. 11, pp. 301-311.

Local and International conference papers

- (4) **Paul, SC &** van Zijl, GPAG & James, L 2015, ‘Influence of cracks in chloride penetration and corrosion of fibre reinforced strain hardening materials under sustained loading condition’, *accepted and in proceeding of the ConMat15 conference, Whistler, Canada*.
- (5) **Paul, SC**, Ebell, G, van Zijl, GPAG & Schmidt, W 2014, ‘Cracked and uncracked SHCC specimens under different exposure conditions’, *in proceeding of the SHCC3 3rd RILEM conference on Strain Hardening Cementitious Composite, Dordrecht, Netherland, Schlangen et al. (eds), © 2014 RILEM – Tous droits reserves, ISBN:978-2-35158-150-6, p:25-32*.
- (6) van Zijl, GPAG, **Paul, SC &** Rens, JP 2014, ‘Corrosion of steel reinforcing bars in strain hardening cement-based composite under sustained loads’, *In proceeding of the SHCC3 3rd RILEM conference on Strain Hardening Cementitious Composite, Dordrecht, Netherland, Schlangen et al. (eds), © 2014 RILEM – Tous droits reserves, ISBN:978-2-35158-150-6, p:69-76*.
- (7) **Paul, SC &** van Zijl, GPAG 2013, ‘Assessment of fracture toughness in strain hardening cement-based composite (SHCC) made from fine and coarse sand’, *in proceeding of the fifth SEMC conference, Cape Town, South Africa, Research and Applications in Structural Engineering, Mechanics and Computation, Cape Town, South Africa, Zingoni (eds) © 2013 Taylor & Francis Group, London, ISBN:978-1-138-00061-2, p:619-624*.
- (8) **Paul, SC**, Theunissen, AI & van Zijl, GPAG 2013, ‘Chloride Induced Corrosion in Cracked Reinforced Strain Hardening Cement-Based Composite (R/SHCC)’, *in proceeding of International Conference on Sustainable Construction Materials & Technologies (SCMT3), Kyoto, Japan (received paper award)*.
- (9) van Zijl, GPAG & **Paul, SC** 2013, ‘Crack spacing in steel bar reinforced strain hardening cement-based composites (R/SHCC), towards corrosion modelling’, *in proceeding of International Conference on Sustainable Construction Materials & Technologies (SCMT3), Kyoto, Japan*.
- (10) **Paul, SC &** van Zijl, GPAG 2013, ‘Strain Hardening Cement Based Composite (SHCC) with fine and coarse sand under tensile load and chloride attack’, *in proceeding*

of 8th International Conference on Fracture Mechanics of Concrete and Concrete Structures (Framcos8), Toledo, Spain, J.G.M. Van Mier, G. Ruiz, C. Andrade, R.C. Yu and X.X. Zhang (eds).

- (11) **Paul, SC &** van Zijl, GPAG 2013, ‘Mechanical behaviour of strain hardening cement-based composites (SHCC) based on micromechanical design’, *in proceeding of International Conference on Advances in Cement and Concrete Technology in Africa (ACCTA), Johannesburg, South Africa (received best paper award).*

Notations

A_f	The ratio of total area of fibres
A_r	Steel reduced area due to corrosion
A_s	Area of steel
C	Cover depth of steel
C_c	Chloride conductivity index
C_s	% of surface chloride concentration
Cl	Chloride-content
Cl_{free}	Free chloride-content
C_x	% of chloride at distance x
D_{app}	Apparent diffusion coefficient of chloride
d_c	Corroded depth
d_f	Fibre diameter
d_p	Corrosion pitting depth
E_{corr}	Corrosion potential
$E-mod$	Modulus of elasticity
E_{pit}	Pitting potential
E_{pro}	Protection potential
f_{cu}	Ultimate compressive strength
g	Gravitational acceleration
G_f	Fracture energy
i_{corr}	Corrosion current density
ΔiR	Ohmic drop
K_{IC}	Matrix fracture toughness
M_{loss}	Mass loss of steel
m_1	Mass of steel per unit length
m_2	Corrosion mass loss per unit length
mS	millisecond
mV	millivolt
mA	milliamp
R_e	Electrical concrete resistance
R_{Ω}	Electrolyte resistance
S	Fibre spacing
S_{cr}	Crack spacing
P	Concrete resistivity
ρ_s	Density of steel
V_{corr}	Corrosion rate
W_{cr}	Crack widths
$W_{cr,ave}$	Average crack widths
$W_{cr,tot}$	Total crack widths
Y_{loss}	Loss of yield force of steel
σ_y	Yield strength of steel

Abbreviations

AASHTO	American association of State Highway and Transport Officials
a/b	Aggregate to binder ratio
ACI	American concrete institute
ACW	Average crack widths
AE	Acoustic emission
AEA	Air entraining agent
AgNO ₃	Silver nitrate
Ag/AgCl	Silver to silver chloride
ASTM	American Standard Testing materials
Ave	Average value
C ₃ A	Tri-calcium aluminate
CAW	Capillary water absorption
CE	Counter electrode
CEM I	Portland cement type I
CEM II	Portland cement type II
CDF	Capillary suction of de-icing solution and freeze-thaw testing
CoV	Coefficient of variation
CSE	Copper-copper sulphate electrode
CS	Coarse sand
CS-SHCC	Strain hardening cement-based composite with coarse sand
CMOD	Crack mouth opening displacement
CMTM	Contest materials testing machine
Cu/CuSO ₄	Copper to copper sulphate
DFRCC	Ductile fibre reinforced cementitious composite
ECC	Engineered cementitious composite
EIS	Electrochemical impedance spectroscopy
EN	Electrochemical noise
EPR	Electrochemical potentiokinetic reactivation
ER	Electrical resistivity
FRC	Fibre reinforced concrete
FPB	Four-point bending
FS	Fine sand
FS-SHCC	Strain hardening cement-based composite with fine sand
GE	Guard electrode
GGBS	Ground granulated blast-furnace slag
GPa	Gigapascals
GPT	Galvanostatic pulse technique
HCP	Half-cell potential
HNO ₃	Nitric acid
HPC	High performance concrete
HPFRCC	High performance fibre reinforced cementitious composite
HSC	High strength concrete

LRP	Linear polarization resistance
LVDT	Linear variable differential transformer
MCW	Maximum crack widths
MPa	Megapascals
NC	Normal concrete
$\text{NH}_4\text{Fe}(\text{SO}_4)_2$	Ammonium iron sulphate
NH_4SCN	Ammonium thiocyanate
NOC	Number of cracks
OPC	Ordinary Portland Cement
PE	Polyethylene
PFA	Pulverised fuel ash
PPC	Potentiodynamic polarization curves
PVA	Polyvinyl alcohol
RC	Reinforced concrete
RCM	Rapid chloride migration
RCS	Reinforced concrete structure
RE	Reference electrode
RH	Relative humidity
R/mortar	Reinforced mortar
RPC	Reactive powder concrete
R/SHCC	Reinforced strain hardening cement-based composite
s/b	Sand to binder ratio
SCE	Silver-silver chloride electrode
SF	Silica fume
SHCC	Strain hardening cement-based composite
SHRCC	Strain hardening fibre-reinforced cementitious composite
SP	Super plasticizer
SSC	Stress-strain curve
TCW	Total crack widths
TPB	Three-point bending
UC	Uncracked
UL	Ultimate load
UHSC	Ultra high strength concrete
UHPC	Ultra high performance concrete
VMA	Viscosity modifying agent
w/b	Water to binder ratio
w/c	Water to cement ratio
WE	Working electrode
WPF	Weighted peak frequency
XCT	X-ray computer tomography
XRF	X-ray fluorescence

Table of Contents

Abstract	i-ii
Acknowledgement	iii
Thesis layout	v-vi
List of publications	vii-viii
Notations	ix
Abbreviations	x-xi

Chapter 1: Introduction

1. General discussion	1
1.1. Materials sustainability	1-2
1.2. Development of new materials	2
1.3. Discovering the strain hardening cement-based composite (SHCC)	2-4
1.4. The main problem statement	4-5
1.5. Scope of the research	5-6
1.6. Purposes of the research	6-7
1.7. Hypothesis of the research	7
1.8. Limitations of the research	7-8
1.9. Concluding remarks	8
1.10. References	8-9

Chapter 2: Existing Results on SHCC (A Literature Survey)

2. General overview	10
2.1. Fresh properties of SHCC	10-11
2.2. Mechanical behaviour of SHCC	12
2.2.1. Compressive strength and E-mod of SHCC	12-13
2.2.2. Tensile stress and strain	13-14
2.2.2.1. Influence of loading rate on strength	14
2.2.2.2. Influence of binder and water content on strength	14-15
2.2.2.3. Influence of water repellent agent on strength	15
2.2.2.4. Influence of loading type and age on strength	15-16
2.2.2.5. Influence of curing on strength	16
2.2.3. Flexural strength	16-17
2.2.4. Tensile cracks in SHCC	17-18
2.2.5. Flexural cracks in SHCC	18-19

2.2.6. SHCC performance under combined loads	19
2.2.7. Fracture toughness of SHCC	20
2.3. Durability performance in SHCC and mortar	20
2.3.1. Rate of corrosion in SHCC and mortar	20-22
2.3.2. Chloride penetration in SHCC and mortar specimen	22
2.3.2.1. Chloride penetration in cracked specimens	23
2.3.2.2. Chloride penetration in different exposures conditions of specimen	24
2.3.2.3. Influence of compressive load on chloride penetration in SHCC specimen	24
2.3.3. Water penetration in SHCC	24
2.3.3.1. Permeability of water	24
2.3.3.2. Capillary suction of water	24-26
2.4. Other important characteristics of SHCC	26
2.4.1. Self-healing in SHCC	26-28
2.4.2. Micro-cell corrosion in SHCC	28
2.5. Current applications of SHCC	28-29
2.6. Concluding remarks	29
2.7. References	29-33

Chapter 3: Influence of Cracks and Chlorides in Concrete Structures

3. General discussions	34-35
3.1. Cracks in concrete structures	35
3.1.1. Types of cracks in concrete structures	35
3.1.1.1. Crack due to static or dynamic loads	36
3.1.1.2. Cracks due to shrinkage	36
3.1.1.3. Cracks due to temperature	36
3.2. Findings on crack widths and frequency in concrete structures	36-38
3.3. Chloride in concrete	39-40
3.3.1. Free and bound chloride in concrete	40
3.3.2. Critical/threshold chloride level for concrete	40-43
3.3.3. Chloride profile and diffusion coefficients of concrete	43-44
3.3.4. Methods of determining chloride profiles in concrete	44-45
3.3.5. Relationship between crack, chloride and corrosion in concrete structures	45-46
3.4. Carbonation corrosion in concrete	47-48
3.5. Influence of cyclic wetting and drying in concrete durability	48-49
3.6. Concluding remarks	49
3.6. References	49-53

Chapter 4: Reinforcement Corrosion Mechanism and Measurement Methods

4. General aspects	54
4.1. Corrosion mechanism in concrete	54-55
4.1.1. Initiation and propagation period of concrete	55-56
4.1.2. Mechanism of breaking passive film	56
4.1.3. Micro-cell and Macro-cell corrosion	56
4.1.4. Re-passivation of corrosion	56-57
4.1.5. Corrosion rate of steel in concrete	57-58
4.1.5.1. Factors influencing the corrosion rate in concrete	58-59
4.1.5.2. Corrosion products	59
4.2. Types of corrosion	59-60
4.2.1. Uniform corrosion	60-61
4.2.2. Galvanic corrosion	61
4.2.3. Localized corrosion	61
4.3. Methods of corrosion rate determination in concrete	61
4.3.1. Half-cell potential (HCP) method	61-63
4.3.1.1. Factors influencing HCP reading	63-64
4.3.2. Electrochemical Corrosion Test	64
4.3.2.1. Polarization resistance technique	64-66
4.3.2.2. Potentiodynamic polarization curves (PPC)	66
4.3.2.3. Electrochemical Impedance Spectroscopy (EIS)	66-67
4.3.2.4. Transient techniques	67-72
4.3.2.5. Ohmic drop (iR drop)	72
4.4. Advantage and disadvantage of using a Coulostatic method	72
4.5. Important notes before using a Coulostatic method	72-74
4.6. Possible protective measures against corrosion of steel in concrete	74
4.6.1. Organic and metal coating on steel bars	74
4.6.2. Corrosion inhibitors	74
4.6.3. Non-metallic reinforcement in concrete	74
4.6.4. Stainless steel in concrete	74
4.7. Concluding summary	75
4.8. References	75-78

Chapter 5: Experimental Methodology

5. General discussion	79
-----------------------------	----

5.1. Type of materials used	79-80
5.1.1. Cement and fly-ash	80
5.1.2. Sand	80-81
5.1.3. Fibre	81
5.1.4. Water	81
5.1.5. Supporting materials	81-82
5.1.6. X-ray fluorescence (XRF) for detecting elements in the different materials	82
5.2. Mix design of SHCC and mortar	82-84
5.3. Properties of fresh SHCC and mortar	84-85
5.4. Types of specimens used	85-87
5.5. Methods of casting and de-moulding	87
5.6. Methods of curing	87-88
5.7. Preparing specimens for mechanical testing	88
5.7.1. Cubes and cylinders for compressive strength and E-mod	88-89
5.7.2. Dumbbells for tensile strength	89-90
5.7.3. Measurement of cracks in dumbbells	90-91
5.7.4. Flexural behaviour of reinforced and un-reinforced beams	91-92
5.7.5. Method of measuring flexural cracks	92-93
5.7.6. Acoustic emission (AE) sensors for characterizing the cracks	93-94
5.7.7. Fracture toughness testing	94-96
5.7.8. Fibre distribution in SHCC matrix	96-97
5.8. Preparing specimens for durability testing of SHCC	97
5.8.1. Corrosion in SHCC and mortar	97-101
5.8.1.1. Corrosion potential	101-102
5.8.1.2. Corrosion rate	102-103
5.8.2. Chloride testing in SHCC and mortar	103
5.8.2.1. Rapid chloride migration (RCM) testing for un-reinforced specimens	103-105
5.8.2.2. Chloride penetration testing in cracked unreinforced SHCC specimens ...	105-108
5.8.2.3. Chloride profiling by X-ray fluorescence (XRF) and chemical testing	108-109
5.8.2.3.1. Chemical testing for total chloride content	110-111
5.8.2.3.2. Chemical testing for free chloride content	111-112
5.8.3. Freeze-thawing testing	112-113
5.8.4. Capillary water absorption testing	114
5.8.5. Electrical resistivity testing	114-115
5.9. Concluding summary	115-116
5.10. References	116-118

Chapter 6: Fresh and Mechanical Behaviour of SHCC

6. Introduction	119
6.1. Fresh properties of SHCC and mortar concrete	119-120
6.2. Mechanical properties of SHCC and mortar	120
6.2.1. Compressive strength and E-mod	120-122
6.2.2. Tensile stress and strain of SHCC	122-126
6.2.3. Number of tensile cracks and crack widths in un-reinforced SHCC	126-131
6.2.4. Flexural strength of SHCC and mortar	131-136
6.2.5. Flexural cracks	136
6.2.5.1. Flexural cracks in un-reinforced specimens	136-137
6.2.5.2. Flexural cracks in reinforced specimens	138-140
6.2.5.3. Relationship between cracks and cover depths	140-143
6.2.5.4. Relationship between cracks and deflection level	143
6.2.6. AE response in SHCC and mortar cracking behaviour	144-146
6.3. Fracture energy of SHCC and mortar	146-148
6.4. Fibre distribution in SHCC matrix	148-150
6.5. General discussion	150-151
6.6. References	151

Chapter 7: Chloride Ingress and Reinforcement Corrosion in SHCC

7. Introduction	152
7.1. Corrosion potential of R/SHCC and R/mortar specimens	152-157
7.1.1. Reason for higher/more negative half-cell potential values	157-158
7.1.2. Corrosion potential mapping	158-159
7.1.3. Relationship between corrosion potential and cracks	159-160
7.2. Corrosion performance of R/SHCC and R/mortar specimens	161
7.2.1. Corrosion rate in R/SHCC and R/mortar specimens	161-165
7.2.2. Verification of corrosion activities in the R/SHCC and R/mortar specimens	165-167
7.2.3. Steel mass loss due to corrosion	167-168
7.2.4. Loss of steel yield resistance due to corrosion	168-169
7.2.5. Pitting depths in steel due to corrosion	169-171
7.2.6. Relationship between corrosion potential, corrosion rate and moisture content in the specimen	172-173
7.3. Chloride (Cl) profile in SHCC and mortar specimens	173
7.3.1. Influence of cracks on penetration of chloride profile in SHCC	173
7.3.2. Chloride penetration in un-reinforced SHCC	173

7.3.2.1. Chloride penetration in un-reinforced SHCC using AgNO ₃	173-175
7.3.2.2. Chloride profile in un-reinforced SHCC using XRF	175-176
7.3.2.3. Chloride profile in un-reinforced SHCC using chemical testing	176-177
7.3.3. XRF chloride profile in R/SHCC and R/mortar specimens	178-179
7.3.4. Chemical total and free chloride profile in R/SHCC and R/mortar specimens	179-180
7.3.5. Relationship among XRF and chemical total, free chloride and corrosion	180-184
7.3.6. RCM coefficient of SHCC and mortar	184-185
7.4. Performance of SHCC against freeze and thaw attack	185-186
7.5. Capillary water absorption (CWA) in SHCC and mortar specimens	187
7.6. Electrical resistivity (ER) in SHCC and mortar concrete	188
7.7. Concluding remarks	188-189
7.8. References	190

Chapter 8: Towards Corrosion Modelling of R/SHCC

8. Introduction	191-192
8.1. Background of the Study	192-193
8.2. Existing modelling on corrosion	193-194
8.3. Factors involved in the error of corrosion prediction	195-196
8.4. Towards the modelling of corrosion in R/SHCC	196
8.4.1. Influence of cracks in R/SHCC	196
8.4.1.1. Cracks and corrosion in R/SHCC	197-199
8.4.1.2. Cracks and chloride in R/SHCC	200
8.4.2. Influence of cover depths in corrosion of R/SHCC	200-202
8.4.3. Consequences of chloride and corrosion of steel bars in R/SHCC	202-204
8.4.4. Proposed corrosion modelling of R/SHCC	204-207
8.4.5. Model validation	207-208
8.5. Important observations and comparison of results	208-211
8.6. Concluding remarks	211-212
8.7. References	212-214

Chapter 9: Conclusions and Recommendations

9. Introduction	215
9.1. Role of slump flow and air in SHCC	215
9.2. Role of aggregate size and binder content in SHCC	215-216
9.3. Mechanical performances of SHCC and mortar	216
9.3.1. Compressive strength and E-mod	216

9.3.2. Tensile strength and cracks	216-217
9.3.3. Flexural strength and cracks	217
9.3.4. AE responses in SHCC	217
9.3.5. Fracture energy of SHCC	218
9.4. Corrosion and chloride attack in SHCC and mortar	218
9.4.1. Corrosion potential values of R/SHCC and R/mortar specimens	218-219
9.4.2. Corrosion rate in R/SHCC and R/mortar specimens	219-220
9.4.3. Chloride profile in the SHCC and mortar specimens	220
9.4.3.1. Chloride profile in un-reinforced SHCC specimens	220-221
9.4.3.2. Chloride profile in the R/SHCC and R/mortar specimens	221
9.4.3.3. Chloride diffusion coefficient	221-222
9.5. Freeze-thaw attack, water absorption and electrical resistivity of SHCC and mortar specimens	222
9.6. Empirical corrosion modelling of R/SHCC	222
9.7. Research hypothesis and findings	223
9.8. General conclusion	223
9.9. Recommendations for future work	223-225

Appendix – A:

A.1. Application of SHCC	226-227
--------------------------------	---------

Appendix – B:

B.1. Apparatus used in the research experiments	228
---	-----

Appendix – C:

C.1. Different strengths properties of FS-SHCC and CS-SHCC	229-233
C.2. Tensile and flexural cracking behaviour of SHCC specimens	234-240
C.3. Corrosion potential mapping in R/mortar specimens	241
C.4. Corrosion damage in the steel bars	241-242
C.5. Chloride penetration in SHCC and mortar specimens in rapid chloride migration test	243
C.6. Capillary water absorption in SHCC and mortar specimens in rapid chloride migration test	244

List of Figures

Figure 1.1: Tensile stress-strain and cracking behaviour of SHCC and fibre-reinforced concrete (FRC) (reproduced from Weimann & Li, 2003)	3
Figure 1.2: Cracking behaviour in reinforced concrete (RC) and R/SHCC (reproduced from Fischer & Li, 2004)	3
Figure 2.1: SEM images of (a) poor and (b) good fibre dispersion ((reproduced from van Dyk, 2005)	11
Figure 2.2: Development of SHCC (a) compressive strength and (b) E-mod with time in high volume of SHCC mix (reproduced from Stander, 2004)	12
Figure 2.3: (a) Tensile strength development (reproduced from Stander, 2004) and (b) effects of loading rate in the tensile response of SHCC (reproduced from Yang & Li, 2006)	14
Figure 2.4: Influence of sand-binder ration on SHCC (a) first cracking strength and (b) ultimate tensile strength (reproduced from van Dyk, 2005)	15
Figure 2.5: Crack width stage on CC and SHFRCC over time in Michigan bridge deck (MODT report, 2001)	18
Figure 2.6: Observed corrosion in (a) HFRCC and (b) SHCC in comparison with mortar (reproduced from Mihashi <i>et al.</i> 2011 and Sahmaran <i>et al.</i> 2007)	21
Figure 2.7: Applied HPRCC in the reinforced NC specimens (reproduced from Kobayashi <i>et al.</i> 2010)	22
Figure 2.8: Effective chloride diffusion in cracked SHCC and mortar as function of deflection (reproduced from Sahmaran <i>et al.</i> 2007 and van Zijl, 2010)	23
Figure 2.9: Observed water permeability in SHCC, mortar and cracked concrete (reproduced from Lepech & Li 2005; Wang <i>et al.</i> 1997; van Zijl 2010)	25
Figure 2.10: Capillary water observed in neat SHCC as a function of time (reproduced from Wittmann <i>et al.</i> 2009)	25
Figure 2.11: Neutron radiography images for capillary water suction observed in un-reinforced SHCC as function of time (reproduced from Zhang <i>et al.</i> 2010)	26
Figure 2.12: Difference in the number of cracks at 0 weeks (W) (before the starting of accelerated exposure) to 108 weeks in cracked R/SHCC specimens	27
Figure 2.13: Forming white crystalline as part of self-healing of fine cracks in cementitious materials (reproduced from Qian <i>et al.</i> 2009).....	27
Figure 3.1: (a) Cracks and corrosion stains in RCS (b) spalling of cover concrete (reproduced from Verma, 2013)	35
Figure 3.2: Crack patterns observed in mortar, SHFRCC with PE fibre and SHFRCC with a mix of PE and hybrid steel fibre specimens under tensile test (reproduced from Ahmed & Mihashi, 2010)	38
Figure 3.3: Influence of cracks in mass loss of steel in corrosion testing (reproduced from Ahmed & Mihashi, 2010)	38

Figure 3.4: (a) Chloride profile of a highway bridge deck (Broomfield, 2007), (b) Chloride profile in SHCC with different fibre percentage (Wittmann <i>et al.</i> 2011)	39
Figure 3.5: Chloride threshold as a function of interfacial voids in concrete (reproduced from Glass & Buenfeld, 2000)	41
Figure 3.6: CEB recommended critical level of chloride for steel corrosion in concrete (CEB: 1989)	41
Figure 3.7: Influence of binder types on threshold chloride (Cl) value (reproduced from Ann & Song, 2007)	43
Figure 3.8: Influence of apparent diffusion coefficient (D_{app}) in (a) concrete cover depths after 10 years of exposure and (b) corrosion initiation for a threshold chloride of 1% due to 5% surface chloride concentration (reproduced from Bertolini <i>et al.</i> 2004)	44
Figure 3.9: Determination of chloride (Cl) in cracked concrete by LIBS analysis (reproduced from Savija <i>et al.</i> 2014)	45
Figure 3.10: Cracks, chloride and corrosion in NC (reproduced from Berke <i>et al.</i> 1993; Huang, 2006)	46
Figure 3.11: Rate of corrosion status at different pH levels of concrete (reproduced from Roberge, 1999)	47
Figure 3.12: Influence of relative humidity on corrosion in mortar with and without mixed chloride (reproduced from Glass <i>et al.</i> 1991)	48
Figure 4.1: RCS service life prediction model (reproduced from Liu & Weyers, 1998)	55
Figure 4.2: A representation of cyclic anode polarization curve of an active-passive material in chloride-laden environment (modified and imitative from Bertolini, 2004)	57
Figure 4.3: Different corrosion products and their volume (reproduced from Cement Concrete & Aggregates Australia, 2009)	59
Figure 4.4: Formation of corrosion microcell in concrete (reproduced from Czarnecki <i>et al.</i> 2010)	60
Figure 4.5: A representation of CSE half-cell with different components	62
Figure 4.6: Modulated guard ring setup (imitative from Wojtas, 2004)	65
Figure 4.7: Non-uniform current distribution under small counter electrode (reproduced from Andrade & Alonso, 2004)	65
Figure 4.8: Effect of localised corrosion (reproduced from Andrade & Alonso, 2004)	66
Figure 4.9: Confined current distribution by modulated guard ring (reproduced from Andrade & Alonso, 2004)	66
Figure 4.10: Randles equivalent circuit used to explain the reaction of a steel bar to the electrical signal (imitative from Gonzalez <i>et al.</i> 2001)	67
Figure 4.11: Magnified raw data of perturbation, recorded at about 1200 samples/second .	69
Figure 4.12: Filtered data for the raw record in Fig 4.11	70
Figure 4.13: Exponential function fitted to the measured decaying voltage	70

Figure 4.14: Corrosion rate measuring procedure using the Coulostatic technique in capillary specimens	71
Figure 4.15: Corrosion rate measuring procedure using the Coulostatic technique in ponding specimens	71
Figure 4.16: Downward response of perturbation vs time curve due to faulty connections in a Coulostatic method	73
Figure 4.17: Upward response of perturbation vs time curve due to faulty connections in a Coulostatic method	73
Figure 5.1: Grading of fine and coarse sand used in this study	81
Figure 5.2: Different elements, peak amplitude (count/sec) in (a) cement and fly-ash and in (b) FS and CS detected by XRF	82
Figure 5.3: Typical mixing procedures of SHCC	84
Figure 5.4: Apparatus used for measuring the slump flow of SHCC and mortar mix	85
Figure 5.5: Apparatus used for measuring the air content in SHCC and mortar mix	85
Figure 5.6: Tangent and secant methods of determining E-modulus of elasticity (imitated from Paul, 2011)	89
Figure 5.7: Dumbbell size and set-up for direct tensile testing	90
Figure 5.8: Preparation of specimen for measuring cracks data by using ARAMIS	91
Figure 5.9: TPB testing set-up with (a) two and (b) one LVDT	92
Figure 5.10: (a) Location of the number of cracks measured on the beam crack face (b) use of template (c) mobi-camera (d) crack width measurement using mobi-camera software	93
Figure 5.11: Dumbbell specimen with AE sensors in direct tensile testing	94
Figure 5.12: Position of AE sensor in flexural beam specimen during bending testing	94
Figure 5.13: Specimen setup for fracture energy testing	95
Figure 5.14: Calculation of fracture energy from the specimen response in flexural testing	95
Figure 5.15: Corrosion measuring set-up for the cracked specimen in Series One	98
Figure 5.16: Sustained loading set-up of R/SHCC beams for accelerated corrosion testing in Series Two and Three	99
Figure 5.17: Notched specimens under sustained loads in Series Three corrosion testing ..	100
Figure 5.18: (a) Sustained loading set-up of specimens (b) position of ERE 20 reference electrode inside specimen in Series Four	101
Figure 5.19: Methods of taking corrosion potential reading in the specimens	102
Figure 5.20: (a) Test set up for rapid chloride migration test (b) preparation of specimen for RCM test	104
Figure 5.21: Details specimens outline for long term chloride penetration testing in FS11 and CS11	106
Figure 5.22: Preparation of specimens for chloride penetration test using AgNO ₃	107
Figure 5.23: Detailed specimen outline for short-term chloride-penetration testing in FS2 and CS2	107

Figure 5.24: Detailed specimen outline for short-term chloride-penetration testing in FS32 and FS5	108
Figure 5.25: Colour changes of the sample during total chloride testing (a) before the test (b) after the test	110
Figure 5.26: Changes of potential (E) due to adding AgNO ₃ solution for (a) lower free Cl and (b) higher free Cl content in the samples	112
Figure 5.27: Specimens in the chamber for freezing and thawing test	113
Figure 5.28: Applied temperature for freeze-thaw testing	113
Figure 5.29: Specimens experimental set-up under (a) CWA and (b) ER testing	114
Figure 5.30: Details of the exposure periods in different series of testing	116
Figure 6.1: Slump flow measured in SHCC and mortar	120
Figure 6.2: Typical SSC response of SHCC and mortar specimens under compressive strength testing	121
Figure 6.3: Compressive strength development in SHCC and mortar (reference strength: 120 days in each case)	122
Figure 6.4: SHCC stress vs strain response in direct tensile testing at 14 days	123
Figure 6.5: SHCC stress vs strain response in direct tensile testing at 28 days	124
Figure 6.6: SHCC stress vs strain response in direct tensile testing at 56 days	124
Figure 6.7: Strength development in different types of SHCCs' ultimate and cracking strength at 14 days (reference strength: FS11)	125
Figure 6.8: Strength development in different types of SHCCs' ultimate and cracking strength at 28 days (reference strength: FS11)	125
Figure 6.9: Relationship between FS11 ultimate tensile ($f_{u,st}$) and cracking strength ($f_{cr,st}$) to the ultimate strain at 14 days	126
Figure 6.10: Tensile cracks at the age of 14 days of FS11 specimens at different strain (%) levels	126
Figure 6.11: Tensile cracks in CS11 specimens at the age of 14 days at different strain (%) levels	127
Figure 6.12: Tensile cracks in FS11 specimens at the age of 28 days at different strain (%) levels	127
Figure 6.13: Tensile cracks in CS11 specimens at the age of 28 days at different strain (%) levels	127
Figure 6.14: Average no of cracks and crack widths at the age of 14 days of FS11 specimens	128
Figure 6.15: Average no of cracks and crack widths at the age of 14 days of CS11 specimens	128
Figure 6.16: ACW and MCW at different strain levels in different FS specimens at 28 days	129
Figure 6.17: ACW and MCW at different strain levels in different CS specimens at 28 days	

.....	129
Figure 6.18: Formation of cracks in FS11 and CS11 during tensile testing	130
Figure 6.19: Relationship between crack spacing and strain in both FS11 and CS11	130
Figure 6.20: Relationship between total crack widths (TCW) vs different strain levels of FS11 and CS11 at 14 days	131
Figure 6.21: Relationship between average nr of cracks and strain in FS-SHCC at 28 days	131
Figure 6.22: Un-reinforced SHCC specimen response in flexural testing at 28 days	133
Figure 6.23: R/SHCC specimen response in flexural testing at the age of 14 days	134
Figure 6.24: R/SHCC specimen response in flexural testing at the age of 14 days	134
Figure 6.25: R/FS3 specimen response in flexural testing at the age of 14 days	135
Figure 6.26: Different un-reinforced SHCCs ultimate-flexural and first-crack strengths at the age of 28 days	135
Figure 6.27: Flexural strength development of un-reinforced SHCC and mortar	136
Figure 6.28: Flexural cracks in un-reinforced SHCC at ultimate deflection level	137
Figure 6.29: Average flexural crack widths (ACW) in un-reinforced notched specimens of (a) FS32 and (b) FS5 at ultimate and 1 mm deflection levels	137
Figure 6.30: Average nr of cracks vs crack widths in R/FS2 specimens with single and double bars at different cover depths	138
Figure 6.31: Average nr of cracks vs crack widths in R/CS2 specimens with single and double bars at different cover depths	138
Figure 6.32: Average nr of cracks vs crack widths in R/Mortar specimens at 15 mm cover depth with single steel bar	139
Figure 6.33: Average nr of cracks vs crack widths of R/FS3 specimens with different cover at two levels of deflection	139
Figure 6.34: Crack pattern in 15 mm cover of R/FS2 and CS2 specimens with single and double bars in Series One	140
Figure 6.35: Average crack spacing vs cover depth in R/FS2 and CS2 at 3.5 mm levels of deflection with single and double bars in Series One	141
Figure 6.36: Average crack spacing vs cover depth in R/FS3 at different level of deflection in Series Two	141
Figure 6.37: Average crack widths vs cover depth in R/FS2 and CS2 at 3.5 mm level of deflection in Series One	142
Figure 6.38: Maximum crack widths vs cover depth in R/FS2 and CS2 at 3.5 mm level of deflection in Series One	142
Figure 6.39: Average crack widths (ACW) and maximum crack widths (MCW) vs cover depth in R/FS3 at different levels of deflection in Series Two	143
Figure 6.40: Relationship between cracks and deflections in R/SHCC specimens	143
Figure 6.41: Amplitude of AE signals (dots) at different stress-strain level	144

Figure 6.42: Amplitude of AE Signals with different frequencies versus strain of FM3 dumbbell specimens in direct tensile testing	145
Figure 6.43: AE response of FS4 beam specimen in flexural test	145
Figure 6.44: AE response of FM3 beam specimen in flexural test	146
Figure 6.45: Un-reinforced FS and CS-SHCC notch specimen responses in flexural testing	147
Figure 6.46: Un-reinforced FS and CS-mortar notch specimen responses in flexural testing	147
Figure 6.47: Fracture-energy (G_f) variations in different mortar types	148
Figure 6.48: Fracture toughness (K_{IC}) vs critical crack length (a_c) in different mortar types	148
Figure 6.49: Fibre distribution (as black dots) in the dumbbell cross-section	149
Figure 6.50: Fibre spacing in SHCC using different equations	150
Figure 7.1: Corrosion potential in different R/SHCC and R/mortar specimens for different cover depths in different series	153
Figure 7.2: Corrosion potential in cracked and un-cracked R/FS4, R/FM3 and R/HM3 with B1 and C15 in Series Four	155
Figure 7.3: Corrosion potential in cracked and un-cracked specimens in Series Four	155
Figure 7.4: Centre versus side corrosion potential reading in Series One	156
Figure 7.5: Corrosion status in the cracked (a) R/FS4 (b) R/FM3 and (c) R/HM3 specimens after 60 days of accelerated chloride exposure of the Series Four specimens	157
Figure 7.6: Capillary chloride penetration in cracked SHCC beam	157
Figure 7.7: Positions of taking corrosion mapping data in the specimen cross section	159
Figure 7.8: Corrosion potential mapping in un-cracked and cracked FS4 specimen at 65 days	159
Figure 7.9: Relationship between cracks and corrosion potential in SHCC specimens	160
Figure 7.10: Relationship between cracks and corrosion potential in mortar specimens ...	160
Figure 7.11: R/SHCC with B1 specimens (a) corrosion rate and (b) estimated corroded depth in Series One	161
Figure 7.12: R/SHCC with B2 specimens (a) corrosion rate and (b) estimated corroded depth in Series One	162
Figure 7.13: R/mortar with B1 specimens (a) corrosion rate and (b) estimated corroded depth in Series One	162
Figure 7.14: R/SHCC specimens (a) corrosion rate and (b) estimated corroded depth in Series Two	162
Figure 7.15: R/SHCC specimens (a) corrosion rate and (b) estimated corroded depth in Series Three	163
Figure 7.16: R/mortar specimens (a) corrosion rate and (b) estimated corroded depth in Series Three	163

Figure 7.17: Observed corrosion stains in C15B1 specimens after 6 months of exposure	164
Figure 7.18: XCT images showing corrosion status inside the R/SHCC specimen	164
Figure 7.19: Corrosion inspection by destruction method (a) virgin steel (b) R/FS31_C15D5 steel before cleaning and (c) R/FS31_C15D5 steel after cleaning with HCl	166
Figure 7.20: Inspection of corrosion in the reinforcing bars by destruction of R/SHCC specimens	166
Figure 7.21: Inspection of corrosion in the reinforcing bars by destruction of R/mortar specimens	167
Figure 7.22: Estimated and actual mass loss of steel in R/FS32 and R/FM2 specimens in Series Three	168
Figure 7.23: Difference of analytical and experimental yield forces in different R/SHCC and R/mortar specimens due to loss of section in corrosion	169
Figure 7.24: Average pitting depths in the single steel bars (B1) at different series	170
Figure 7.25: Pitting depths versus loss of yield resistance of steel bars	171
Figure 7.26: Relationship between corrosion potential (E_{corr}) and rate (V_{corr}) in the cracked R/SHCC specimens at different days	172
Figure 7.27: Relationship between corrosion rate (V_{corr}) and moisture content in the specimens	173
Figure 7.28: Chloride penetration in R/FS1 and R/CS1 at different exposure cycles	174
Figure 7.29: Chloride penetration in R/FS2 and R/CS2 at different time periods	175
Figure 7.30: Chloride penetration in R/FS5 and R/FS32 after different exposure periods ..	175
Figure 7.31: Chloride profiles in FS32 and FS5 specimens for different notch spacing for different exposure periods	177
Figure 7.32: Comparison of XRF and chemical chloride profile in (a) FS32 and (b) FS5 specimens	177
Figure 7.33: XRF chloride profile in different (a-e) R/SHCC and (f) R/mortar specimens after different weeks (W)	178
Figure 7.34: Chloride profile for the entire depth of different cracked and un-cracked (UC) R/SHCC specimens after different exposure weeks (W)	179
Figure 7.35: Chemical total and free chloride profile in different R/SHCC specimens	180
Figure 7.36: XRF total and chemical free chloride content in different R/mortar specimens	180
Figure 7.37: Chemical versus XRF total chloride content profile in R/SHCC specimens ..	181
Figure 7.38: Total versus free chloride relationship in R/SHCC specimens	181
Figure 7.39: (a to c) Different chloride content profile with respect to the cover depth and (d) the difference of total and free chloride at different depth	182
Figure 7.40: XRF chloride content versus total crack width relationship in different specimens	182

Figure 7.41: Influence of exposure period on the chloride content at the steel bar surface in the specimens in Series One	183
Figure 7.42: Corroded depths versus different chloride content relationship in R/SHCC specimens	183
Figure 7.43: Comparison of chloride content at the level of the steel bar in the R/SHCC and R/mortar specimens	184
Figure 7.44: Cl penetration during RCM test in un-cracked FS4, FM3 and HM3 specimens in Series Four	185
Figure 7.45: Diffusion coefficient (D_{cl}) and penetration depth (X_d) in un-cracked FS4, FM3 and HM3 specimens in Series Four	185
Figure 7.46: Mass loss of un-cracked FS4, FM3 and HM3 specimens in freeze-thaw test in Series Four	186
Figure 7.47: Mass loss from the freeze-thaw testing in the different specimens after 28 and 42 cycles in Series Four	186
Figure 7.48: Capillary water absorption in un-cracked FS4, FM3 and HM3 specimens in Series Four	187
Figure 7.49: Water gains by different specimens during capillary absorption testing in Series Four	187
Figure 7.50: Electrical resistivity of un-cracked FS4, FM3 and HM3 specimens at different frequency in Series Four	188
Figure 8.1: Typical modes of attack in reinforced concrete structures	191
Figure 8.2: Influence of crack widths and spacing on corroded depths in R/FS31 specimens after 57 weeks of exposure	197
Figure 8.3: Pitting depths with different numbers of cracks in R/SHCC specimens at the end of their exposure period	198
Figure 8.4: Pitting depths versus total crack widths (TCW) in R/SHCC specimens at the end of their exposures period	198
Figure 8.5: Relationship between pitting depths and crack spacing in R/SHCC specimens at the end of their exposures period	199
Figure 8.6: Pitting area in steel due to different number of cracks in the R/SHCC specimens	199
Figure 8.7: Pitting diameter in steel due to different crack widths in NC (reproduced from Mohammed <i>et al.</i> 2001)	199
Figure 8.8: XRF total chloride (Cl) and average crack widths (ACW) relationship in R/SHCC specimens after (a) 108 weeks and (b) 57 weeks of chloride exposure	200
Figure 8.9: XRF total chloride (Cl) and total crack widths (TCW) relationship in R/SHCC specimens after (a) 108 weeks and (b) 57 weeks of chloride exposure	201
Figure 8.10: XRF total chloride (Cl) at the cover depths on R/SHCC specimens	201
Figure 8.11: Relationship between the corroded depths calculated from corrosion rate readings by Eqs. (4.22 & 4.23) and cover depths (a) average crack widths/cover depth ($W_{cr,ave}$)	

/C) (b) total crack widths/cover depth ($W_{cr,tot}/C$) and (c) crack spacing/cover depth (S_{cr}/C) in R/FS2 & R/CS2 specimens at 108 weeks of exposures periods	202
Figure 8.12: Corroded depths and actual mass loss of steel in the specimens in Series Three	203
Figure 8.13: Relationship between loss of yield force and actual mass loss in the specimens in Series Three	203
Figure 8.14: Corrosion modelling using Eq (8.8) of cracked R/SHCC specimens with a single crack	206
Figure 8.15: Corrosion modelling using Eq (8.9) of cracked R/SHCC specimens with multiple cracks	206
Figure 8.16: Validation of proposed corrosion modelling for single crack specimens using Eq. (8.8) (a) for 20 mm cover depths (C20) (b) for 40 mm cover depths (C40) of steel	207
Figure 8.17: Observed mass loss due to different crack widths in NC	208
Figure 8.18: Relationship between XRF total chloride (Cl) content and total crack widths (TCW) in unreinforced SHCC specimens (reproduced from Kojima <i>et al.</i> 2014)	209
Figure 8.19: Chloride content and corrosion area at different total crack widths (TCW) in NC (reproduced from Mohammed <i>et al.</i> 2001)	210
Figure 8.20: Corrosion in steel due to different average crack widths (ACW) in SHCC and NC	210
Figure 8.21: (a) Measured corrosion current (I_{corr}) in steel using different measuring techniques by Liu & Weyers, (1998) (b) normalised corrosion current after multiplying with the calibration factors	211
Figure A.1: Application of HPFRCC (a type of SHCC) in Mihara Bridge in Japan (imitated from Mitamura <i>et al.</i> 2005)	226
Figure A.2: Surface repair of concrete dam using sprayable SHCC in Japan (imitated from Kojima <i>et al.</i> 2004)	226
Figure A.3: Application of ECC (a type of SHCC) in bridge deck repair in Michigan, USA (imitated from Li <i>et al.</i> 2005)	227
Figure A.4: HPFRCC used as damper in high building in Japan (imitated from Mitamura <i>et al.</i> 2005)	227
Figure B.1: Set up for corrosion pitting depths measurements in the steel bar	228
Figure B.2: Titrator used for determining the free chloride-content in SHCC and mortar powder	228
Figure C.1: Formation of tensile cracks in different FS-SHCC and CS-SHCC specimens ..	234
Figure C.2: Observed crack pattern in R/FS2 & R/CS2 specimens	234
Figure C.3: Observed crack pattern in R/FM1 & R/CM1 specimens	234
Figure C.4: Observed crack pattern in unreinforced FS11 & CS11 specimens	235
Figure C.5: Flexural cracks in individual specimens of R/FS2 with B1 at D3.5	235
Figure C.6: Flexural cracks in individual specimens of R/CS2 with B1 at D3.5	236

Figure C.7: Flexural cracks in individual specimens of R/FS2 with B2 at D3.5	237
Figure C.8: Flexural cracks in individual specimens of R/CS2 with B2 at D3.5	238
Figure C.9: Flexural cracks in individual specimens of R/FS31 with B1 at D5	239
Figure C.10: Flexural cracks in individual specimens of R/FS31 with B1 at D7	240
Figure C.11: Corrosion potential mapping in uncracked R/FM3 specimen in Series Four .	241
Figure C.12: Corrosion potential mapping in uncracked R/HM3 specimen in Series Four	241
Figure C.13: Corrosion in steel bars in Series One	241
Figure C.14: Corrosion in steel bars in Series Two	242
Figure C.15: Corrosion in steel bars in Series Three	242
Figure C.16: Chloride penetration during RCM test in cracked FS4 specimens loaded at different levels of deformation in Series Four	243
Figure C.17: Chloride penetration during RCM test in FM3 and HM3 specimens loaded at different levels of deformation in Series Four	243
Figure C.18: Water gains by different specimens during capillary absorption testing in Series Four	244

List of Tables

Table 3.1: ACI committee 224 acceptable crack widths for RC under service loads	37
Table 3.2: Threshold crack width for different exposure conditions in different countries ...	37
Table 3.3: Threshold chloride level for concrete described in different codes and literatures	42
Table 3.4: Relationship between crack widths, chloride content, corroded area and corrosion rate in concrete	46
Table 4.1: Relationship between corrosion rate, resistivity and severity in concrete	55
Table 4.2: Corrosion condition related to half-cell potential (ASTM C876)	62
Table 4.3: Effect of different factors on HCP readings and corrosion probability (Gu & Beaudoin 1998)	63
Table 5.1: Oxide compositions (% of total wt) of different materials used in the research ...	80
Table 5.2: Properties of PVA fibre used (Ogawa & Hoshiro, 2011)	81
Table 5.3: Amount of materials (kg/m^3) used in this research	83
Table 5.4: Details of specimen types and numbers used in this research	86
Table 5.5: Details of reinforced SHCC and mortar specimen types, number, size, exposure types and methods of making cracks	87
Table 5.6: Details of number of specimens, crack and crack widths in series three	99
Table 5.7: Details of unreinforced FS32 and FS5 notched specimens used in XRF and chemical testing	109
Table 5.8: Details of R/SHCC and R/mortar specimens used in XRF and chemical testing	109
Table 6.1: Fresh properties of SHCC and mortar mixes	119
Table 6.2: SHCC and mortar 28 days ultimate compressive strength (f_{cu}) and E-mod with their CoV (%)	121
Table 6.3: SHCC tensile strength and strain at different days	123
Table 6.4: Ultimate-flexural ($f_{u,ft}$) and first-cracking ($f_{cr,ft}$) strengths at 28 days for SHCC and mortar	132
Table 6.5: Different reinforced SHCC beam responses in three-point bending testing at 14 days	133
Table 6.6: Matrix fracture toughness (K_{IC}), crack tip toughness (J_{tip}) and fracture energy (G_I)	146
Table 7.1: Specimen details in different series of corrosion testing in this research	152
Table 7.2: Average and maximum pitting depths in the steel bars in different series at the end of testing period as reported in Table 7.1	171
Table 8.1: Proposed estimated corrosion rate (V_{corr}) in steel bars at different exposure classes (EN 206)	192

Table 8.2: Observed corroded depth relationships with time, cracks, cover depths and chloride	206
Table C.1: SHCC mix 1	229
Table C.2: FS-SHCC 28 days ultimate compressive strength and strain at ultimate strength for mix 1	229
Table C.3: FS-SHCC 28 days flexural resistance and deformation for mix 1	230
Table C.4: CS-SHCC 28 days flexural resistance and deformation for mix 1	230
Table C.5: FS-SHCC tensile resistance for mix 1	231
Table C.6: CS-SHCC tensile resistance for mix 1	232
Table C.7: SHCC mix 2	232
Table C.8: FS-SHCC tensile resistance for mix 2	233
Table C.9: CS-SHCC tensile resistance for mix 2	233

Chapter 1

Whatever the mind of man can conceive and believe, it can achieve.

- Napoleon Hill

Introduction

1. General discussion

Concrete is one of the most widely-used construction materials. The Romans used to think of concrete as a revolutionary material for its versatility over many other materials like steel, timber, aluminium, glass, etc. It is still uncertain exactly when first concrete came to the construction industry. However it is believed that concrete already existed in 800 B.C (Merusin, 1996) and now there is no other construction material used in such vast quantities as concrete. Global concrete production is roughly about 25 billion tonnes and that means about 3.8 tonnes/per person/per year (WBCSD report, 2014) and this amount is increasing every year due to the booming of construction works in many countries. In today's corporate world, the concrete sector is a vital one. Continued strong population and industrial growth are accompanied by increasing concrete consumption world-wide. According to the NRMCA report (2013) in 2015 the projected global revenue of concrete ready-mix companies will be over \$100 billion. The present concrete constituents and construction techniques are quite different than those of ancient period concrete. Every day's upgrading of technology in many fields brings new changes to past traditional methods. Also modern civilization and progress are almost wholly dependent on developments in the fields of engineering and technology which are always changing with the inclusion of new ideas, innovations and skills. On the other hand limited natural resources can be a big burden for the future generation. Therefore, it is very important to implement a durable design or production method of any material to serve or improve the structural performance and meet the present demands without necessitating any major repair works. In this regard, researchers from all over the world have been contributing significantly in many ways in the different fields. The introduction of fibre-reinforced concrete in today's construction industry is one of the great achievements.

1.1. Materials sustainability

For society to continue developing in the way it has done, it is necessary to pay more attention to the environment and its sustainability. Sustainable development involves maintaining the current rate of development whilst leaving sufficient and suitable resources behind for later generations to develop. Therefore, environmental problems must be tackled by considering their relationship with both the state of the economy and the well-being of

Introduction

society. So, new materials that are being added to the construction sector need more research to determine their behaviour under various conditions.

Once concrete was thought of as a durable material needing little repair throughout its lifetime. This hypothesis is correct indeed, except when the environment surrounding concrete is highly hostile and beyond its performance level (Shetty, 1982). In the last few decades global warming has changed the earth's climate, ultimately influencing the performance of materials as well as of whole structures (Natesan *et al.* 2003). Inconsistency in the environment has brought to attention the influence thereof in numerous fields and many studies have been carried out to find the proper solution. Also the harsh environments e.g. in coastal areas, the practice of de-icing, industrial gases, etc. are usually causes for deterioration such as carbonation, corrosion, etc. As a result, some structures built more than 40-50 years ago have already deteriorated in many countries and about 50% of construction expenditure in developed countries is spent on repairs and maintenance (ISO 15686-1:2000). Many concrete structures may need repair work on a regular basis say every 5 or 7 years until the end of their service life. In the USA, every year almost \$18-\$21 billion is spent by owners for repairing, strengthening and protection of their concrete structures until the end of their service life (Goodwin, 2012). Additionally, new construction needs to meet present demands. However, material durability and environmental sustainability should be given the highest priority during any construction work.

1.2. Development of new materials

The main dilemma of the existing reinforced concrete structure (RCS) is that it is not resistant to the present climate condition of many countries. The conventional RCS faces many problems such as the formation of wide cracks due to its brittleness, the changing of live loads over time as well as climate. The introduction of different kinds of fibre-reinforced concrete (FRC), various types of high strength concrete (HSC), ultra-high performance concrete (UHPC) and reactive powder concretes (RPC) etc. have therefore resulted in significant changes in today's concrete mix design compared to the design practices 50 years ago (Bentz *et al.* 1999). The structures made from these materials are assumed to have a considerable increase in their maintenance/repair-free lifetime, although the production costs of these types of concrete are higher than those of conventional concrete. However, the in-depth knowledge of the durability-performance of these new generation concretes is still lacking and research needs to continue in order to increase the knowledge on this topic.

1.3. Discovering the strain hardening cement-based composite (SHCC)

According to published literature, strain hardening cement-based composite (SHCC) came to light in 1990 for its extraordinary performance of higher strain/ductility as well as strength (Li *et al.* 1990; Li, 1992, 1993) when compared to that of traditional normal concrete (NC) as well as FRC. The typical stress-strain responses and the crack width of SHCC and FRC in direct tensile testing are shown in Fig 1.1. Up to the elastic region of both SHCC and FRC,

Introduction

the stress increases as the strain increases. After the first cracking, the stress reduces significantly for FRC while the fibre bridging capacity of SHCC leads to increased stress upon further strain increase. This so-called strain hardening continues until localisation occurs in a crack, which leads to the onset of strain softening. In the strain hardening part, multiple fine cracks are appear and the average crack width typically remains below 0.1 mm, although the maximum crack widths can be larger than 0.15 mm.

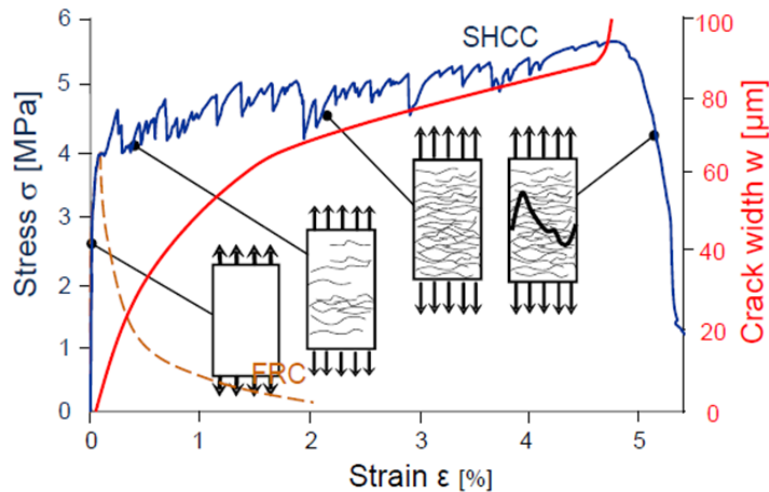


Figure 1.1: Tensile stress-strain and cracking behaviour of SHCC and fibre-reinforced concrete (FRC) (reproduced from Weimann & Li, 2003).

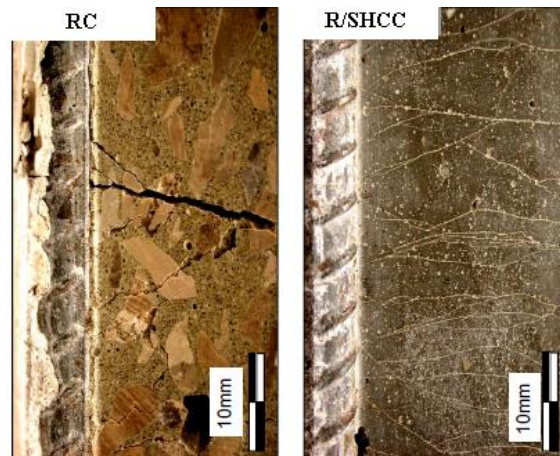


Figure 1.2: Cracking behaviour in reinforced concrete (RC) and R/SHCC (reproduced from Fischer & Li, 2004).

Higher strain capacity of concrete is a very important feature as protection against any kind of tensile load caused by hazardous environments, seismic action, wind load, tidal load, etc. on the RCS. Note that the tidal load only applies on the bridge due to the extreme tides. It is because of the variation of pressure in the earth due to the movement of the water caused by the tide. Researchers discovered that the aforementioned problems can be solved by using

Introduction

highly ductile materials like SHCC, rather than repairing with NC every time. It is now well known that NC has lower tensile strength and ductility which are counteracted by the inclusion of extra reinforcement. Therefore in RCS if sufficient tensile strength and ductility are not provided, cracks may appear which allow aggressive chemical substances to enter to the concrete and ultimately leads to corrosion in the steel bar. Typically tensile strain values of NC range between 0.015-0.02%, while more than 4% strain can be obtained for SHCC (Sahmaran *et al.* 2008). It means that compared to NC, 300-500 times more strain can be achieved in SHCC before strain softening starts. Therefore by using the high ductile behaviour of SHCC, the repair as well as the service lifetime of structures can also be increased (Lepech & Li, 2006). It is also worth mentioning that the compressive strength of SHCC can be designed to be as high as NC, however, but the Young's Modulus (E-mod) of this material is typically lower compared to NC due to exclusion of large aggregate and overall lower proportion of aggregate in SHCC. The higher ductility of SHCC is mainly achieved due to the formation of multiple fine cracks in the SHCC specimen as the applied load is increased. Fig 1.2 shows the cracking behaviour in reinforced concrete and in reinforced SHCC (R/SHCC) (Fischer & Li, 2004). Until now SHCC has been used in many countries as a repair material for bridge decks, tunnels, retaining walls and offshore structures. Full scale SHCC in structures is not yet generally done and the reasons behind it may be the initial high cost of SHCC and also the limited information available on SHCC performance as it is a relatively new material.

1.4. The main problem statement

In current practice, concrete specifications are mainly characterised by the slump value and compressive strength as well as by its flexural strength, direct or indirect tensile strength and E-mod, which are often calculated from the compressive strength value by using empirical relations recommended in different codes. This is not sufficient and does not guarantee the durability of concrete (Richard & Cheyrezy, 1994; Saravanan *et al.* 2010). The compressive strength of the concrete is a bulk property, while the durability is strongly affected by the properties of the surface and near-surface of the concrete structures. Additionally, transport (gas, liquid and water) is a characteristic controlled by the overall percolation of the pore network, while strength is controlled usually by the pore size in a concrete matrix. The durability is mostly influenced by the transport properties of the concrete such as diffusivity, permeability, and sorptivity. Thus, in order to ensure durability of concrete, it is required that properties other than compressive strength must also be stipulated.

The interaction of the surface layer of the concrete with the external surroundings is of the utmost importance in many degradation processes (ingress of sulphates and chlorides, carbonation, wetting/drying cycles). For this reason, an evaluation of the transport properties of this surface layer should provide a valuable indication of the durability of a given concrete (Bentz *et al.* 1999). Also as mentioned in a previous section, many RCS often face the dilemma of lower strain and strength resulting in excessive durability problems especially

Introduction

due to the formation of cracks in the structure. Often these cracks are the main passage of dangerous substances and when reaching the steel bars corrosion of the steel starts.

Cracks in the RCS are often unavoidable due to the inherent properties of concrete. However, if the crack widths can be controlled up to a certain limit, it might solve some of the problems. As mentioned earlier, the strain-hardening behaviour of SHCC is accompanied by multiple fine cracks and controlled fine crack widths which are believed to improve structural durability, by controlling the rates of ingress of deleterious materials. So far, the existing research on SHCC has shown promising outcomes in different fields such as cracking, corrosion, water and chloride penetration, free-thaw resistance, etc. (Li *et al.* 1990; Lepech & Li, 2005; Wittmann *et al.* 2009). However, the major backlogs in previous studies are (i) the number of tests was limited and (ii) studies did not link up with the real deterioration of structures and so not enough was done to come up with a design guideline.

1.5. Scope of the research

This research was commenced to generate more information on cracks, chloride ingress and corrosion in SHCC specimens made with polyvinyl alcohol (PVA) fibres in a broad sense. SHCC crack widths at different strain and deflection levels, chloride ingress through cracked and un-cracked specimens and corrosion damages in the steel bar were the main focuses of this research work. Some supporting experiments on durability such as freeze-thaw resistance, rapid chloride migration testing, water absorption and electrical resistivity testing were also performed. The experiments were designed in such a way that the outcomes from the research can also be used as references for future modelling such as corrosion linked to the concrete cracks, steel mass loss, etc. of a structure where SHCC is used.

The experimental work was started in February 2012 after performing a broad literature survey. Large numbers of SHCC dumbbells, cubes, cylinders and beam specimens were prepared containing various percentages of fibres to determine the mechanical characteristics of the materials. In the same year in late July, a total of 36 R/SHCC beams with two different levels of steel bars for three different cover depths were made for the accelerated corrosion testing. All the specimens were pre-cracked in flexure, subjected to chloride by capillary absorption and only corrosion potential readings were recorded until the corrosion rate measuring set-up was developed. Again in February 2013 a total of 5 beams from reinforced mortar (R/mortar), in July 2013 a total of 16 beams from both R/SHCC and R/mortar, in September 2013 a total of 18 beams from R/SHCC and in March 2014 a total of 22 beams from both R/SHCC and R/mortar were prepared respectively for the accelerated chloride-induced corrosion testing on them. Because of specimens different casting periods, the corrosion testing in this research was divided in to four series and details are discussed in Chapter 5.

Copper/copper-sulphate and manganese half-cells were used for measuring the corrosion potential. Later the Coulostatic method was used to determine the corrosion rate in the steel

Introduction

bars of R/SHCC and R/mortar specimens. Both corrosion potential and rate were measured in an indoor laboratory ambient temperature condition / climate. Since chloride-induced corrosion was monitored in the specimens, the actual chloride (% by binder weight) content at the steel bar surface level was also determined. In this regard, chloride profiling in the reinforced and un-reinforced specimens was determined by X-ray fluorescence (XRF) method as well as by the chemical testing recommended by the RILEM TC 178. Destructive and non-destructive (using X-ray Computer Tomography (XCT)) methods were also followed to monitor the real corrosion damage in the steel bars. The actual mass loss of steel due to corrosion, the loss of yield force resistance and the pitting depths and areas were also obtained from the destructive tests. The results reported here were obtained during a period of more than two years. Although the main focus of this research is corrosion at cracked stage of R/SHCC, however, corrosion does occur at uncracked stage of R/SHCC as well. In this case, long time may require noticing any corrosion activities in the R/SHCC and that is why the corrosion test in this research at uncracked R/SHCC and R/mortar specimens is limited.

1.6. Purposes of the research

As mentioned before, the lack of or limited information and knowledge are the main obstacles to using SHCC in large structures and therefore in this study, the focus is to induce cracking and corrosion in the SHCC under certain strain or load levels, for a specific composite. Most of the previous research reports on SHCC were where specially graded fine sand (FS) (particle size up to 0.30 mm) was used as aggregate. However, this research also investigated SHCC using local coarse sand (CS) with particle size up to 2.36 mm. Successful application of local sand can also help to reduce the production cost of this material. Different mechanical properties such as compressive, tensile and flexural strengths together with the tensile and flexural crack patterns in SHCC specimens were examined extensively over a large number of specimens to contribute to a pool of knowledge to assist in increasing confidence in using this material in structural applications.

One of the major purposes of this research was to lay the basis for the development of a durability design guideline for SHCC in structural applications. From the chloride-induced accelerated corrosion testing on about 100 different R/SHCC and R/mortar specimens, different types of relationships were drawn from the outcomes. The results obtained from this experiment can be used to validate the reinforcement corrosion in FS-SHCC, CS-SHCC and in mortar specimens. The outcome of this research may provide the basis for using SHCC in structures to protect reinforcement against corrosion in a chloride environment and also contribute to the knowledge of typical corrosion problems in concrete. It may also help to predict the service life of finely cracked structures when corrosion starts. In this sense, this research work is more directly applicable to new construction. However, many aspects of this work are relevant for repair also, if the steel bar is embedded in the SHCC part to sufficient depth. Finally a successful application of SHCC in structures can reduce the repair cost as well as increase service life of structures. Obviously durability potential and increase of

Introduction

structural service life remains to be verified. Therefore, the main purposes of this research are:

- Investigate the crack properties such as average, maximum and total crack widths in un-reinforced SHCC specimens under direct tensile testing and in R/SHCC specimens under three-point bending/flexural testing.
- Quantify corrosion rate in steel bars in cracked R/SHCC and reinforced mortar (R/mortar) specimens under both pre-cracked and uncracked states.
- Observe chloride penetration profiles in both cracked and un-cracked reinforced and unreinforced SHCC and mortar specimens.
- Establish the ratio of total and free chloride content in the SHCC matrix with a large volume of fly-ash.
- A primary approach towards the durability design modelling of a structure with SHCC.

1.7. Hypothesis of the research

This research is designed to assess the following hypotheses:

Firstly, the laboratory experimental corrosion rate measurement in the steel bar will represent to a satisfactory level, the real corrosion damage of steel bar.

Secondly, the corrosion rate in specimens with smaller crack spacing is lower than the corrosion rate for larger crack spacing in R/SHCC specimens and

Finally, the lower chloride penetration through finer crack widths will cause a lower corrosion rate in the steel bars of R/SHCC specimens.

1.8. Limitations of the research

This study is limited to the corrosion in finely cracked R/SHCC under chloride attack for a period of two years. However, corrosion also accelerates by carbonation attack and in most cases both chloride and carbonation attacks act together. Because of the time constraint for this research work, carbonation corrosion was not included here. Another important issue is that only two different strength classes of SHCCs for nearly the same mix proportions are reported here. However, in comparison of experimental results in terms of different water to binder ratios (w/b), it is important to have a noticeable difference in the strength class. As a result, it becomes easier to compare the outcomes from different strength classes of concrete which is also limited in this research. Finally and most importantly, currently there is no real data available on the corrosion rate in SHCC and neither is there any existing modelling on this particular type of high volume fly-ash SHCC. This research work therefore is the first approach to corrosion modelling on SHCC and the modelling reported here was not validated by real structures in actual field conditions. Of course the experimental corrosion rates measured in the R/SHCC specimens were verified by measuring actual steel mass loss,

Introduction

pitting depth and loss of yield resistance after destruction of the specimens. It was found that the analytical methods followed in this research also meet the outcomes from the aforementioned actual measurements to a satisfactory level.

1.9. Concluding remarks

Introducing new materials and their improved properties is bringing new dimensions and possibilities to present construction work. However, durability should be the main focus in choosing new materials for construction work since it is argued that overall structural cost, i.e. over its entire life span is influenced most strongly by cost saving through durable construction material. The practice of using durable materials in proper ways can save our environment as well as costs and energy. Entire SHCC structures may not be the suitable or optimal option in many cases because of the higher initial cost as well lower E-mod value. However, partial replacement by SHCC may be suitable in the RCS where large extension due to dynamic load, higher flexural deformation and severe exposure is expected. SHCC has significant resistance against wide cracking as well as against penetration by dangerous substances to the steel bar position and therefore alters the deterioration process favourably.

1.10. References

Bentz, DP, Clifton, JR, Ferraris, CF & Garboczi, EJ 1999, Transport properties and durability of concrete: Literature review and research plan, Building and Fire Research Laboratory, NIST, USA.

Cement Sustainability Initiative 2014, WBCSD-World Business Council for Sustainable Development. [Retrieved 15 September 2014].

Fischer, G & Li, VC 2004, 'Effect of fibre reinforcement on the response of structural members', proceedings of the Fracture Mechanics of Concrete and Concrete Structures, Vail, USA, pp. 831-838.

Goodwin, F 2012, 'The concrete life cycle: Maintain to Sustain', proceedings of the ICRI fall convention, November 7-9, Rancho Mirage, Canada.

ISO 15686-1 2000, Building and Constructed Assets – Service Planning, Part 1: General principles.

Lepech, MD & Li, VC 2005, 'Water permeability of cracked cementitious composites', proceedings of ICF11, Turin, Italy, pp. 20-25.

Lepech, MD & Li, VC 2006, 'Long term durability performance of engineered cementitious composites', International Journal for Restoration of Buildings and Monuments, vol. 12, pp. 119-132.

Li, VC, Wang, Y & Backer, S 1990, 'Effect of inclined angle bundling and surface treatment on synthetic fibre pull-out from a cement matrix', Composites, vol. 21, no. 2, pp. 132-140.

Li, VC 1992, 'Post crack scaling relations for fibre reinforced cementitious composites', ASCE Journal of Materials in Civil Engineering, vol. 4, no. 1, pp. 41-57.

Introduction

Li, VC 1993, 'From micromechanics to structural Engineering – The design of cementitious composites for civil engineering applications', *J. Struct. Mech. Earthquake Eng.*, vol. 10, pp. 37-48.

Marusin, SL 1996, 'Ancient Concrete Structures, *Concrete International*', vol. 18 no.1, pp. 56–58.

Natesan, M, Smith, S, Humphreys, K & Kaya, Y 2003, 'The Cement Industry and Global Climate Change: Current and Potential Future Cement Industry CO₂Emissions', *Greenhouse Gas Control Technologies – 6th International Conference*, Oxford: Pergamon. pp. 995–1000. doi:10.1016/B978-008044276-1/50157-4. ISBN 978-0-08-044276-1.

Paul, SC & van Zijl, GPAG 2013, 'Mechanically induced cracking behaviour in fine and coarse sand strain hardening cement-based composite (SHCC) at different load levels', *Journal of Advanced Concrete Technology*, vol. 11, pp. 301-311.

Ready Mixed Concrete Production Statistics 2013, NRMCA-National Ready Mixed Concrete Association. [Retrieved 10 January 2013].

Richard, P & Cheyrezy, MH 1994, 'Reactive Powder Concretes with High Ductility and Compressive Strength. *Concrete Technology: Past, Present, and Future*', proceedings of the V. Mohan Malhotra Symposium, ACI SP-144, S. Francisco, pp. 507 518. Editor: P.K. Mehta.

Sahmaran, M, Li, VC & Andrade, C 2008, 'Corrosion resistance performance of steel-reinforced engineered cementitious composite beams', *ACI Materials Journal*, vol. 105, no.3, pp. 243-250.

Saravanan, J, Suguna, K & Raghunath, PN 2010, 'Confined high strength concrete columns: An experimental study', *American J. of Engineering and Applied Sciences*, vol. 3, no. 1, pp. 133-137.

Shetty, MS 1982, *Concrete Technology, Theory and Practice*, New Delhi, S. Chand & Company Ltd.

Wittmann, FH, Zaho, T, Tian, L, Wang, F & Wang, L 2009, 'Aspect of durability of strain hardening cement-based composites under imposed strain' proceedings of the *Advances in Cement based Materials*, van Zijl and Boshoff (eds), pp.173-179.

Weimann, MB & Li, VC 2003, 'Hygral behaviour of engineered cementitious composites (ECC)', *International Journal for Restoration of Building and Monuments*, vol. 9, no. 5, pp. 513-534.

Chapter 2

Start where you are. Use what you have. Do what you can.

– Arthur Ashe

Existing Results on SHCC (A Literature Survey)

2. General overview

This chapter of the research work covers the current state of understanding and cases of successful applications of innovative materials in the field of concrete and in particular the current and possible future uses of SHCC in structural and non-structural concrete. It also presents an extensive overview on existing results and background of the study of mechanical and durability aspects of SHCC as well as reference concretes such as NC, HPC and UHPC etc. The materials selection for SHCC mix design is different than the conventional concrete mix. Typically huge volume of binder, especially graded fine sand, water and micro fibres such as PVA or polyethylene (PE) are required for SHCC. In last decade, many researchers have attempted to develop the SHCC as one of green construction materials. In this regard the amount of cement content in the SHCC mix has been replaced by the by-products such as fly-ash, slag and limestone powder (Yang *et al.* 2009; Qian *et al.* 2009). However, the micromechanical behaviours due to addition of these by-products are the same as SHCC made from only cement (Kobayashi *et al.* 2010).

Present articles on SHCC indicate that its pseudo strain-hardening behaviour can be an alternative solution to the impasse of NC in ductility, tensile and flexural strength and crack widths since SHCC has been shown to have a better performance in this regard by different researchers like Li *et al.* (2004) and Kanda & Li (2006). Successful researches have been conducted in many countries in Europe, the USA, Japan, etc. However, as a new material, the literature on SHCC especially on its durability properties is still limited and the existing results have not yet been compared on the actual field structural level and this may be the main reason of the limited applications of SHCC. The background information reviewed in this chapter forms the basis for a formulation of the hypothesis and objectives of this research work. Some of the outcomes of the literature survey on SHCC are discussed below.

2.1. Fresh properties of SHCC

Fresh properties such as slump flow value (small cone) and air content are important for the strain-hardening behaviour of SHCC. Uniform dispersion of fibres in the matrix is important

Existing Results on SHCC (A Literature Survey)

for achieving the multiple cracking behaviour of SHCC. It is obtained by careful mix design, which includes proper grading of fine aggregates, optimal fibre content and the use of chemical additives. Fibre distribution in the matrix is influenced by the slump flow and because of poor fibre distribution as shown in Fig 2.1, lower strain and fewer cracks can be found in SHCC. In this case, crack widths will be wider and the complementary energy loss will also be higher. Typically, the slump flow of SHCC is measured with a small cone as specified by different design codes and the flow value varies from 160 mm to 220 mm. However, slump value often depends on the percentage of fibres, water to binder ratio (w/b) and aggregate sizes in the matrix. Nevertheless, by using a super plasticizer (SP) and a viscosity-modifying agent (VMA), it is possible to control the slump flow up to an expected limit. Usually a lower fibre content ($\leq 1\%$ by volume) gives a higher flow value of SHCC (Bruedern *et al.* 2009). SHCC can also be made self-compacting; however, the focus of this research is not the materials development, but corrosion. Similarly, air content in the matrix also depends on the amount of fibre. An almost 30% higher air content was found in SHCC by increasing the fibre content from 0.75% to 1.5% (Kobayashi *et al.* 2010). A maximum 22% air content was observed in SHCC with a fibre content of 1.5% by Kobayashi *et al.* (2010). Air/voids in the matrix form fine flaws, which assist in formation of multiple cracks in the matrix and also help fibre to be pulled out rather than to break/rupture in the matrix. Adding air-entraining agents (AEA) helps to form air/voids inside the matrix. However, in both cases (slump flow & air) the difference in the results can be attained by the different aggregate to binder ratio (a/b), w/b and also the type of fibre (PVA or PE) used in the SHCC mix. So far, not many researchers have reported the results on SHCC slump and air content and there is currently no conclusive evidence of slump and air content influence in SHCC mechanical and durability properties. More research is needed to fill these gaps.

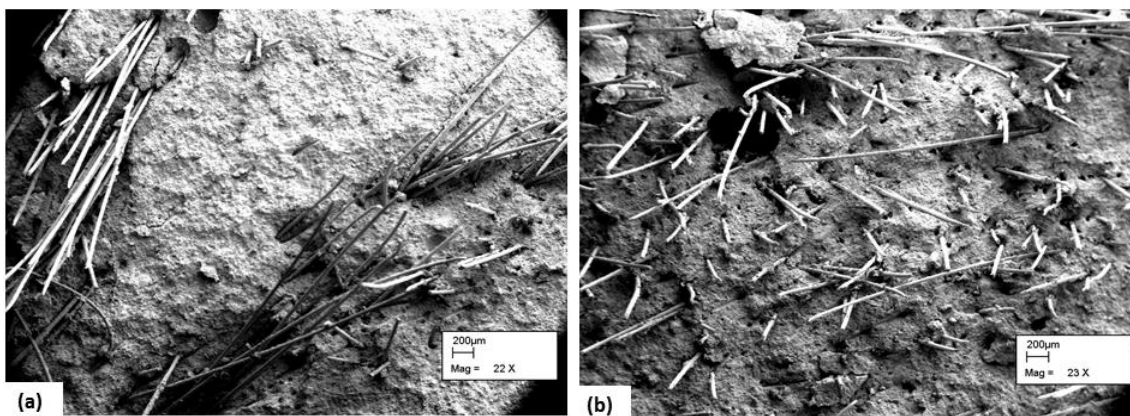


Figure 2.1: SEM images of (a) poor and (b) good fibre dispersion (reproduced from van Dyk, 2004).

2.2. Mechanical behaviour of SHCC

In ultimate compressive and tensile strength, SHCC response may be similar to that of NC, but in flexure it has a factor of 2 to 4 times the resistance. Although not enough research has been done in this area, so far the results have shown promising mechanical behaviour of SHCC (Wang & Li, 2007; Shamaran *et al.* 2008; Qian *et al.* 2009; Kobayashi *et al.* 2010). Some of the mechanical properties, especially different strength properties, E-mod and crack properties of SHCC are discussed in this section.

2.2.1. Compressive strength and E-mod of SHCC

Recently developed advanced cement-based materials, including high strength concrete (HSC), ultra-high strength concrete (UHSC), HPC, UHPC and reactive powder concrete (RPC), etc. have shown drastic improvement particular in the mechanical properties of concrete including compressive strength, E-mod, flexural strength and tensile strength (Richard & Cheyrezy, 1994; Benjamin, 2006; Saravanan *et al.* 2010). Depending on the mix design, SHCC ultimate compressive strength varies from 24-60 MPa (Li *et al.* 1995; Shamaran *et al.* 2008; Filho & Magalhaes, 2009). SHCC ultimate compressive strength (f_{cu}) and E-mod are mostly influenced by its materials compositions, rate of loading and type of loading condition. Li *et al.* (1995) found significant improvement in the strength and E-mod when sand was added to the SHCC mix with higher water/cement ratio (w/c) than the mix without sand. An almost similar or 2.45% higher compressive strength was also found in SHCC in comparison with the same mix of mortar matrix by Sahmaran *et al.* (2007, 2008). However, Kobayashi *et al.* (2010) found that higher fibre volume in SHCC leads to lower compressive strength.

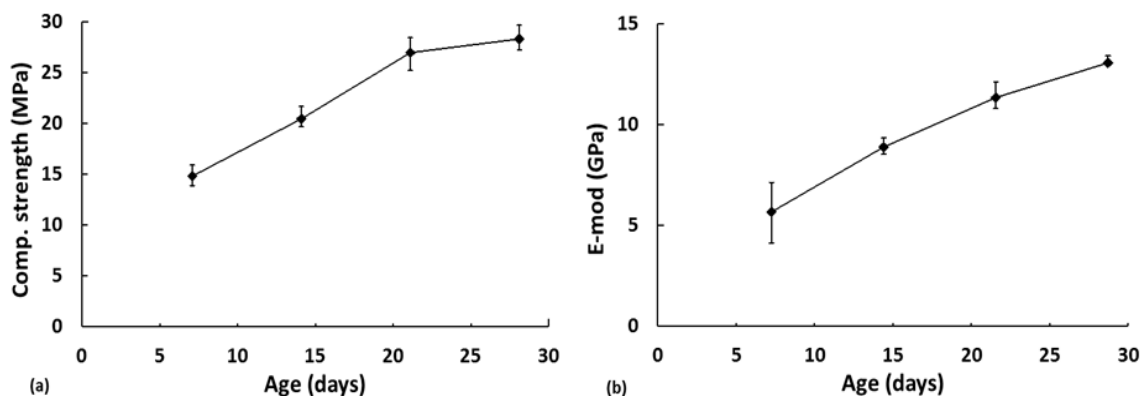


Figure 2.2: Development of SHCC (a) compressive strength and (b) E-mod with time in high volume of SHCC mix (reproduced from Stander, 2004).

The presence of fibre also has an influence on the E-mod value and as a result a lower E-mod value was found for SHCC than for the same mix of mortar matrix (Paul & van Zijl, 2013). Jun & Mechtcherine (2010) calculated the E-mod at the unloading stage of SHCC specimens

Existing Results on SHCC (A Literature Survey)

at different strain levels and they observed a more than 60% reduction in E-mod at increased strain from 0.5% to 2%. SHCC compressive strength behaviour was also observed under different cyclic exposure conditions. A reduction of 7.8% and 2.6% in strength was observed in the SHCC specimen after 180 and 300 cycles of freezing and thawing testing than in the 28 days virgin SHCC strength (Yun & Rokugo, 2011). A high volume of fly-ash in SHCC contributes to developing strength and E-mod gaining as can be seen from Fig 2.2a&b (Stander, 2004; Wang & Li, 2007). Specimens from the different SHCC mixes were tested for investigating the strength development for 8 months by Wang & Li (2007). Strength developments in the SHCC specimens were linearly increased with time while in reference M45 grade concrete after 28 days of testing, the rate of strength development was not that noticeable. The hydration process in fly-ash concrete is slower and in presence of moisture this hydration process continues for a long time causing strength and E-mod increase in SHCC as shown in Fig 2.2a&b.

2.2.2. Tensile stress and strain

One of the major disadvantages of NC, HSC, etc. is that they have low strain/ductility and low performance in crack control, which is very important for the durability of any concrete structure. Strain and crack widths are very important features for structures, especially structures in seismic and hostile environment regions. Therefore designers need to provide extra reinforcement in structures to ensure enough strain capacity and to control crack width. So far SHCC has shown better performance in this regard (Li *et al.* 2002). In spite of the fact that the initial cost of the SHCC is higher than that of conventional concrete, the higher strain capacity of SHCC can improve structural performance against seismic action as well as hazardous environmental impact.

Higher ultimate tensile strength and strain was found in SHCC than in the typical NC used in concrete structures in several studies (Kanda & Li 2006; Sahmaran *et al.* 2007; Qian *et al.* 2009; Witmann *et al.* 2009; Zhang *et al.* 2010) and like compressive strength, tensile strength was also found to increase with time (see Fig 2.3a). It is because the fibres in SHCC allow an increase in the tensile resistance and deformation even after cracks form in the specimen, whereas after cracks appear in NC, its resistance does not increase upon increased strain/deformation and it tends to fail. In a good SHCC matrix, 300 to 500 times higher ultimate tensile strain can be achieved than the typical ultimate strain level of 0.02% of NC. SHCC ultimate tensile resistance and ultimate strain also depend on many factors such as casting methods, types of binder, loading rate, etc. Wang & Li (2007) performed tensile testing for different types (bottom fly-ash, fine fly-ash and class F fly-ash) and percentages of fly-ash on SHCC using 2% of PVA fibres. In a control SHCC mix without fly-ash, authors had found more than 4.5 MPa of ultimate tensile resistance and about 5% of ultimate strain. On the other hand, for others SHCC mixes by replacement of cement with different fly-ash content, although similar strengths were found in the SHCC specimens, strain was significantly lower than the control mix. The authors concluded that the weakening by fly-ash may be explained by the change of matrix chemical composition and coating effect of inert

Existing Results on SHCC (A Literature Survey)

particles on the fibre surface. Typically Al^{3+} and Ca^{2+} are responsible for the formation of strong interfaces between the cement grain and PVA. In Portland cement Al^{3+} exists in the forms of C_3A and C_4AF . However, in fly-ash Al^{3+} and Ca^{2+} are not free hence the high volume of low calcium class F fly-ash dilutes the concentration of Al^{3+} and Ca^{2+} in matrix and reduces the possibilities of strong chemical bonding. It is important to note that in FRC, fibres become active when the cracks are formed in the specimen and in the crack region the matrix stress is zero while the stresses in the fibres are higher. Tanaka *et al.* (2013) investigated tensile behaviour of SHCC with and without vibrating the mould of specimen. Significant improvement in the strength and strain was observed in SHCC by vibrating the mould during casting.

2.2.2.1. Influence of loading rate on strength

Mechtcherine *et al.* (2011) and Yang & Li (2006) studied the effects of different loading rates (strain rate control 0.00001 to 0.01/S) on the tensile strength and strain of SHCC. The rate-dependent results of Yang & Li are shown in Fig 2.3b. They reported that although higher strength can be found at higher strain rate in SHCC in the quasi-static range, the strain capacity reduces linearly as rates increase. On the other hand, Boshoff & van Zijl (2007) found an insignificant reduction in ultimate strain with increased loading rate. By material modification, also Yang & Li (2006) improved the loss of tensile ultimate strain with increased loading rate.

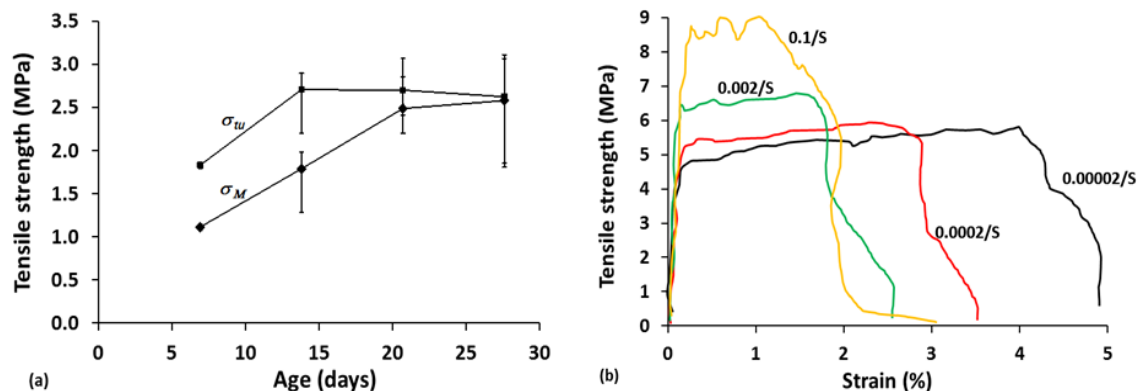


Figure 2.3: (a) Tensile strength development (reproduced from Stander, 2004) and (b) effects of loading rate in the tensile response of SHCC (reproduced from Yang & Li, 2006).

2.2.2.2. Influence of binder and water content on strength

As in the case of compressive strength and E-mod, the tensile strength and strain of SHCC is also influenced by the material mix design. A study by van Dyk (2004) found that although the increased sand/binder ratio (s/b) improves the first cracking strength of SHCC, it gradually reduces the ultimate tensile strength as s/b is increased as shown in Fig 2.4a&b. Significantly higher strength and ultimate strain were observed in the SHCC with the same amount of fibre content when w/c was increased and sand was added to the mix (Li *et al.*

Existing Results on SHCC (A Literature Survey)

1995). For the same fibre content but different sand/cement ratios (s/c) (from 0.5 to 2) in SHCC the strength and strain were significantly higher for higher w/c (0.45) compared to lower w/c (0.35). The authors also found that for the same w/c increased fibre (PVA) diameter from 14 to 40 μm , decrease the matrix tensile strength but increase the strain. Keeping the same w/c ratio, but replacing 10 kg/m^3 of cement by tri-calcium aluminate (C_3A) in the SHCC mix, Bruedern *et al.* (2009) found substantial changes in strain (1.3% to 0.8%) but almost similar strength. It must be kept in mind that careful mix design is required for this relatively young construction material. A critical, minimum amount of fibre is essential to enable strain hardening behaviour, which amount is related to matrix strength and toughness, as well as fibre type. All the above findings must be seen in light of the particular mixes and approaches followed by the respective research groups.

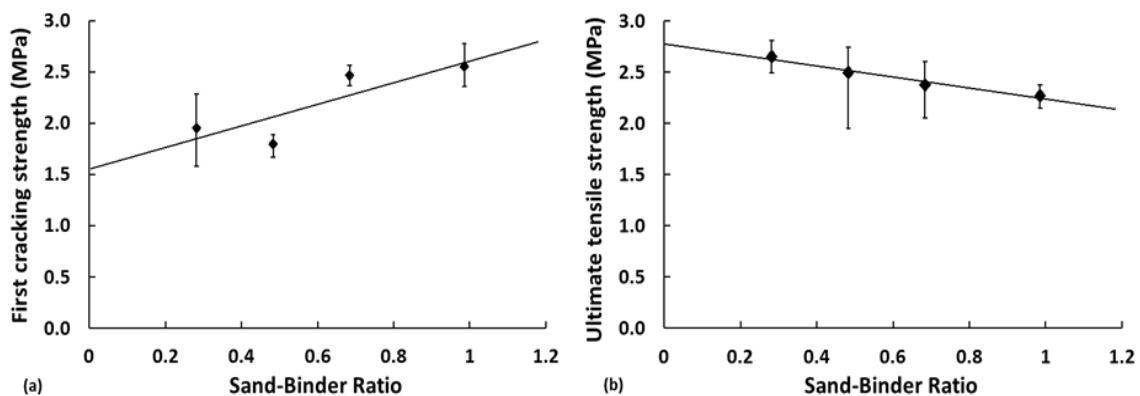


Figure 2.4: Influence of sand-binder ration on SHCC (a) first cracking strength and (b) ultimate tensile strength (reproduced from van Dyk, 2004).

2.2.2.3. Influence of water repellent agent on strength

In a study performed by Zhang *et al.* (2010), two different SHCC mixes were prepared and water repellent agent was mixed in with the fibres. For 2% of fibre in the SHCC, the water repellent mix showed a slightly higher ultimate stress but a lower strain than the SHCC mix without any water repellent. The reason was not described fully by the authors and they suspected that the bond strength of PVA fibres with cement matrix might have improved with the water repellent agent.

2.2.2.4. Influence of loading type and age on strength

SHCC tensile strength behaviour under monotonic and cyclic tensile loading was also observed by Jun & Mechtcherine (2010). Insignificant reduction in strength and strain was observed after 24 loading cycles in SHCC compared with the resistance under monotonic loading (1 cycle).

Although SHCC tensile strength increases with age, similar to NC, the strain capacity can be reduced significantly (Wang & Li, 2007). The experimental results showed that with age

Existing Results on SHCC (A Literature Survey)

SHCC becomes more brittle in direct tensile testing. The reason can be the complex behaviour of binder, sand, fibre and matrix/fibre interface properties which influence the strain capacity of SHCC during aging (van Zijl, 2011).

2.2.2.5. Influence of curing on strength

The influence of curing methods and size of specimens on the strength and strain of SHCC were also examined by Mechtcherine & Schulze (2005). Sealed small and large specimens showed higher strength and strain than the specimens which were kept in water. However in both curing conditions smaller specimens showed slightly higher strength but significantly lower strain under ultimate loading conditions. SHCC strength, strain and E-mod were also observed in the specimen under hot water (60°C) immersion exposure condition by Li *et al.* (2004). After 26 weeks of hot water curing, only little change in the result was observed when compared with specimens under normal curing conditions.

2.2.3. Flexural strength

Typically addition of fibre in concrete tends to increase its flexural resistance. However, as mentioned before the fibre content should not cross the optimum level. The optimum fibre content depends on the types of fibres (macro or micro) used in the matrix. At the optimum fibre content the matrix tensile resistance retained despite tensile strain exceeding the first cracking strain, which may lead to the formation of a tensile stress-block before the strain softening of the matrix starts. In SHCC, the ultimate flexural capacity can be 2-4 times higher than that of the matrix without fibre (Ahamed, 2012).

The flexural strength capacity of strain hardening materials influenced by the many factors such as binder type, curing methods, sand/binder (s/b) content, maximum sand size (S_{max}), exposure conditions, etc. A study conducted by Qian *et al.* (2009) on the flexural strength capacity in SHCC beams (dimension 160 mm x 40 mm x 40mm) mixed with cement, fly-ash, blast furnace slag (BFS) and lime stone powder. After casting all the specimens were sealed and left for 28 days in a control room at 20°C temperature. There were total four different mixes of SHCC and from each mix the specimens were divided in to three sets. From each mix, one set of specimens (controlled specimens) were tested in four-point bending (FPB) test for the ultimate flexural resistance of 2.9, 3.8, 4.2 and 3 mm deformation levels. Second and third sets of specimens were also tested in TPB up to a deflection level of 2.4 mm. In second set the specimens were again cured in water and in third set they were cured in air for another 28 days and tested again at TPB at 56 days for the ultimate flexural resistance. From the same mix, after 56 days a noticeable improvement in the ultimate flexural resistance was observed in the specimens made from cement, fly-ash and limestone powder mix than the same specimens which were tested at 28 days. On the other hand SHCC made from cement, BFS and limestone the different in the results between 28 and 56 days were not significant. However, significantly lower deformations were observed in all specimens of second and third sets from four different mix designs because of pre-cracking.

Existing Results on SHCC (A Literature Survey)

Deflection hardening behaviour due to the changes of s/b content and sand size (0.6 and 1.18 mm) in ductile fibre reinforced cementitious composite (DFRCC) and ductile fibre reinforced geopolymer composite (DFRGC) made from different percentage of PVA and steel fibres (1% and 2%) was studied by Shaikh (2013). DFRCC with 2% PVA and $S_{max} = 0.6$ mm, the flexural resistance was about 30% lower for s/b = 0.5 than s/b = 0.75. In case of DFRGC, completely opposite result was found however the difference was more than 500%. When the S_{max} was changed to 1.18 mm, in DFRCC again the lower strength was observed for s/b = 0.5 than s/b = 0.75. However, in DFRGC almost similar results were observed with the larger sand size but different s/b content.

Sahmaran *et al.* (2008) observed the loss of flexural strength capacity on the SHCC specimens with and without being kept in an aggressive exposure condition. For similar types (size and shape) of mortar specimens after 50 hours of accelerated chloride exposure (by means of immersion), the mortar specimen showed 34% reduction in ultimate flexural resistance compared with the control specimen, i.e. not exposed to the aggressive environment. However, after 50 hours of the same accelerated test there was no reduction in the strength capacity of the SHCC beam. 45% ultimate strength was retained in the SHCC beam even after 300 hours of accelerated testing.

Research conducted by Yun & Rokugo (2011) has shown that the initial load vs deflection slope in flexural testing of SHCC specimens becomes steeper and that the ultimate load deflection reduces under freezing and thawing exposure while no significant changes were shown in the ultimate load capacity of the specimen.

2.2.4. Tensile cracks in SHCC

The crack bridging capacity under any kind of loading in SHCC is one of the major advantages of using this material and to ensure that a sufficient amount of fibre must be present in the matrix. Li *et al.* (2001) found that at 1% tensile strain level the average crack width in SHCC with 2% fibre is about 55 μm while at ultimate strain (3.8%) level crack width still remains below 60 μm . For similar fibre content, Wang & Li (2007) also observed exactly the similar cracking behaviour in SHCC. The number of cracks increases with the increase in strain hardening and in the strain softening part a wider crack widths form at the weak region of matrix before it fails or strain softening starts. Several researchers, including Li *et al.* (2001), Wang & Li (2007), Mihashi *et al.* (2011) found that a maximum of 1.5% to 2% of PVA or PE fibre in SHCC satisfies the above statement, and lead to ultimate tensile strain capacity of up to 3%.

Cracks in SHCC were also monitored in real structures and compared with conventional repair mortar. In Michigan, USA, SHCC and repair mortar were used as a link slab and cracks were monitored in both repair materials. Two days after casting, almost 0.3 mm wide

Existing Results on SHCC (A Literature Survey)

shrinkage cracks were monitored over a patch made with repair mortar. On the other hand and at the same time, there were no cracks in the SHCC patch area. After four months of Michigan winter exposure, cracks up to 2 mm wide were found in the mortar patch, while many fine micro cracks of up to 50 μm width were found in the SHCC patch (Lepech & Li 2005). Even after 900 days of continuous weather exposure and traffic movement over the bridge deck, the maximum crack width in SHCC was limited to 50 μm but the mortar patch was severely deteriorated (crack width was about 3.8 mm) as it is shown in Fig 2.5.

Laboratory experiments carried out by Ahmed *et al.* (2007) on shrinkage cracks in strain hardening materials has also shown significantly higher number of cracks at different days than the two premix reference mortars. In less than 70 days of testing, a maximum of 49 cracks were seen in strain hardening materials while in a mortar mix 6 cracks were found at the same time. In the mortar mix the average crack width was 1.4 mm while in strain hardening materials it was less than 0.2 mm.

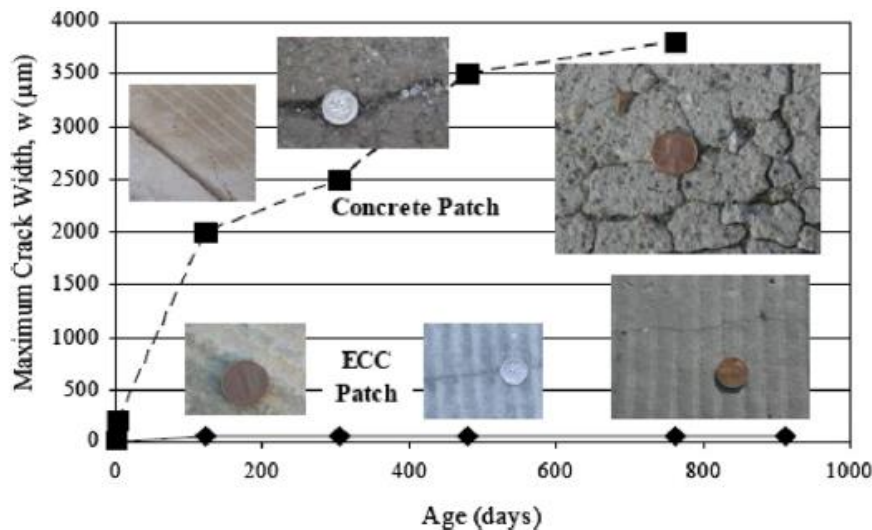


Figure 2.5: Crack width stage on CC and SHFRCC over time in Michigan bridge deck (MODT report, 2001).

2.2.5. Flexural cracks in SHCC

Multiple cracks were found in SHCC tested in flexure by several researchers (Ahmed, 2012; Sahmaran *et al.* 2008). In un-reinforced SHCC beam specimens at maximum resistance level, the average crack widths remain below 100 μm and at 30% of maximum resistance level it was found to be 50 μm in the un-loaded state of the specimen (Paul & van Zijl, 2013). Not enough information is available to date on the number of cracks and crack widths at different deflection levels of SHCC under flexural load. Most research results on SHCC flexural beam test mention that multiple cracks are formed during flexural test. They however do not quantify or analyse the above aspects in their test (Bruedern *et al.* 2009; Yun & Rokugo, 2011).

Existing Results on SHCC (A Literature Survey)

In a recent study by Kobayashi & Rokugo (2013) high-performance fibre-reinforced cementitious composite (HPFRCC) was used in a patch repair in corroded reinforced concrete specimens with size of 100 mm x 100 mm x 1600 mm. A maximum of 28 cracks were found in the high performance fibre reinforced cementitious composite (HPFRCC) specimens and crack widths varied from 0.02 mm to 0.9 mm in flexural testing up to 40% of ultimate deflection level. At the same level of deflection in monolithic specimens (without HPFRCC patch) only 3 cracks were found and crack widths varied from 0.2 mm to > 1mm. The same specimens were loaded up to 15 mm deflection level and maximum crack widths were also measured. In this case, in monolithic specimens the maximum crack widths were more than 1.5 mm wide, while in HPFRCC specimens they were below 1 mm and localised. Related study was also performed by Ahmed (2012) on DFRCC where the author used different lengths (8 and 12 mm) of PVA fibre as well steel fibre. DFRCC was used as a repair material in 125 mm x 150 mm x 600 mm size of RC beams. However, crack properties were not discussed broadly.

2.2.6. SHCC performance under combined loads

The superiority of SHCC behaviours under different types of mechanical loads has already been indicated by many researchers and also discussed in previous sections. However, during the total life time of a structure it is subjected to many types of loads in different forms. Therefore a single load on a structure does not really show the actual behaviour of structural concrete under different loads (Wittmann, 2011). To come to a definite decision to use SHCC structurally, its behaviour under combined loads must also be understood and evaluated. To some extent, this was done by some researchers (Nemecek *et al.* 2007; Sahmaran & Li, 2007; Filho *et al.* 2011). Significant E-mod reduction was observed in the fibres of SHCC materials after an accelerated chemical (KNO_3 , NH_4NO_3) leaching test. The transition zone around the fibres was damaged significantly due to this accelerated leaching test and as a result lower E-mod was found in the matrix than for the unexposed matrix. SHCC contains more fine particles, un-hydrated cementitious composites and short micro fibres which result in the formation of fine cracks. These fine cracks of SHCC have a self-healing capacity due to fact that during the immersion period (in NaCl solution) of SHCC specimens, calcium hydroxide (CH) and NaCl ions enter through the cracks and start the hydration process. In damp weather, fine cracks of SHCC are closed by the hydration process. As a result there is no loss of strength and strain monitored in SHCC even after 50 freezing and thawing cycles. A similar trend was observed in the case of mass loss per unit surface area by Filho *et al.* (2011). After 28 cycles of freezing and thawing, the mass loss per unit surface area in the reference mortar specimen was 395% higher than in the SHCC specimen. Also heat in concrete can significantly change the properties. At extreme temperature fibre will melt and it will lead to concrete spalling. Not much research has been done on this topic to date, but research so far has found that an extreme situation can occur in SHCC with PVA fibre if the temperature reaches 263°C (Yoshitake *et al.* 2006).

Existing Results on SHCC (A Literature Survey)

2.2.7. Fracture toughness of SHCC

Fracture toughness of concrete describes its resistance to fracture when a crack is present. Fracture energy is a measure of the energy dissipated per square meter of cracked face. Fracture toughness of concrete is influenced by the specimen size, binder and aggregate content, etc. SHCC fracture toughness was observed by several researchers like Li *et al.* (1995), Lin *et al.* (1999), Wang & Li (2007) and Mihashi *et al.* (2011). Matrix fracture toughness was found to increase as s/c ratio also increased (Li *et al.* 1995). Fracture energy is also influenced by the fly-ash/cement ratio (f/c) as well as by the fibre content. Wang & Li (2007) revealed that increased f/c from 0.1 to 0.2 had no influence on the matrix toughness while an increase in f/c from 0.8 to 1.5 caused a linear reduction in the matrix toughness. A change of PVA fibre content from 1.5% to 2 % in the composite matrix was found to have more than 2 times higher fracture energy (Lin *et al.* 1999). Considerably higher fracture energy in cementitious composite than in the reference mortar was also observed by Mihashi *et al.* (2011). A study by van Zijl (2010b) observed strain rate-independent fracture energy in SHCC. Fracture energy was determined by inverse analysis of SHCC tensile tests and it was found that the energy increased as the strain rate increased.

2.3. Durability performance in SHCC and mortar

The main focus of this section is to highlight some of the existing results of corrosion damage as well as chloride and water penetration in cracked and un-cracked SHCC or related materials. Details are discussed in the following sub-sections.

2.3.1. Rate of corrosion in SHCC and mortar

The corrosion rate in SHCC-related materials was examined by several researchers (Sahmaran *et al.* 2007, 2008; Kobayashi *et al.* 2010; Mihashi *et al.* 2011) over the last few years and almost everyone reported better performance of SHCC materials compared to materials used in mortar and conventional concrete. However none of the researchers used the same methodology for corrosion measurement and the link to the specific process is not yet clear. Some of the previous experimental findings on corrosion rate in SHCC and mortar concrete are discussed in this section.

Mihashi *et al.* (2011) applied about 3 Volt to a steel bar and the corrosion current was recorded for up to 52 weeks in un-cracked beam specimens containing a single steel bar. Using Faraday's law (Gene & Aaron, 1954) mass loss was calculated in SHCC specimens as well as in mortar specimens. After one year of alternative wetting (only specimens' bottom surface in 3% NaCl solution for 3.5 days) and drying (3.5 days), only 10 gm of mass loss was found in the HPFRCC specimen while in the mortar specimen mass loss was more than 50 gm as shown in Fig 2.6a. Also 100% steel area was affected by corrosion in mortar specimen with corrosion depth of about 3.1 mm of total 13mm diameter of polish rebar. In SHCC, only 65% of the steel area was affected by corrosion and the depth of corrosion was only 1.2 mm.

Existing Results on SHCC (A Literature Survey)

The authors concluded that the better crack-bridging and self-healing capacity of HPFRCC may be the reason for the lower mass loss in the steel than in the steel of the mortar specimen.

Similarly, Sahmaran *et al.* (2008) applied about 30 Volt to the steel bar and cracks due to the corrosion of the steel bar were monitored in both un-cracked SHCC and in mortar specimens. Both specimens were partially exposed to 5% NaCl solution. After 300 hrs of testing, the corrosion current in the SHCC specimen was below 1 ampere (A) while it was more than 1.5A after 75 hrs of testing in the mortar specimen (see Fig 2.6b). It was also observed that one large crack formed (about 2 mm wide) in the mortar specimen while multiple fine cracks (about 0.01 mm wide) were found in SHCC specimens after the same accelerated corrosion testing. Almost 12% mass loss of steel was observed in the mortar specimen at 75 hours accelerated corrosion testing while none or insignificant mass loss was noticed in the SHCC specimen. After 300 hours of accelerated testing, only 18% of mass loss was observed in the steel bar in the SHCC specimen. They concluded that if 0.3 mm crack width is considered as a serviceability limit state of a structure then the service life of reinforced SHCC will be 15 times higher than the reinforced mortar concrete structures. Note that in Fig 2.6b reported engineering cementitious composite (ECC) is a type of SHCC.

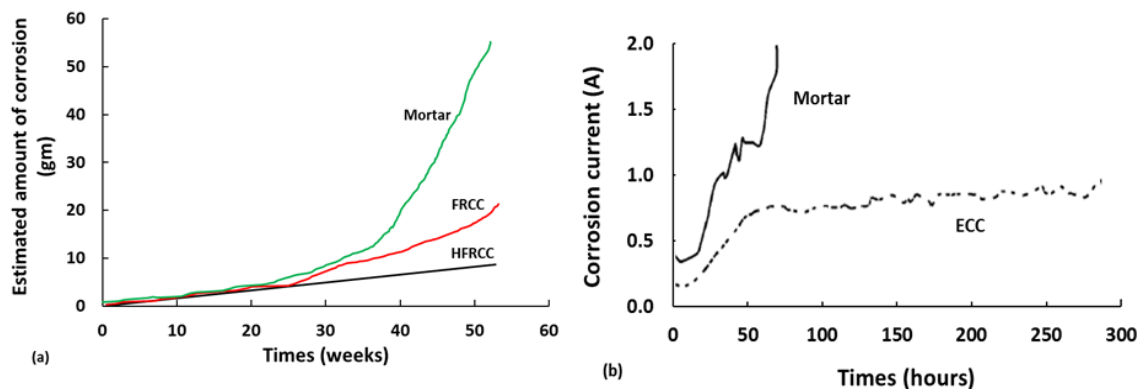


Figure 2.6: Observed corrosion in (a) HFRCC and (b) SHCC in comparison with mortar (reproduced from Mihashi *et al.* 2011; Sahmaran *et al.* 2007).

Kobayashi *et al.* (2010) used HPFRCC (containing three different fibres percentage) as a surface coating as well as a patching material (see Fig 2.7) on the reinforced NC specimen while the corrosion protection performance was observed. Cracks were formed in the specimens by tensile testing and then 3% NaCl solution was sprayed over the specimens for 5 minutes every 6 hours for 60 days of accelerated corrosion testing. The corroded area was expressed as percentage of the total bar surface area. A minimum of 2% to a maximum of 10% corrosion area was observed in all steel bars in surface coated specimens. However, in the patched specimens, no signs of corrosion areas were noted in the steel bars. There was no significant difference in the performance of SHCC with three different fibre contents.

Existing Results on SHCC (A Literature Survey)

Miyazato & Hiraishi (2013) also investigated the corrosion rate in flexurally-cracked SHCC and mortar specimens with w/c of 0.3. Specimens were exposed to 3% NaCl solution (penetration was allowed only through the cracked face of the specimen, the other faces were sealed with epoxy resin) for 2 days and dried for 5 days and this cycle was followed for 28 days and after that the corrosion rate was calculated for the specimen. Using the polarization corrosion measurement technique, for w/c of 0.3, 0.082 mm/year and 0.004 mm/year corrosion rates found respectively were in SHCC and mortar specimens. The reason for the lower corrosion rate of SHCC was explained by the shallower crack depth and smaller crack width of SHCC specimens than of mortar specimen which caused a minimum amount of chloride penetration into the specimens.

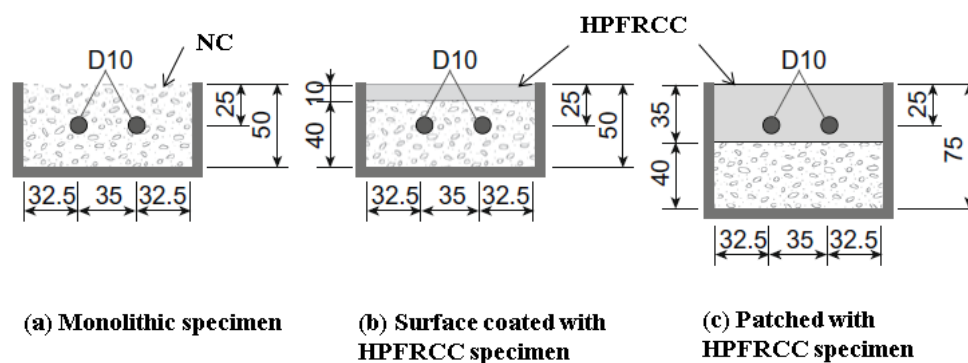


Figure 2.7: Applied HPCRCC in the reinforced NC specimens (reproduced from Kobayashi *et al.* 2010).

All of the aforementioned results were obtained from the accelerated corrosion tests to be able to compare the corrosion rate in SHCC with that in mortar. The question remains what the actual steel corrosion rate in real structures is under certain exposure conditions and this is one of the important issues researchers have been trying to solve over the last few decades (Otieno *et al.* 2011). However, it is not an easy task to determine the actual corrosion rate in steel and long term experiments and field data are required. Also in these present experiments, researchers did not certain some important aspects such as the corrosion rate with respect to the number of the cracks and crack widths and spacing in the specimens nor the number of cracks and crack widths due to different corrosion rates in the steel bar. Therefore, in this dissertation it is the aim to determine the above information which is believed to be the most important parameters for corrosion modelling of SHCC structures. More details will be discussed in the subsequent chapters.

2.3.2. Chloride penetration in SHCC and mortar specimen

The presence of chloride in concrete accelerates the corrosion process of steel bars. Chloride penetration in concrete is influenced by many factors such as cracks, types of exposures, etc. and some of them are discussed in this section.

Existing Results on SHCC (A Literature Survey)

2.3.2.1. Chloride penetration in cracked specimens

The presence of cracks in concrete allow chloride to penetrate and when the amount of chloride reaches beyond the threshold level it breaks the corrosion protective layer of the steel bar and corrosion starts (Tutti, 1982). However, chloride penetration in SHCC specimens is much lower than in mortar specimens (Miyazato & Hiraishi, 2013; Kobayashi *et al.* 2010; Sahmaran *et al.* 2007) because of the formation of multiple fine cracks in SHCC as opposed to fewer and wider cracks. Lower effective chloride diffusion was observed in SHCC specimens than in mortar specimens when loaded at different deflection levels during flexural testing as shown in Fig 2.8. In SHCC specimens at 2 mm deflection level the average crack width was found to be 0.05 mm and chloride diffusion was 50×10^{-10} (m^2/s). In the case of mortar specimens, 0.4 mm crack width was found at less than 1 mm deflection level and chloride diffusion was also more than 2×10^{-10} m^2/s .

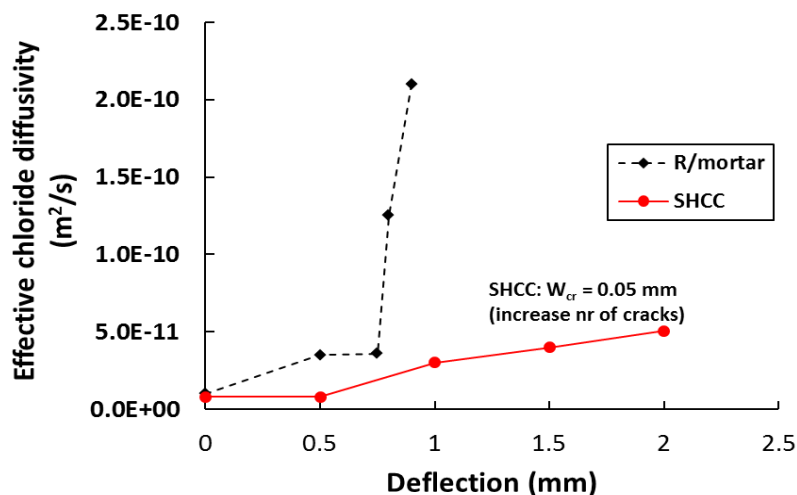


Figure 2.8: Effective chloride diffusion in cracked SHCC and mortar as function of deflection (reproduced from Sahmaran *et al.* 2007; van Zijl, 2010a).

Miyazato & Hiraishi (2013) performed accelerated chloride penetration testing in both cracked and un-cracked SHCC and mortar (same as SHCC mix without fibre) specimens with two different w/c ratios of 0.3 and 0.6. In un-cracked SHCC a higher penetration was found compared to mortar specimens because of higher air content and a lower fine aggregate content. However, in cracked SHCC a much lower chloride penetration was found due to the presence of finer cracks than the larger cracks in the mortar specimens. Also, a lower w/c ratio showed shallower penetration of chloride in both SHCC and mortar specimens. The authors concluded that the chloride penetration in SHCC and mortar specimens depends on the air content, the amount of fines, the w/c ratio and the flexural crack properties such as depth, width, etc. No comparisons were found in the influence of chloride penetration for difference exposures condition of specimens such as submerged versus partially submerged, capillary suction versus ponding, etc.

2.3.2.2. Chloride penetration in different exposures conditions of specimen

After 30 days of ponding test of 3% NaCl solution over cracked mortar (without fly-ash) and SHCC (with fly-ash) specimens (76.2 mm depth specimen), Sahmaran *et al.* (2007) observed about 40 to 70 mm penetration of chloride in mortar specimens. In the case of SHCC the penetration depth was 0 to 40 mm. The authors concluded that the deeper and wider cracks in mortar specimens allow chloride to more easily penetrate them. The crack bridging capacity of SHCC prevents specimens from forming deeper and wider cracks which ultimately lead to lower chloride penetration. Also, the self-healing capacity of micro cracks in SHCC prevents from chloride penetration as the crack closes due to self-healing (Qian *et al.* 2009; RILEM TC 221-SHC 2013).

2.3.2.3. Influence of compressive load on chloride penetration in SHCC specimen

Wittmann *et al.* (2009) studied the influence of different compressive force levels on the neat SHCC specimens. 90 mm x 65 mm x 30 mm size of blocks were obtained by cutting from the 90 mm widths 30 mm thick and 300 mm length of dumbbell specimen. The surface of block (90 mm x 60 mm) was kept contact with 5% NaCl solution for 10.75 hours and after that the powder samples were collected by grinding the surface. In this case the grinding layer was 1 mm and powder samples were collected up to 15 mm. Chloride content was determined by the aid of ion sensitive electrode. At 9 mm depth of specimen, the chloride penetration (% wt of cement) in the unloaded specimen was about 0.13%. However, when the specimen was loaded up to 50% and 100% of maximum resistance, the penetration was about 0.25% and 0.38% respectively. Not much research on SHCC was found in this regard.

2.3.3. Water penetration in SHCC

2.3.3.1. Permeability of water

Water permeability was observed as a function of different crack widths and strain levels in SHCC and mortar specimens by several researchers (Wang *et al.* 1997; Lepech & Li, 2009; Wittmann *et al.* 2009; Zhang *et al.* 2010). As shown in Fig 2.9, for different crack widths, the water permeability was observed in SHCC, R/mortar and NC by Lepech & Li (2009), Wang *et al.* (1997). For crack width ranges of 0 to <0.1 mm, almost similar water penetration was observed in SHCC and NC specimens. However, water penetration in wider crack widths of SHCC specimens was not observed and as a result no comparison was possible with NC and mortar specimens from their experiments.

2.3.3.2. Capillary suction of water

Capillary water penetration in SHCC specimens was found to increase as the strain was increased in the specimens during tensile testing (see Fig 2.10). Increased strain from 0% to 0.5% caused an almost 72% higher water absorption in the SHCC specimens, 42% higher for

Existing Results on SHCC (A Literature Survey)

strains from 0.5% to 1% and 7% higher for strains from 1% to 2% (Wittmann *et al.* 2009). Therefore as the strain level increased, water penetration did not increase linearly.

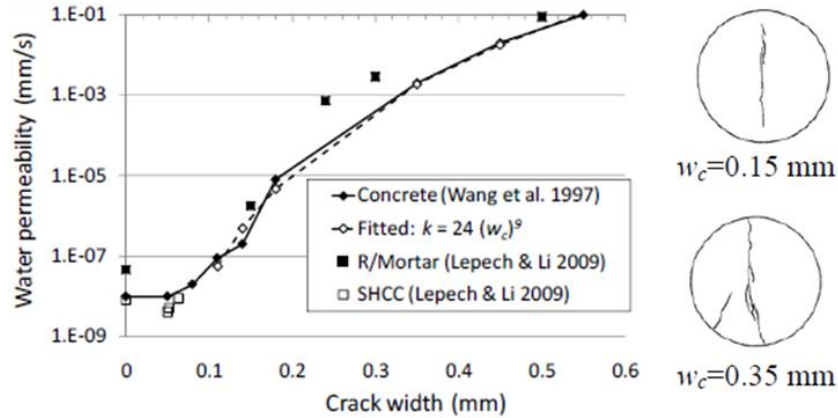


Figure 2.9: Observed water permeability in SHCC, mortar and cracked concrete (reproduced from Lepech & Li, 2005; Wang *et al.* 1997; van Zijl, 2010a).

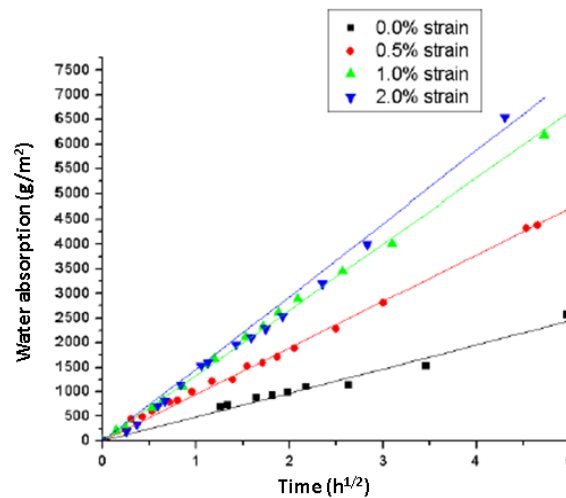


Figure 2.10: Capillary water observed in neat SHCC as a function of time (reproduced from Wittmann *et al.* 2009).

Capillary water suction in cracked un-reinforced SHCC was also observed by means of neutron radiography analysis where two-dimensional penetration depths were recorded in the specimens for different short periods of time (0 to 120 minutes) as shown in Fig 2.11 by Zhang *et al.* (2010). Note that water content in the sample is shown on the vertical axis and the specimen width is on the horizontal axis. It was found that within 1 minute, water penetrates to about 80 mm of the total 90 mm crack depth and after 15 minutes, water penetrates to the whole depth of cracks and with more time, penetration becomes wider, i.e. spreads at right angles to the crack direction. Water content in the samples an increased gradually with time. Interestingly it was also observed from the specimen after a longer

Existing Results on SHCC (A Literature Survey)

period of testing (here it was 120 minutes) that water content was found to be higher at the upper crack surface than at the lower crack surface which was kept in contact with water.

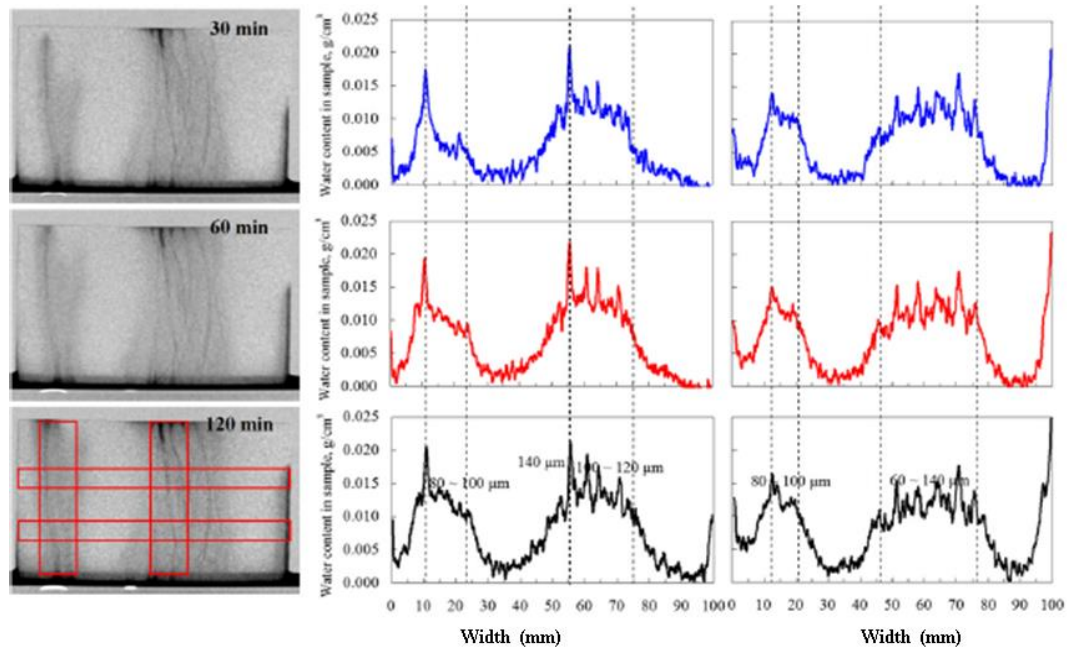


Figure 2.11: Neutron radiography images for capillary water suction observed in unreinforced SHCC as function of time (reproduced from Zhang *et al.* 2010).

2.4. Other important characteristics of SHCC

Apart from forming multiple finer cracks, higher tensile and flexural resistance and lower water and chloride penetration, SHCC also has other characteristics such as self-healing and forming micro-cell corrosion in the specimen.

2.4.1. Self-healing in SHCC

Self-healing of SHCC depends on the availability of unhydrated binders such as fly-ash, slag etc. (Qian *et al.* 2009). Although in this research work there was no experiment performed on the self-healing of SHCC, it was in fact noticed in the specimens under accelerated exposure conditions. After almost 2 years of accelerated exposure, a significant reduction in the number of cracks was noticed in the R/SHCC specimens tested in this research as shown in Fig 2.12. The specimens' details will be discussed in Chapters 5 to 7. Many researchers had also reported on this issue in their research papers but only a few of them really worked on it (Sahmaran *et al.* 2007; Mihashi *et al.* 2011). The self-healing in concrete is attributed to the formation of calcium carbonate or calcium hydroxide due to the reaction of calcium ion in the concrete with rainwater and carbon dioxide in the air (Edvardsen, 1999). In high volume of binder concrete, unhydrated binder particles also play a role in self-healing. Self-healing in finer cracks of cementitious materials is illustrated in Fig 2.13. This phenomenon can also be

Existing Results on SHCC (A Literature Survey)

observed in old concrete structures where smaller crack widths (< 0.3 mm) have sealed themselves with white crystalline material. In water retaining structures, over time a significant reduction in the water permeability was noticed due to the self-healing (Wang *et al.* 1997).

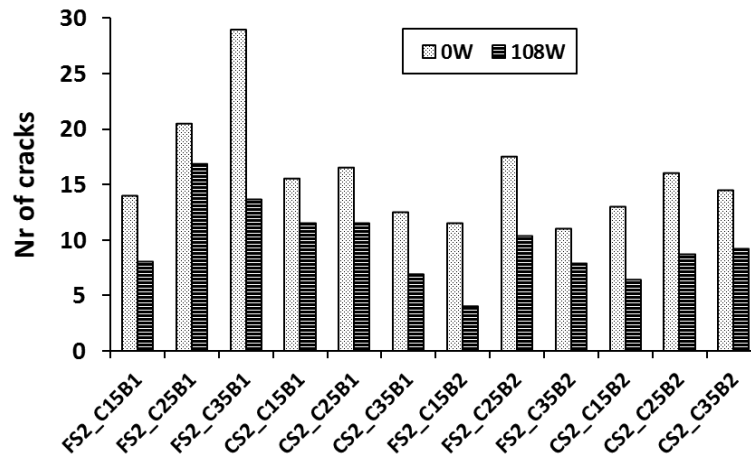


Figure 2.12: Difference in the number of cracks at 0 weeks (W) (before the starting of accelerated exposure) to 108 weeks in cracked R/SHCC specimens.

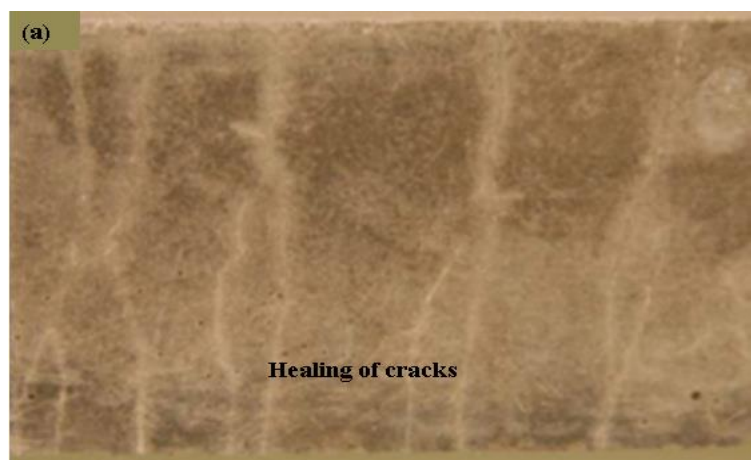


Figure 2.13: Forming white crystalline as part of self-healing of fine cracks in cementitious materials (reproduced from Qian *et al.* 2009).

Modern admixtures are also used to heal the cracks. A study by Jonker & Schlangen (2009) focused on bacterial crack healing, in which the bacteria themselves act largely as a reagent and convert an originator compound into an appropriate filler material. However, the lifetime of this bacterial micro-organism was very short (a few months only). As a result, a two-component biochemical healing agent, composed of bacterial micro-organisms and an appropriate organic bio-cement originator compound, was used. The authors concluded that

Existing Results on SHCC (A Literature Survey)

the bacterial concrete is much more effective because of the animated metabolic adaptation of calcium lactate in the presence of bacteria.

Qian *et al.* (2009) studied the self-healing behaviour of SHCC that contained local waste materials. Compared to un-cracked virgin specimens nearly 65-105% was recovered by self-healing in the specimens under submersed water curing, while in air cured specimens less recovery (40-60%) was observed. Finer cracks of SHCC are the key of being self-healed with time and improve the mechanical and durability properties.

2.4.2. Micro-cell corrosion in SHCC

Another important consequence of the multiple cracking characteristic of SHCC is the formation of micro-cell corrosion in the steel bar subjected to corrosive exposure. Corrosion in a steel bar inside concrete continues by the formation of anodes and cathodes. As it is discussed in the Chapter 4, corrosion damage in steel bars is often defined by local and general corrosion. Although it is difficult to predict whether pitting or uniform corrosion will occur in a steel bar inside concrete, typically corrosion is dominantly local, and damage can be seen even on a few centimetres of a couple of meters long clean bar (Broomfield, 2007). In chloride-laden exposure, corrosion damage is well separated by the cathode and anode part of steel. This phenomenon is called macro-cell corrosion. On the other hand, carbonation attack in concrete is dryer (only in a dry environment can carbon dioxide (CO₂) enter concrete) and as a result, corrosion continues along the whole length of steel and is called microcell corrosion. When the anode area is smaller than the cathode area, there is a big possibility of the formation pitting in the steel bar which is not good for the steel bar since its capacity is reduced significantly. Miyazato & Hiraishi (2005) reported that micro cell corrosion could be observed in finely-cracked R/SHCC specimens, as opposed to significant macro-cell corrosion in R/mortar specimens.

2.5. Current applications of SHCC

As already mentioned, the applications of SHCC are limited. From published literature it was found that SHCC is mostly used in Japan on some existing structures. After experiencing the 1995 Kobe earthquake, many existing structures were strengthened using these strain hardening materials and some of the pictures are shown in Appendix A, Figs A.1 to A.3. This research is not intended to discuss details of SHCC applications, however, if readers are interested they can find them in the references given in this section. As far as the author is concerned, most SHCC applications are in Japan and only limited applications are reported to be in the USA and Germany. Some of the SHCC applications are listed below (source: ECC Technology Network 2009; Kunieda & Rokugo, 2006; Lepech & Li, 2005; RILEM State-of-the-Art Report, 2013):

- SHCC dampers for improving structural safety by reducing response drift in the RC shear wall

Existing Results on SHCC (A Literature Survey)

- SHCC wall with large opening
- SHCC lining to improve the tensile performance of tunnel
- SHCC overlay patch repair and link slab retrofitting in the bridge deck
- Steel protection against carbonation
- R/SHCC in coupling beams in tall structure building

2.6. Concluding remarks

This chapter has mapped out the existing results of both mechanical and durability testing on SHCC. The influence of different loading rate, binder content, age, curing, exposure types, crack widths, level of deformation on the mechanical and durability properties of SHCC has been addressed here and all these factors need to be considered before the limits for designing this material. Current knowledge of SHCC indicates that the mechanical behaviour of this material is suitable for improving structural performance due to the fact that it has higher tensile and flexural strength, ductility and most importantly, finer average crack widths at ultimate tensile and flexural resistance (Li *et al.* 1995; Li *et al.* 2001). However, lack of information on the long term behaviour of SHCC is still a major obstacle in designing the durability performance of a RC structure with SHCC. A general framework in dealing with the problems of such material in terms of durability is necessary (Mechtcherine, 2012). At present there is limited information available on the corrosion damage of steel bar in SHCC at cracked stage as well as at the amount of total and free chloride at the surface level of the steel bar. Also, there is no specific method for corrosion testing in SHCC and most of the corrosion measuring methods reported in the literature were not compared to the real damage in the steel bar due to corrosion. Therefore, the literature gave rise to the need to investigate the aforementioned limitations which are the aims and hypothesis of this research. From this point of view, this research can provide a general overview of SHCC durability performance which can be used as a basis for a future durability framework for the application of SHCC in RC structures.

2.7. References

Ahmed, SFU, Mihashi, H & Suzuki, S 2007, 'Experimental study on restrained shrinkage-induced cracking of mortars with different toughness', proceeding of fifth international conference on concrete under severe conditions (CONSEC07), Environment and loading, Tours, France.

Ahmed, SFU 2012, 'Flexural performance of repaired reinforced concrete beam containing DFRCC materials', proceeding of Concrete Repair, Rehabilitation and Retrofitting III – Alexander et al. (eds), Taylor & Francis Group, London, ISBN 978-0-415-89952-9.

Benjamin, AG 2006, Material property characterization of ultra-high performance concrete. US Department of transport, Publication No.FHWA-HRT-06-103.

Boshoff, WP & van Zijl, GPAG 2007, 'Time-dependent response of ECC: Characterisation of creep and rate dependence', Cement and Concrete Research, vol. 37, pp. 725–734.

Existing Results on SHCC (A Literature Survey)

- Broomfield, JP 2007, Corrosion of steel in concrete understanding, investigating and repair, 2nd edition, Taylor & Francis, USA & Canada.
- Bruedern, AE, Abecasis, D & Mechtcherine, V 2009, ‘Development of Strain-Hardening Cement-based Composites for the strengthening of masonry’, proceeding of Concrete Repair, Rehabilitation and Retrofitting II – Alexander et al (eds), Taylor & Francis Group, London, ISBN 978-0-415-46850-3.
- ECC Technology Network 2009, Ann Arbor, Michigan, USA.
- Edvardsen, C 1999, ‘Water permeability and autogenous healing of cracks in concrete’, ACI Materials Journal, vol. 96, no. 4, pp. 448–455.
- Filho, RDT, Fairbairn, EMR & Slowik, V 2011, ‘Durability under thermal loads’, van Zijl & Wittmann (eds.), Durability of strain-hardening fibre-reinforced cement-based composite, pp. 59-71.
- Filho, RDT & Magalhaes, MS 2009, ‘RILEM TC 208 HFC’, Durability of strain-hardening fibre-reinforced cement-based composite (SHCC).
- Gene, RE & Aaron, I 1954, ‘Faraday's Electrochemical Laws and the Determination of Equivalent Weights’, Journal of Chemical Education, vol. 31, pp. 226–232.
- Jonkers, HM & Schlangen, E 2009, ‘Bacteria-based self-healing concrete’, International journal of restoration of buildings and monuments, vol. 15, no. 4, pp. 255-265.
- Jun, P & Mechtcherine, V 2010, ‘Behaviour of Strain-hardening Cement-based Composites (SHCC) under monotonic and cyclic tensile loading Part 1 – Experimental investigations’, Cement & Concrete Composites, vol. 32, pp. 801–809.
- Kanda, T & Li, VC 2006, ‘Practical design criteria for saturated pseudo strain hardening behaviour in ECC’, Journal of Advanced Concrete Technology, vol. 4, no.1, pp. 59-72.
- Kobayashi, K, Iizuka, T, Kurachi, H & Rokugo, K 2010, ‘Corrosion protection performance of high performance fibre reinforced cement composites as a repair material’, Cement & Concrete Composite, vol. 32, pp. 411-420.
- Kobayashi, K & Rokugo, K 2013, ‘Mechanical performance of corroded RC member repaired by HPFRCC patching’, Construction and Building Materials, vol. 39, pp. 139-147.
- Kunieda, M & Rokugo, K 2006, ‘Recent progress on HPFRCC in Japan’, Journal of Advantage Concrete Technology, vol. 4, no. 1, pp. 19-33.
- Lepech, M & Li, VC 2005, ‘Design and field demonstration of ECC link slabs for joint less bridge decks’, proceeding of ConMat’05, Vancouver, Canada.
- Lepech M & Li VC 2009, ‘Water permeability of engineered cementitious composites’, Cement and Concrete Composites, vol. 31, pp. 744-753.
- Li, VC, Horikoshi, T, Ogawa, A, Torigoe, S & Saito, T 2004, ‘Micromechanics-based durability study of Polyvinyl Alcohol-Engineered Cementitious Composite’, ACI Materials Journal, vol. 101, no. 3, pp. 242-248.
- Li, VC, Mishra, DK & Wu, H 1995, ‘Matrix design for pseudo-strain-hardening reinforced cementitious composites’, Materials and structures, vol. 28, p: 586-595.

Existing Results on SHCC (A Literature Survey)

- Li, VC, Wang, S & Wu, C 2001, 'Tensile strain-hardening behaviour of polyvinyl alcohol engineered cementitious composite (PVA-ECC)', *ACI Materials Journal*, vol. 98, No. 6, pp. 483-492.
- Lin, Z, Kanda, T & Li, VC 1999, 'On interface property characterization and performance of fibre-reinforced cementitious composites', *Concrete Science and Engineering*, vol. 1, pp. 173-174.
- Mechtcherine, V & Schulze, J 2005, 'Ultra-ductile concrete-Material design and testing', proceeding for Ultra-ductile Concrete with Short Fibres – Development, Testing, Applications, Mechtcherine (Ed.), ibidem-Verlag, Stuttgart, Germany, pp. 11-36 [in German].
- Mechtcherine, V, Silva, FA, Butler, M, Zhu, D, Mobasher, B, Gao, SL & Mader, E 2011, 'Behaviour of strain hardening cement-based composite under high strain rates', *Journal of Advanced Concrete Technology*, vol. 9, no.1, pp. 51-62.
- Mechtcherine, V 2012, 'Towards a durability framework for structural elements and structures made of strengthened with high-performance fibre-reinforced composites', *Construction and Building Materials*, vol. 31, pp. 94-104.
- Mihashi, H, Ahmed, SFU & Kobayakawa, A 2011, 'Corrosion of reinforcing steel in fibre reinforced cementitious composites', *Journal of Advantage Concrete Technology*, vol. 9, no. 2, pp. 159-167.
- Miyazato, S & Hiraishi, Y 2005, 'Transport properties and steel corrosion in ductile fibre reinforced composites', proceeding of high performance fibre reinforced cement composites as a repair material, ICF, Vol. 11, Torino.
- Miyazato, S & Hiraishi, Y 2013, 'Durability against steel corrosion of HPFRCC with bending cracks', *Journal of Advantage Concrete Technology*, vol. 11, pp. 135-143.
- Nemecek, J, Kabele, P, Kopecky, L & Bittnar, Z 2007, 'Effect of chemical exposure on fibre reinforced cementitious matrix', in proceeding of third international conference on structural engineering, mechanics and computation (SEMC), Cape Town, South Africa.
- Otieno, M, Beushausen, H & Alexander, M 2011, 'Prediction of corrosion rate in RC structures- A critical review', Andrade & Mancini (eds.), *Modelling of Corroding Concrete Structures*, RILEM Bookseries 5, DOI 10.1007/978-94-007-0677-4_2, © RILEM 2011.
- Paul, SC & van Zijl, GPAG 2013, 'Mechanically induced cracking behaviour in fine and coarse sand strain hardening cement based composites (SHCC) at different load levels', *Journal of Advanced Concrete Technology*, vol. 11 pp. 301-311.
- Qian, S, Zhou, J, de Rooij, MR, Schlangen, E, Ye, G & van Breugel, K 2009, 'Self-healing behavior of strain hardening cementitious composites incorporating local waste materials', *Cement & Concrete Composites*, vol. 31, pp. 613–621.
- Richard, P & Cheyrezy, MH 1994, 'Reactive Powder Concretes with High Ductility and 200 800 MPa Compressive Strength. Concrete Technology: Past, Present, and Future', in proceedings of the V. Mohan Malhotra Symposium, ACI SP-144, S. Francisco, pp. 507 518. Editor: P.K. Mehta.

Existing Results on SHCC (A Literature Survey)

RILEM TC 221-SHC 2013, Self-healing phenomena in cement-based materials, Schlangen et al. (eds), Springer, ISBN 978-94-007-6623-5.

RILEM State-of-the-Art Report 2013, Strain hardening cement composite: structural design and performance, Toshiyuki *et al.* (eds), vol.6, pp. 90.

Sahmaran, M, Li, VC & Andrade, C 2008, 'Corrosion resistance performance of steel reinforced engineered cementitious composite beams', *ACI Materials Journal*, vol. 105, no. 3, pp. 604–611.

Sahmaran, M, Li, M & Li, VC 2007, 'Transport properties of engineered cementitious composite under chloride exposure', *ACI Materials Journal*, vol. 104, no. 6, pp. 243–50.

Saravanan, J, Suguna, K & Raghunath, PN 2010, 'Confined high strength concrete columns: An experimental study', *American J. of Engineering and Applied Sciences*, vol. 3, no. 1, pp. 133-137.

Shaikh, FUA 2013, 'Deflection hardening behaviour of short fibre reinforced fly-ash based geopolymer composites', *Materials and Design*, vol. 50, pp. 674-682.

Stander, H, 2004, The role of admixtures in cementitious composite materials, Final year BSc project report. University of Stellenbosch, South Africa.

Tanaka, R, Takada, H, Asano, Y, Kobayashi, K & Rokugo, K 2013, 'Uniaxial tension test method using SHCC prism moulded into dumbbell shape', in proceeding for FraMCoS-8, Toledo, Spain.

Tutti, K 1982, 'Corrosion of steel in concrete', Swedish Cement and Concrete Research Institute, CBI Research Report 4, Sweden.

Van Dyk, WD 2004, Development of thin fibre reinforced cementitious plates and investigating influence of sand on ECC Behaviour. Final year BSc project report, University of Stellenbosch, South Africa.

Van Zijl, GPAG 2010a, 'Crack distribution characterisation, towards a framework for durability design of SHCC', proceedings of the SHCC2-Rio International RILEM Conference, Brazil.

Van Zijl, GPAG 2010b, 'Modelling the rate effects in cracking and fracture of strain hardening cement-based composite (SHCC)', proceeding for Fracture and Damage of Advanced Fibre-reinforced Cement-based Materials, 18th European Conference on Fracture, Dresden, Germany, pp. 185-193.

Van Zijl, GPAG 2011, 'Durability under mechanical load-micro-crack formation (ductility)', G van Zijl and Wittmann (eds), RILEM state of the art, Durability of strain-hardening fibre-reinforced cement-based composite (SHCC), pp.9-39.

Wang, K, Jansen, DC, Shah, SP & Karr, AF 1997, 'Permeability study of cracked concrete', *Cement and Concrete Research*, vol. 27, pp. 381–393.

Wang, S & Li, VC 2007, 'Engineered cementitious composites with high-volume fly ash', *ACI Materials Journal*, vol. 104, no. 3, pp. 233-241.

Existing Results on SHCC (A Literature Survey)

- Wittmann, FH 2011, 'Durability under combined loads', van zijl & Wittmann (eds.), Durability of strain-hardening fibre-reinforced cement-based composites (SHCC), pp. 73-79.
- Wittmann, FH, Zhao, T, Tian, L, Wang, F & Wang, L 2009, 'Aspects of durability of strain hardening cement-based composites under imposed strain', proceeding for ACM conference, van Zijl & Boshoff (eds), South Africa.
- Yang, E & Li, VC 2006, 'Rate dependence in engineered cementitious composites', proceeding for workshop on high performance fibre reinforced cementitious composites in structural applications, Fischer & Li (eds), pp. 83-92.
- Yang, Y, Lepech, MD, Yang, EH & Li, VC 2009, 'Autogenous healing of engineered cementitious composite under wet-dry cycles', Cement and Concrete Research, vol. 39, pp. 382-390.
- Yoshitake, I, Baba, K, Ito, T & Nakagawa, K 2006, 'Behaviour of fibre reinforced concrete under fire temperature, in proceeding of the international workshop on HPRFRC in structural applications, Honolulu, Hawaii, USA.
- Yun, HD & Rokugo, K 2011, 'Mechanical properties of sustainable strain hardening cement-based composites after exposure to rapid freeze-thaw cycle', Fib symposium Prague, pp. 345-348.
- Zhang, P, Wittmann, FH, Zhao, TJ, Lehmann, EH, Tian, L & Vontobel, P 2010, 'Observation and quantification of water penetration into strain hardening cement-based composite (SHCC) with multiple cracks by means of neutron radiography', Nuclear Instruments and Methods in Physics Research A, vol. 620, p. 414-420.

Chapter 3

Challenges are what makes life interesting and overcoming them is what makes life meaningful. - Joshua J. Marine

Influence of Cracks and Chlorides in Concrete Structures

3. General discussions

The durability of concrete can be described by its performance against environmental actions such as chemical attacks, freezing, hot weather, permeation, etc. The concrete is said to be durable when it will not change its form, quality and serviceability under the above actions. At present, durability of RCS is a most discussed issue all over the world since many of the RCS are expected to be repaired or rehabilitated before their design life periods are reached. A large portion of many countries' annual budgets are being used to repair those RCS which are already being seriously affected by man-made and natural exposure environments (Goodwin, 2012).

One of the major durability problems occurs due to the corrosion of steel bar inside concrete. Typically the matrix properties surrounding the steel/concrete interface influence the corrosion of steel. Corrosion of steel will not happen in the presence of chloride and carbonation unless other contributing aggressive substances enter the concrete. For instance, the carbonation process mostly affects the concrete microstructure, which is not generally harmful. Also chloride and carbonation cannot impair the integrity of concrete. However, concrete integrity may be considered to have been impaired once chloride ingress and / or carbonation occur, as the potential for corrosion then arises. Some acid and aggressive ions such as sulphate destroy concrete integrity and subsequently allow chloride, carbon dioxide and oxygen ingress, and the corrosion problem starts. Sulphate attack and acid attack break the integrity of concrete cover which ultimately helps corrosion to take place in the steel bar. So, several degradation processes in concrete may be the cause of corrosion. For instance, it is very difficult for carbon dioxide to penetrate into concrete unless concrete is significantly damaged. In this regard the cover depth and type of concrete near the steel surface is very important. If sufficient cover depth to steel can be provided or protective materials which have higher resistance against penetration of carbonation or chloride can be used on the surface of concrete, the RCS durability will be increased significantly. The consequences of cracks, chloride and corrosion in RCS are shown in Figs 3.1a&b. It can be seen that cracks arise due to the chloride-induced corrosion in the steel bar and when the stress caused by the increased volume of corrosion product becomes higher than the concrete cover stress,

Influence of Cracks and Chlorides in Concrete Structures

spalling of concrete can be seen. Spalling of concrete cover depth and corrosion stains are the common problems of RCS due to cracks, chloride and corrosion.

In general, concrete durability increases the service life of the structures. Therefore designers must pay enough attention to this during the design of concrete structures. It can be achieved in several ways, viz. by providing sufficient cover in concrete, proper curing, higher concrete strength, adding water repellent agents, using anti-corrosion steel bars, etc. Prevention through early attention can save significant cost for the repair or rehabilitation of structures through their life spans. This chapter aims to provide important aspects regarding durability of RCS and their possible solutions.

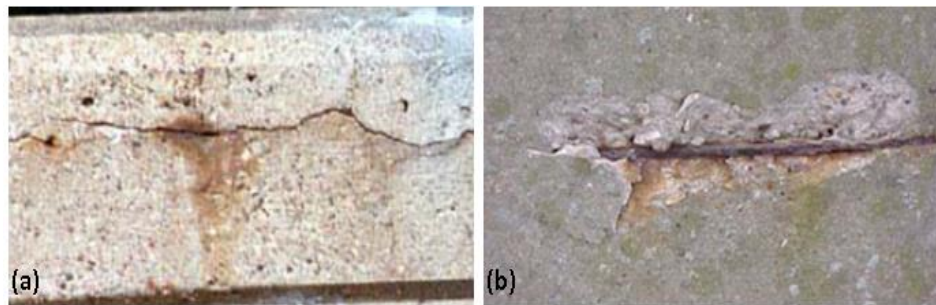


Figure 3.1: (a) Cracks and corrosion stains in RCS (b) spalling of cover concrete (reproduced from Verma, 2013).

3.1. Cracks in concrete structures

The presence of cracks in concrete structures especially in the coastal environments or exposed to de-icing salts may create major durability problems in infrastructure. In such chloride exposure conditions, corrosion of steel starts in the presence of enough oxygen and water in concrete. In RCS, it appears that if the crack width is controlled to a level below a certain threshold limit, the ingress rate of water, gas and chlorides may not be significant (Bertolini *et al.* 2004). However, it is often quite difficult to control crack widths in the structures made from NC because of concrete's inherent low tensile strength and brittleness. In this regard, SHCC displays self-controlled crack width which is a great advantage, as the crack widths in SHCC are small compared to those in NC which is usually used in RCS (Sahmaran *et al.* 2008; Kobayashi *et al.* 2010; Mihashi *et al.* 2011; Kobayashi & Rokugo, 2013; Paul & van Zijl, 2014). This particular character of SHCC makes it useful for repairing RCS structural elements, or to be used as structural elements.

3.1.1. Types of cracks in concrete structures

Due to the low strain capacity of NC, it is virtually impossible to avoid the formation of cracks in RCS. However, cracks in RCS can occur due to design faults. Precautions may limit the crack widths. Some of the reasons why cracks form are discussed in this section.

3.1.1.1. Crack due to static or dynamic loads

Cracks in concrete structures due to loads acting on them are categorised as flexural cracks, tensile cracks, shear cracks and torsional cracks. These cracks appear when the applied load on the structure causes internal strains higher than the concrete tensile strain capacity. In RCS when the strain created by the static loads such as self-weight of structural elements beams, slabs, columns, etc. and the dynamic loads such as earth quake, wind, moving loads, etc. reach beyond the capacity of concrete elastic strain, cracks are formed. By providing sufficient reinforcement and ensuring proper detailing of reinforcements the severity of cracks can be minimized.

3.1.1.2. Cracks due to shrinkage

Shrinkage of fresh concrete is a phenomenon which can be ascribed to several mechanisms such as volume change due to hydration and volume reduction due to solidification of free water. Typically shrinkage is classified as drying shrinkage, autogenous shrinkage, carbonation shrinkage and chemical shrinkage. Before fresh concrete sets and when the evaporation water loss due to evaporation is higher than the concrete's bleeding rate, plastic shrinkage cracks may arise (Combrinck & Boshoff, 2013). In hardened, young concrete, drying of the concrete due to water migration and evaporation from its surface with time causes shrinkage of the concrete. Typically shrinkage is not a problem if the structural element can shrink freely, as it means that no stress arises. However, if there is a restraint to shrinkage, it leads to tensile mechanical strain and associated tensile stress and when this reaches the tensile capacity of the concrete, drying shrinkage cracks will appear in the concrete. So far limited research has been carried out on shrinkage behaviour of SHCC (Boshoff, 2007) and more research is needed in this regard.

3.1.1.3. Cracks due to temperature

As is the case with drying shrinkage, the restraint to volume change (thermal elongation or contraction) leads to mechanical strain, and if this exceeds the tensile cracking strain of concrete, cracks will arise. To protect concrete structures from this problem extra steel reinforcement bars are provided during the design of structures. Different design standards (*fib* model code 2010; ACI 318; EN 10080) have suggested different percentages of reinforcement in designing the structures against temperature cracking.

3.2. Findings on crack widths and frequency in concrete structures

The degradation process in un-cracked concrete is not that significant in the presence of static water i.e. the structure remains submerged and does not experience cyclic wetting and drying (Mitchell, 1991). However, cracked concrete in contact with static water may not have the same behaviour. The same crack may be accelerating the degradation rate if water is frequently penetrating the crack, such as in dried out and rewetted concrete exposed to the atmosphere (Hausmann, 1967). The degradation process differs in cracks of different widths

Influence of Cracks and Chlorides in Concrete Structures

in concrete. From the literature it appears that a threshold crack width exists for concrete, below which degradation processes are slow. Once the threshold crack width is exceeded, orders of magnitude of acceleration of the degradation process occur (Lepech & Li, 2009; Wang *et al.* 1997). So, the limitation of crack width in a concrete structure is considered to be very important. According to a report by VicRoads (2010), crack widths in concrete of 0.3 mm or less do not pose a threat under normal exposure conditions. However, in a corrosive environment and alternative drying and wetting exposures, a safer crack width range is 0.1-0.2 mm. Therefore it appears that there is no unique threshold crack width in concrete and depending on the type and exposure conditions of concrete structures, different standards have suggested different crack width limits as shown in Tables 3.1 & 3.2. If good quality of concrete and proper cover depth can be ensured, the threshold crack width limit can also be higher under the governing loading condition.

Table 3.1: ACI committee 224 acceptable crack widths for RC under service loads

Exposure type	Acceptable crack width (mm)
Dry air or protective membrane	0.41
Humidity, moist air, soil	0.30
De-icing chemicals	0.18
Seawater and seawater spray, wetting and drying	0.15
Water-retaining structures	0.10

Table 3.2: Threshold crack width for different exposure conditions in different countries

Codes/ authors	Allowable crack width (mm)
BS 8110 (1997) & EN (1991-1-1)	0.30
ACI (1994)	0.15
Dutch code NEN 6720	0.20
CEB Bulletin 182 (1987)	0.40

Limited research was carried out on the influence of crack frequency reinforced concrete (RC) specimens. Arya & Ofori-Darko (1996) tested 1.36 m long RC beams with different number of cracks such as 0, 1, 4, 8, 12, 16 & 20 and observed the corrosion rate of the steel bars under chloride exposure of such specimens. Note that in the above experiments, although the numbers of cracks were different but the total crack width was kept constant at 2.4 mm. When the crack frequency was higher, increased cumulative mass loss of steel bars was noticed. However, in the same study, lower mass loss of steel was found in the specimens with 20 cracks than in the specimens with 8, 12 and 16 cracks respectively. No definite relationship could be drawn between crack frequency and mass loss from such limited work. In strain hardening materials crack frequency has been found to be related to the corrosion rate in the specimens. A study conducted by Ahmad & Mihashi (2010) found corrosion to be worse in specimens with a single crack in reinforced mortar than in multiple cracked strain hardening materials as shown in Figs 3.2 & 3.3. On the other hand, multiple cracks in strain hardening materials made from PE and hybrid steel fibres were found to

Influence of Cracks and Chlorides in Concrete Structures

perform better, with reduced corrosion rates. After almost 100 days of testing, smaller crack frequency of strain hardening fibre-reinforced cementitious composite (SHFRCC) specimens made from PE and steel fibre, showed 97% and 96% lower mass loss than the specimens made from SHFRCC with only PE and plain mortar specimens. The reduced corrosion rate in steel fibre concrete is attributed to the sacrificial anode effect of fibre. Note that in the above experiment the materials compositions for mortar and SHFRCC were the same except there was no fibre in the mortar mix.

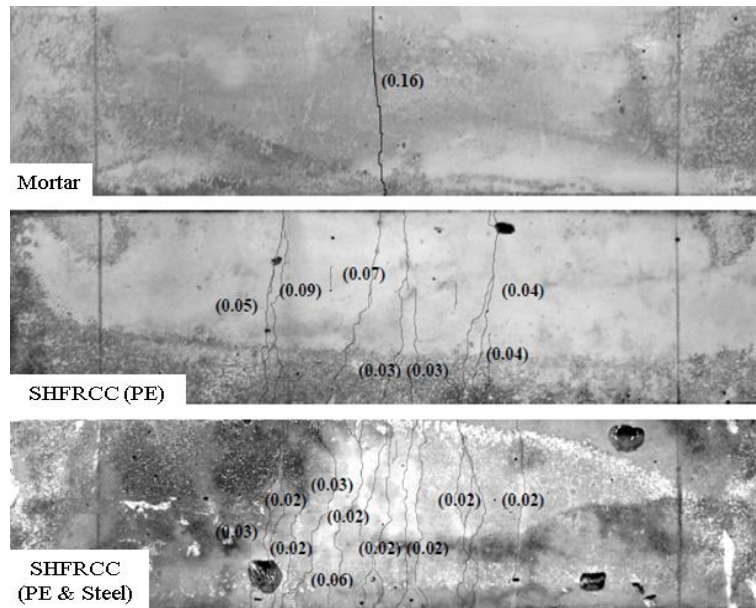


Figure 3.2: Crack patterns observed in mortar, SHFRCC with PE fibre and SHFRCC with a mix of PE and hybrid steel fibre specimens under tensile test (reproduced from Ahmed & Mihashi, 2010).

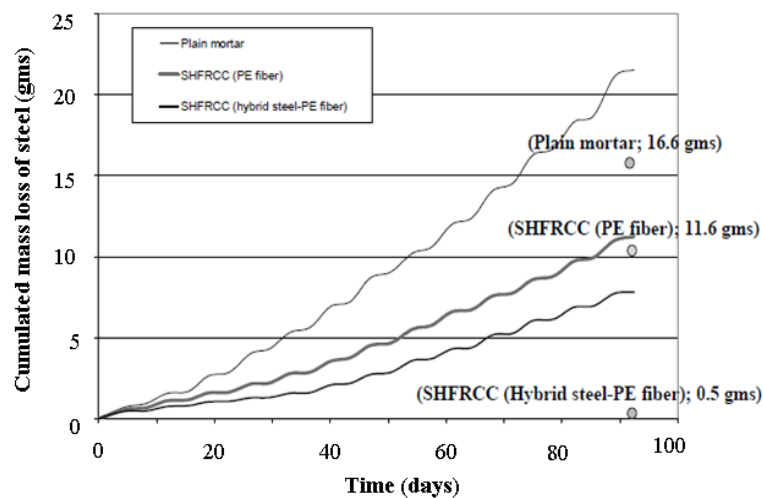


Figure 3.3: Influence of cracks in mass loss of steel in corrosion testing (reproduced from Ahmed & Mihashi, 2010).

3.3. Chloride in concrete

Chloride-induced corrosion is the most severe problem in most RCS. It can be explained by the fact that in chloride-induced corrosion, the anode and cathode area are well separated, therefore the ions from the cathode area can easily move and increase the corrosion rate. Chloride may come into concrete in different ways such as deliberate addition of chloride as accelerators, chloride contaminated water and aggregates, sea salt spray or direct sea water wetting, deicing salts, use of chemicals, etc. (Broomfield, 2007). Chloride penetration in both marine and road structures exposed to de-icing salts produces a profile in the concrete categorized by high chloride content near the external surface and decreasing contents at greater depths as shown in Fig 3.4a. Depending on the size of specimens, the presence of cracks and exposure conditions, the chloride content may also be higher at the opposite surface of specimens (see Fig 3.4b). Fig 3.4b shows the chloride profile in 2 mm layers of 30 mm deep SHCC and mortar specimens.

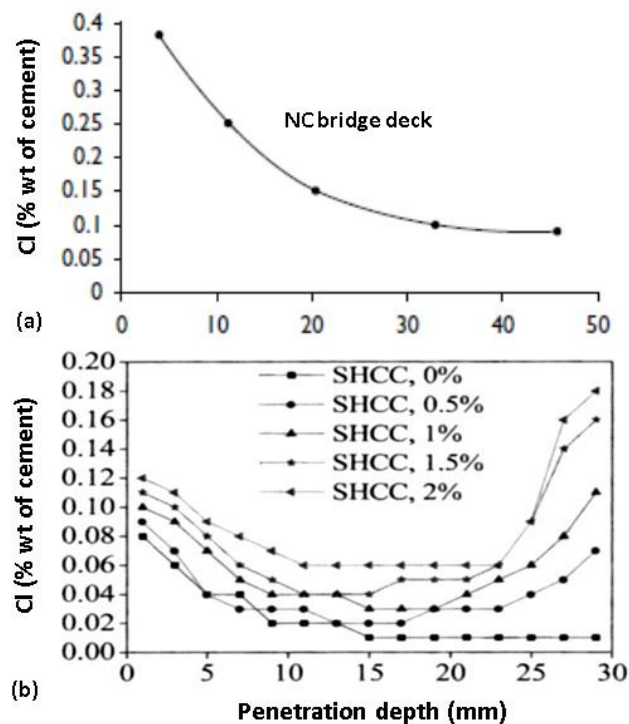


Figure 3.4: (a) Chloride profile of a highway bridge deck (Broomfield, 2007), (b) Chloride profile in SHCC with different fibre percentage (Wittmann *et al.* 2011).

A significantly higher amount of chloride was observed at the opposite side of SHCC specimens than of the mortar specimens. In SHCC the amount of chloride was higher as the fibre content increased. This can be explained by the inclusion of fibre which produces some air/voids in the matrix and ultimately increases the permeability of SHCC. The higher the fibre content, the more the permeability of SHCC. This may be the reason for higher chloride content in the SHCC with higher fibre content. Higher chloride at greater depth can also be

Influence of Cracks and Chlorides in Concrete Structures

found in NC, and the reason is discussed in Section 3.5. This section discusses the influence of chloride content in concrete, the threshold level of chloride content, and the relationship between cracks, chloride and corrosion in concrete.

3.3.1. Free and bound chloride in concrete

The chloride content can be expressed as either the free chloride or the total chloride in the concrete. Free chloride typically dissolves in the concrete pore solution. Some of the chlorides bind with the concrete ingredients especially with the binders. This is known as bound chloride and is commonly referred to as Friedel's salt ($3\text{CaO}\cdot\text{Al}_2\text{O}_3\cdot\text{CaCl}_2\cdot 10\text{H}_2\text{O}$). The total chloride content is the combination of free and bound chloride in concrete. It is usually thought that only free chloride ions can contribute to the corrosion, while those chemically bound to constituents of the cement paste, such as chlorides adsorbed on C-S-H or bound to tricalcium aluminate (e.g. as Friedel's salt) do not (Bertolini *et al.* 2004). In contrast to the above statement, a study performed by Glass & Buenfeld (1997) revealed that some of the bound chloride may also contribute to the corrosion. A significant portion of the bound chloride may become unbound as soon as the pH value of concrete drops below 12, which may happen locally if there are enough voids at the steel/concrete interface. Because the presence of voids allows some chemical matter to enter the concrete, which then leads to a drop in pH. Therefore the presence of voids is very important for the durability of RCS. In the voids, the bound chloride dissolves and may subsequently be involved in the initiation of corrosion. Another research by Glass *et al.* (1997) discovered that materials such as C_3A , slag, pulverised fuel ash (PFA) and silica fume when used as binders in concrete also influence the level of free and bound chloride. The authors found that the free chloride content was reduced by 50% and 9% by replacing cement with 65% slag and 35% pulverised fly ash (PFA) respectively. However, free chloride content increased when cement was replaced with silica fume (SF). About 50% more free chloride was found in concrete by replacing 20% of cement with silica fume. Therefore, depending on binder types and matrix compositions the difference between the free and total chloride (bound chloride) content in concrete can be in the range 10%-53% (Gaynor, 1985; Dhir *et al.* 1990; Liu, 1996).

3.3.2. Critical/threshold chloride level for concrete

A chloride threshold level in concrete means that the presence of a certain minimum amount of chloride which is required at the steel surface to start corrosion. This threshold chloride level also depends on many factors such as pH level, the presence of microscopic voids, types of binders, etc. Most researches do not mention whether the threshold chloride is the free or total chloride. However, reporting the amount of free chloride in concrete may be more representative than reporting the total chloride content. German & Zaborski (2011) suggested that a threshold value of free chloride is about 0.35 (% by concrete wt) in concrete.

Fig 3.5 shows the influence of interfacial voids and the total chloride content threshold (% cement by weight) level of concrete made with different binder types. The results in the

 Influence of Cracks and Chlorides in Concrete Structures

figure indicate that the chloride threshold value is higher when there are fewer voids inside the concrete. Committee Euro-International du Beton (CEB) has drawn a relationship between chloride threshold value and humidity in concrete as is shown in Fig 3.6. Chloride threshold is higher for constantly dry and wet condition of concrete. However, in constantly higher humidity the threshold value is lower in both bad and good quality concrete.

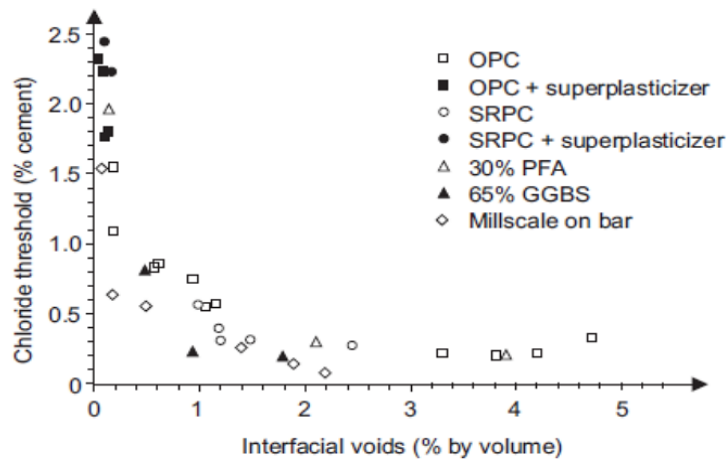


Figure 3.5: Chloride threshold as a function of interfacial voids in concrete (reproduced from Glass & Buenfeld, 2000).

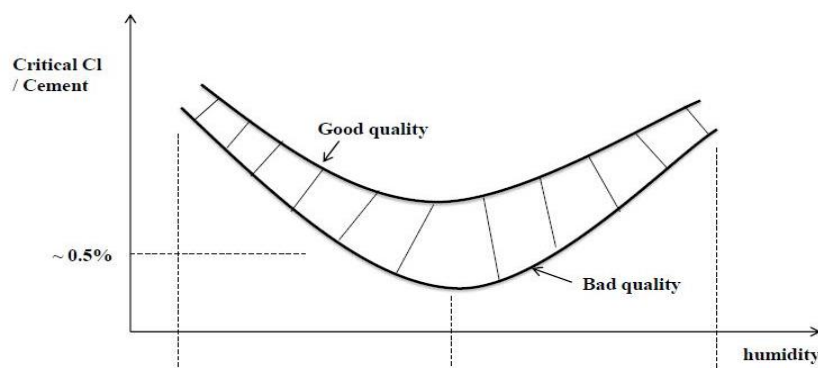


Figure 3.6: CEB recommended critical level of chloride for steel corrosion in concrete (CEB: 1989).

As for total and free chloride, the threshold chloride value also depends on the type of binder, structure, environmental conditions, etc. As shown in Table 3.3, depending on exposure types, DuraCrete (2000) has suggested a threshold range 0.5%-2.3% (by wt of binder) of chloride in concrete structures. For concrete containing normal reinforcing steel and pre-stressing steel, EN 206 (2001) suggests a range of 0.1%-0.4% (by wt of cement) of maximum acceptable total chloride ion which is harmless for steel in concrete. The threshold chloride value also depends on the position of the structural elements. The influence of binder types such as PFA and GGBS on threshold chloride value in external and internal structure elements is shown in Figs 3.7a&b. The difference in the chloride value in external and

Influence of Cracks and Chlorides in Concrete Structures

internal elements can be explained by the entrance of different level of oxygen and water therefore the level of threshold chloride can also be tolerated before corrosion starts.

Table 3.3: Threshold chloride level for concrete described in different codes and literatures

References	w/b	Conditions	Maximum chloride content (% by weight)	
			Binder	Cement
DuraCrete (2000)	0.5	Submerged	1.6	-
	0.4	Submerged	2.1	-
	0.3	Submerged	2.3	-
	0.5	Splash and tidal	0.5	-
	0.4	Splash and tidal	0.8	-
	0.3	Splash and tidal	0.9	-
EN 206 (2001)	-	Concrete containing embedded steel or metal	-	0.2-0.4
	-	Concrete containing pre-stressing steel	-	0.1-0.2
Gouda & Halaka (1970)	-	Concrete mixed with chloride	-	3.04
Kayyali & Haque (1995)	-	Cement with 2.43% C ₃ A in concrete	-	0.14
	-	Cement with 7.59% C ₃ A in concrete	-	0.17
	-	Cement with 14% C ₃ A in concrete	-	0.22
Thomas (1996)	-	Concrete in marine exposure with 0% fly-ash	-	0.70
	-	15% fly-ash	-	0.65
	-	30% fly-ash	-	0.50
	-	50% fly-ash	-	0.20

Some other researchers also suggested different threshold values for concrete. A study conducted by Hausmann (1967) suggested that the critical total chloride content (% by cement wt) is about 0.06%-1.0% while Pettersson (1993), Schiessl (1986) and Broomfield (2007) mentioned different ranges of 0.9%-1.8%, 0.48%-2.02% and 0.2%-0.4% respectively. It is also worth mentioning that all these chloride ranges mentioned here are valid for Portland cement (CEM I).

Influence of Cracks and Chlorides in Concrete Structures

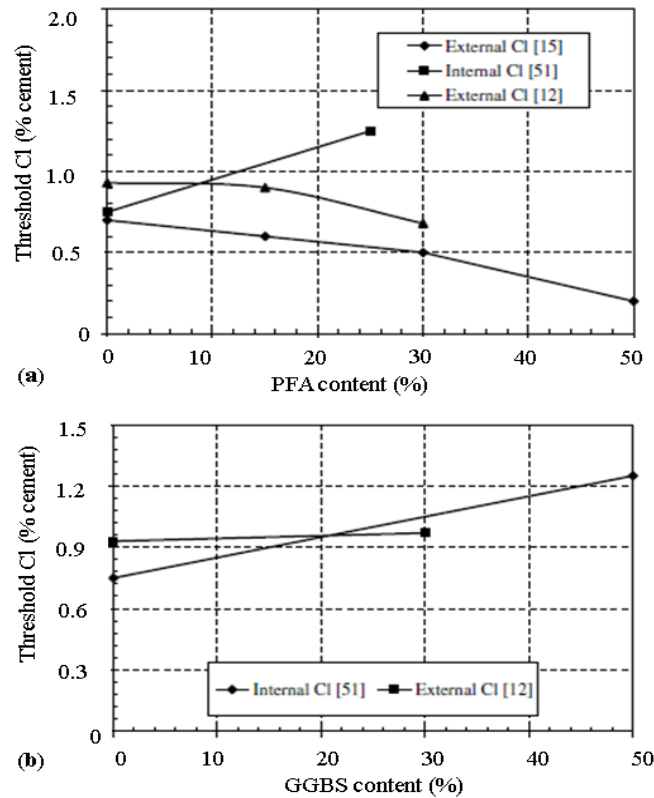


Figure 3.7: Influence of binder types on threshold chloride (Cl) value (reproduced from Ann & Song, 2007).

3.3.3. Chloride profile and diffusion coefficients of concrete

The chloride diffusion coefficient is an indication of concrete performance against the penetration of chloride into concrete and often used as parameter for the durability design of concrete structures. Fick's law as shown in Eq (3.1) is generally used to calculate the chloride profile in concrete.

$$C_x = C_s \left(1 - \operatorname{erf} \frac{x}{2\sqrt{D_{app} \cdot t}} \right) \quad (3.1)$$

where: C_x is the % of chloride (by wt of binder or concrete) at time t (in sec); x is the depth from the concrete surface (m); C_s is the % of surface chloride concentration; D_{app} is the apparent diffusion coefficient of chloride (m^2/s).

The apparent diffusion coefficient (D_{app}) of concrete can be determined by laboratory testing of rapid chloride penetration suggested by the AASHTO T277, NT BUILD 492 (1999), etc. The details about the rapid chloride penetration testing are discussed in Chapter 4. Chloride penetration resistance of concrete is described by the D_{app} value. Lower D_{app} indicates higher resistance to chloride ingress in the concrete. D_{app} also depends on exposure time and

 Influence of Cracks and Chlorides in Concrete Structures

conditions. However, in most test methods the D_{app} value is obtained from a short period of testing time which may not be suitable for the assessment of concrete resistance in the long term exposure conditions. In this case other methods as described in the next section are more suitable than the rapid chloride migration testing. Figs 3.8a&b show the influence of different D_{app} values on the penetration of chloride in concrete cover depths and corrosion initiation periods. As shown in Fig 3.8a the chloride penetration is lower due to a lower D_{app} value of concrete. The corrosion initiation period is lower for a higher D_{app} value of concrete as shown in Fig 3.8b.

3.3.4. Methods of determining chloride profiles in concrete

Concrete chloride profiles can be determined in various ways. The most common method of determining the chloride profile in concrete is by chemical testing. Chemical testing is performed on concrete powder samples obtained by destructive methods such as by grinding and drilling. Presence of chloride in concrete can also be seen using non-destructive methods such as painting silver nitrate (AgNO_3) solution. Recent work by Savija *et al.* (2014) where authors used laser-induced breakdown spectroscopy (LIBS) which is a micro-scale technique to determine the chloride profile by means of mapping in cracked concrete (see Figs 3.9a-c). However, the results obtained from this method have not yet been validated by careful comparison with the chemical tests recommended by the AASHTO T260, RILEM TC178 and ASTM C1152, C1218. Painting AgNO_3 solution only gives a perspective of chloride by discolouration in the presence of a sufficient amount of chloride in concrete, not the actual chloride content. The methods for determining the chloride profile in this research work are discussed in Chapters 4 and 6.

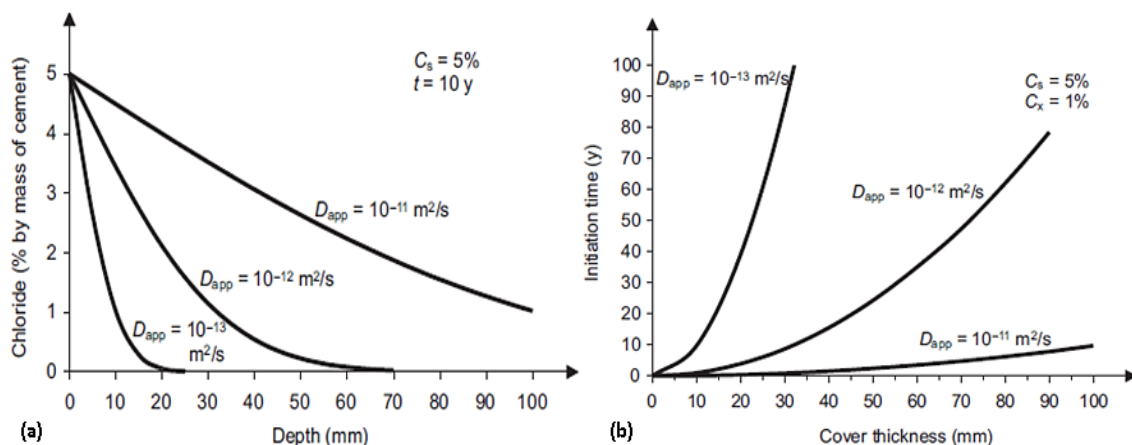


Figure 3.8: Influence of apparent diffusion coefficient (D_{app}) in (a) concrete cover depths after 10 years of exposure and (b) corrosion initiation for a threshold chloride of 1% due to 5% surface chloride concentration (reproduced from Bertolini *et al.* 2004).

Influence of Cracks and Chlorides in Concrete Structures

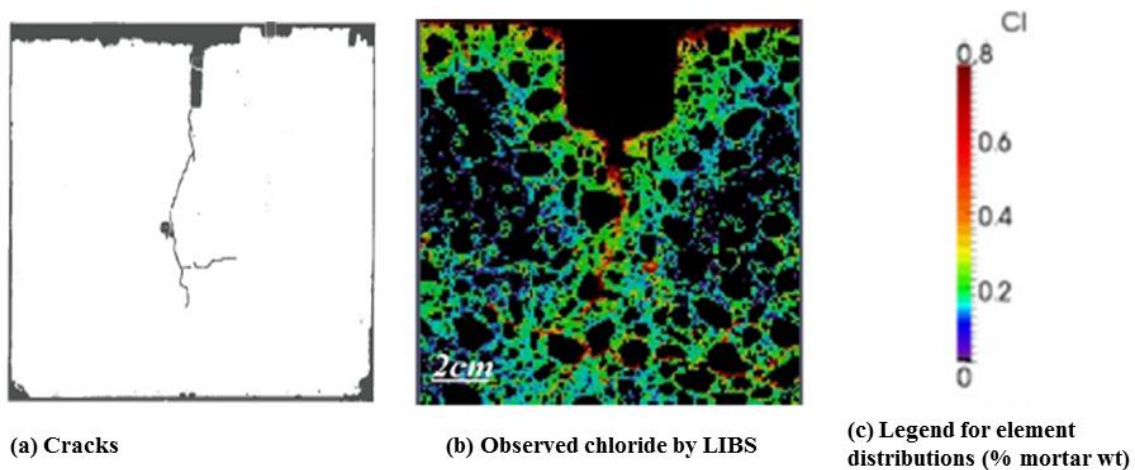


Figure 3.9: Determination of chloride (Cl) in cracked concrete by LIBS analysis (reproduced from Savija *et al.* 2014).

3.3.5. Relationship between crack, chloride and corrosion in concrete structures

In previous sections, the limiting crack widths and critical chloride levels in concrete to protect steel bars from corrosion, have already been discussed. A threshold crack width is still a disputed issue amongst researchers since some believe wider cracks cause greater corrosion and some argue that the crack spacing may be a more important parameter than the crack widths in concrete. Several researchers tried to develop a relationship between the crack width, chloride level and corrosion in concrete as shown in Table 3.4. Figs 3.10a&b show the relationship between the crack, chloride and corrosion in NC by Berke *et al.* (1993) and Huang (2006). No direct relationship was found. The reason may be that the smaller crack widths might have been blocked by the corrosion product at the start of, or early in the exposure period. Corrosion stains at fine cracks present evidence in this regard. Also the possible self-healing capability of concrete in finer cracks may stop the corrosion of steel bars (Fagerlund & Hassanzadeh, 2010). Therefore it indicates that a limiting crack width might exist in concrete and that below that limit no solid relationship can be found between corrosion rate and cracks.

Another study was conducted by Mohammed *et al.* (2001) on the corrosion of steel in concrete containing different crack widths. The authors concluded that the crack widths are correlated to the corrosion rate in the very early exposure condition only and that the period is very short in comparison to the service life of a RCS. The authors also concluded that corrosion rate correlation with the crack width is less clear. Similar conclusions were also made by the other researchers, where they suggested that the concrete cover and quality should be the relevant parameters for durability design, since they influence the chloride-induced corrosion more significantly than the crack widths (Adiyastuti, 2005; Audenaert *et al.* 2009). At the earlier stage of corrosion, wider crack widths (range of 0.1-0.5 mm) in concrete influence the corrosion rate of steel bars because of forming macro-cell corrosion.

Influence of Cracks and Chlorides in Concrete Structures

However, in the long run, the corrosion rate is mostly influenced by the cover depth and concrete quality (Schiessl & Raupach, 1997). The macro-cell corrosion matter will be discussed in the next Chapter 4.

Table 3.4: Relationship between crack widths, chloride content, corroded area and corrosion rate in concrete

References	Crack widths (W_{cr}) (mm)	Chloride concentration	Corroded area (mm^2)	Corrosion rate (mm/year)
Mohammed <i>et al.</i> (2001)	0.05	0.62 (wt % of cement)	960	-
	0.10	0.7-0.74 (wt % of cement)	840-960	-
	0.15	0.65 (wt % of cement)	620	-
	0.20	0.68-0.96 (wt % of cement)	580-1180	-
Berke <i>et al.</i> (1993)	0.25	8.4-9.7 (kg/m^3)	850-9800	-
	0.50	8.4 (kg/m^3)	9850	-
Huang, (2006)	$0.02 < W_{cr} < 0.04$	-	-	0.0575-0.07
	$0.08 < W_{cr} < 0.10$	-	-	0.062-0.07
Verbetskii <i>et al.</i> (1986)	0.2 mm	-	-	0.1

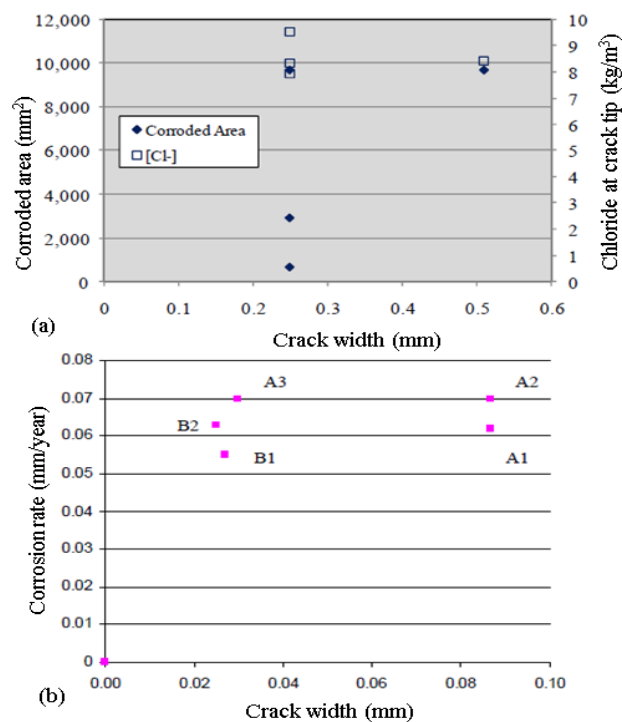


Figure 3.10: Cracks, chloride and corrosion in NC (reproduced from Berke *et al.* 1993; Huang, 2006).

3.4. Carbonation corrosion in concrete

In drying exposure, moisture from concrete evaporates and creates small voids allowing the penetration of air. Air contains different types of gases including CO₂ which basically reacts with different oxides in the alkaline portion of concrete and reduces concrete alkalinity. The reaction between alkaline hydroxides in concrete and atmospheric carbon dioxide gas is termed carbonation. When CO₂ dissolves in water, it forms an acid called carbonic acid. There is no reaction between this carbonic acid with cement paste, but calcium carbonate is formed which basically diminish the alkalinities and corrosion of steel will occur if oxygen and moisture are available. The carbonic reactions in concrete are shown in Eqs (3.2) & (3.3).

Gas water carbonic acid



Carbonic pore acid solution



The presence of much calcium, sodium and potassium hydroxide in concrete pores maintain the pH level even if there is carbon dioxide. However, this carbon dioxide starts reacting with the calcium hydroxides and forms CaCO₃ which causes a lower pH value in concrete and as a result corrosion starts in steel bars. If there is not enough concrete cover, the carbonation attack will be faster/sooner. Also if there are voids in concrete which allow rapid ingress of CO₂, the carbonation attack might happen faster even if the concrete cover is large. It is more prominent in higher w/c, low binder content, and poorly cured and poorly compacted concrete. The influence of pH values on the corrosion rate of steel bars in concrete is shown in Fig 3.11.

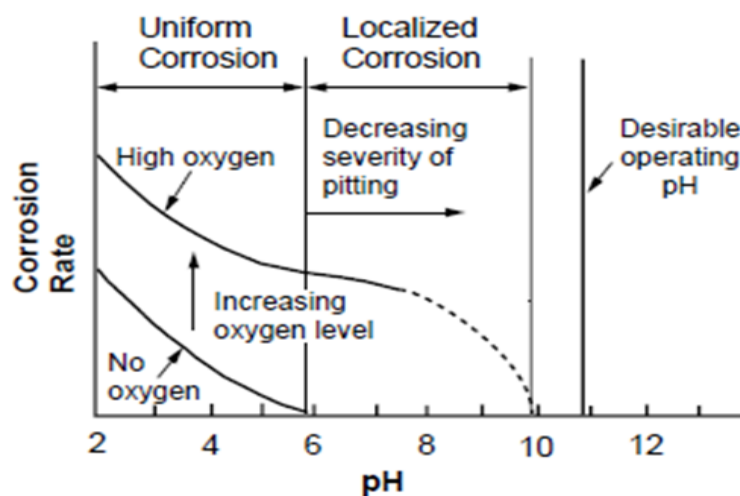


Figure 3.11: Rate of corrosion status at different pH levels of concrete (reproduced from Roberge, 1999).

Influence of Cracks and Chlorides in Concrete Structures

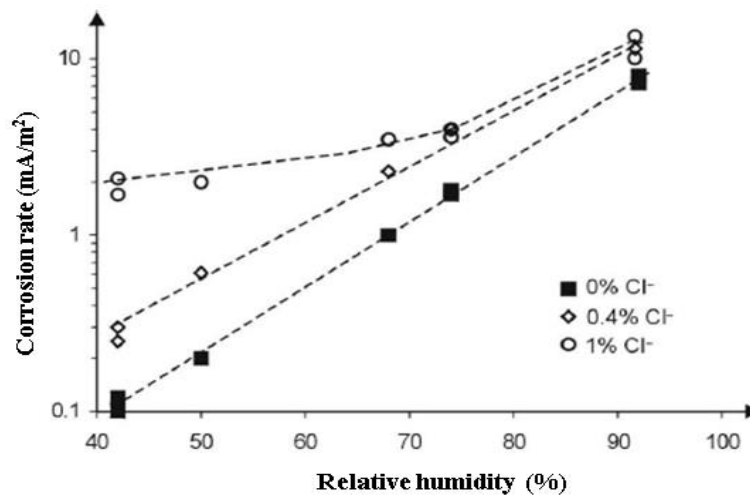


Figure 3.12: Influence of relative humidity on corrosion in mortar with and without mixed chloride (reproduced from Glass *et al.* 1991).

As mentioned before, temperature and relative humidity (RH) play an important role in both chloride and carbonation-induced corrosion in concrete. Fig 3.12 shows the corrosion rate versus RH in mortar mixed with and without chloride. A higher concentration of chloride causes faster corrosion at higher RH values. It is worth mentioning that in this research work the influence of temperature and RH in corrosion rate was not investigated, and as a result, no relationships were drawn between them.

3.5. Influence of cyclic wetting and drying in concrete durability

For laboratory chloride-induced corrosion testing, a common accelerated exposure method is the cyclic wetting and drying of the RC specimen. Under normal exposure condition, it takes a long time for corrosion activities in RCS to become noticeable. Therefore, in this research work the accelerated cyclic wetting and drying exposure was also followed. This is discussed in detail in Chapters 5 and 7. Cyclic wetting and drying allows continuous movement of moisture through pores in concrete. It is considered to be very harmful for RCS since it allows motion and accumulation of aggressive substances such as chloride, sulphates, acids, alkalis, etc. RCS in the marine environment (splash and tidal zones area), as well as highway structures exposed to deicing salts are in fact subjected to cyclic wetting and drying. When dry concrete comes in contact with salt water, it absorbs the salt water by capillary suction. As a result, a chloride concentration gradient will develop in concrete. In a dry environment water from the pores will evaporate, and salts that were originally in solution may precipitate out in the pores near to the surface. At this point chloride may now exist within the concrete (Hong, 1998).

The rate of chloride penetration into concrete depends on the duration of wetting and drying periods as well. At the wet stage of concrete, some salts may migrate deep into concrete by diffusion. Therefore, higher chloride concentration can also be seen at the opposite face of

Influence of Cracks and Chlorides in Concrete Structures

exposed surface of concrete as it is also shown in Fig 3.4b. In general, cyclic wetting and drying in concrete increase the concentration of ions such as chloride due to subsequent ingress and evaporating of water. The drying exposure increases the availability of oxygen in concrete since oxygen has a significantly lower diffusion coefficient in saturated concrete. Therefore in dry concrete, oxygen has a better chance to diffuse and attain the level necessary to induce and sustain corrosion (Hong, 1998). For example, RCS permanently submerged into seawater are less prone to corrosion than RCS subjected to seawater wetting and drying exposure (Abdul-Hamid, 1990).

The ingress rate of chlorides into concrete is also influenced by the duration as well as the sequence of drying and wetting. The degrees of dryness are very important since drier concrete allows subsequent wettings to carry the chloride in deeper, thus speeding up the penetration of chloride ions (Neville, 1996). Dryness is directly related to the concrete durability since oxygen level and moisture content at the rebar level, and the magnitude of the capillary suction forces are related to the dry exposure (Hong, 1998).

3.6. Concluding remarks

Concrete durability is related to many things like cracks, chloride, exposures conditions, moisture content, oxygen ingress, etc. and it is a difficult task to control all of them so that they have minimum influence on durability throughout the whole design life of a RCS. A durability design model is necessary to predict the expected design life of RCS after being affected by the chloride and carbonation attack in the presence of cracks. At the design stage some important measurements must be performed which includes crack width limitation by design, larger cover depth or low permeable concrete, to ensure a sufficiently long design life span or a limited number of maintenance/repair cycles during the life span to minimize overall cost. Current durability research outcomes on SHCC are limited and as a result it is difficult to develop a rigorous and reliable durability design model at this stage. Even in NC, the information is not clear and researchers have suggested different crack width limits and chloride threshold values to prevent durability problems. It may be because of different researchers having used different mix designs and all the limiting parameters (chloride, carbonation, etc.). So for SHCC, a research data base will help to come up with a durability model and to determine the expected remaining design life of a structure where SHCC is used.

3.6. References

- AASHTO T259 1986, Method of Test for Resistance of Concrete to Chloride Ion Penetration Methods of Sampling and Testing, 444 N. Capitol St., NW, Washington, DC 20001.
- Abdul-Hamid, Al-Tayyib, J & Al-Zahrani, MM 1990, 'Use of polypropylene fibres to enhance deterioration resistance of concrete surface skin subjected to cyclic wet/dry sea water exposure', *ACI Materials Journal*, vol. 87, no. 4, pp. 363-370.

Influence of Cracks and Chlorides in Concrete Structures

- Adiyastuti, SM 2005, Influence of cracks on chloride induced corrosion in reinforced concrete flexural members. PhD thesis, The University of New South Wales, Sydney, Australia.
- Ahmed, SFU & Mihashi, H 2010, 'Corrosion durability of strain hardening fibre-reinforced cementitious composites', Australian Journal of Civil Engineering, Paper C09-644, pp. 27-39.
- Alekseev, SN 1993, Corrosion of Steel Reinforcement, Durability of Reinforced Concrete in Aggressive Media, Malliek (eds), Russian Translation Series 96, Brookfield, pp. 164-247.
- Ann, KY & Song, HW 2007, 'Chloride threshold level for corrosion of steel in concrete', Corrosion Science, vol. 49, pp. 4113-4133.
- Arya, C & Ofori-Darko, FK 1996, 'Influence of crack frequency on reinforcement corrosion in concrete', Cement and Concrete Research, vol. 26, no. 3, pp. 345-353.
- ASTM C1202 2012, Standard Test Method for Electrical Indication of Concrete's Ability to Resist Chloride Ion Penetration, ASTM International, West Conshohocken, PA.
- ASTM C1152 2004, Standard test method for acid soluble chloride in mortar and concrete, ASTM International, West Conshohocken, PA.
- ASTM C1218 1999, Standard test method for water soluble chloride in mortar and concrete, ASTM International, West Conshohocken, PA.
- Audenaert, K, Marsavina, L & De Schutter, G 2009, 'Influence of cracks on the service life of concrete structures in a marine environment', Key Engineering Materials, vol. 399, pp. 153-160.
- Bertolini, L, Elsener, B, Pedferri, P & Polder, RP 2004, Corrosion of Steel in Concrete, Copyright © WILEY-VCH Verlag GmbH & Co. KGaA, Weinheim, ISBN: 3-527-30800-8.
- Berke, NS, Hicks, MC & Tournay PG 1993, 'Evaluation of concrete corrosion inhibitors', in proceeding 12th international corrosion congress, Houston, Texas, pp. 3271-3286.
- Boshoff, WP 2007, Time-dependant behaviour of engineered cement-based composite, PhD thesis, Stellenbosch University, South Africa.
- Broomfield, JP 2007, Corrosion of steel in concrete understanding, investigating and repair, 2nd edition, Taylor & Francis, USA & Canada.
- CEB 1989, Durable Concrete Structures, CEB Design Guide, Bulletin d'information 182.
- Combrinck, R & Boshoff, WP 2013, 'Typical plastic shrinkage cracking behaviour of concrete', Magazine of Concrete Research, vol. 65, no. 8, pp. 486-493.
- Dhir, RK, Jones, MR & Ahmed, HEH 1990, 'Determination of total and soluble chloride in concrete', Cement and Concrete Research, vol. 20, no. 4, pp. 579.
- DuraCrete R17 2000, DuraCrete Final Technical Report, "The European Union – Brite EuRam III, DuraCrete – Probabilistic performance based durability design of concrete structures, Document BE95-1347/ R17, CUR, Gouda, The Netherlands.

Influence of Cracks and Chlorides in Concrete Structures

- DuraCrete R9 2000, Statistical quantifications of the variables in the limit state functions, Document BE95- 1347/R9, The European Union - Brite EuRam III, DuraCrete – Probabilistic Performance based Durability Design of Concrete Structures.
- EN 206-1 2001, Concrete – Part 1. Specification, Performance, Production and Conformity, European Committee for Standardization.
- Fagerlund, G & Hassanzadeh, M 2010, Self-healing of cracks in concrete long-term exposed to different types of water, Results after 1 year exposure, Div. Building Research, Lund Institute of technology, Report TVBM-3156.
- Gaynor, R 1985, Understanding chloride percentage, *Concrete International*, pp. 35.
- German M & Zaborski, A 2011, ‘Numerical analysis of chloride corrosion of reinforced concrete, Biblioteka Cyfrowa Politechniki Krakowskiej, Technical Transmission, vol. 3, pp. 47-59.
- Glass, GK & Buenfeld, NR 2000, ‘The inhibitive effects of electrochemical treatment applied to steel in concrete’, *Corrosion Science*, vol. 42, pp. 923–927.
- Glass, GK & Buenfeld, NR 1997, ‘Chloride threshold level for corrosion of steel in concrete’, *Corrosion Science*, vol. 39, pp. 1001–1013.
- Glass, GK, Hassanein, NM & Buenfeld, NR 1997, ‘Neural network modelling of chloride binding’, *Magazine of Concrete Research*, vol. 49, pp. 323–335.
- Glass, GK, Page, CL & Short, NR 1991, ‘Factors affecting the corrosion of steel in carbonated mortars’, *Corrosion Science*, vol. 32, pp. 1283.
- Goodwin, F 2012, ‘The concrete life cycle: Maintain to Sustain’, proceedings of the ICRI fall convention, November 7-9, Rancho mirage, Canada.
- Gouda, VK & Halaka, WY 1970, ‘Corrosion and corrosion inhibition of reinforced steel’, *British Corrosion Journal*, vol. 5 pp. 204-208.
- Hausmann, DA 1967, ‘Steel corrosion in concrete’, *Materials Protection*, vol. 6, pp. 19-23.
- Hong, K 1998, Cyclic wetting and drying and its effects on chloride ingress in concrete. MSc thesis, University of Toronto, Canada.
- Huang, Q 2006, Influence of cracks on chloride-induced corrosion in reinforced concrete structures. MSc thesis, Chalmers University of Technology, Sweden.
- Kayyali, OA & Haque, MA 1995, ‘The ratio of Cl/OH in chloride contaminated concrete, A most important criterion’, *Magazine of Concrete Research*, vol. 47, pp. 235-242.
- Kobayashi, K, Iizuka, T, Kurachi, H & Rokugo, K 2010, ‘Corrosion protection performance of high performance fibre reinforced cement composites as a repair material’, *Cement & Concrete Composite*, vol. 32, pp. 411-420.
- Kobayashi, K & Rokugo, K 2013, ‘Mechanical performance of corroded RC member repaired by HPRCC patching’, *Construction and Building Materials*, vol. 39, pp. 139-147.
- Lepech M & Li VC 2009, ‘Water permeability of engineered cementitious composites’, *Cement and Concrete Composites*, vol. 31, pp. 744-753.

Influence of Cracks and Chlorides in Concrete Structures

- Liu, Y 1996, Modelling the time-to-corrosion cracking of the cover concrete in chloride contaminated reinforced concrete structures, PhD thesis, Virginia Polytechnic Institute and State University, USA.
- Mitchell, JK 1991, Fundamentals of soil behaviour, John Wiley & Sons, Inc., New York, pp. 47-53.
- Mihashi, H, Ahmed, SFU & Kobayakawa, A 2011, 'Corrosion of reinforcing steel in fibre reinforced cementitious composites', Journal of Advantage Concrete Technology, vol. 9, no. 2, pp. 159-167.
- Mohammed, TU, Otsuki, N, Hisada, M & Shibata, T 2001, 'Effect of crack width and bar types on corrosion of steel in concrete', Journal of Materials in Civil Engineering, vol. 13, pp. 194-201.
- Moskvina, V, Lvanov, F, Alekseyev, S & Guzeyev, E 1980, 'Concrete and reinforced concrete deterioration and protection', Mir Publishers, Moscow, pp. 292-305.
- Naville, AM 1996, Properties of concrete, 4th edition, New York, NY USA.
- NT BUILD 492: 1999-11: Chloride migration coefficient from non-steady-state migration experiments. ISSN 0283-7153.
- Paul, SC & van Zijl, GPAG 2014, 'Crack formation and chloride induced corrosion in reinforced strain hardening cement-based composites (R/SHCC)', Journal of Advanced Concrete Technology, vol. 12 pp. 340-351.
- Pettersson, K 1993, 'Corrosion of steel in high performance concrete', proceeding for 3rd international symposium on utilization of high strength concrete, Lillehammer, Norway.
- Roberge, PR 1999, Handbook of corrosion engineering, McGraw-Hill, New York, NY 10011, ISBN 0-07-076516-2.
- RILEM TC 178-TMC 2002, Testing and modelling chloride penetration in concrete, Analysis of water soluble chloride content in concrete, Materials and Structures, vol. 35, pp: 586-588.
- RILEM TC 178-TMC 2001, Testing and modelling chloride penetration in concrete, Analysis of total chloride content in concrete, Materials and Structures, Vol. 35, pp: 583-585.
- Savija, B, Schlangen, E, Pacheco, J, Millar, S, Eichler, T & Wilsch, G 2014, 'Chloride ingress in cracked concrete: a laser induced breakdown spectroscopy (LIBS) study', Journal of Advanced Concrete Technology, vol. 12, pp. 425-442.
- Schiessl, P 1986, The influence of cracks on the durability of reinforced concrete and prestressed concrete (in German). Ernst & Sohn, Deutscher Ausschuss für Stahlbeton, Heft 370, Berlin, Germany.
- Schiessl, P & Raupach, M 1997, 'Laboratory studies and calculations on the influence of crack width on chloride-induced corrosion of steel in concrete', ACI Materials Journal, vol. 94, no. 1, pp. 56-62.
- Sahmaran, M, Li, VC & Andrade, C 2008, 'Corrosion resistance performance of steel reinforced engineered cementitious composite beams', ACI Materials Journal, vol. 105, no. 3, pp. 604-611.

Influence of Cracks and Chlorides in Concrete Structures

Thomas, M 1996, 'Chloride thresholds in marine concrete', *Cement and Concrete Research*, vol. 26, no. 4, pp. 513-519.

Verbetskii, GP, Chogovadze, GI & Daneliya, AI 1987, 'Enlargement of concrete blocks of arch dams with allowance of the formation of radial cracks', *Hydrotechnical Construction*, vol. 21, no. 10, pp. 49-51.

Verma, N 2013, *Corrosion of steel reinforcements in concrete*, Research project MME 480, Indian Institute of Technology, Kanpur, India.

VicRoads Standard Specification Section 687 2010, *Repair of Concrete Cracks*, Technical Note, No.38.

Wang, K, Jansen, DC & Shah, SP 1997, 'Permeability study of cracked concrete', *Cement and Concrete Research*, vol. 27, no. 3, pp. 381-393.

Wittmann, FH, Wang, P, Zhang, P, Tie-Jun, Z & Betzung, F 2011, 'Capillary absorption and chloride penetration in neat and water repellent SHCC under imposed strain' proceeding for 2nd International Conference on Strain Hardening Cementitious Composites, 165-172. Brazil.

Chapter 4

Limitations live only in our minds. But if we use our imaginations, our possibilities become limitless. –Jamie Paolinetti

Reinforcement Corrosion Mechanism and Measurement Methods

4. General aspects

Corrosion is a radical destructive process which takes place in a material, causing the material to deteriorate and to finally ruin it. The economic loss due to corrosion damage of highway bridge decks, motorways and other infrastructure is high in many countries, and reported to be US\$300-400 million dollars per year required in the USA alone for renovation of bridges and car park alone. In the UK, £500 million is spent on concrete repair per year while in China the annual loss due to corrosion has reached 100 billion RMB (Li *et al.* 2009). Improving material performance against corrosion can therefore make significant savings over the service lifespan of infrastructure. Typically, corrosion of a material is an impact of a changing internal environmental process which is influenced by the external environment. In its total lifespan, material often experiences different types of corrosion and each material has different corrosion resistance depending on its internal structure and composition. Indeed material corrosion is a very complex subject since all physical (external forces, temperature, water and cyclic dampness), chemical (presence of chloride and alkali aggregate reaction) and biological (fungi, micro-organisms and insects) changes influence the corrosion process.

4.1. Corrosion mechanism in concrete

In concrete, the corrosion of steel is an electrochemical process where current passes from one medium to another (anode to cathode) as in an electrical circuit. In the hydration process of cement in concrete, a highly alkaline (sodium and potassium hydroxide) environment ($12.5 < \text{pH} < 14$) is formed. However, lower pH and carbonation are also causes of corrosion. Lower the pH, lowers the amount of chloride ions needed to promote corrosion in the steel bar. The alkaline environment (pH above 12.5) in concrete helps in forming a thin protective layer also called a passive film on the surface of steel. Typically this passive film is composed of different degrees of hydrated iron oxide Fe^{2+} and Fe^{3+} and it is only a few nanometres thick. Usually the passive film of steel is secure from any kind of mechanical damage. The whole process of corrosion in the steel is called depassivation. The time for such process to lead to corrosion, is referred to as the initiation period of corrosion of steel in concrete (see Fig 4.1). By providing good quality, less permeable concrete and higher cover

Reinforcement Corrosion Mechanism and Measurement Methods

depth, the initiation period can be increased in RCS. So the resistivity of concrete is related to the severity of corrosion and Table 4.1 shows the limit of resistivity and corresponding possible corrosion in concrete.

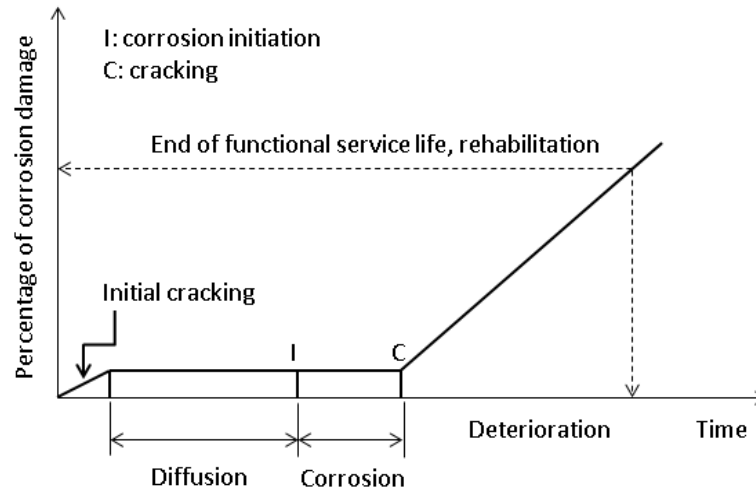


Figure 4.1: RCS service life prediction model schematisation (reproduced from Liu & Weyers, 1998).

Table 4.1: Relationship between corrosion rate, resistivity and severity in concrete

Severity	Resistivity of concrete (k Ω .cm)	Corrosion rate (μ m/year)	
	(Langford & Broomfield, 1987)	(Langford & Broomfield, 1987)	(Bertolini, 2004)
Low corrosion rate	>20	Up to 2	2-4
Low to moderate corrosion	10-20	2-6	5-9
Moderate to high corrosion	5-10	6-12	10-49
Very high corrosion rate	<5	>12	50-99

4.1.1. Initiation and propagation period of concrete

Tutti (1982) has developed a simple corrosion model which was then modified by Liu & Weyers (1998) with more graphical representation. Their model shows the different stages of the corrosion scenario in RCS (see Fig 4.1). According to the Tutti model, the total service life of a RCS can be divided into two major phases, (i) the initiation period and (ii) the propagation period. In the initiation period, carbonation and chloride ingress take place in the concrete as discussed in previous sections. The propagation period starts when the steel is fully depassivated and reaches a limiting state when corrosion is no longer acceptable. Water and oxygen must be present for corrosion to take place because in the absence of either water or oxygen, the corrosion process will not take place or will be very insignificant. Therefore it

Reinforcement Corrosion Mechanism and Measurement Methods

can be said that the presence of wider cracks in concrete might reduce the service life of RCS since water, carbon and oxygen can easily penetrate the concrete and reach the steel.

4.1.2. Mechanism of breaking passive film

The process of depassivation of reinforcing steel in concrete is not yet clearly understood because of its complexity and also because many factors are involved in the process. Typically, the passive film is a very thin layer and it is inside the concrete which makes it difficult to examine correctly. The hypothesis is that when chloride comes into contact with the passive film, it reduces the resistance of the passive film. However, in concrete, the contact between chloride and the passive film is not uniform and where it happens, an anodic region forms more rapidly and corrosion continues. On the other hand, the unaffected or remaining area of steel bar remains passive. Another hypothesis is that chloride ions form a dissolvent compound with Fe^{2+} ions, and as a result a passive film cannot form and the process encourages further metal corrosion (Hansson *et al.* 2007).

4.1.3. Micro-cell and Macro-cell corrosion

In any corrosion process, the steel surface is affected such that part of the steel acts as an anode and other, adjacent parts act as the cathode. The corrosion rate in the steel is highly influenced by these two zones. Depending on their positions in the steel bar, corrosion can be classified as either micro-cell or macro-cell corrosion. The formation of micro-cell and macro-cell corrosion in cracked concrete is discussed below:

Micro-cell corrosion: When the distance between the anode and the cathode is very small or difficult to separate it is called micro-cell corrosion. So in finely distributed cracks in concrete like SHCC, there is a big possibility of forming micro-cell corrosion. In this case, typically cracks act as a path for oxygen penetration to the cathode. Since the cathodic area is small, it is expected that there will be less damage in the RCS from this type of corrosion process (Andrade & Gonzalez, 1978; Bertolini *et al.* 2004; Broomfield, 2007).

Macro-cell corrosion: In this case the anode and cathode areas are far apart and the anode area is limited to the crack zone. Here, oxygen penetrates to the cathode part through the uncracked portion of concrete. Since the cathode area in the macro-cell corrosion process is much larger than in micro-cell corrosion, the corrosion rate due to macro-cells is also higher (Vennesland & Gjrv, 1981; Okada & Miyagava, 1989; Makita *et al.* 1989).

4.1.4. Re-passivation of corrosion

Once corrosion starts in the steel it is not always certain that the corrosion rate will increase. Due to the complex electro-chemical mechanism of steel corrosion in concrete, the rate of corrosion may decrease or stop. Typically when pitting corrosion takes place, current circulation in the anodic part incites and gradually increases the chloride content and acidity, so that propagation may take place even if the potential of the steel is reduced, e.g. owing to

 Reinforcement Corrosion Mechanism and Measurement Methods

an external cathodic polarization. This activity is illustrated in Fig 4.2. It can be seen that the current growth replaced anodically during cyclic polarization in which the potential of the steel (by external polarization) is first raised above pitting potential (E_{pit}) to initiate localized attack and then lowered until conditions of passivity are established again. It can be seen how, to stop the attack, it is necessary to reach a potential value, called the protection potential (E_{pro}) which is more negative than E_{pit} . Thus the interval of potential between E_{pit} and E_{pro} is characterized by the fact that it does not initiate the attack, but if the attack has already begun, it permits propagation of the attack. E_{pro} varies, as does E_{pit} , with the chloride level, pH, and temperature. Depending on the potential of steel and chloride content in the concrete, it is possible to define different domains where pitting corrosion can or cannot initiate and propagate and other effects may take place (Bertolini, 2004). This phenomenon can only be valid in chloride-induced corrosion since the localized pitting corrosion mostly occurs in a chloride-laden environment.

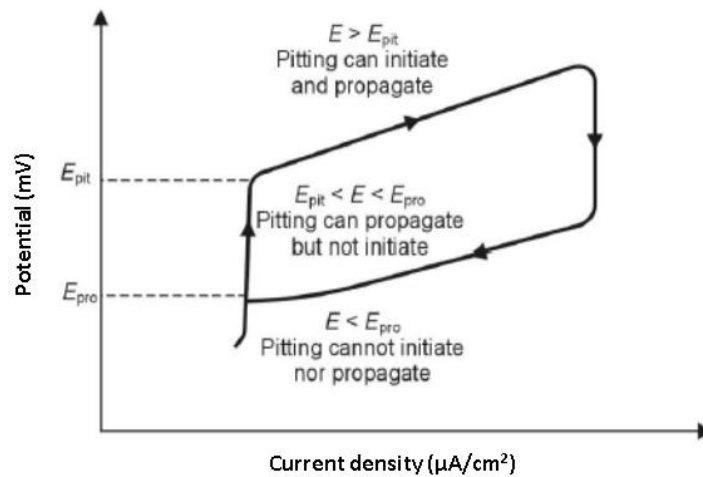


Figure 4.2: A representation of cyclic anode polarization curve of an active-passive material in chloride-laden environment (reproduced from Bertolini, 2004)

Another reason for the reduction in corrosion rate may be due to the self-healing behaviour of materials. Not many studies have been done on this issue since it is complicated by the formation of oxides, crack patterns and different chemical reactions. If self-healing can take place in concrete, it can also reduce the further penetration of chemical substances resulting in a lower rate of corrosion (Mihashi *et al.* 2011; Rooij *et al.* 2013). It has also been postulated that the steel bar interface with the surrounding cement-based matrix plays a significant role in corrosion protection. Experimental evidence has shown that a strong interface layer surrounding the steel increases the corrosion initiation period (Mohammed *et al.* 2002).

4.1.5. Corrosion rate of steel in concrete

Typically, damage of steel in concrete is determined by the corrosion rate. Depending on the exposure type, the corrosion rate in RCS can vary from 2 to 100 $\mu\text{m}/\text{year}$ as the relative

Reinforcement Corrosion Mechanism and Measurement Methods

humidity (RH), CO₂ and chloride concentration at the reinforcement level changes with time (see Table 4.1). Corrosion rate also increases in more harsh exposure conditions. A higher corrosion rate can be observed in RCS in coastal regions as well as in structures where salt is used to dissolve ice such as bridge decks, motorways, etc. since the chloride concentration level in such structures is very high. Until now the corrosion mechanism is not fully understood because many factors are involved. However, it is suggested that higher resistivity of concrete can lead to lowering the corrosion rate because when the reinforcing steel bar corrodes, electrons flow through the bar and ions flow through the concrete. The ion flow in concrete is controlled by the resistivity or electrical conductance of concrete and therefore lower resistivity means a higher ion flow and as a result higher corrosion is expected in concrete.

The preconditions for corrosion to occur are follows (fib Bulletin 3, 1999):

- The depassivation of the steel bar must be developed to create a place for developing the anodic process.
- The anode and cathode area must be connected electrolytically in order to movement of ions between these two areas.
- Sufficient moisture must be available in order to migrate the ions between the anode and cathode area i.e. the resistivity of concrete must be sufficiently low.
- There must be enough oxygen available at the steel bar in the cathode area in order to sustain the cathodic process creating hydroxyl ions, but also at the anode, where the type and volume of rust determines by the availability of oxygen.

4.1.5.1. Factors influencing the corrosion rate in concrete

As mentioned before, in a chloride-laden environment when the amount of chloride reaches the threshold level, it creates an environment to damage the protective film also known as passive film of steel bars embedded in concrete. At this stage, factors that influence the corrosion rate of steel bars are as follows:

- Amount of oxygen and moisture in concrete
- Steel surface area ratio at the anode to cathode area
- Concrete resistivity
- Humidity and temperature in concrete
- Formation of microstructures in concrete

In the corrosion process, the presence of oxygen accelerates the corrosion rate of a steel bar. However it also depends on the amount of moisture present in the concrete. If the concrete is fully saturated, the oxygen diffusion rate is lower because oxygen cannot diffuse through moisture. However in dry concrete, oxygen can easily diffuse through pores or cracks in the concrete. It is found that the wetting and drying cycles of concrete accelerates the steel corrosion process. In the wetting process, the presence of moisture in concrete acts as an electrolyte which causes lower resistivity of concrete than in the drying process. As a result higher half-cell potential values can be found in concrete when it is in contact with moisture

Reinforcement Corrosion Mechanism and Measurement Methods

than when it is in a dry environment. A sufficient amount of oxygen is also necessary in the rapid corrosion process. Concentrated polarization occurs when there is not a sufficient amount of oxygen in the concrete for the cathodic reaction, and so the corrosion current is reduced (Carino & Clifton, 1995).

4.1.5.2. Corrosion products

After corrosion initiation in reinforced concrete, steel corrosion propagates and produces expansive rust surrounding the steel bar (mainly ferrous and ferric hydroxide $\text{Fe}(\text{OH})_2$ and $\text{Fe}(\text{OH})_3$), that occupies a much larger volume than the original reinforcement and thereby generates radial stress in the surrounding concrete at the interface between the reinforcement and concrete. Fig 4.3 shows the corrosion products and their relative volumes. When the stress from these products exceeds the maximum tensile capacity of the concrete cover, the concrete cracks and may eventually spall off. This scenario is very common in RCS and it can also be observed visually.

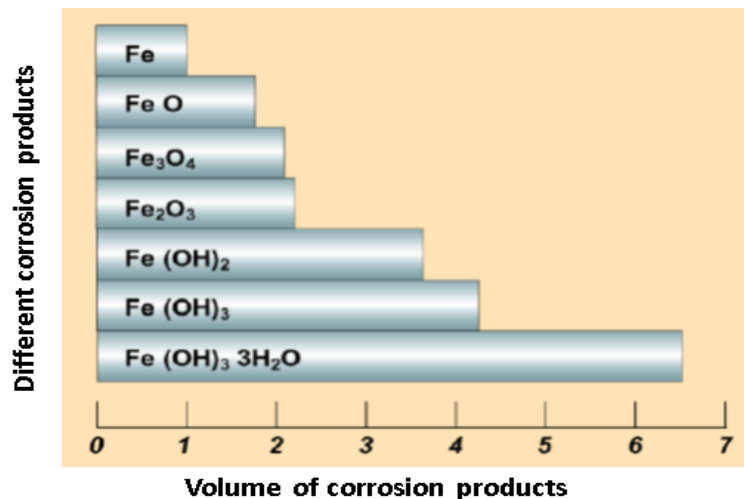


Figure 4.3: Different corrosion products and their volume (reproduced from Cement Concrete & Aggregates Australia, 2009).

4.2. Types of corrosion

Depending on the types of materials and their exposure conditions, different types of corrosion exist. The corrosion mechanism in different materials is also different since the element compositions are not the same. In reinforcing steel inside the concrete, different potential may exist in different places, which may form corrosion cells by continuous chemical processes that cause a flow of electrons or ions from one position to another. In electrochemical corrosion, the anode serves as an electrode which normally releases electrons while the cathode receives electrons. In both anodic and cathodic processes, the total load exchanged must be equal. Typically, the cathodic process is slower and the speed of corrosion is typically determined from this process (Czarnecki *et al.* 2010). Fig 4.4 shows the

 Reinforcement Corrosion Mechanism and Measurement Methods

reactions that take place in the anode and cathode areas during the corrosion process. Some of the oxidations in different environments are shown below:

Oxygen reduction in aqueous environment:



Hydrogen reduction in acidic environment:



Metal oxidation in anode due to environmental reaction:

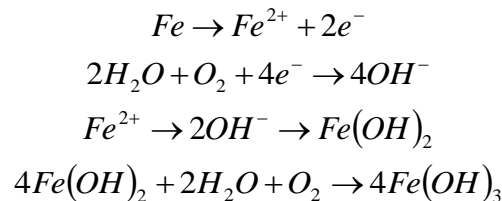
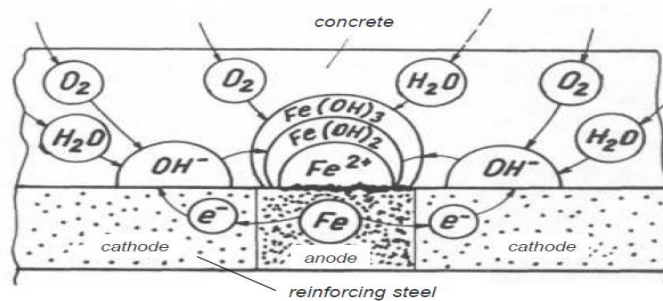
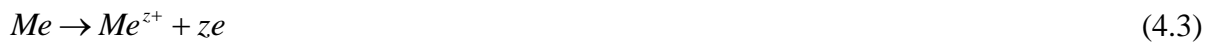


Figure 4.4: Formation of corrosion microcell in concrete (reproduced from Czarnecki *et al.* 2010).

The corrosion types can be classified in different ways based on the corrosion mechanism, final damage appearances, environment induced corrosion, etc. The classification of corrosion types is not absolute and the definition of corrosion type can only be applicable under certain conditions (Song & Shayan, 1998). Corrosion types according to corrosion mechanisms are described in this section.

4.2.1. Uniform corrosion

When the distance between the anodic and cathodic areas is small uniform corrosion is typically the effect. It is common in carbonated concrete structures since the carbonation of concrete normally proceeds in all the exposed areas of concrete structure and the decrease of pH value would be expected over a relatively large area. Oxygen is also available over the

Reinforcement Corrosion Mechanism and Measurement Methods

exposed area. As a result, anodic and cathodic area may possibly be distributed over the rebar surface (Song & Shayan, 1998).

4.2.2. Galvanic corrosion

In reality it is often impossible to form uniform corrosion over the whole length of rebar because of concrete heterogeneity. Depending on the exposure types, the cathodic process in most sites is stronger than the anodic process, while at some sites anodic reaction can be faster than the cathodic reaction (Broomfield, 2007). Higher cathodic and anodic ratios will also produce more concentrated corrosion damage to the rebar. In large dimensioned concrete structures, galvanic corrosion plays an important role because of the fact that the oxygen, carbonation and chloride attack simultaneously and the possible breakdown of passive film is not constant over the total length of rebar (Song & Shayan, 1998).

4.2.3. Localized corrosion

The corrosion damage morphology can be referred as the localized corrosion. It can also be classified as pitting or crevice corrosion. In this case the anodic to cathodic area ratio is very small (localized corrosion), but the corrosion penetration rate in the anodic area is relatively higher (Broomfield, 2007). Localized corrosion mostly happens due to the chloride attack in concrete on some particular sites. In this case, the chloride ions tend to accumulate in the affected/pit area and the pH of the solution decrease drastically, so the environment in the pit area becomes aggressive; this in turn further accelerates the anodic dissolution of steel in the pits. The loss of rebar cross-section and strength is a major concern for pitting corrosion. Therefore, a relatively small amount of pitting corrosion can induce significant damage to the reinforcement (Song & Shayan, 1998) due to the localised damage and reduction of the cross-section.

4.3. Methods of corrosion rate determination in concrete

Information regarding the corrosion rate of steel bars is an important parameter for the evaluation of the service life as well as the required repair pattern (extensive or normal) of any RCS. Measuring the real corrosion rate in steel is a difficult task. Currently there are several methods to measure the corrosion potential and/or rate of steel in concrete and some of them are discussed in this section.

4.3.1. Half-cell potential (HCP) method

The half-cell potential (HCP) measuring technique is a standard method for the inspection of corrosion probability in reinforced concrete structures as set out by the American National Standards (ASTM C876). Typically two types of half-cell, namely a copper-copper sulphate electrode (CSE) and a silver-silver chloride electrode (SCE) are used to measure the corrosion potential (E_{corr}) in millivolt (mV). The test is limited by the fact that a direct connection to the reinforcing steel has to be made. It is also only applicable to uncoated

Reinforcement Corrosion Mechanism and Measurement Methods

reinforcing steel imbedded in concrete where the surface has not been coated with a dielectric material. The half-cell is composed of an unreactive outer sleeve with a copper rod that is suspended in a saturated solution of copper sulphate. A saturated solution is maintained by ensuring that un-dissolved crystal copper sulphate is visible in the distilled water solution within the half-cell. The tip of the half-cell (also referred to as a reference electrode) is made of a porous material, normally wood or ceramic, which allows it to remain wet by capillary action. The half-cell is connected as illustrated in Fig 4.5 and a voltmeter is used to measure the potential difference between the steel and the reference electrode.

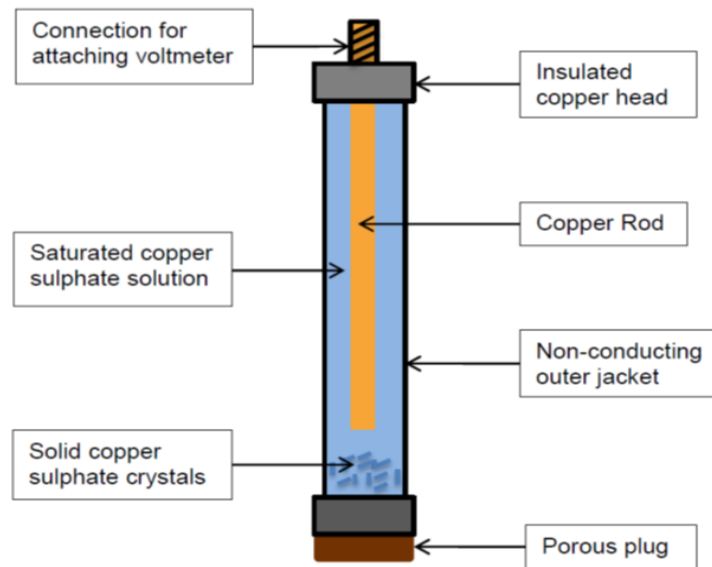


Figure 4.5: A representation of CSE half-cell with different components.

Table 4.2: Corrosion condition related to half-cell potential (ASTM C876)

Corrosion potential (E_{corr}) values		Corrosion probability (%)
(mV vs. SCE*)	(mV vs. CSE ⁺)	
$E_{corr} > -125$	$E_{corr} > -200$	10 (low risk of corrosion)
$-126 \leq E_{corr} \leq -275$	$-200 \leq E_{corr} \leq -350$	Intermediate
$E_{corr} < -276$	$E_{corr} < -350$	90 (high risk of corrosion)
$E_{corr} < -426$	$E_{corr} < -500$	Severe corrosion

Note: *Ag/AgCl and ⁺Cu/CuSO₄ half-cell

The potential value measured can only be used to give a general indication of the probability of corrosion activities. The measurements are interpreted according to Table 4.2. It must be noted that certain conditions may arise where potential readings will reflect values more negative than -350 mV without having significant corrosion activity occurring. This may be as a result of a polarisation phenomenon created by limited oxygen diffusion. Also Table 4.2 is only applicable for NC, and it has not been calibrated for SHCC. So these potential ranges may not be suitable for SHCC since the matrix compositions are not the same as in NC. Concrete resistivity is depended on matrix properties and the HCP reading is influenced by

 Reinforcement Corrosion Mechanism and Measurement Methods

the resistivity. Also a significant difference may be seen in the potential value when cracks are present as salt water penetrates through the cracks in concrete which also has not been calibrated before.

4.3.1.1. Factors influencing HCP reading

As mentioned before, the HCP reading in concrete can be more negative/higher than the typical range of potential values recommended by the ASTM. This is due to the fact that the polarisation phenomenon is significantly affected by the slow oxygen diffusion in concrete (Arup, 1983; Gu & Beaudoin, 1998). A study by Gu & Beaudoin (1998) summarized a number of factors influencing the HCP reading and suitability of following ASTM guidelines in determining the corrosion probability of steel in concrete as shown in Table 4.3.

Table 4.3: Effect of different factors on HCP readings and corrosion probability (Gu & Beaudoin, 1998)

Conditions	HCP reading	Rate of corrosion in steel bar	Applicable to ASTM C876
Lower oxygen	to negative	may not increase	no
Carbonation/lower pH	to negative	increase	yes
Higher chloride	to negative	increase	yes
Anodic corrosion inhibitor	to positive	decrease	yes
Cathodic corrosion inhibitor	to negative	decrease	no
Mixed corrosion inhibitor	to positive or negative	decrease	no
Epoxy-coated rebar	to positive	not related	no
Galvanized rebar	to negative	not related	no
Dense concrete cover	to negative	not related	no
Concrete resistance	to positive	not related	no
Dry concrete	to positive	not related	no
Coating and sealers	to positive	not related	no
Concrete repair patch	to positive or negative	not related	no

Various factors such as oxygen, corrosion inhibitors, carbonation, epoxy coating in steel, types of steel, concrete density, etc. significantly influence the HCP reading. Insufficient oxygen in concrete causes steel to become more active even if there is no sign of corrosion and as a result a more negative potential value may be obtained in concrete from a half-cell reading. HCP value can also be influenced by the higher density of the concrete layer above reinforcing steel. Dense concrete provides a strong barrier against chloride reaching the steel as well as limiting oxygen diffusion. Typically HCP readings are taken at a distance from the reinforcing steel which is inside the concrete at a depth varying according to the designed cover depth. In this case, the obtained HCP readings are actually of mixed potential. This implies that the cathodic region influences the potential readings and hence the readings are more negative than the actual potential near to the reinforcing steel (Montemor *et al.* 2003). Cusson & Qian (2009) concluded that if concrete permeability can be reduced the oxygen

Reinforcement Corrosion Mechanism and Measurement Methods

level the near reinforcing steel will also be reduced and this may cause more negative HCP readings in the steel bar.

4.3.2. Electrochemical Corrosion Test

As mentioned earlier, before the corrosion behaviour in concrete is an electrochemical process, and therefore the potential and current due to reduction/oxidation of reinforcing steel can be measured by electrochemical testing. There are several possible ways in which these two variables can be measured while all the techniques force a potential on the working electrode and measure the resulting current or vice versa. So, ultimately the corrosion process in RCS can be monitored by this technique without any destruction. It is due to the fact that all electrochemical tests follow some fundamental model of the electrode kinetics associated with corrosion processes to quantify corrosion rates. The magnification of the electrical signals created during these tests permits very precise and sensitive measurements to be carried out.

Some of the electrochemical corrosion testing techniques are listed below:

- Linear polarization resistance (LPR) measurements
- Potentiodynamic polarization curves (PPC)
- Electrochemical potentiokinetic reactivation (EPR) measurements for intergranular corrosion
- Current vs time curves (at a given potential)
- Electrochemical impedance spectroscopy (EIS)
- Transient techniques
- Electrochemical noise (EN) measurements

4.3.2.1. Polarization resistance technique

The polarisation resistance (R_p) technique may be considered to be the most encompassing and attainable method of measuring the rate of corrosion in steel at present. It has been used for nearly three decades with continuous improvements with respect to the accuracy of its application found in literature over the years. The method uses the measurement of the instantaneous corrosion current density i_{corr} ($\mu\text{A}/\text{cm}^2$), to determine the rate of degradation of a concrete structure affected by corrosion. However, the method is limited by not being able to quantify the loss of steel cross-section, but will be able to distinguish between areas of active and passive corrosion (Andrade & Alonso, 2004). The free corrosion potential (E_{corr}) as described in the section 4.3.1 and the electrical concrete resistance (R_e) are used to validate and add to the reliability of the method.

The most accurate setup required to measure the R_p effect is a so-called modulated guard ring technique. The setup is an improvement of the DC polarisation resistance measurement with ohmic drop that has been used since the 1970's. It comprises of a central reference electrode (RE) surrounded by two concentric electrodes, one acting as a counter electrode (CE) and the

Reinforcement Corrosion Mechanism and Measurement Methods

outer electrode as a guard electrode (GE). Fig 4.6 depicts the setup of the whole system. The steel reinforcing acts as the working electrode (WE) and is connected, with the other electrodes, to a potentiostat. The guard ring technique is further modulated by two reference electrodes between the CE and GE which help to control the polarisation of the electrodes and the concrete beneath them.

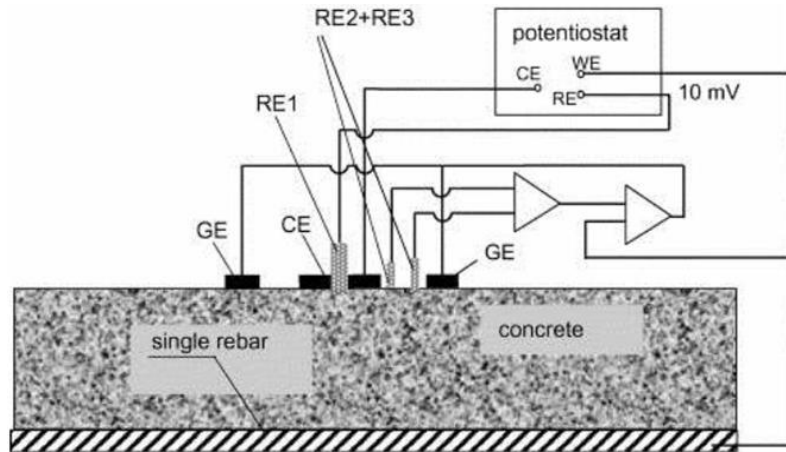


Figure 4.6: Modulated guard ring setup (imitative from Wojtas, 2004).

The greatest problem in obtaining reliable R_p measurements, and the cause for the need of the guard ring technique, is the non-uniform current distribution between the counter electrode and the steel reinforcing in the concrete (Wojtas, 2004). Fig 4.7 shows how the current will be distributed between a small counter electrode and the steel reinforcing when no guard ring is present. This distribution allows for a much larger area of steel to be polarised than the area right beneath the electrodes. This is a particular problem when localised corrosion occurs. It may yield elevated corrosion rates without actually having any corrosion occurring under the area of study, see Fig 4.8. It is because the polarization current is confined with a guard ring electrode. The confining effect ensures that the critical length of steel that the reference electrode is exposed to, is equal to the length of contact of the reference electrode itself. Fig 4.9 depicts the ideal current distribution when a modulated guard ring electrode is used.

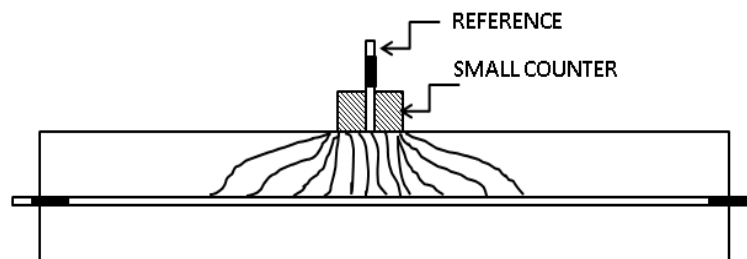


Figure 4.7: Non-uniform current distribution under small counter electrode (reproduced from Andrade & Alonso, 2004).

Reinforcement Corrosion Mechanism and Measurement Methods

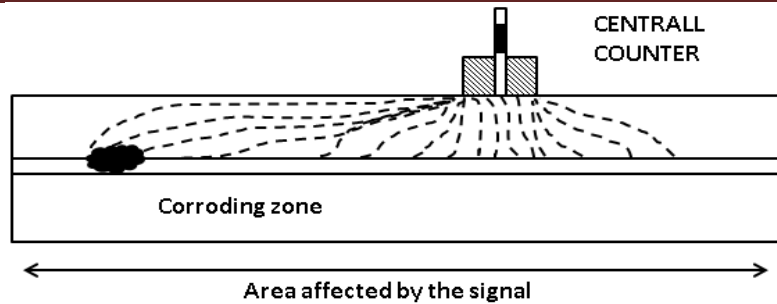


Figure 4.8: Effect of localised corrosion (reproduced from Andrade & Alonso, 2004).

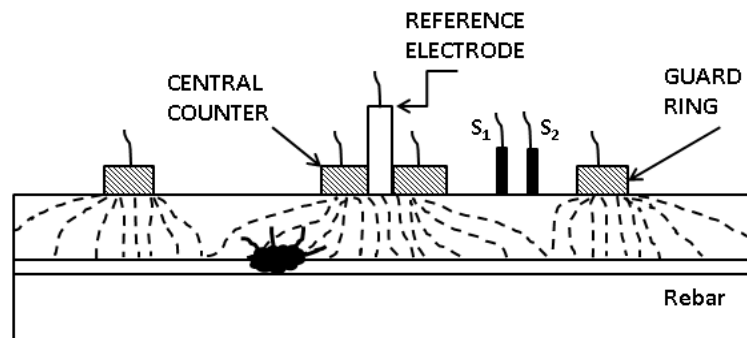


Figure 4.9: Confined current distribution by modulated guard ring (reproduced from Andrade & Alonso, 2004).

4.3.2.2. Potentiodynamic polarization curves (PPC)

The change of electrical potential measurement of a system is described by the PPC. In electrochemical corrosion testing, this term is often used in describing the polarization methods. It is a laboratory-based corrosion-measuring technique which helps provide valuable information regarding corrosion mechanism, rate and probability in selected environments (ASTM G61).

4.3.2.3. Electrochemical Impedance Spectroscopy (EIS)

Electrochemical impedance spectroscopy (EIS) is a corrosion measuring technique that works in the frequency domain. It postulates that an electrochemical interface, as found on the surface of corroding steel reinforcing, can be interpreted as a combination of electrical circuit elements such as resistance, capacitance and inductance. EIS has many advantages in comparison with other electrochemical techniques. During EIS experiments, an alternating voltage is applied to the elements and the resulting current is computed using Ohm's law. Therefore, it is a non-destructive method for the evaluation of a wide range of materials, including coatings, anodized films and corrosion inhibitors. It can also provide detailed information of the systems under examination; parameters such as corrosion rate, electrochemical mechanisms and reaction kinetics and detection of localized corrosion, can all be determined from these data (Hamdy *et al.* 2006). This method is still in a development

 Reinforcement Corrosion Mechanism and Measurement Methods

phase, but research has suggested that it gives a better insight into the corrosion process. It is stated that smaller interpretations are necessary to obtain results from EIS than for the polarisation resistance technique (Montemor *et al.* 2003). However, the application of EIS for on-site measurements is still very complex and not feasible (Andrade & Alonso, 2004).

4.3.2.4. Transient techniques

This method includes techniques such as the galvanostatic pulse technique (GPT) also called potentiostatic method and Coulostatic method. These methods work in the time domain and may be preferred because of the slow steel/concrete interface reactions (Montemor *et al.* 2003). The GPT is similar to the polarisation technique, however, a small current is applied to the reinforcing steel and the transient potential is then recorded. In this research work a Coulostatic method was used in determining the corrosion rate and detailed measuring techniques are described here.

In a Coulostatic method a known amount of small current (10 - 20 mA) is injected into the reinforced concrete for certain amount of time (< 10 mS) and then potential decay is observed for a few seconds. The potential decay due to corrosion of steel in concrete may be described by a Randles equivalent circuit shown in Fig 4.10. A Randles circuit entails an active electrolyte resistance (R_{Ω}) in series with the parallel combination of the double layer capacitance (C) and an impedance of a faradic reaction. This model can be used to calculate the Polarization resistance (R_p).

$$\eta_T = \Delta I R_{\Omega} + \Delta I R_p \left(\exp \left(\frac{-t}{\tau_c} \right) \right) \quad (4.4)$$

where: η_T is the total potential change in the working electrode (WE), $\Delta I R_{\Omega}$ is the ohmic drop between the WE and the reference electrode (RE) in the concrete, $\Delta I R_p$ is the effective polarisation at charging time, R_p is the polarisation resistance of the rebar, and τ_c is the Coulostatic time constant.

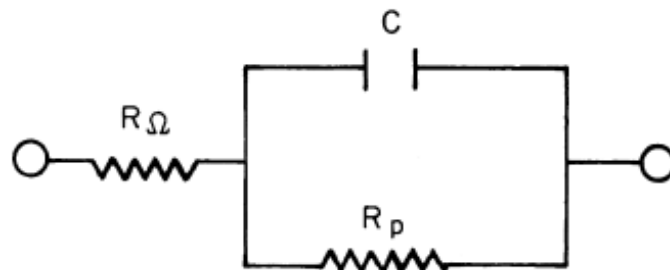


Figure 4.10: Randles equivalent circuit used to explain the reaction of a steel bar to the electrical signal (imitative from Gonzalez *et al.* 2001).

The moment current is disturbed the charge attained by the interfacial layer, also called double layer (it refers to two parallel layers of charge surrounding the object), is gradually

 Reinforcement Corrosion Mechanism and Measurement Methods

used in the corrosion reaction. Because the electrode potential immediately loses the ohmic drop (ΔIR_O) contribution, and its measurement expresses its actual polarisation. So during corrosion testing, if no further current is applied to the steel bar, the potential decays can be represented exponentially with time as follows:

$$\eta_t = \eta_0 \exp\left(\frac{-t}{\tau_c}\right) \quad (4.5)$$

where: η_t is the potential shift (ΔE) at time t and η_0 is the initial potential shift. Polarization resistance R_p is then obtained from the time constant (τ_c) and interfacial C as follows:

$$R_p = \frac{\tau_c}{C} \quad (4.6)$$

$$C = \frac{q_s}{A\eta_0} \quad (4.7)$$

$$q_s = \Delta i x \Delta t \quad (4.8)$$

$$I_{corr} = \frac{B}{R_p} \quad (4.9)$$

$$V_{corr} = 0.0116 I_{corr} \quad (4.10)$$

where: q_s is the amount of charge, Δi is the amount of current sent, Δt is the pulse duration. η_0 and τ_c values can be determined by drawing an exponential function is fitted to the perturbation (mV) vs time (sec) curve. A is steel surface area ($\pi d_s L_s$) and B is the Stern-Geary constant varying from 26 to 52 mV depending on the passive and active corrosion. In this research project the B value was considered to be 26 mV. This corrosion rate measuring technique was broadly explained by the Glass (1995), Gonzalez *et al.* (2001), Andrade & Alonso (2004) and Otieno *et al.* (2010).

Due to corrosion in steel bars, the consequences such as loss of rebar tensile resistance and pitting depths from this observation were then compared with the experimental outcomes. In this regard, Eqs (4.11), (4.12) and (4.13) estimate uniformly-corroded depth (d_c) with time, estimate mass loss with time $m_c(t)$ and change in rebar yield resistance due to cross section reduction (ΔF_y):

$$d_c(t) = d_{c0} + \int_0^t V_{corr} dt = d_{c0} + \sum_{i=1}^{N_t} \frac{1}{2} (V_{corr} + V_{corr,i-1})(t_i - t_{i-1}) \quad (4.11)$$

$$m_c(t) = \frac{\pi \rho_s L_s}{4} [d_s^2 - (d_s - 2d_c)^2] \quad (4.12)$$

Reinforcement Corrosion Mechanism and Measurement Methods

$$\Delta F_y(t) = \frac{\pi \sigma_y}{4} [d_s - 2d_c(t)]^2 \quad (4.13)$$

In these equations d_{c0} is the initial corroded depth, t_i corroding period, ρ_s is the steel density, L_s is the length of steel (here it was assumed to be 500 mm), d_s is the steel diameter and σ_y is the nominal yield stress of steel.

Researchers (Hassanein *et al.* 1998) suggest that the perturbations should be kept small (no more than ± 20 mV). However, with this particular test setup and the equipment being used, measurements of such small voltages can prove to be difficult. The large volume of unshielded material (concrete and steel) picks up a lot of high frequency, especially radio frequency noise. A typical set of raw data is shown in Fig 4.11. However, the high frequency noise can be filtered out effectively by taking a 10-20 points moving average, and the offset above zero can be corrected by subtracting the average value of all the data points before the start of the pulse, from all the data points in the record. This results in the graph shown in Fig 4.12 below. The vertical axis is millivolt (mV) and the horizontal axis is time in milliseconds (mS). Note that, because of the very low series resistance, the vertical wiggles before and after the upward sloping line is missing or very small. The upward sloping line indicates the charging of the internal capacitance. The perturbation range throughout the time of taking readings fell between 100 and 1500 mV which are higher than typical ranges found in normal concrete. This higher perturbation found in SHCC materials could be explained by the vastly different matrix when compared to normal concrete. Further, the higher resistivity, lower permeability and fewer voids found in SHCC materials might play a large role when the current is applied to the specimens. So far no research has been found where this method has been applied to R/SHCC materials.

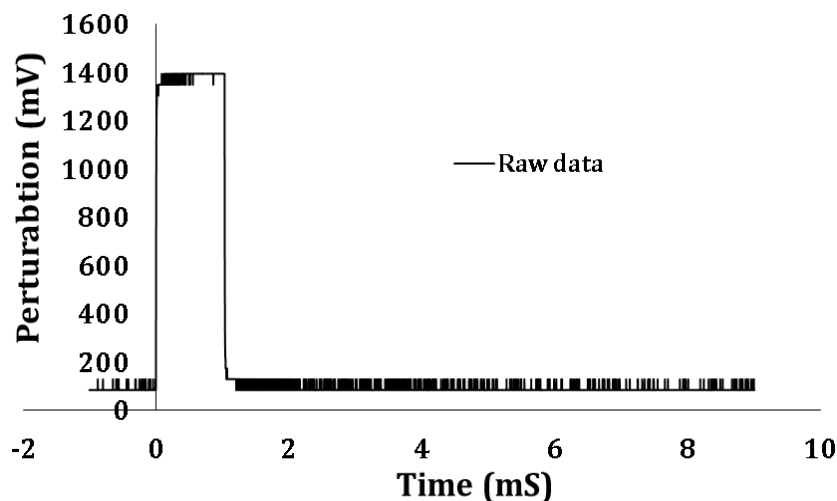


Figure 4.11: Magnified raw data of perturbation, recorded at about 1200 samples/second.

Considering Figs 4.11 & 4.12, where perturbation in mV and time in mS are represented on the vertical and horizontal axis respectively, it can be seen that when the pulse current is

Reinforcement Corrosion Mechanism and Measurement Methods

applied to the counter electrode (CE) the perturbation spikes and remains at this height for a specific time Δt until it drops suddenly once again. This sudden drop is called the ohmic drop (point *c* to *d*, on Fig 4.12) which is related to the concrete resistance and has no use for the calculation of corrosion rate. Fig 4.13 is a magnified image of the curve starting at point *d* in Fig 4.12 which is the only relevant part of the graph used for calculating. An exponential function is fitted to the curve as shown in Fig 4.13 from which η_0 and τ_c values can be determined.

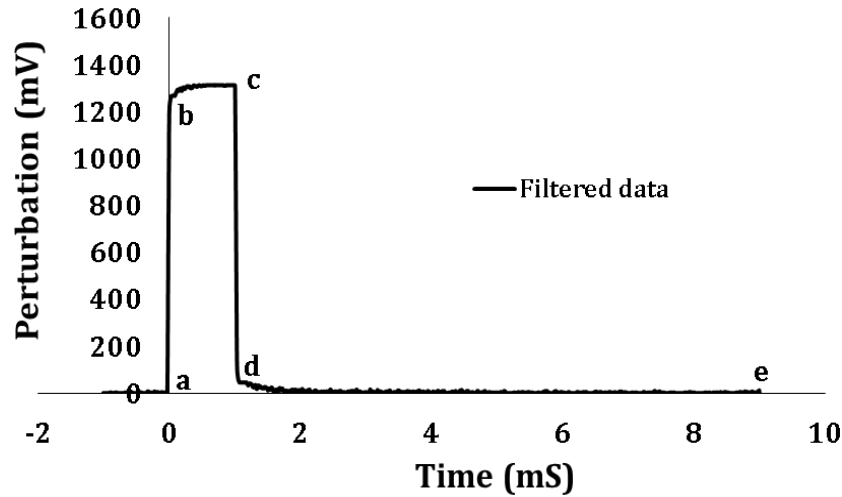


Figure 4.12: Filtered data for the raw record in Fig 4.11.

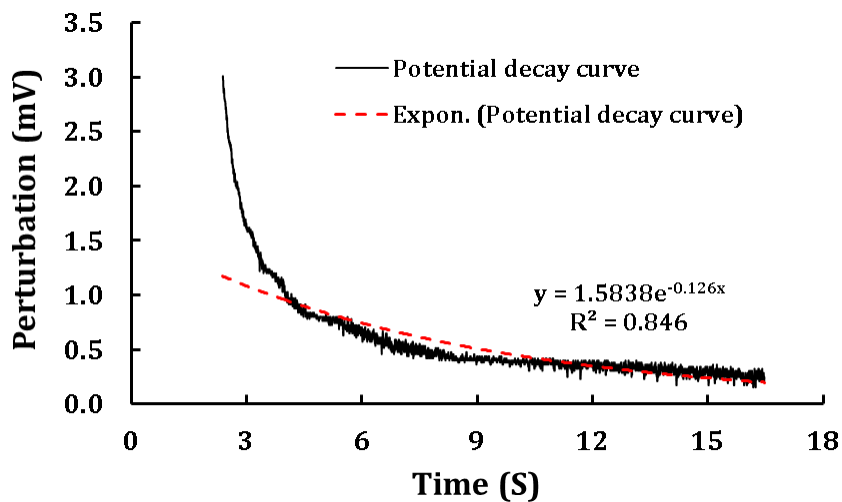


Figure 4.13: Exponential function fitted to the measured decaying voltage.

In this research work all capillary absorption and ponding specimens (details are discussed in Chapter 5) were cast using a Y10 (10 mm diameter) steel reinforcing bar acting as the WE. In case of capillary absorption specimens, a 15 mm thick and 120 mm long steel plate was used as a CE and placed on top of each specimen as seen in Fig 4.14 during corrosion measurement. A 5 mm diameter stainless steel bar with the same length of WE was used as a

Reinforcement Corrosion Mechanism and Measurement Methods

CE in all ponding specimens. In both types of specimens, an Ag/AgCl half-cell was used as the reference electrode (RE) as seen in Fig 4.15. For the corrosion rate measurement, the Spider8 data logger was used while in most specimens (except six) a current of 4 mA was applied to each of the specimens for a period of 5 mS by a laboratory-built current pulse generator.

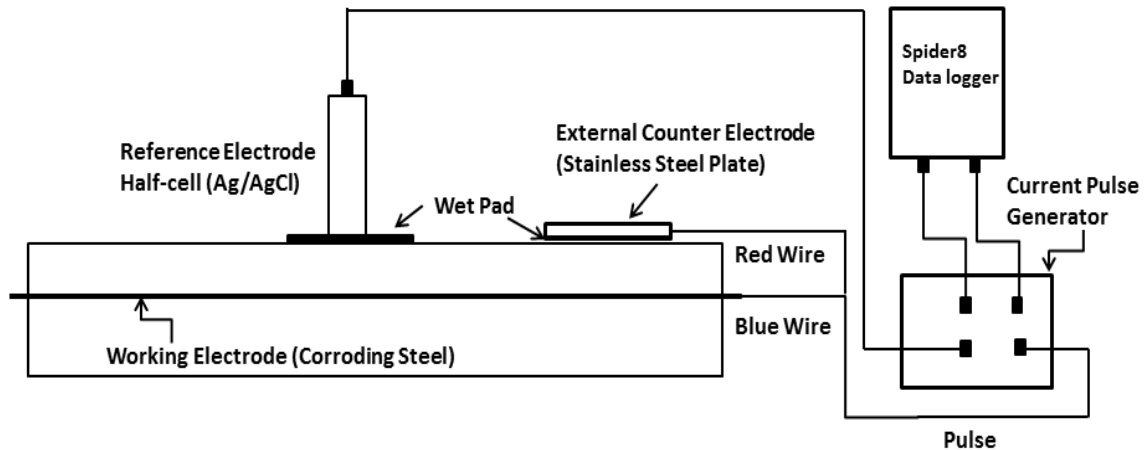


Figure 4.14: Corrosion rate measuring procedure using the Coulostatic technique in capillary absorption specimens.

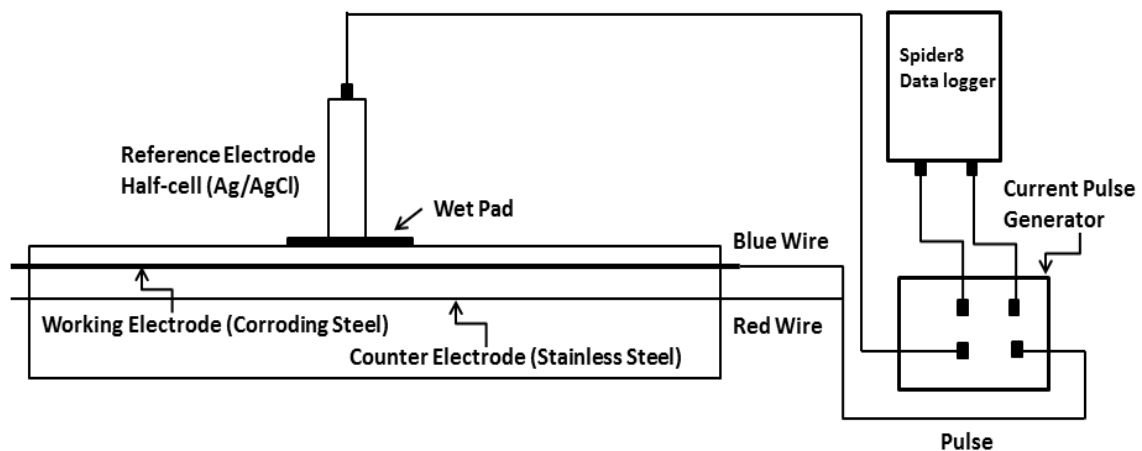


Figure 4.15: Corrosion rate measuring procedure using the Coulostatic technique in ponding specimens.

The corrosion part of this research work was divided into four parts based on exposures type, loading condition and forming cracks in the specimens and will be discussed broadly in Chapters 5 and 7. In series two of this research work, a total of six specimens with a cover depth of 15 mm (specimen's details are discussed in Chapter 5), a different current of 10 mA for a period of 6 mS were used. The reason was the very low perturbation when the applied current was 4 mA for a period of 5 mS in these specimens. Also it was difficult to have a good perturbation versus time curve because of limited available data produced from the

Reinforcement Corrosion Mechanism and Measurement Methods

specified current (4 mA) and time (5 mS) in these specimens. As a result a higher value of current for slightly longer time period was applied in these six specimens.

4.3.2.5. Ohmic drop (*iR* drop)

Ohmic potential drop also known as *iR* drop (as shown in Fig 4.12) is potential drop due to solution resistance which is the difference in potential required to move ions through the solution. The *iR* drop effects will become more evident when the applied current is increased. *iR* drop can be minimized by placing the RE tip as near to the WE as possible. Another way to reduce the *iR* drop is to apply a smaller current.

4.4. Advantage and disadvantage of using a Coulostatic method

As mentioned earlier, until now no research was found on SHCC where a Coulostatic method was used to measure the corrosion rate. Therefore, from this research work the author has discovered the following advantages and disadvantages of using this method in SHCC:

Advantages:

- Easy and quick. In less than 1 minute readings can be obtained on corrosion rate using this method.
- The instrument set-up is quite simple.
- It is a less expensive way of measuring corrosion rate. A laboratory version of the Coulostatic equipment could be developed for about \$1000, apart from the computer and data collection equipment.

Disadvantages:

- It is not an automatic way of determining the corrosion rate such as Gecor (Tang *et al.* 2001). Manually a potential vs time curve needs to be drawn from the recorded data in the data logger and then the exponential curve is drawn to get the initial potential shift (η_0) and time constant (τ_c) for Eq (4.17).
- Much attention must be given to carefully connecting all the cables with CE, WE and in establishing good contact between the concrete surface and that of the half-cell as shown in Figs 4.14 & 4.15.

4.5. Important notes before using a Coulostatic method

Some notes have been made by the author for future work before using a Coulostatic method:

- It is preferable that the cable connection with the CE and WE should be done before casting concrete and left in position throughout the tests series. Sometimes the results might have some errors due to loose connections. However, in this research work all the connections were checked each time for the next reading. Care was taken before

Reinforcement Corrosion Mechanism and Measurement Methods

taking any reading by checking all the connections, cleaning the part of the steel bar where cable connections were made, etc. Poor connections may lead to strange potential vs time curve responses as shown in Figs 4.16 & 4.17. If this problem occurs, all the connections need to be checked carefully and the reading should be taken again.

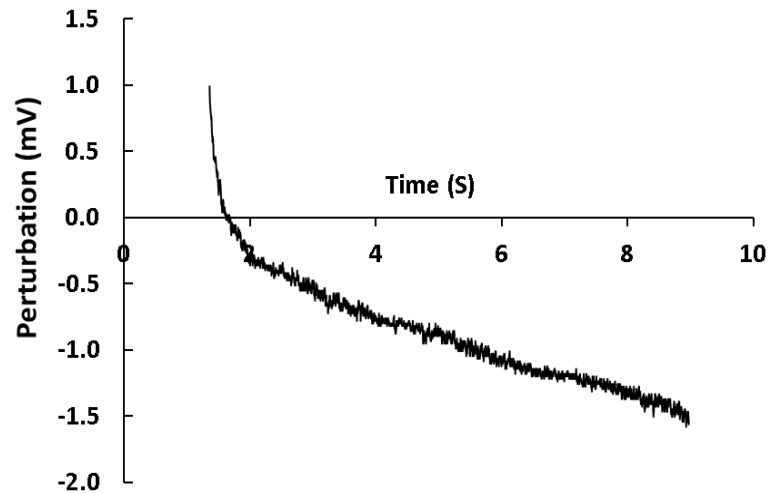


Figure 4.16: Downward response of perturbation vs time curve due to faulty connections in a Coulostatic method.

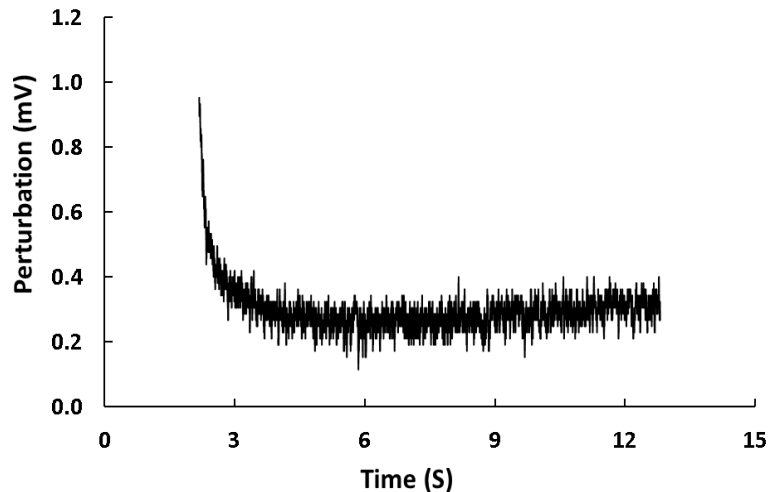


Figure 4.17: Upward response of perturbation vs time curve due to faulty connections in a Coulostatic method.

- Since a small current is applied for a short period, the data logger must have higher resolution and logging frequency to pick up the response (potential vs time) from the specimen. The smoothness of this curve is dependent on the number of data points logged over the short time period. This is important for fitting an exponential curve to the measured potential vs time curve. In this research, a maximum of 1200 readings

Reinforcement Corrosion Mechanism and Measurement Methods

per second were used. For lower values like 600 and 800 readings per second (600 – 800 Hz), a noticeable difference was observed in the exponential curve.

- It is also preferable to insert the CE inside the concrete to avoid any possible loss of applied current. In case of an outer CE, attention needs to be given to better contact between the CE and concrete surfaces. A wet pad should be used (preferably wet with NaCl solution) in between the CE and concrete surface for making better contact.

4.6. Possible protective measures against corrosion of steel in concrete

Protection methods such as using epoxy coating, stainless steel and non-metallic reinforcement can also influence the deterioration process in concrete. A brief discussion in this regard is given in this section.

4.6.1. Organic and metal coating on steel bars

Organic coatings such as epoxy resins may constrain the movement of oxygen and dangerous ions on the surface of steel bars inside the concrete and may delay the corrosion process. Like epoxy, hot dipped metal zinc coating also resists steel corrosion. However, these methods are expensive and may not be suitable for large construction work. It may also influence bond characteristics by changing the mechanical behaviour in structural response to actions (Selvaraj & Bhuvaneshwari, 2009).

4.6.2. Corrosion inhibitors

Steel protection by corrosion inhibitors can be done by either the inhibition of the anodic dissolution of iron or by the inhibition of cathodic reduction of oxygen. Chromium and nickel in combination with iron and oxygen form a protective oxide immune to chloride, thus preventing chloride-induced corrosion of steel (Sandberg, 1995).

4.6.3. Non-metallic reinforcement in concrete

Fibres, such as glass, aramid or carbon fibre embedded in polymers can be used as a non-metallic reinforcement in concrete. However, the use of this type of reinforcement is limited due to its lower E-mod and typically lower bond with concrete (Sivakumar & Santhanam, 2007).

4.6.4. Stainless steel in concrete

The probability of corrosion in high alloy stainless steel is much lower because of the presence of chloride-resisting oxide such as Cr_2O_3 and other corrosion resistant oxides (Sandberg, 1995). However, the use of stainless steel as the main reinforcement in concrete structures will be much more expensive.

4.7. Concluding summary

In this Chapter details of corrosion mechanisms such as how they take place inside concrete and the parameters which contribute to the corrosion process, are described. Indeed it is a difficult task to measure the actual damage in steel due to corrosion. However, using the corrosion measuring techniques described in this chapter, it is possible to estimate the possible damage in steel due to corrosion. Of course the results obtained from different methods may be different but they may be sufficient to represent the corrosion damage with acceptable reliability for decision on repair. Future research would be helpful to link these different corrosion methods. The Coulostatic technique which is used in this research is a simple way of measuring the corrosion rate and it is already acknowledged by many researchers. In this technique, as only a small amount of current is applied to the CE, it is assumed that no disturbance of electrons happens inside the steel bar which may contribute to the wrong calculation of the corrosion rate. As mentioned in Chapters 2 and 3, where researchers have applied large voltages (up to 60 Volt) which actually accelerate the real corrosion mechanism of a steel bar inside concrete and the corrosion rates reported from these tests are not real corrosion damages for a particular exposure condition (Sahmaran *et al.* 2008; Mihashi *et al.* 2011). In this regard, corrosion rate using a Coulostatic technique may be considered to be more representative of the real corrosion damage in steel. Some further improvements might be necessary to improve the corrosion rate measurement using Coulostatic technique. One of them may be the inclusion of guard ring as it seems to be important as described in Section 4.3.2.1. Future research will be helpful in this regard.

4.8. References

- Andrade, C & Gonzalez, JA 1978, 'Quantitative measurements of corrosion rate of reinforcing steels embedded in concrete using polarization resistance measurements', *Werkstoffe und Korrosion*, vol. 29, pp. 515-519..
- Andrade, C & Alonso, C 2004, 'Test Methods for on-site corrosion rate of steel reinforcing in concrete by means of the polarization resistance method', *Materials and Structures*, vol. 37, no. 9, pp. 623-643.
- Arup, H 1983, *Corrosion of reinforcement in concrete construction*, Page et al (eds), The royal society of chemistry, London, UK, p: 151.
- ASTM Standards 1999, *Half-Cell Potentials of Uncoated Reinforcing Steel in Concrete*, in ASTM Standards.
- ASTM C876 1999, *Standard test method for half-cell potentials of uncoated reinforcing steel in concrete*, in ASTM Standards.
- ASTM Standard G61, *Test methods for conducting cyclic potentiodynamic polarization measurements for localized corrosion susceptibility of iron, nickel or cobalt-based alloys*, In ASTM Standards.
- ASTM International 2003, *Flow Table for Use in Tests of Hydraulic Cement*, in ASTM International.

Reinforcement Corrosion Mechanism and Measurement Methods

Bertolini, L, Elsener, B, Pedferri, P & Polder, RP 2004, Corrosion of Steel in Concrete, WILEY-VCH Verlag GmbH & Co. KGaA, Weinheim, ISBN: 3-527-30800-8.

Broomfield, JP 2007, Corrosion of steel in concrete understanding, investigating and repair, 2nd edition, Taylor & Francis, USA & Canada.

Carino, NJ & Clifton, JR 1995, Prediction of cracking in reinforced concrete structures, Building and Fire Research Laboratory National Institute of Standards and Technology (NISTIR 5634), U.S. Department of Commerce, Gaithersburg, MD 20899.

Cement Concrete & Aggregates Australia 2009: Chloride resistance of concrete, pp. 37.

Cusson, D & Qian, S 2009, 'Ten-year field evaluation of corrosion inhibiting systems in concrete bridge barrier walls', ACI Materials Journal, vol. 106, no. 3, pp. 291-300.

Czarnecki, L, Loukowski, P, Garbacz, A & Chimielewska, B 2010, 'Corrosion of construction materials', *CHEMIK*, vol. 64, no. 9, pp. 573-582.

Fib Bulletin 3: 1999, Structural concrete- Textbook on behaviour, design and performance, vol. 3.

Ekstrom, T 2000, 'Leaching of concrete experiment and modelling', Licentiate thesis report TVBM-7153, Division of Building Materials, Lund Institute of Technology.

Glass, GK 1995, 'An assessment of the coulometric method applied to the corrosion of steel in concrete', Corrosion Science, vol. 37, no. 4, pp. 597-605.

Gonzalez, JA, Cobo, A, Gonzalez, MN & Feliu, S 2001, 'On-site determination of corrosion rate in reinforced concrete structures by use of galvanostatic pulses', Corrosion Science, vol. 43, pp. 611-625.

Gu, P & Beaudoin, JJ 1998, Obtaining effective half-cell potential measurements in reinforced concrete structures, National Research Council of Canada, Construction Technology Update No.1, ISSN 1206-1220.

Hamdy, AS, El-Shenawy, E & El-Bitar, T 2006, Electrochemical Impedance Spectroscopy Study of the Corrosion Behavior of Some Niobium Bearing Stainless Steels in 3.5% NaCl', International Journal of Electrochemical Science, vol. 1, pp. 171-180.

Hansson, CM, Poursace, A & Jaffer, SJ 2007, Corrosion of reinforcing bars in concrete, R&D serial No. 3013a, Portland Cement Association, Skokie, Illinois, USA, 33 pages.

Hassanein, AM, Glass, GK & Buenfeld, NR 1998, 'The use of small electrochemical perturbations to assess the corrosion of steel in concrete', NDT&E International, vol. 31, no. 4, pp. 265-272.

Langford, P & Broomfield, J 1987, 'Monitoring the corrosion of reinforcing steel', Construction Repair, vol. 1, no. 2, pp. 32-36.

Little, BJ & Lee, JS 2007, Microbiologically influenced corrosion, John Wiley & Sons, Inc., Hoboken, New Jersey.

Li, Z, Leung, C & Xi, Y, 2009. Structural renovation in concrete, Book published by Taylor & Francis, NY, USA, ISBN 0-203-93136.

Reinforcement Corrosion Mechanism and Measurement Methods

Liu, Y & Weyers, RE 1998, 'Modelling the time-to-corrosion cracking in chloride contaminated reinforced concrete structures', *ACI Materials Journal*, vol. 95, no. 6, pp. 675-681.

Makita, M, Mory, Y & Katawaki, K 1989, Marine corrosion behaviour of reinforced concrete exposed at Tokyo Bay, *ACI, SP-65, In Performance of Concrete in Marine Environment*, Detroit, Michigan, pp 271-290.

Mihashi, H, Ahmed, SFU & Kobayakawa, A 2011, 'Corrosion of reinforcing steel in fibre reinforced cementitious composites', *Journal of Advantage Concrete Technology*, vol. 9, no. 2, pp. 159-167.

Mohammed, TU, Otsuki, N, Hamada, H & Yamaji, T 2002, 'Chloride-induced corrosion of steel bars in concrete with presence of gap at steel-concrete', *ACI Materials Journal*, vol. 99, no. 2, pp. 149-156.

Montemor, MF, Simoes, AMP & Ferreira, MGS 2003, 'Chloride-induced corrosion on reinforcing steel: from the fundamental to the monitoring techniques', *Cement & Concrete Composite*, vol: 25, pp. 491-502.

Otieno, MB, Alexander, MG & Beushausen, HD 2010, 'Corrosion in cracked and un-cracked concrete influence of crack width, concrete quality and crack reopening', *Magazine of Concrete Research*, vol. 62, no. 6, pp. 393-404.

Okada, K & Miyagawa, T 1989, Chloride Corrosion of Reinforcing Steel in Cracked Concrete, *ACI, SP-65, In Performance of Concrete in Marine Environment*, Detroit, Michigan, pp 237-254.

Rooij, MR, Schlangen, E & Joseph, C 2013, *Self-healing phenomena in cement-based materials*, Springer publication, ISBN 978-94-007-6623-5.

Sandberg, P 1995, Critical evaluation of factors affecting chloride initiated reinforcement corrosion in concrete, Report TVBM-3068, University of Lund, Sweden, ISRN LUTVDG/TVBM-95/3068-SE(1-116).

Sahmaran, M, Li, VC & Andrade, C 2008, 'Corrosion resistance performance of steel reinforced engineered cementitious composite beams', *ACI Materials Journal*, vol. 105, no. 3, pp. 243-250.

Selvaraj, R & Bhuvaneshwari, B 2009, Characterization and development of organic coatings for steel rebars in concrete, *Portugaliae Electrochimica Acta*, vol. 27, no. 6, pp. 657-670. DOI: 10.4152/pea.200906657.

Song, G & Shayan, A 1998, Corrosion of steel in concrete: causes, detection and prediction, A state-of-the-art review, *ARRB Transport Research Ltd, Review Report 4*.

Sivakumar, A & Santhanam, M 2007, 'Mechanical properties of high strength concrete reinforced with metallic and non-metallic fibres', *Cement & Concrete Composite*, vol. 29, no. 8, pp. 603-608.

Tang, L, Frølund, T, Skoglund, P & Fedjstød, P 2001, Calibration of the Electrochemical Methods for the Corrosion Rate Measurement of Steel in Concrete, Nordtes project No. 1531-01, SP Swedish National Testing and Research Institute, Borås, Sweden.

Reinforcement Corrosion Mechanism and Measurement Methods

Tutti, K 1982, 'Corrosion of steel in concrete', Swedish Cement and Concrete Research Institute, vol. 82-84 of CBI research, pp. 468.

Vennesland, Ø & Gjørsv, OE 1981, Effect of cracks in submerged concrete sea structures on steel corrosion, *Material Performance*, pp: 49-51.

Winter, N 2009, *Understanding Cement*, WHD Microanalysis Consultants Ltd, UK.

Wojtas, H 2004, Determination of corrosion rate of reinforcement with a modulated guard ring electrode analysis of errors due to lateral current distribution', *Corrosion Science*, vol. 46, pp.1621-1632.

Chapter 5

Definiteness of purpose is the starting point of all achievement.

–W. Clement Stone

Experimental Methodology

5. General discussion

The main objective of this research was to monitor the corrosion rate in cracked R/SHCC and R/mortar specimens due to chloride attack. It is very important for the engineer or designer to know whether SHCC can protect steel from corrosion or what will be the corrosion rate of steel if chloride or any other chemical substance enters the reinforced structure where SHCC is being used. For this purpose, a significant number of different types of SHCC and mortar specimens were made and tested, and this maps out the way all the experiments were designed and conducted to achieve the aforementioned research objectives. The types of materials, mix designs and test procedures for obtaining the research results are highlighted here.

Over the whole period of this research, the properties of local materials such as cement and sand changed when new batches of these materials, collected from the local providers were used. As a result, the initial mix design of the matrix had also to be adapted slightly for every new batch of materials. Therefore a number of different mix designs were used to achieve the goal of this research as is discussed later in this chapter. The mechanical properties of the matrix made from different mixes were determined by means of different strengths (compressive, flexural and tensile), E-mod, cracks and fracture-energy tests and different types, sizes and shapes of specimens were used which are also discussed here. In determining the durability properties such as the chloride profile and content, the corrosion rate and freeze-thaw testing of SHCC and mortar, the research program was divided into four series based on their different mix designs, exposure types, loading conditions and specimen sizes. Details of these durability property tests are discussed broadly in this chapter. Note that part of this research was performed in collaboration with the Federal Institute for Materials Research and Testing (BAM), Germany. Since the ingredient material properties in Germany and South Africa vary the mix design which was used in South Africa was adjusted slightly and this has also created a separate series of work (as defined by series four).

5.1. Type of materials used

SHCC is different from conventional concrete that is typically used in modern RCS. Conventional concrete consists of a large volume of coarse aggregate (up to a size of 25 mm)

Experimental Methodology

which plays a key role because of its major mechanical properties. On the other hand, SHCC is a sensitive composite which requires finely-graded sand (in most cases up to a size of 0.30 mm) and a large volume of binder such as cement, fly-ash, or slag. In addition micro fibres such as PVA and high molecular weight PE are key ingredients in achieving the strain-hardening behaviour in SHCC. The details regarding the materials which were used in this research work and their properties are discussed below.

5.1.1. Cement and fly-ash

Ordinary Portland Cement (CEM I 42.5 and 52.5 under the brand PPC, South Africa) and class F Fly-ash were used as the main binders in SHCC. Some of the oxide compositions of the CEM I 52.5 cement and fly-ash are shown in Table 5.1. The quantities of the typical constituents of Portland cement CaO, SiO₂, and Al₂O₃ are respectively 61-67%, 19-23% and 2.5-6% by total weight. The chemical analysis of various fly ashes has indicated a wide range of compositions, reflecting wide variations in the coal used in power plants over the world (Berry, 1976). In the US, a typical chemical analysis for low-calcium fly ashes (>10% CaO), usually formed by the combustion of bituminous coal, shows SiO₂ content of 45–65%, Al₂O₃ at 20–30% and Fe₂O₃ at 4–20%. The high-calcium fly ashes (<10 % CaO) formed by the combustion of subbituminous and lignite coal typically contain 20–50% SiO₂, 15–20% Al₂O₃ and 3–5% Fe₂O₃ (Mehta, 1994; Cabrera & Hopkins, 1982; ACI Committee 226).

Table 5.1: Oxide compositions (% of total wt) of different materials used in the research

Type	Cement CEM I 52.5	Fly-ash	Fine sand	Coarse sand
MgO	0.00	0.00	0.81	0.00
Al ₂ O ₃	0.91	9.28	0.60	1.17
SiO ₂	9.36	28.69	50.58	53.25
K ₂ O	0.59	0.62	0.14	0.10
CaO	59.93	4.04	0.91	0.89
TiO ₂	0.08	1.47	0.41	0.19
MnO	0.07	0.00	0.00	0.00
FeO ₃	2.56	3.10	0.22	0.21
CuO	0.00	0.01	0.00	0.00
ZnO	0.00	0.01	0.00	0.00

5.1.2. Sand

Two types of locally available natural sand called fine grain Phillippi sand (graded to ASTM F95) (FS) (size up to 0.30 mm) with fineness modulus (FM) of 1.9 and Malmesbury coarse sand (CS) (size up to 2.36 mm) with FM of 3.3 were used in this research. In some of the experiments, the results of SHCC made from FS were also compared with those of SHCC made from CS. The particle size distributions of these two types of sand are shown in Fig 5.1.

Experimental Methodology

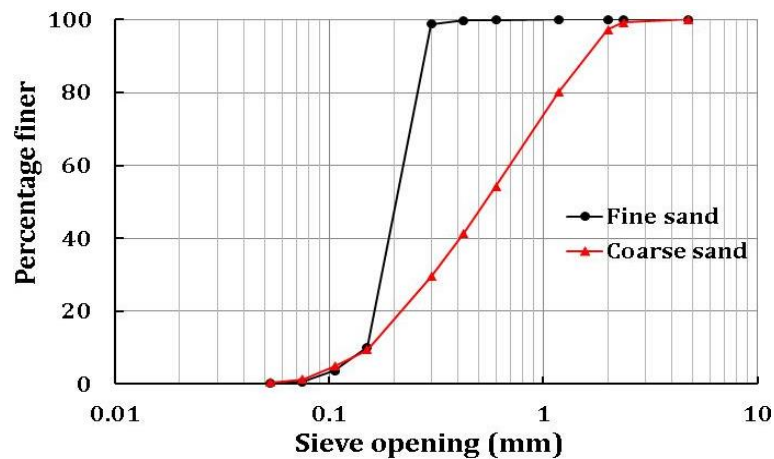


Figure 5.1: Grading of fine and coarse sand used in this study.

5.1.3. Fibre

Various kinds of fibre for improving the quality as well as the durability of concrete structures have been introduced during the last few decades. One of the relatively new types of fibre for construction materials is called Polyvinyl Alcohol (PVA) with the product name REC15, which has been developed for SHCC materials. Mostly high-molecular weight PE and PVA fibres have been used in SHCC in the last decade of research on SHCC. PE fibre is significantly more expensive than PVA, and as a result PVA fibres supplied by Kuraray Co. Ltd. of Japan were used here in this research work. Fibre specifications can be found in Table 5.2.

Table 5.2: Properties of PVA fibre used (Ogawa & Hoshiro, 2011)

Type	Length (mm)	Diameter (mm)	Tensile strength (MPa)	E-mod (GPa)	Elongation capacity (%)	Density (g/cm ³)
REC 15 Polyvinyl alcohol (PVA)	12	0.04	1600	41	6.5	1.30

5.1.4. Water

Impurities in mixing water might play an important role in concrete setting time, volume change as well as in the corrosion of steel bars. In this research work, normal tap water (potable water) was used.

5.1.5. Supporting materials

Dynamo SP1 super plasticizer (SP) was used as an admixture which is based on modified acrylic polymer supplied by MAPEI South Africa. To prevent segregation of a mix with a high w/c ratio, a viscosity-modifying agent (VMA) was used together with an air-entraining

Experimental Methodology

agent (AEA) to ensure good fibre distribution and the associated formation of multiple cracks in SHCC. Note that VMA and AEA were supplied by CHRYSO and MAPEI South Africa.

5.1.6. X-ray fluorescence (XRF) for detecting elements in the different materials

As explained in Chapter 2 the chemical composition of cement and fly-ash influences the bonding behaviour between the surface of PVA fibre and the cement particles, therefore the major chemical elements in cement, fly-ash, FS and CS were detected by XRF and it is shown in Figs 5.2a&b. As it is known that the chemical compositions of different materials depend on their source and concrete durability is also depended on the materials chemical composition. Although this was not the focus of this research and it remains for the further studies related to the influence of types of materials on durability of SHCC. However, author believes this figure will be very useful if someone consider studying chemical compositions of different materials and their influence on the durability of SHCC. The highest amplitude (count/sec) of Ca and Fe were observed in cement and fly-ash. In CS, slightly more Si was found than in FS. Note that apart from the elements shown in Figs 5.2a&b, there are many more elements that were detected by the XRF. However, the amounts of those elements were quite low when compared to those of the elements shown in the figures, and as a result they have not been shown here.

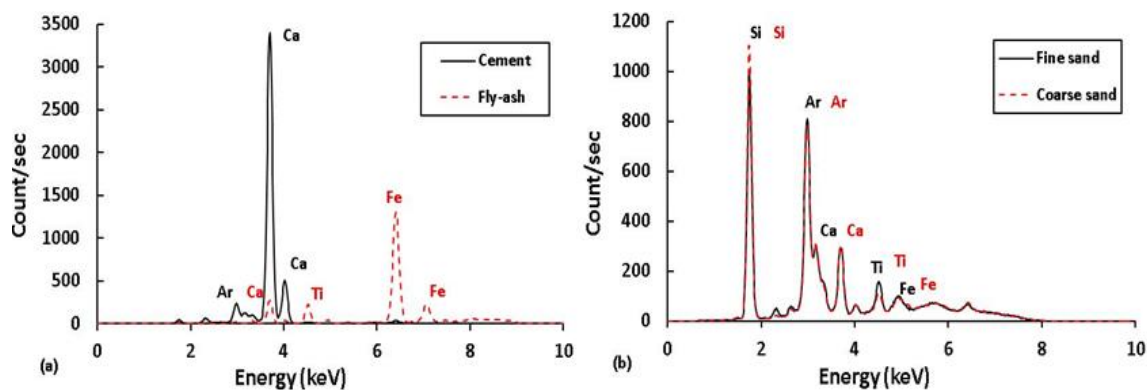


Figure 5.2: Different elements, peak amplitude (count/sec) in (a) cement and fly-ash and in (b) FS and CS detected by XRF.

5.2. Mix design of SHCC and mortar

To achieve the ductile behaviour of SHCC, it is necessary to have a carefully designed mixture. In this research, a total of 18 mix designs were made for both SHCC and mortar made with FS and CS and they are shown in Table 5.3. Note that in some cases for the same mix design of SHCC, different cement types were used and were classified as different SHCC (e.g. FS2, FS31, and FS32) in Table 5.3. The mixes were not specifically designed for this research program, but are typically used in the research group in Stellenbosch. A part of this research (series four) was carried out in a different laboratory in Germany (Federal Institute for Material Research and Testing, BAM) where the materials were different than the materials in South Africa. As a result, the mix design was slightly adjusted.

Experimental Methodology

Table 5.3: Amount of materials (kg/m^3) used in this research

Type	Id*	Cement	Fly-ash	Sand	Water	Fibre (%)	SP	VMA	AEA
FS-SHCC	FS11	441 (42.5)	657	539	387	2.2	1.89	0.95	0.51
FS-SHCC	FS12	445 (42.5)	662	544	390	1.5	-	0.97	0.52
FS-SHCC	FS13	447 (42.5)	665	546	392	1.0	-	0.97	0.53
FS-SHCC	FS2	392 (42.5)	674	553	392	2.0	1.99	0.54	0.54
FS-SHCC	FS31 & FS32	392 (52.5)	674	553	392	2.0	1.99	0.54	0.54
FS-SHCC	FS4	361 (42.5)	361	620	509	1.9	1.81	0.18	0.55
FS-SHCC	FS5	698 (52.5)	406	573	406	1.9	2.01	0.18	0.55
CS-SHCC (2.36 mm)	CS11	442 (42.5)	658	540	388	2.0	2.54	0.95	0.51
CS-SHCC (2.36 mm)	CS12	445 (42.5)	662	544	390	1.5	-	0.97	0.52
CS-SHCC (2.36 mm)	CS13	447 (42.5)	665	546	392	1.0	-	0.97	0.53
CS-SHCC (1.70 mm)	CS2	392 (42.5)	674	553	392	2.0	1.99	0.54	0.54
FS-Mortar	FM1	401 (42.5)	688	565	401	-	-	1.0	-
FS-Mortar	FM2	401 (52.5)	688	565	401	-	-	1.0	-
FS-Mortar	FM3	368 (42.5)	632	519	368	-	-	0.42	-
FS-Mortar	FM4	451 (42.5)	672	552	396	-	-	1.0	-
CS-Mortar (1.70 mm)	CM1	401 (42.5)	688	565	401	-	-	1.0	-
CS-Mortar (2.36 mm)	CM4	451 (42.5)	672	552	396	-	-	1.0	-
HS-Mortar	HM3	495 (42.5)	-	1525	233	-	6.35	-	-

Note: *These id numbers are used in the text and graphs to introduce the different SHCC and mortar types used in this research work, CEM I 41.5 and 52.5 cement types are in brackets, SP = super plasticizer, VMA = viscosity modifying agent and AEA = air entraining agent. In all fine sand the maximum particle size was 0.30 mm and in coarse sand the maximum particle size is given in brackets.

Experimental Methodology

Also for the SHCC and mortar with different types of sand (FS and CS), mixes were classified as different mix designs e.g. FS12-CS12, FS13-CS13, FS2-CS2, FM1-CM1 and FM4-CM4. The SHCC mix is sensitive to ingredient material changes, when received in different batches from industry. For instance, the cement supplied to Stellenbosch University has recently been in a developmental phase, and the local coarse sand varies considerably in grading and particle shape from batch to batch. Because of these different batches of materials, SHCC mix design was also adjusted. The micro-mechanical parameters in SHCC, especially the crack tip toughness, are sensitive to ingredient material variations and the designer or engineer must be careful in the selection of materials since they vary from one source to another. This sensitivity is not only applicable to SHCC but the varying ingredient material properties also influence normal concrete mix design significantly.

Although different mixes were used, the strain hardening and multiple cracking behaviour of SHCC were checked in all the mixes. The mixing procedures and duration are shown in Fig 5.3. Note that for the mortar mixes, the total duration of mixing was about 5 minutes.

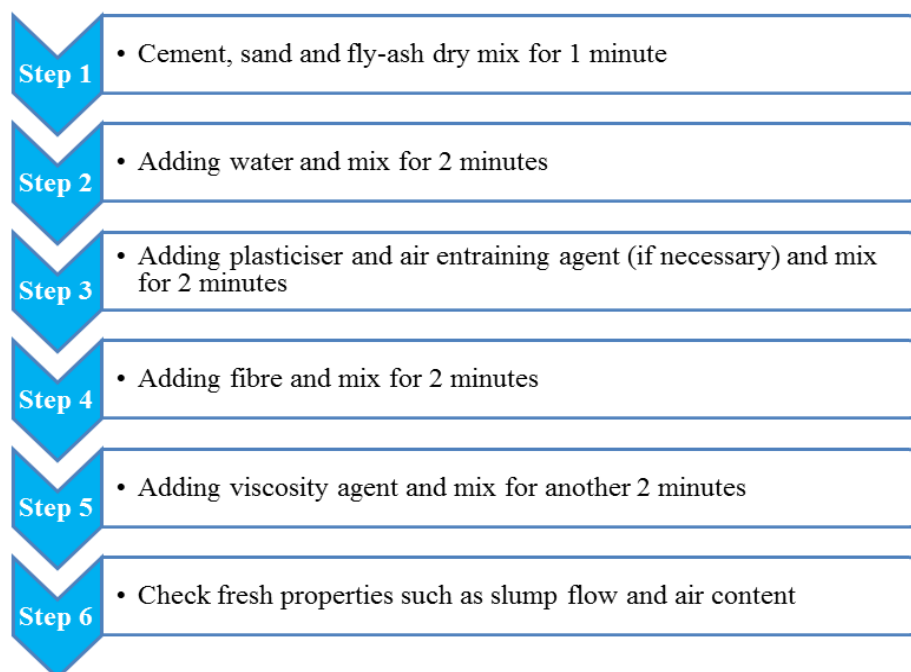


Figure 5.3: Typical mixing procedures of SHCC.

5.3. Properties of fresh SHCC and mortar

The rheology of fibre concrete to a large extent determines its fibre dispersion and, together with its casting or placement method, also fibre orientation, as has been shown by several researchers (Song & van Zijl, 2004; Adendorff *et al.* 2009). After mixing, the slump flow in the mix was checked according to ASTM C1611 and the air content according to ASTM C231 for both fresh SHCC and mortar. Figs 5.4 & 5.5 show the apparatus used for measuring slump flow and air content in SHCC and mortar.

Experimental Methodology



Figure 5.4: Apparatus used for measuring the slump flow of SHCC and mortar mix.



Figure 5.5: Apparatus used for measuring the air content in SHCC and mortar mix.

5.4. Types of specimens used

Cubes, beams and cylinders made of SHCC and mortar were prepared and subjected to various types of mechanical and durability tests. Cubes and cylinders were used for determining the compressive strength and E-mod of the different matrixes. For uni-axial tensile testing of unreinforced SHCC, dumbbell shaped specimens (approximate cross section 30 x 16 mm) were used. Both beams and small prism-shaped specimens were used in three-point bending (TPB) tests for the different levels of flexural load of SHCC and mortar used. The same beam specimens which were used in flexural testing were also used in chloride penetration profiling tests in SHCC. For the corrosion testing, reinforced beam specimens were used containing single and double steel bars for three (15, 25 & 35 mm) different cover depths. Corrosion testing in this research was performed mostly in cracked specimens (only limited specimens were un-cracked) and in both the loaded and unloaded state of the specimens. Cracks were formed in the reinforced beams by loading them to different

Experimental Methodology

deflection levels (3.5, 5 & 7 mm) in TPB testing. Note that these deformation levels were also the ultimate deformation capacity of the specimens from a particular mix of SHCC and details will be discussed in Section 6.2.4. Before choosing the TPB tests, some extra specimens were used in both TPB and in four-point bending (FPB) tests. It was found that most specimens failed in shear in FPB testing. As a result, TPB was chosen for the flexural testing of both SHCC and mortar specimens. Since in SHCC specimens, cracks close when unloading them after TPB testing, some specimens were again loaded in the steel frame to keep the crack widths open. In one series, cracks were formed in the specimens directly after placing them into the steel frame and this is discussed in Section 5.8.1. The specimen details and their estimated total number are shown in Table 5.4.

Table 5.4: Details of specimen types and numbers used in this research

Type of specimens	Type of testing	Nr of specimens	Curing duration (days)	Followed guideline
Cube (100 mm)	Compressive strength	> 100	28	BS-EN 12390:2002, ASTM C 39
Cylinder (Ø100 mm & l = 200 mm)	Compressive strength, E-mod	> 80	14 & 28	ASTM 469
Dumbbell (30 x 16 mm cross section)	Tensile strength & cracks	> 150	14, 28 & 56	RILEM
Unreinforced beams (100 x 100 x 500 mm & 150 x 150 x 700 mm)	Flexural strength, flexural cracks, fracture energy & chloride testing	> 50	14 & 28	SANS 586:1994, Literatures & ASTM E399
Reinforced beams (100 x 100 x 500 mm & 80 x 100 x 490 mm)	Flexural cracks & corrosion	> 100	14	Literatures & author own
Small prism (16 x 16 x 160 mm)	Flexural strength	48	28, 56, 90 & 120	DIN EN 20178
Prism (150 x 150 x 50 mm)	Freeze-thaw test*	12	14, 28, 42 & 56	DIN CEN/TS 12390-9
Disc (Ø100 mm & t = 50 mm)	Rapid chloride migration (RCM) test*	15	28	BAW Merkblatt 2004
Small disc (Ø100 mm & t = 20 mm)	Water permeability ⁺	12	14	DIN 52617
Small cylinder (Ø50 mm & l = 50 mm)	Electrical resistivity	9	90	ASTM C611

*Specimens were collected from the unreinforced flexural beams & ⁺specimens were air cured in a controlled temperature room.

Table 5.5 is an extension of Table 5.4 where the details of the reinforced SHCC and mortar specimens are shown separately. More than 100 reinforced specimens were made and 98 of

Experimental Methodology

them were directly used in accelerated corrosion testing. The rest of the specimens were used for determining the ultimate load capacity in flexural testing and based on the flexural results, different deformation levels were chosen for specimens as shown in Table 5.5. The guideline for different types of testing is given in Table 5.4. Types of exposure, specimens testing condition (loaded or unloaded) and ways of forming cracks in the specimens are also shown in Table 5.5.

Table 5.5: Details of reinforced SHCC and mortar specimen types, number, size, exposure types and methods of making cracks

Series	Id	Total nr of specimens	Size in mm (d x b x L)	Cover depth (mm)	Types of exposure & load	Formation of cracking method
One	R/FS2, R/CS2, R/FM1 and R/CM1	18+18+3+3 = 42	100 x 100 x 500	15, 25 and 35	Capillary absorption (unloaded)	3.5 & 1.5 mm deflection in TPB
Two	R/FS31	18	80 x 100 x 490	15, 25 and 35	Ponding (loaded)	5 & 7 mm deflection in TPB
Three	R/FS32* and R/FM2*	18+4 = 22	80 x 100 x 490	15 and 25	Ponding (loaded)	In the frame
Four	R/FS4, R/FM3 and R/HM3	8+4+4 = 16	100 x 100 x 500	15	Ponding (loaded)	In the frame

* Note that these are notched specimens for TPB (three point bending) testing as discussed in section 5.8.1.

5.5. Methods of casting and de-moulding

After mixing (by following the steps as shown in Fig 5.3), the fresh material was poured in the specific moulds as soon as possible. A vibrating table was used for better compaction of SHCC and mortar in the moulds. Almost the same vibrating speed (frequency of vibration is about 3000-4000 rpm) was used for all specimens and the maximum vibration time was about one minute. After pouring, moulds were covered with plastic to prevent evaporation of water from the mix. De-moulding was performed approximately 48 hours after casting.

5.6. Methods of curing

Curing is very important for concrete to achieve the expected properties. Except for water absorption testing (after demoulding all the specimens were stored in a controlled temperature and RH room until testing), the method of curing was in water. All specimens were put in a water tank (approximately at $21 \pm 2^\circ\text{C}$ temperature) directly after stripping from the moulds, until they were used for testing. At the time of testing, the cube, cylinder, small prism and unreinforced beam specimens for compressive and flexural strength testing were taken out of the water and tests were done within a short period of time. After seven days of

Experimental Methodology

water curing all the dumbbell and reinforced beam specimens were taken out and left in a control room (temperature $21 \pm 2^\circ\text{C}$ and humidity $60 \pm 5\%$) until they were tested at different ages.

5.7. Preparing specimens for mechanical testing

For construction materials, their mechanical properties play an important role in structural design and performance and hence testing of mechanical behaviours is necessary. Also the materials' durability performance is often associated with a particular set of mechanical properties so that the designer can consider the durability of the construction material used in the design. For instance if the lower crack widths and smaller crack spacing of SHCC under tensile or flexural testing can be confirmed, it may expect lower durability problem in the structure made from SHCC as this matter already discussed in Chapter 2 and 3. In this research, strength (compressive, tensile and flexural), E-mod, fracture toughness and crack properties of SHCC and mortar were examined.

5.7.1. Cubes and cylinders for compressive strength and E-mod

A minimum of six cubes (with sides of 100 mm) and four cylinders (100 mm in diameter and 200 mm in length) were tested from each type SHCC and mortar for compressive strength and E-mod calculation. The compressive strength is calculated from the failure load, divided by the cross-sectional area (cube or cylinder) under the load, and is reported in units of megapascal (MPa). The methodology of compressive strength testing according to BS-EN 12390:2002, ASTM C 39 and SANS 5863:1994 was followed. A 200 ton Contest Materials Testing Machine (CMTM) was used for testing all cubes and cylinders and the loading rate was maintained at about 3 kN/s. ASTM 469 was followed in determining the E-mod of the cylinder specimens. For uniform distribution of loading, every cylinder top was saw-cut to obtain a uniform surface and parallel ends before testing in compression. The E-modulus was calculated using the secant method shown in Fig 5.6 and recommended by ASTM 469. For accurate determination of the E-mod, an HBM 2000 kN load cell was placed over the specimen and three HBM 10 mm linear variable-differential transformers (LVDTs) were used to determine the deformation of the specimens. The setup also consisted of a Contest compression testing machine, a Spider8 data collector and a computer to download the data of the test. The loading rate used was the same as that for the compressive strength test. The data from the load cell (in the compression testing machine) and the LVDTs were recorded by a computer data acquisition system (Spider8).

In order to calculate E-mod, the stress-strain response at 30% - 40% of the ultimate compressive strength was used. In total, four cylinders per set were tested to determine their ultimate compressive strength and E-mod in each case at 28 days. Eqs (5.1) & (5.2) were used to calculate the compressive strength and E-mod of concrete.

Experimental Methodology

$$\sigma_c = \frac{F}{A} \quad (5.1)$$

$$E_c = \frac{\sigma_1 - \sigma_0}{\varepsilon_1 - \varepsilon_0} \quad (5.2)$$

where: σ_c is the compressive stress, F is the applied force (N), A is the cross-section area under load (mm^2), E_c is the E-mod of concrete, σ_1 and ε_1 is the stress and strain pair corresponding to the 30% - 40% of ultimate load, and σ_0 and ε_0 are the stress and strain pair corresponding to a small non-zero load (stress corresponding to 0.05% of strain was used here).

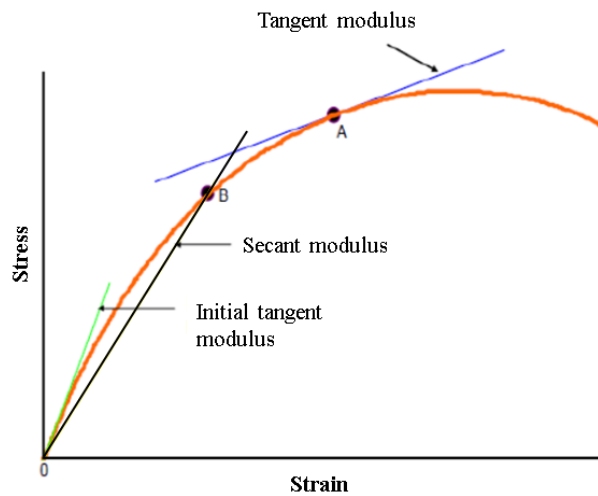


Figure 5.6: Tangent and secant methods of determining E-mod in concrete (imitated from Paul, 2011).

5.7.2. Dumbbells for tensile strength

Small dumbbell-shaped specimens with cross-sectional dimensions of 30 ± 2 mm by 16 ± 2 mm were used in uniaxial tensile tests. A minimum of four specimens were tested per set and the average value was recorded for each type of SHCC. Loads and deformations are measured by an HBM 1 kN load cell and HBM DD1 extensometer over a gauge length of 77 mm. All data is collected via a Spider8 data-collecting system connected to a computer. The direct tensile tests on dumbbell specimens are performed in a Zwick Z250 Materials Testing machine at a constant deformation rate of 0.0075 mm/s. Fig 5.7 shows the setup for dumbbell direct tensile testing.

Experimental Methodology

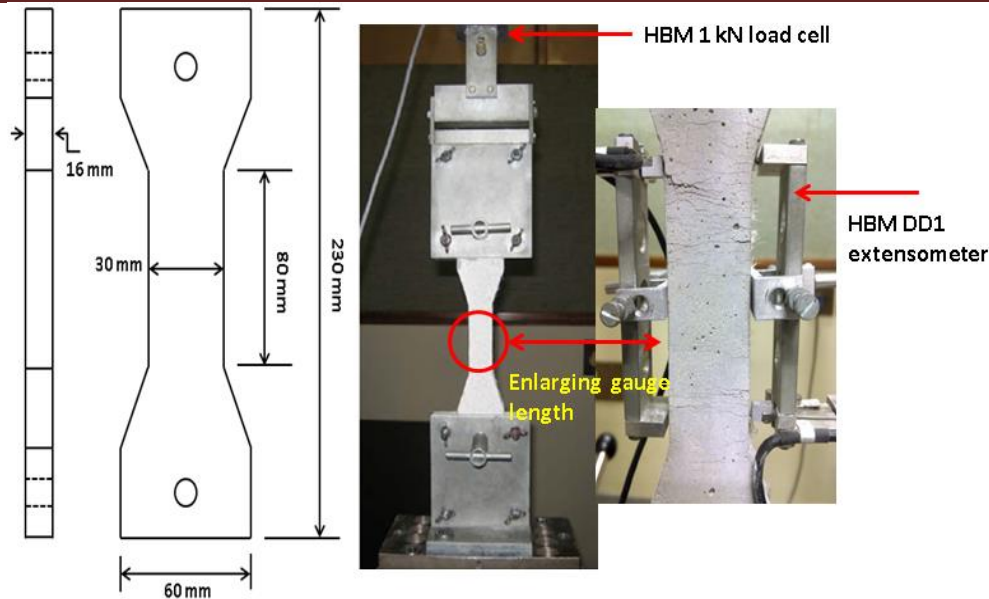


Figure 5.7: Dumbbell size and set-up for direct tensile testing.

5.7.3. Measurement of cracks in dumbbells

The crack width of each crack, from which the subsequent calculation of the number of cracks (NOC), the average crack widths (ACW) and the maximum crack widths (MCW) in the dumbbell specimens were determined, was measured using a contactless deformation measurement system and ARAMIS software. Note that ARAMIS was used only on dumbbell specimens. Special care is needed to prepare the surface of the specimen for measuring the crack properties. Typically in the ARAMIS system, the crack opening displacement (COD) is defined by the relative distance between two adjacent points on opposite sides of a crack, measured during the crack propagation in the specimen. In this regard, similar-sized small paint speckles should be prepared (as shown in Fig 5.8a) by spraying black speckles on the surface, which has preferably been given a white colour as contrasting background to ensure appropriate deformation tracking. This means that the dumbbell specimen tensile cracks reported here are at the loaded state, because monotonic loading was applied and images were recorded during the loading at various stages of the test. Typically ARAMIS takes images during testing and then the COD value is calculated for each recorded image, processing the displacement fields obtained from the y-axis of proposed lines – see Fig 5.8b. In this study it was assumed that deformations exceeding 15 μm between two speckles (roughly 1 mm apart) in the direct tensile test were cracks. It is worth mentioning that the cracks were counted at the intersections with three lines (1, 2 & 3) drawn vertically along the 77 mm gauge length of the dumbbell specimen as shown in Fig 5.8b. Also, all the results shown here are the average values of 3 sections from a total of 3 specimens for each type of SHCC. Readers are referred to Nieuwoudt (2012) and Chinn (2013) for detailed descriptions of the method of crack measurement via the digital image correlation method as described here.

 Experimental Methodology

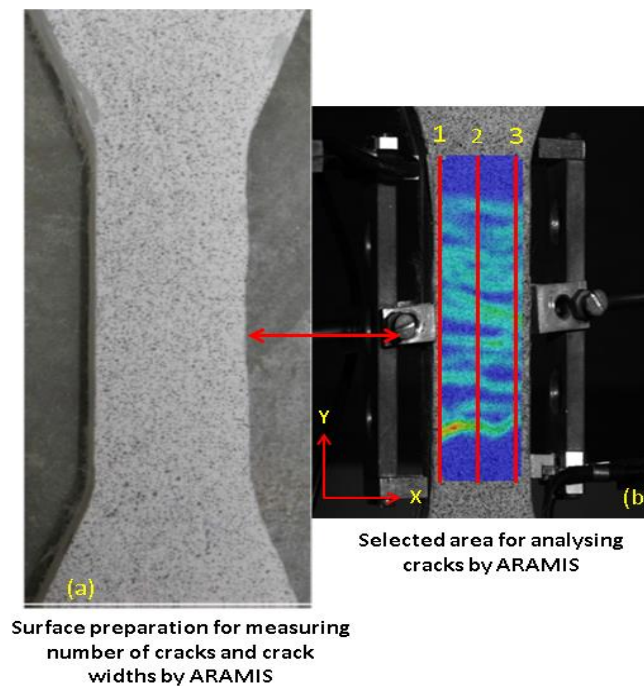


Figure 5.8: Preparation of specimen for measuring cracks data by using ARAMIS.

5.7.4. Flexural behaviour of reinforced and un-reinforced beams

The three point bending (TPB) method was used for the flexural strength test of SHCC and mortar. The test was carried out in the Zwick Z250 material testing machine at a force rate of 0.03 kN/s for determining the ultimate flexural strength. Since the beam specimens were used for different purposes such as flexural strength, fracture energy and corrosion testing, different dimensions of beams were used in different test procedures. Four different sizes of specimens (1) 40 x 40 x 160 mm (also called small prism specimen for flexural strength testing), (2) 80 x 100 x 490 mm (for pre-cracking for corrosion testing) (3) 100 x 100 x 500 mm (flexural strength, fracture energy and corrosion testing) and (4) 150 x 150 x 700 mm (rapid chloride migration and freeze-thaw testing) respectively were used. One 200 kN load cell and two 10 mm LVDT's (for measuring deflection) were connected to a Spider8 to plot a load versus deflection graph for the beam. By using the formula suggested by SANS 5864:1994 as shown in Eq (5.3), the flexural strength of each beam was calculated and the average value was reported. For the flexural load vs deflection curve, the two LVDT's were placed (Fig 5.9a) on both sides of the beam and connected to the frame. The frame was securely fixed to the specimen so that it remained fixed in its position relative to the beam. On the other hand, in most corrosion specimens, deflections were measured in the bottom face of specimens by using only one LVDT (Fig 5.9b).

$$f_{ft} = \frac{3Pl}{2bd^2} \quad (5.3)$$

Experimental Methodology

where: f_{ft} is the flexural strength, P is the load on the specimen which caused it to yield, b and d are respectively cross-sectional width and height of the specimen (mm) and l is the loading span. In this research l was 350 mm for 500 mm and 490 mm beam lengths and 450 mm for 700 mm beam length.

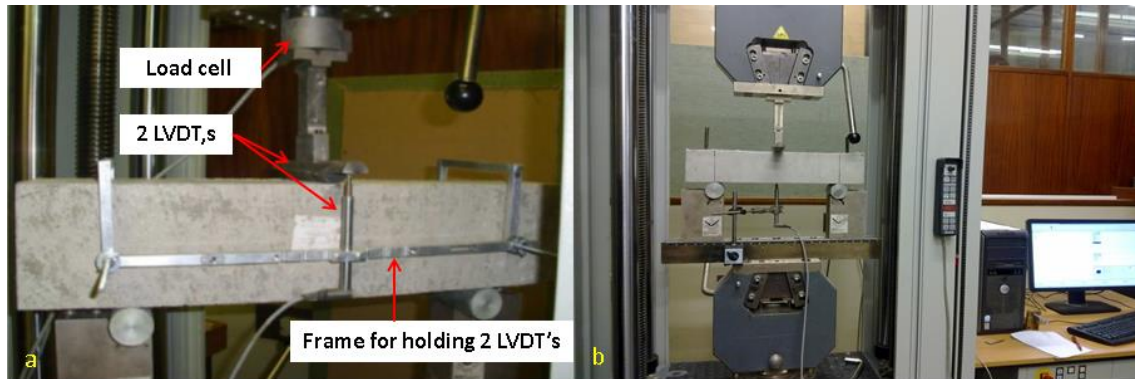


Figure 5.9: TPB testing set-up with (a) two and (b) one LVDT.

5.7.5. Method of measuring flexural cracks

Unless noted otherwise, the crack widths reported (both in tensile and flexural testing) in this research were measured on the surface of specimens. Therefore the influence of specimens' depth on the crack widths was not overserved. The total number of cracks and crack widths were also examined in the beam specimens after the flexural tests. Cracks in both reinforced and unreinforced beams were examined after the test, i.e. in the unloaded state, as opposed to the crack width observations in tensile specimens in the loaded state. In unreinforced SHCC, cracks were examined after loading to the ultimate load state as well as at a deflection level of 1.0 mm. For crack width measurement, different apparatus and methods were used separately such as a Leica MZ 7.5 microscope, a line-width template, a German-made portable, high-resolution mobi-camera (specially made for crack width measuring with 500 x zoom and 12 Megapixel), and AutoCAD software. In R/SHCC specimens, most cracks were localized in the central 150 to 200 mm section and cracks were measured only in that specific region. For measuring the number of cracks, at least three lines similar to those used on the dumbbell specimens were drawn on the cracked face as shown in Fig 5.10a. A Leica MZ 7.5 microscope was used to magnify the cracks and then a template was used to measure the crack widths although a template has a limitation of measuring crack widths (minimum 50 μm). AutoCAD was also found to be very difficult for measuring fine crack widths and in this regard, the portable mobi-camera was found to be the best way of measuring finer cracks in SHCC. This digital mobi-camera must be placed at a known distance from the object while the magnification factor is known (it can be adjusted). After taking photos, software provided with camera is used to measure the crack width for that known magnification factor. In this research, most flexural crack results were measured by using this mobi-camera. Fig 5.10b shows the crack width measurement using a template. Figs 5.10c&d show the portable digital

Experimental Methodology

mobi-camera and the crack width measurement technique using mobi-camera software for a known magnification factor.

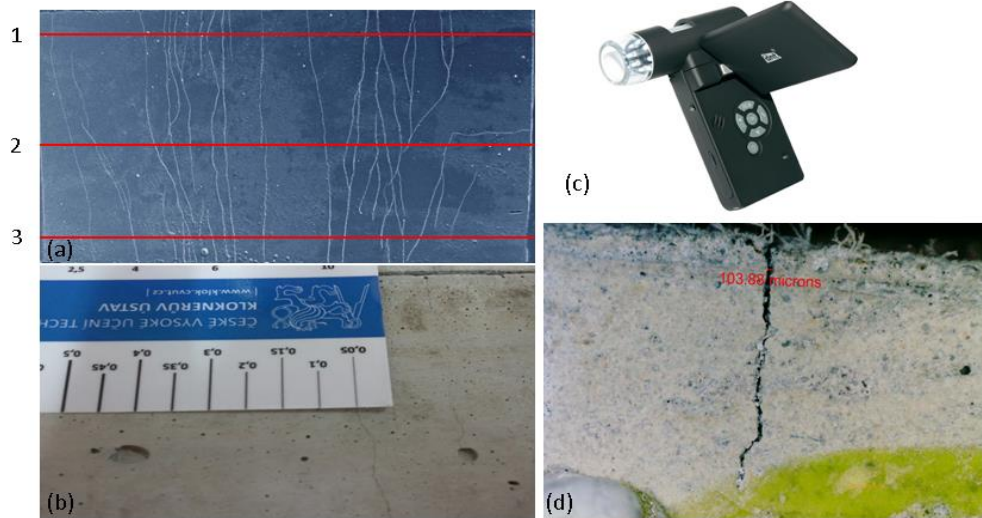


Figure 5.10: (a) Location of the number of cracks measured on the beam crack face (b) use of template (c) mobi-camera (d) crack width measurement using mobi-camera software.

5.7.6. Acoustic emission (AE) sensors for characterizing the cracks

It is the first time that SHCC Acoustic Emission (AE) sensors were used for characterizing the tensile and flexural cracks in both FS4 and FM3 specimens. In direct tensile tests on dumbbell specimens, two AE sensors (type VS 150 MS) were coupled by an adhesive putty (BOSTIK) at the wide ends of the dumbbell specimens. An AMSY-6 system was used to process and store the acoustic emission signals. The frequency filter was set to 25 - 850 kHz, covering the complete nominal bandwidth (100 - 450 kHz) of the sensors. To synchronise the AE signals and strain and tensile stress, the data measured by the controller of the testing machine were transferred to the AE system as analogue voltage signals (Paul *et al.* 2015).

Dumbbell-shaped specimens with an approximate cross-section of 30 mm x 16 mm and 100 mm gauge length were prepared for AE sensors in direct tensile testing as shown in Fig 5.11. The applied geometry (previous gauge length was about 80 mm) provides more space for the coupling of AE sensors and for clamping the specimen.

A total of 6 beam specimens (3 FS4 and 3 FM3) with a size of 100 mm x 100 mm x 500 mm were used in flexural testing with AE sensors. A total of 8 AE sensors (2 at the bottom face and 3 on both the vertical surfaces as shown in Fig 5.12) type VS 150 MS and coupled with an adhesive, were used on each specimen for detecting cracking activities during testing. All the specimens were tested after 28 days of water curing. Note that the loading span for flexural testing was 350 mm.

Experimental Methodology

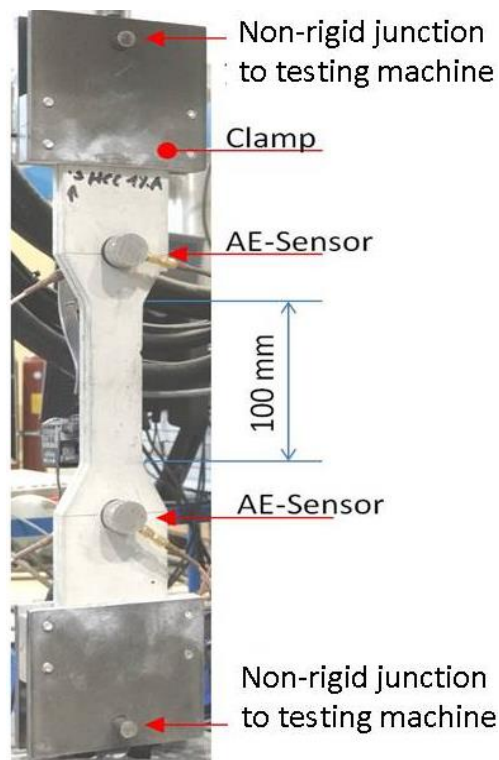


Figure 5.11: Dumbbell specimen with AE sensors in direct tensile testing.

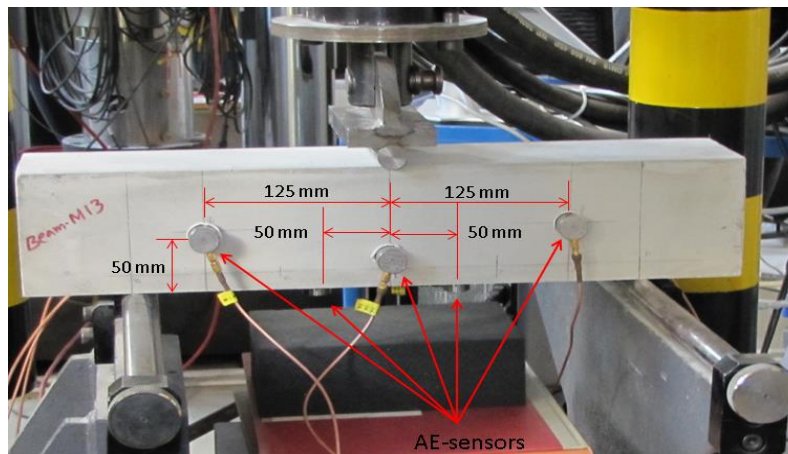


Figure 5.12: Position of AE sensor in flexural beam specimen during bending testing.

5.7.7. Fracture toughness testing

In most materials the failure mechanism of crack development can be examined by fracture mechanics. For the strain hardening behaviour of SHCC it is one of the conditions of having steady state crack propagation i.e. good micromechanical behaviour of stress and crack opening relationship. Steady state crack propagation means that a crack elongates at constant ambient tensile stress while crack opening become constant (Li & Leung, 1992). In this

Experimental Methodology

regard the matrix fracture toughness (K_{IC}) is very important for the strain hardening materials like SHCC.

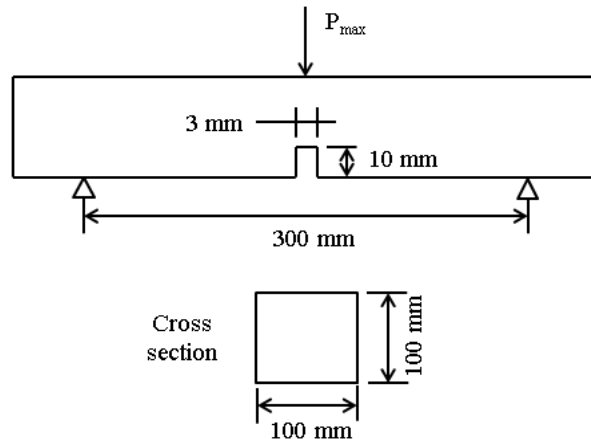


Figure 5.13: Specimen setup for fracture energy testing.

SHCC and mortar beams 100 mm x 100 mm x 500 mm in size were tested for TPB in the Zwick Z250 machine at a constant deflection rate of 0.005 mm/s for determining K_{IC} according to ASTM E399-09. A 10 mm deep and 3 mm wide central notch was created and the crack mouth opening displacement (CMOD) across the notch was recorded. An HBM 20 ton load cell was used to record the force and one 10 mm LVDT was used to measure CMOD (see Fig 5.13). Finally a Load-CMOD graph was used to calculate the fracture toughness of concrete as shown in Fig 5.14.

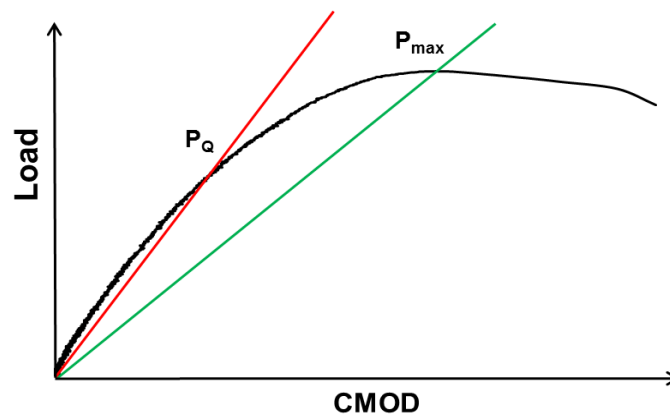


Figure 5.14: Calculation of fracture energy from the specimen response in flexural testing.

According to the recommendations by ASTM E399-09, each specimen was verified under certain conditions. To establish valid matrix toughness, conditional results of K_{IC} need to be calculated from the Load-CMOD curve. In the Load-CMOD curve a best-fit straight line first needs to be drawn to obtain the slope of the curve ($\tan \theta$) after which a second best-fit line with compliance 5% greater than that of the initial, line needs to be drawn. If the maximum flexural load (P_{max}) falls in between these two lines, the matrix toughness can be calculated

Experimental Methodology

using the P_{max} value. If the P_{max} value falls outside these two lines, the load must be calculated using the second straight-line connecting-point on the curve (P_Q). For the details see Fig 5.14. Furthermore, if the ratio of $P_{max}/P_Q < 1.1$, P_Q will be used to calculate K_{IC} as otherwise the test is invalid. To recheck the validity of K_{IC} , it is also necessary to check that $2.5(K_{IC}/\sigma_y)^2 < b$ as well as the specimen ligament ($d-a$), where σ_y is the yield strength, b is the specimen width, d is the specimen depth and a is stable crack growth. If the above condition is satisfied the K_{IC} is valid (ASTM E399-09). The reason of aforementioned test validity may be because this test method and equations are empirical, i.e. correlated from many experimental results to give reasonable results of K_{IC} despite the simple nature of the test method. Eqs (5.4) to (5.6) were used to calculate K_{IC} for both the mortar and SHCC specimens.

$$K_{IC} = \frac{3P_{max}S}{2bd} \sqrt{\pi a_1} F(x) \quad (5.4)$$

where: P_{max} is the valid peak load, S is the specimen loading span, b is the width of beam, d is the depth of beam, a_1 is the effective critical crack length at peak load.

$$F(x) = \frac{1}{\sqrt{\pi}} \frac{1.99 - x(1-x)(2.15 - 3.93x + 2.7x^2)}{(1+2x)(1-x)^{3/2}} \quad (5.5)$$

$$x = \frac{a_1}{d} \quad (5.6)$$

5.7.8. Fibre distribution in SHCC matrix

In addition to the matrix fracture toughness, the appropriate packing of aggregates and the distribution of fibres are considered essential for achieving strain hardening. In reality, several factors influence fibre dispersion and orientation. Fibres will not distribute in a described way not only due to their discontinuous nature, but also due to ratios of fibre length to particle size and fibre spacing to particle size. The role of fibre spacing to particle size is investigated here. Within a range of suitable fibre length to particle size ratios and for particle sizes smaller than the average fibre spacing, fibres may distribute in a regular pattern in a good production process and mix consistency. Such a regular dispersion is believed to be highly preferred, if not a physical requirement, for fibre crack-bridging efficiency towards multiple crack formation and strain hardening. Fibre spacing (S) in a regular grid of aligned fibres with circular cross-section can be shown from simple geometrical relations to be given by:

$$S = d_f \left(\sqrt{\frac{\pi}{4A_f}} - 1 \right) \quad (5.7)$$

Experimental Methodology

where: A_f is the ratio of total area of fibres in a cross-section to the cross-section area and d_f is the fibre diameter. Fibre spacing in concrete was also proposed by several other authors (eg. Kelly, 1974; McKee, 1969; Romualdi & Mendal, 1964). Eq (5.8) was proposed by Kelly (1974):

$$S = d_f \left(\sqrt{\frac{\alpha}{V_f}} - 1 \right) \quad (5.8)$$

where: V_f is the fibre volume content ratio and $\alpha = \pi/2\sqrt{3}$ for a regular triangular fibre array and $\alpha = \pi/4$ for a regular square fibre array. McKee (1969) and Mindess & Young (1981) respectively proposed Eqs (5.9) and (5.10) for random-oriented short fibres of length L_f and diameter d_f .

$$S = \sqrt[3]{\frac{\pi d_f^2 L_f}{4V_f}} \quad (5.9)$$

$$S = 0.138 d_f \frac{\sqrt{L_f}}{V_f} \quad (5.10)$$

Eqs (5.7) to (5.10) will be considered in the discussion of fibre spacing in fine and coarse sand SHCC dumbbell specimens investigated in this research, in the next chapter.

5.8. Preparing specimens for durability testing of SHCC

The durability properties of a material give an assessment of its response to extreme exposures and other events that may arise throughout the service life of the material. Since corrosion is thought to be the most widely-occurring problem (quickest deterioration and higher repair cost) of RCS, the major focus of this research is on corrosion of steel reinforcement in SHCC and mortar. As mentioned earlier, the corrosion testing in this project was divided into four series and most testing was performed on the cracked specimens. All specimens in series one to three were cracked and only a limited number of specimens in series four were un-cracked. The detailed specimen conditions (loading, unloading, and exposures) and corrosion testing procedures are discussed here.

5.8.1. Corrosion in SHCC and mortar

Firstly in Series One, both SHCC and mortar types FS2, CS2, FM1 and CM1 were used. R/SHCC and R/mortar beam specimens 100 mm x 100 mm x 500 mm in size and made with two types of sand (FS and CS) were used in this series. Three specimens from each R/FS2 and R/CS2 for two different levels of steel bars (single and double bars) and three different levels of cover depths, therefore a total of $2 \times 2 \times 3 \times 3 = 36$ beams, were prepared from SHCC. Their mix design, loading and exposure conditions are given in Tables 5.3 and 5.5. In the case of mortar, a total of three specimens with only 15 mm cover depth were made from both

Experimental Methodology

R/FM1 and R/CM1, therefore $2 \times 3 = 6$ mortar beams were prepared with a single steel bar. The specimens were cracked in TPB testing in the Zwick Z250 machine up to a vertical deflection level of 3.5 mm just to form several cracks in the specimens. Single and double steel bar (B1 and B2) reinforcements (10 mm diameter, Y10) were used in both R/FS2 and R/CS2 at three different cover depths (C15, C25 and C35 mm). All these specimens were tested under capillary absorption (see Fig 5.15) of 3.5% NaCl solution in cyclic wetting (3 days) and drying (4 days) exposure conditions for more than two years. Only one directional penetration was allowed in the specimens' cracked region (200 mm length seen in Fig 5.15a) by sealing the other surfaces with water proofing material to protect them against NaCl penetration. Fig 5.15b shows the reinforcement cross-section for B1 and B2 in Series One to Four where they are applicable. Note that in this series, for achieving different crack patterns in the specimens' two different levels of rebars were used. Also, the author wanted to study whether possible interaction of the two bars in the chemo-electrical process would alter the corrosion process markedly.

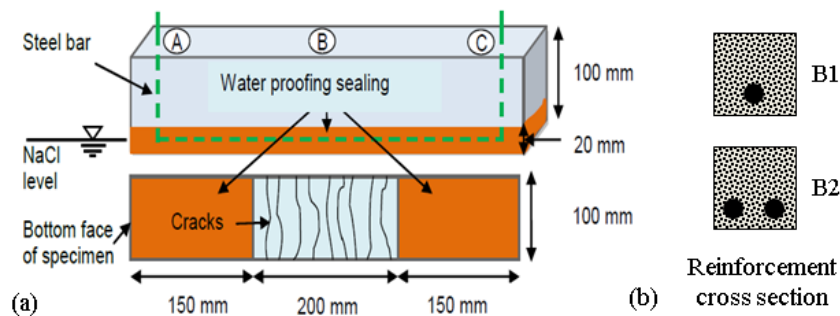


Figure 5.15: Corrosion measuring set-up for the cracked specimen in series one.

Secondly, in Series Two, a total of 18 specimens made from FS31 (refer to Tables 5.3 and 5.5) with dimensions of 80 mm x 100 mm x 490 mm were used. A total of three specimens from each of three different cover depths (C15, C25 and C35 mm) for two different levels of deflection (5 and 7 mm, denoted as D5 and D7) were tested (total specimens $3 \times 3 \times 2 = 18$). This resulted in multiple cracks forming over a length of 150 mm to 180 mm in the middle of the specimens. Note that these specimens were cast with a Y10 steel bar and a 5 mm stainless steel bar which was used as a counter electrode for corrosion testing inside the specimens. After performing the TPB testing in the Zwick Z250 machine up to aforementioned deflection levels, the specimens were further placed in individual steel frames under sustained loads applied by tightening the bolts on both ends to recreate the pre-cracking deflection levels; see Fig 5.16a. Note that two 16 mm holes were made at both ends of each specimen by inserting PVC pipes during the casting of each specimen for later inserting bolts and nuts. A pond for containing @ 3.5% NaCl solution as in series one, was made over the nominal cracked surface of 200 mm x 100 mm as shown in Fig 5.16b, using non-absorbent plastic for containing the chloride solution.

Experimental Methodology

In Series Three FS32 and FM2 types of SHCC and mortar of similar size as those of the specimens in series two, were used. However, the cracks in these specimens were created in a different way. As can be seen in the break-down in Table 5.6, two different cover depths (C15 and C25) were tested for three different crack spacing categories. The three different crack categories are: 5 cracks 20 mm apart, 3 cracks 40 mm apart and one crack in the centre of the upper face of the specimen. Three specimens were made of each category, producing a total of eighteen specimens from R/FS32. Another four specimens were also made from R/FM2 with a single crack.

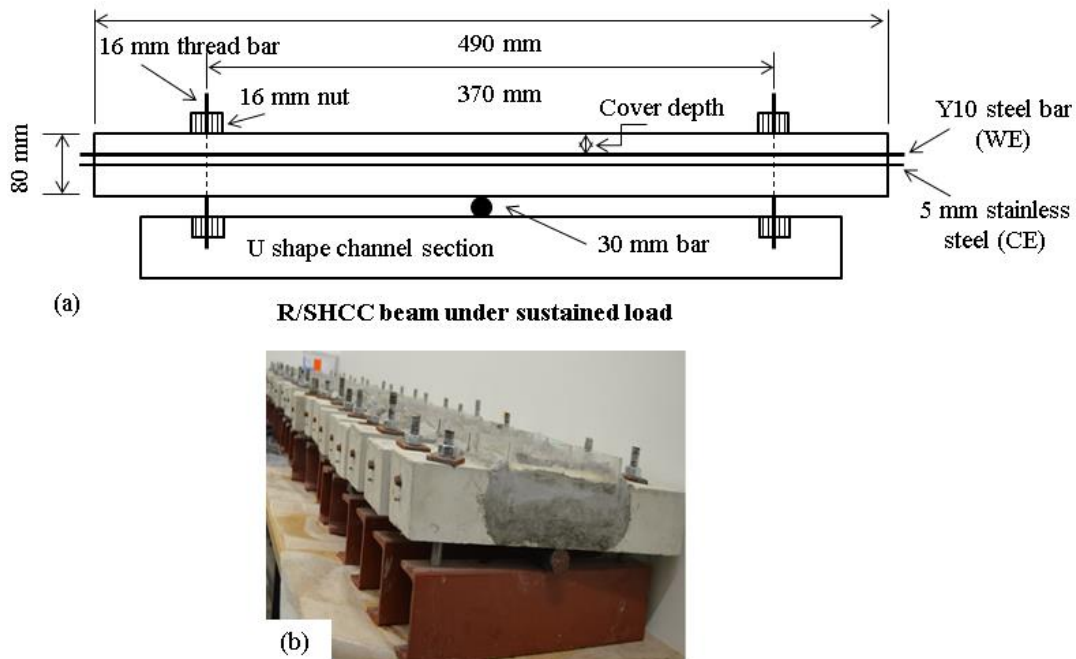


Figure 5.16: Sustained loading set-up of R/SHCC beams for accelerated corrosion testing in Series Two and Three.

Table 5.6: Details of number of specimens, crack and crack widths in series three

Type	Cover (mm)	Nr of specimens	Nr of notch/crack*	Surface strain (mm)
R/FS32	C15	3	1 (N1)	0.30
		3	3 @ 40 mm (N3)	0.90
		3	5 @ 20 mm (N5)	1.50
	C25	3	1 (N1)	0.30
		3	3 @ 40 mm (N3)	0.90
		3	5 @ 20 mm (N5)	1.50
R/FM2	C15	2	1 (N1)	0.15
	C25	2	1 (N1)	0.15

* 3 mm wide and 10 mm deep notches were made to create artificial cracks in the middle of each specimen as shown in Fig 5.17.

Experimental Methodology

Before the specimens were placed on the frames, 10 mm deep and roughly 3 mm wide notches were made on the top face of each specimen. The number of notches in the specimens also represents the number of cracks in them. The purpose of these notches was to force cracks to occur at the desired spacing, namely one crack, three cracks at 40 mm spacing, and five cracks at 20 mm spacing (cover depth measured from the bottom of the notch). The beams were then placed on the frames and cracked in a three point manner by tightening the bolts on either side and causing the specimen to flex over the 30 mm diameter steel bar. Due to the fact that this type of SHCC material is rate sensitive (as discussed in Chapter 2 that stress and strain depends on rate of loading) when considering a typical applied load, it is worth noting that the bolts were tightened simultaneously reaching the desired deformed length in approximately two minutes (see Fig 5.17). To ensure known crack width, the surface strain was measured beyond the notch in the 100 mm gauge length middle portion of each SHCC and mortar specimen.

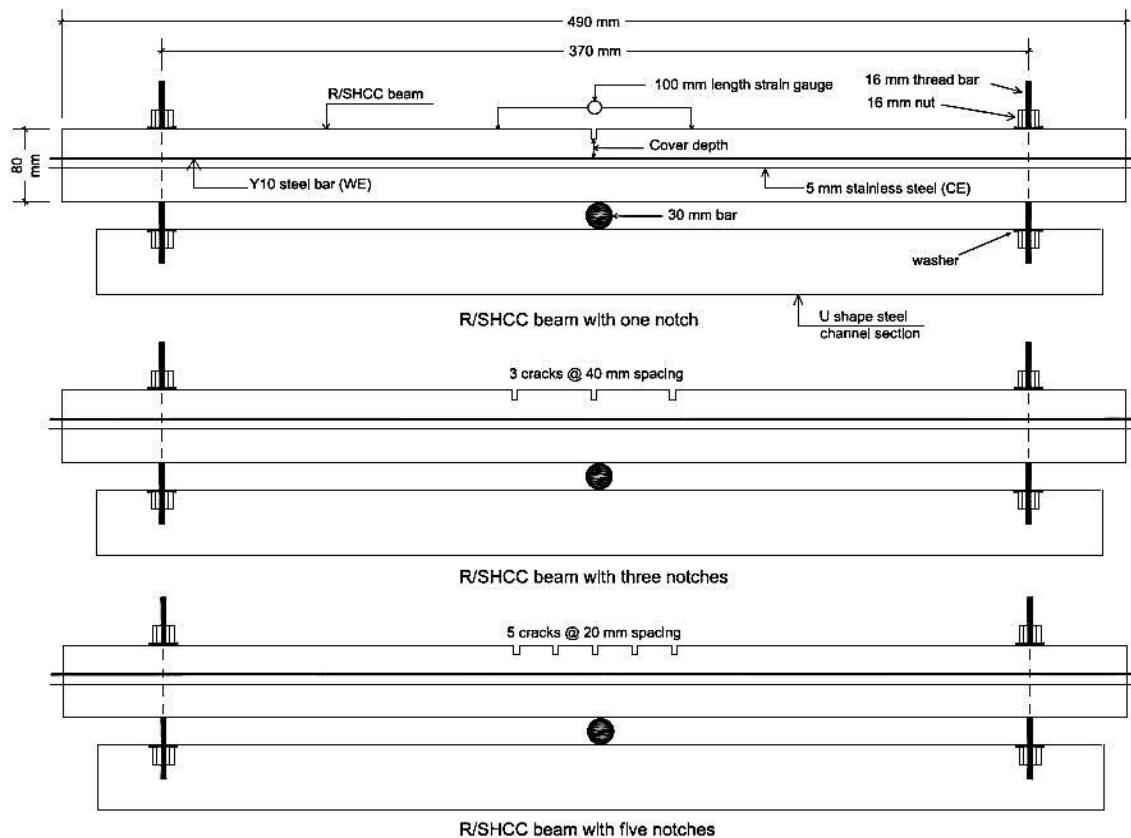


Figure 5.17: Notched specimens under sustained loads in Series Three corrosion testing.

Finally in Series Four, the corrosion potentials of R/FS4, R/FM3 and R/HM3 were studied on a total of 16 beam specimens measuring 100 mm x 100 mm x 500 mm. The reference mortars FM3 is of the same strength class as FS4 without fibre and the other high strength class HM3 was used under the same conditions as FS4. Both cracked and un-cracked specimens were tested here. For the un-cracked reinforced specimen corrosion test, 2 specimens of each material type (a total of $3 \times 2 = 6$) were used. In addition, 6 cracked R/FS4 and 2 from each

Experimental Methodology

cracked R/FM3 and R/HM3 type (a total of 10 specimens) were tested. At 30 days after casting the 10 specimens were pre-cracked directly in the sustained loading frame by TPB testing up to a vertical deflection of approximately 6 mm (see Fig 5.18). In R/FS4 specimens several cracks were formed over a central length of about 150 mm, but in both mortar specimens only a few cracks formed, also in the middle portion of the specimens. Subsequently, ponding of salt water over the cracked area of 200 mm x 100 mm commenced as shown in Fig 5.18a. To monitor the corrosion potential of the specimens, one ERE 20 reference electrode (made from manganese dioxide which has a fixed potential value) was placed inside each specimen near the embedded reinforcement (Y10 mm) before casting the concrete (see Fig 5.18b). The corrosion potential of each specimen was recorded by connecting the ERE 20 reference electrode and steel bar to a data logger. Cyclic wetting (3 days) and drying (4 days) exposure was also carried out for the accelerated corrosion testing.

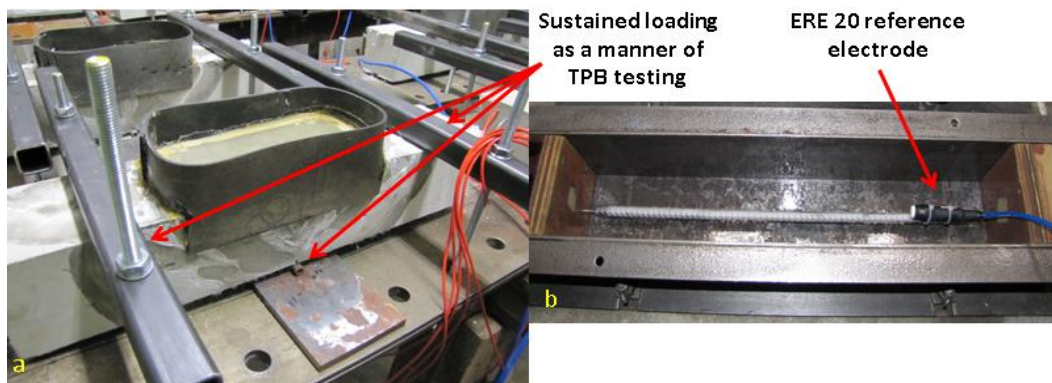


Figure 5.18: (a) Sustained loading set-up of specimens (b) position of ERE 20 reference electrode inside specimen in Series Four.

5.8.1.1. Corrosion potential

A half-cell potential measurement method was used in all the series to obtain the corrosion potential reading in all the specimens. A copper/copper sulphate half-cell (CSE) was used for the measurement of potentials on concrete surfaces. A Fluke 23 (Series II) multi-meter with impedance of 10 M Ω was used with lead wiring as specified by the ASTM C 876 (ASTM Standards, 1999). Fig 5.19 depicts the CSE that was used with a multi-meter to measure the half-cell potential of the samples at various locations. The white circular discs visible in the figure were normal disposable cotton wool sponge pads that were used as electrical junction devices as described by the ASTM standard. Normal tap-water was used as electrical contact solution. It was decided that one measurement in the centre of the top of the each beam sample would suffice with two additional readings 100 mm from the ends of one of the samples per batch. The two additional readings would serve as an indicator of whether the seal managed to restrict the ingress of chloride ions to the area of the exposed surface or not. The same pattern of collecting measurements used and the sponges of all the samples were pre-wetted in the same pattern prior to the measurement of half-cell potentials.

Experimental Methodology

It was understood that the half-cell potential readings may not always have given a direct indication of corrosion due to several other factors that may have influenced it, but the readings were to serve as an indication of when change occurred in the samples. A change in the corrosion, a change in the chloride levels and a change in the moisture content could possibly have influenced the readings, but since the focus of the project was on the effect of early age corrosion it was deemed a practical way of tracking change with the equipment available. It was envisaged that, after an extended period of exposure to the chloride solution, the steel bars would be removed and inspected for corrosion to correlate with the readings. A detailed outcome in this regard is described in Chapter 7.

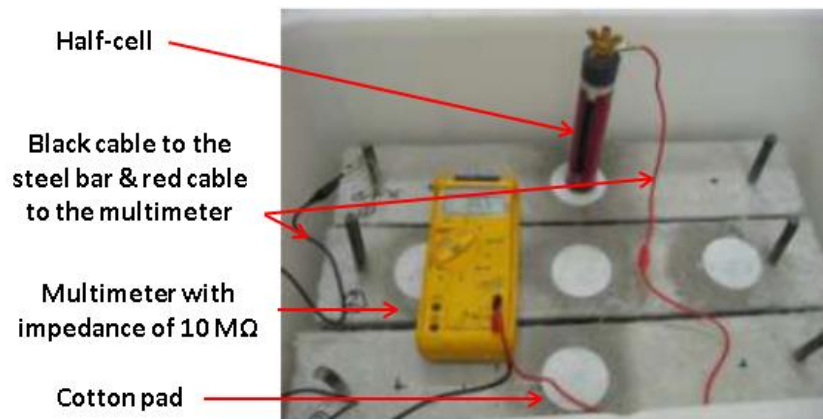


Figure 5.19: Methods of taking corrosion potential reading in the specimens.

5.8.1.2. Corrosion rate

The corrosion rate measuring technique used in this research has already been broadly described in Chapter 4. Except for series four, the corrosion rate was measured in all R/SHCC and R/mortar beams. Note that the Coulostatic measurement device was prepared during the test phase of series one. As a result, corrosion rate measuring was not possible from the beginning of testing in series one. Only in series two and three, the corrosion rate readings were taken from the beginning of the chloride exposure testing. Hence, the taking of corrosion reading in series one and two were started after 480 days (68 weeks).

After corrosion testing, all the steel bars were cleaned with HCl and a wire brush. Depending on the severity of corrosion a minimum 10 minutes to a maximum 20 minutes was required to clean the corroded steel bar with HCl. The pitting depths, loss of yield force and mass loss was also determined in steel bars. For pitting depths measurement, a dial gauge with a resolution of 10 μm (shown in Appendix B, Fig B.1) was used. A minimum of 3 to maximum of 6 pitting were chosen to measure the average and maximum pitting depths in each steel bar. Zwick Z250 machine was used to determine the yield force on corroded steel bars and loss of force was calculated from the yield force found in the reference steel bars. Mass loss of steel bars was determined only in series four. In this case, the initial weight of steel bars was taken before casting them into FS32 and FM3. The final weight of steel bars was taken

Experimental Methodology

by breaking the specimens after the corrosion testing and cleans them in HCl. The differences in two weights were the mass loss of steel in corrosion testing.

5.8.2. Chloride testing in SHCC and mortar

Since the main aim of this research is chloride-induced corrosion testing, the chloride content at the cover depth of SHCC and mortar specimens was also determined. The chloride profile was investigated in both reinforced and unreinforced specimens. The details about the types of tests performed for determining chloride content in the different types of specimens is discussed next.

5.8.2.1. Rapid chloride migration (RCM) testing for un-reinforced specimens

This part of the research work is limited to only FS4, FM3 and HM3 in series four. In rapid chloride migration (RCM) tests both pre-cracked and un-cracked core specimens (100 mm diameter and 50 mm thickness) were tested for all three types of SHCC and mortar. These core specimens were obtained from the 150 mm x 150 mm x 700 mm size beams which were tested in TPB testing at 29 days from the casting date. A total of 8 beams from FS4, 5 from FM3 and 4 from HM3 were used in flexural testing. Two beams from all three types were tested at ultimate load to obtain the ultimate deflection capacity. By knowing the ultimate deflection capacity of beams, a further 6 FS4 beams were pre-cracked at two levels of deflection (3 beams each at 1.67 mm and 3.33 mm levels of deflection), 3 beams from FM3 and two beams from HM3 were tested at one level of deflection (0.73 mm for FM3 and 0.68 mm for HM3). Note that there were no cracks formed in FM3 and HM3 specimens. Details of loads vs deflections, the number of core specimens and the testing age are discussed in the next section. For loaded specimens, 50 mm thick core specimens were collected from the centre of the bottom surface (cracked face) of each beam and this surface was also used for chloride penetration in the RCM test. Un-cracked specimens were collected in the same way as loaded specimens from the two edges of beams. It is worth mentioning that multiple fine cracks were observed in the pre-cracked FS4 beams and the cores collected from these beams were also cracked. The number of cracks and crack widths are described in subsequent sections. FM3 and HM3 beams which were tested up to a certain deflection level did not have cracks and so the cores obtained from these beams were similar to cores obtained from unloaded beams.

Figs 5.20a&b show the test set-up and specimen preparation for the RCM test. For the RCM test, 0.2 N KOH was used as anolyte and 0.2 N KOH + 10% NaCl was used as catholyte solution. In all the core specimens the applied voltage was 30V. The duration of the test depends on the current passing through core specimens when applying this 30V. After the test period core specimens were broken into two parts in the splitting test and then silver nitrate solution was applied to the broken surface to measure the chloride ions penetration depth on each of the core samples. A maximum of 11 readings were taken along the 100 mm length of the core specimen and their average was used to calculate the diffusion coefficient of SHCC and mortar used here. Preparation of the core specimens and details of the test

Experimental Methodology

method of determining the chloride migration coefficient from RCM tests are discussed broadly in the German Federal Institute for Hydraulic Engineering leaflet 2004 (BAW Merkblatt, 2004) which is almost similar to NT BUILD 492-1999-11. The major differences between these two codes are the value of absolute potential difference (U) and the duration of the test based on the current passing through the specimen. In BAW Merkblatt 2004 the applied voltage (E) is considered to be equal to U , whereas in NT BUILD 492-1999-11, the influence of the specimen length to the input and output voltage is considered to be $U = (E - 2)/L$.

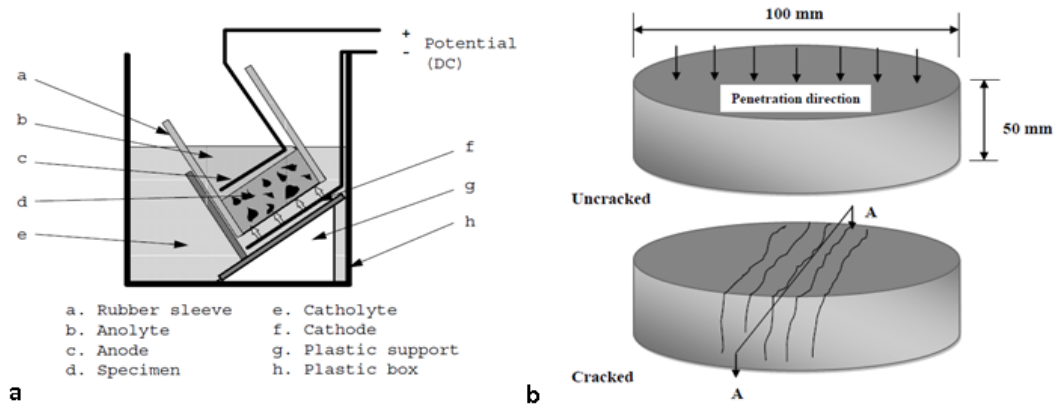


Figure 5.20: (a) Test set up for rapid chloride migration test (b) preparation of specimen for RCM test.

The chloride diffusion coefficient (D_{cl}) was calculated from the RCM test results by using equations (5.11) to (5.14) as recommended in BAW Merkblatt 2004.

$$D_{cl} = \frac{RTh}{zFU} \frac{x_d - \alpha\sqrt{x_d}}{t} \quad (5.11)$$

with:

$$\alpha = 2\sqrt{\frac{RTh}{zFU}} \operatorname{erf}^{-1}\left(1 - \frac{2c_d}{c_o}\right) \quad (5.12)$$

where: D_{cl} is the migration coefficient ($10^{-12} \text{ m}^2/\text{s}$), z is the ion charge ($z = 1$ for chloride), F is the Faraday constant (96495 J/V.mol), U is the absolute potential difference (V), R is the gas constant (8.315 J/K.mol), T is the mean temperature (K), h is the thickness of the specimen (m), x_d is the chloride penetration depth (m), t is the duration of the test (s), erf^{-1} is the error function, c_d is change in colour triggering chloride concentration (0.07 mol/l), and where c_o is the potassium chloride concentration (mol/l).

For 10% NaCl solution the above Eqs (5.11) & (5.12) can be simplified to:

Experimental Methodology

$$D_{cl} = \frac{\beta}{t} (x_d - 2.53\sqrt{\beta x_d}) \quad (5.13)$$

$$\text{with: } \beta = 8.619 \cdot 10^{-5} \frac{hT}{U} \quad (5.14)$$

If D_{cl} value for a concrete type is known, the chloride concentration ($C_{x,t}$) with respect to specimen depth (x) can be calculated from the recommended Eqs (5.15) & (5.16) by Tang and Nilsson (1991).

$$C_{x,t} = \frac{1}{2} c_{sol} \left[\operatorname{erfc} \left(\frac{x - aD_{cl}t}{2\sqrt{D_{cl}t}} \right) + e^{ax} \operatorname{erfc} \left(\frac{x + aD_{cl}t}{2\sqrt{D_{cl}t}} \right) \right] \quad (5.15)$$

$$\text{with: } a = \frac{ZFU}{RTh} \quad (5.16)$$

where: c_{sol} is the concentration of chloride in the bulk solution (g_{cl}/dm^3 solution) and erfc is the complementary error function.

Since diffusion is influenced by the specimen age, Marsavina *et al.* (2009) developed a relationship between the chloride penetration depth at the day of testing (x_t) to the 28 days ($x_{d,28}$) penetration depth in the specimen shown in Eq (5.17).

$$x_{d,28} = x_t \left(\frac{28}{t_n} \right)^\beta \quad (5.17)$$

where: t_n is the specimen age at the day of testing and β is the factor depending on cement types (for Portland cement β is -0.135).

The diffusion rate decreased with time due to the continuous hydration process of binder in the concrete structure. Thomas & Bentz (2000) developed the following relationship shown in Eq (5.18).

$$D_t = D_{ref} \left(\frac{t_{ref}}{t} \right)^m \quad (5.18)$$

where: D_t is the apparent diffusion coefficient at time t , D_{ref} is the reference diffusion coefficient at time t_{ref} and m is a constant depending on the continuous hydration process of binder in concrete. $m = 0.2 + 0.4$ (percentage of fly ash/50+ percentage of slag/70) and the maximum value of m is 0.6.

5.8.2.2. Chloride penetration testing in cracked unreinforced SHCC specimens

Chloride penetration testing in unreinforced SHCC specimens was performed in three ways. Firstly, a total of 6 beams 100 mm x 100 mm x 500 mm in size were made from FS11 and

Experimental Methodology

CS11. All these specimens were tested in TPB at the age of 28 days. Capillary chloride absorption testing was performed in the specimens for up to 30, 60 and 90 days respectively. Besides these 6 specimens, another 2 specimens of each SHCC type were tested to determine their ultimate flexural resistance. The details of these specimens are shown schematically in Fig 5.21. For the preparation of the chloride test specimens, approximately 60% of the ultimate flexural load was applied to cause pre-cracks in the specimens. The reason behind the application of 60% load is to simulate in-service loading conditions, as opposed to ultimate limit state, failure loads. Here the number of cracks on the specimens was found to be about 5 and the average crack width was below 0.50 mm. For the chloride penetration test, a 150 mm length of each cracked specimen was prepared by saw-cutting it from the middle portion of the each beam - see Fig 5.22a. The figure shows that the specimen was collected by sawing along lines A and B. After the chloride penetration test, it was sawn along the C line to observe the chloride penetration. Five faces of the specimens were sealed with a layer of waterproofing material (plascon roof seal product), leaving the cracked face open for penetration (top face in Fig 5.22b). At present there is no specific method for chloride exposure of SHCC and so, different methods were followed by different researchers (Kobayashi *et al.* 2010; Miyazato & Hiraishi, 2005; Wittman *et al.* 2009; Kato *et al.* 2005). In this research paper, only one method was followed which was cyclic wetting (3 days submerged) and drying (4 days). The specimens were submerged into a 3.5% solution of NaCl in water by weight. After 3 days, the specimens were removed and kept in ambient laboratory conditions for 4 days. This cyclic wetting and drying procedure was followed until the specimens were ready for testing at 30 days (4 wet and dry cycles), 60 days (8 cycles) and 90 days (13 cycles) respectively. The NaCl solution concentration was not checked to ensure that it remained at 3.5% over time, but a new mix was made after 30 days to ensure the solution quality. On the above-mentioned day of chloride testing, each specimen was sawn through the middle along the line C in Fig 5.22a (left). After that, 0.1N of AgNO₃ solution was painted on the cutting surface to observe the chloride penetration into the SHCC specimen.

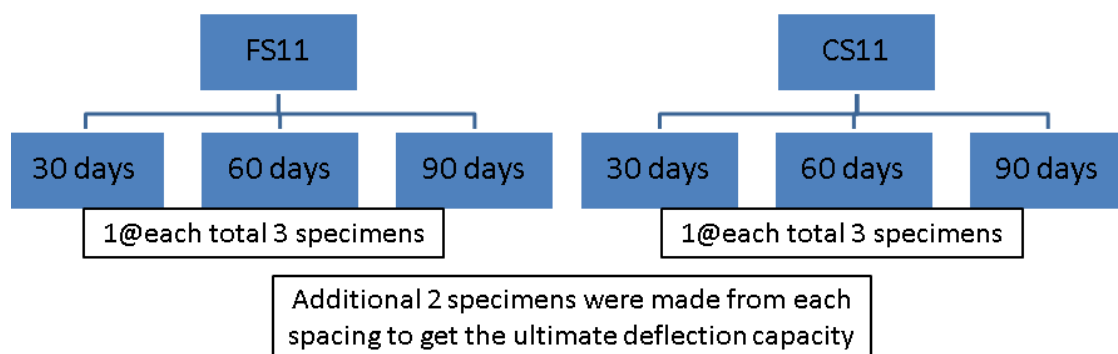


Figure 5.21: Details specimens outline for long term chloride penetration testing in FS11 and CS11.

Secondly, 4 similar sized specimens were made from FS2 and CS2. In this case cracks were formed in the specimens by loading them to a central deflection of 1 mm in TPB testing. A

Experimental Methodology

maximum of 3 cracks were observed in the specimens and the average crack width in the unloaded state of the specimens was 0.50 mm. Capillary chloride absorption testing was performed for 1hr, 3hrs and 6hrs. Note that 3 specimens from FS2 were used for all exposure periods and that only 1 specimen from CS2 was used for the 6hrs exposure time as shown in Fig 5.23. Chloride profiling was done in the same way as in the previous step.

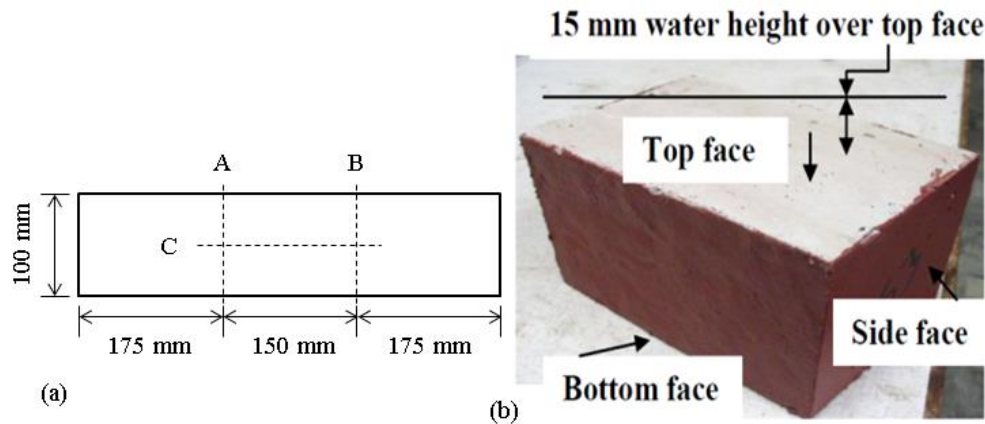


Figure 5.22: Preparation of specimens for chloride penetration test using AgNO_3 .

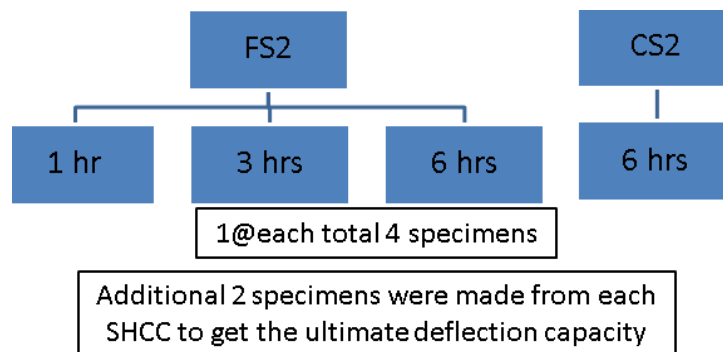


Figure 5.23: Detailed specimen outline for short-term chloride-penetration testing in FS2 and CS2.

Finally, a total of 16 similar-sized specimens as mentioned in the previous steps were used for chloride-penetration under ponding-exposure conditions of FS32 and FS5 specimens. Cracks were made in the specimens by making notches. A total of 5 notches were made on the surface of each specimen. Two different notch spacings were used i.e. from each type of SHCC, 4 specimens had a notch spacing of 20 mm and of 40 mm, giving a total of $4 \times 2 = 8$ specimens of each type as shown in Fig 5.24. One specimen from each notch spacing was used to determine the ultimate deflection capacity in TPB testing. With the knowledge of the ultimate deflection for one specimen type, the other three specimens were loaded to a deflection level of 1 mm. In this case, cracks were successfully formed in the position of the notches. After pre-cracking, 100 mm x 100 mm x 200 mm specimens were cut from the central part of the beam. Ponds made from non-absorption plastic were made on top of each

Experimental Methodology

notch face. Then all the specimens were exposed to 3.5% NaCl solution by means of ponding with an initial depth of between 15-20 mm. Chloride profiles were obtained for specimens after continuous ponding exposure of 1, 3 and 7 days respectively. Therefore, only one specimen from each category was used in each exposure duration.

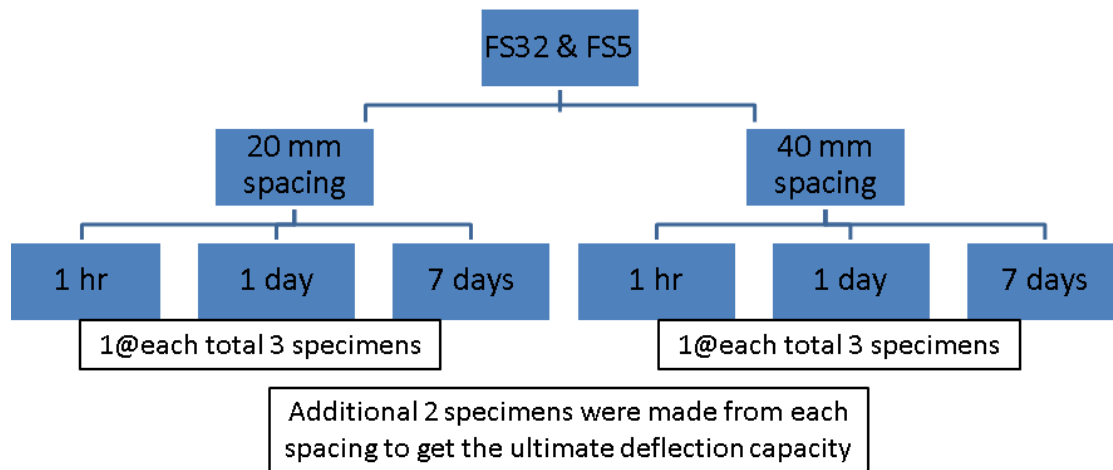


Figure 5.24: Detailed specimen outline for short-term chloride-penetration testing in FS32 and FS5.

5.8.2.3. Chloride profiling by X-ray fluorescence (XRF) and chemical testing

Chloride penetration profiles were also determined for R/SHCC and R/mortar specimens by means of XRF and chemical testing. Typically, XRF is used to measure the total chloride content (% of total weight or ppm) in concrete. Chemical test methods recommended by the ASTM (C1152 and C1218) and RILEM can be used for both total and free chloride content. In this research work both XRF and RILEM chemical test methods were performed for determining the total and free chloride in R/SHCC, R/mortar and also in unreinforced FS32 and FS5 specimens. More than 700 samples from different types of specimens were tested in XRF. In case of R/SHCC and R/mortar, various specimens were chosen after different cyclic chloride-exposure periods. A certain amount of powder sample is necessary for both XRF and chemical testing to determine the level of Cl. Here, the powder samples were obtained by drilling from the specimens exposed surface in layers of 3 mm each, up to a depth of 45 mm. The powder samples thus obtained were then used for XRF to determine the total chloride content in each layer. A drill with diameter of 16 mm was used to ensure sufficient powder per 3 mm layer. Details of chemical testing procedures are discussed in the next section. Note that for XRF testing, no special care needs to be taken for the preparation of powder samples as long as the particles are fine (below 0.30 mm). In this research work, a Niton portable (hand-held) XRF instrument was used and the amount of powder for total chloride testing should be such that a disc with an 8 mm diameter and 10 mm depth can be formed from it. Each powder sample was placed in a sealed plastic bag for protection. Testing can be done on the sample while it is in the thin plastic bag. One test can take up to a maximum of 2 minutes. More importantly, XRF can provide both the elements and oxide forms of different chemicals

Experimental Methodology

in the sample. Specimen details which were tested in both XRF and chemical testing for determining their total and free chloride content are given in Tables 5.7 & 5.8.

Note that in Table 5.7, FS32_20mm@ 1hr and FS5_20mm@ 1hr represent the specimens with 20 mm notched spacing which was loaded up to 30% (1 mm deflection level) of their ultimate resistance capacity and that 3.5% NaCl was applied (by means of ponding) on top of the notched area (100 mm x 200 mm) for 1 hr. 1hr (UL) represents the same specimen but loaded up to its ultimate resistance capacity. Similar conditions are also applied for FS32_40mm and FS5_40mm specimens where the notch spacing was 40 mm.

Table 5.7: Details of unreinforced FS32 and FS5 notched specimens used in XRF and chemical testing

Type	Notch spacing (mm)	Sp. id	XRF (total Cl)	Chemical (total Cl)	Chemical (free Cl)
FS32	20	FS32_20mm@ 1hr, 1hr (UL)*, 1d, 7d	√	-	-
	40	FS32_40mm@ 1hr, 1hr (UL)*, 1d	√	-	-
	40	FS32_40mm@ 7d	√	√	√
FS5	20	FS5_20mm@ 1hr, 1hr (UL)*, 1d, 7d	√	-	-
	40	FS5_40mm@ 1hr, 1hr (UL)*, 1d	√	-	-
	40	FS5_40mm@ 7d	√	√	√

*Note that these specimens were loaded up to ultimate resistance capacity while rest of the specimens were loaded up to 30% (1 mm deflection level) of their ultimate resistance capacity.

Table 5.8: Details of R/SHCC and R/mortar specimens used in XRF and chemical chloride (Cl) testing

Series	Type	Sp. id	XRF (total Cl)	Chemical (total Cl)	Chemical (free Cl)
1	R/FS2	C15B1, C25B1 (2)*, C25B2, C352	√	-	-
		C25B1	√	√	√
	R/CS2	C25B1, C35B1 (2)*, C15B2, C25B2, C35B2	√	-	-
		C35B1	√	√	√
	R/FM1	C15B1	√	√	√
R/CM1	C15B1	√	-	√	
2	R/FS31	C15D5, C25D5 (2)*, C25D5 (2)*, C25D7, C35D5 (2)*, C35D7	√	-	-
		C15D7	√	√	√
3	R/FS32	C15N1, C15N3, C15N5, C25N1, C25N3, C25N5	√	-	-
		C15N5, C25N3	√	√	√
	R/FM2	C25N1	√	-	√

* Note that two specimens were tested from these cases.

Experimental Methodology

5.8.2.3.1. Chemical testing for total chloride content

In the case of chemical testing, the number of specimens was limited because chemical testing is time-consumable. As is shown in Tables 5.7 & 5.8, some of the specimens which were used in XRF testing were again used in chemical testing. Typically, XRF does not alter the chemical content of the powder sample, and the chemical test can be performed on the same sample after XRF testing and give the correct result.

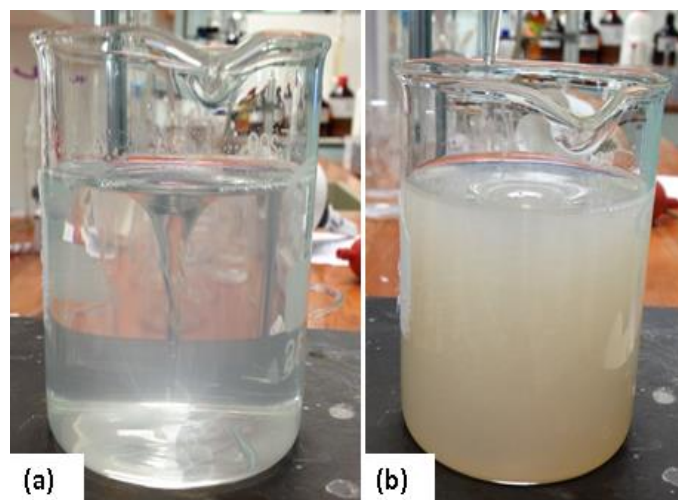


Figure 5.25: Colour changes of the sample during total chloride testing (a) before the test (b) after the test.

The total chloride-content chemical test, also known as the acid soluble test, was performed according to the RILEM TC178-TMC recommendation. In total 40 samples (in powder form) were tested for their total chloride content. In this method, a 1 ± 0.0001 gm powder from one sample is necessary to run the test. For the preparation of this test, the sample was placed in a 250 cm^3 beaker and then 50 cm^3 of HNO_3 (1:2) was added and stirred on a magnetic hotplate. After effervescence (bubbles in a liquid) had stopped, the suspension was heated during continuous agitation until it boiled (process takes a few minutes). Again 10 cm^3 of standardized 0.05M AgNO_3 solution was added into the beaker by means of a pipette. The suspension was allowed to boil for another minute after which it was filtered through filter paper, previously washed with HNO_3 (1:100). The beaker, agitator and filter paper were washed thoroughly with HNO_3 (1:100) until the final volume of the filtrate was about 200 cm^3 . The filtrate was left to cool down to room temperature. 20 drops of indicator solution of ammonium iron sulphate $[\text{NH}_4\text{Fe}(\text{SO}_4)_2 \cdot 12\text{H}_2\text{O}]$ was added and stirred vigorously. The suspension was titrated with 0.05M NH_4SCN (ammonium thiocyanate) solution and stopped when a drop of the NH_4SCN solution produced a slight red brown colour as shown in Fig 5.25, which does not disappear with agitation. The volume of the NH_4SCN solution used was recorded as volume nr 1 (*VI*).

Experimental Methodology

A blank run needs to be conducted beforehand following the same procedure with the same reagents, but without the powder. The spent NH_4SCN solution for the blank run was recorded as volume nr 2 (V_2).

After doing all the preparations and, depending on the amount of total chloride in each individual powder sample, the total time to perform one test ranges between 20 minutes to 1 hour. The chloride content in the material, expressed as a percentage relative to the weight of the dry sample (% Cl), was calculated using the following Eq (5.19):

$$\%Cl = \frac{3.5453V_{Ag}M_{Ag}(V_2 - V_1)}{mV_2} \quad (5.19)$$

where: V_{Ag} is the volume of AgNO_3 added (in cm^3), M_{Ag} is the real molarity of the AgNO_3 solution and m is the mass of the powder sample (grams).

5.8.2.3.2. Chemical testing for free chloride content

Free chloride-content testing, also called water-soluble testing in concrete was also performed according to the RILEM TC 178-TMC recommendation. In this research a total of 52 samples from different specimens were tested for free chloride content. Free chloride indicates that which is not bound, but which is dissolved in the pore water of the sample.

The following procedure was followed in a temperature-controlled room at $20 \pm 2^\circ\text{C}$. A 5 gm powder sample that can pass through a 0.315 mm sieve, and measured with an accuracy of 0.001 gm, was weighed off and placed in a 250 ml beaker. 50 ml of distilled water was added and placed on a magnetic agitation plate for 3 minutes. The solution was filtered and the beaker was rinsed with 10 ml of distilled water. This volume is limited so as to prevent any supplementary extraction of chloride due to dissolution of calcium chloro-aluminates. 2 ml of concentrated nitric acid was then added and the solution was increased to 250 ml with distilled water in a graduated flask. For determining the chloride content, 50 ml of the filtered solution was poured into a beaker and placed in a potentiometric titrator. Typically a titrator contains a probe/half-cell (AgCl) thermometer for observing solution temperature (optional, not necessary for calculating Cl value) and a pipe to drop 0.01 M AgNO_3 (silver nitrate) solution (approximately 0.01 ml/drop) automatically into the filtered solution while it is being stirred. When silver nitrate solution drops into the filtered solution, the potential value (E) of the probe changes as shown in Figs 25a&b. The exact amount of silver nitrate is determined from the curve as shown in Figs 26a&b in the region of b to c where the molar ratio chloride and OH^- become one. This point is also known as the end point of titration. In this region, there is a point where the potential value jumps drastically (not shown here, it can only be seen in the titration display). In this case this point was recorded from the titrator machine. A large value of silver nitrate in the filtered solution indicates a higher free chloride content in the solution as seen in Fig 26b. A photo of the titrator is shown in the Appendix B, Fig B.2.

Experimental Methodology

After doing all the preparation, depending on the amount of total chloride in each individual powder sample, the total time to perform one test ranges between 7 minutes and 40 minutes. The water-soluble (free) chloride content (Cl), expressed as a percentage relative to the weight of the sample (%Cl), is calculated with the Eq (5.20):

$$\%Cl = \frac{3.545C_{AgNO_3}V_eV_f}{M_{pe}V_p} \quad (5.20)$$

where: C_{AgNO_3} is the exact concentration of the silver nitrate solution, V_e is the volume of silver nitrate added during titration, V_f is the volume of filtered solution prepared, V_p is the volume of filtered solution prepared and M_{pe} is the mass of powder sample (grams).

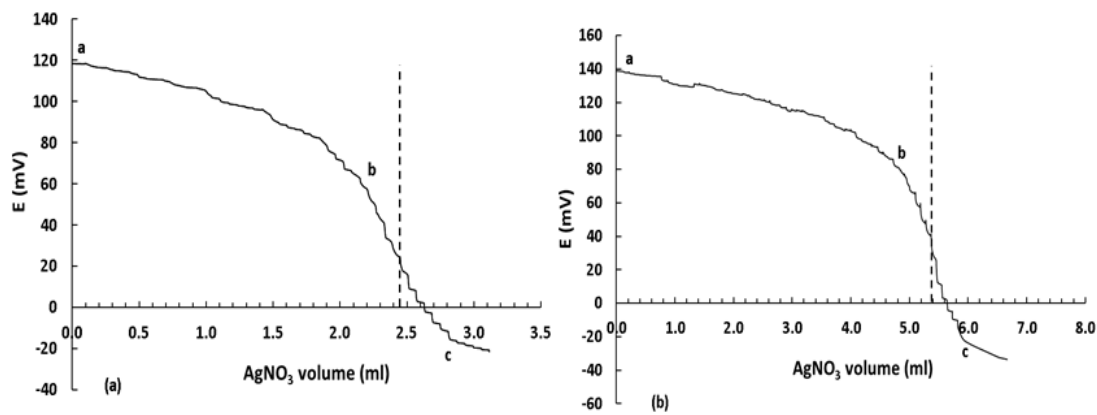


Figure 5.26: Changes of potential (E) due to adding $AgNO_3$ solution for (a) lower free Cl and (b) higher free Cl content in the samples.

5.8.3. Freeze-thaw testing

Capillary suction of de-icing solution and freeze-thaw testing (CDF) was performed to evaluate the resistance to deterioration caused by repeated freezing and thawing in the presence of salt water. The CDF test determines the mass loss of concrete per unit surface area after a number of freezing and thawing cycles while exposed to water or chloride solution. Four specimens measuring 150 mm x 150 mm x 50 mm from each FS4, FM3 and HM3 types were used for CDF tests as shown in Fig 5.27. All these specimens were collected by cutting the 150 mm x 150 mm x 700 mm beam specimens. A maximum of two specimens from each beam were collected. All the specimens were prepared as per DIN CEN/TS 12390-9 recommendation for a maximum of 42 freeze-thaw cycles. Five faces were sealed tightly with rubber strips and glued with silicon to prevent leakage between the concrete surface and the rubber strip. Only one face with a surface area of 150 x 150 mm was left open and this face was subjected to freeze-thaw cycles at a temperature of $\pm 20^\circ C$ as shown in Fig 28. 3% NaCl solution was used on top of the surface and having an approximate depth of 3 mm. Mass loss of the specimens was determined from the scaled materials obtained from 7, 14, 28 and 42 freezing and thawing cycles. All scaled materials were collected from the surface

Experimental Methodology

using a brush during the wet stage and then dried in an oven at a maximum temperature of 110°C. The first freeze-thaw cycle was started when the SHCC specimens were 60 days old and all mortar specimens were 58 days old. Total amount of mass loss ($M_{loss,n}$) of the specimen after “n” cycles is calculated by Eq (5.21).

$$M_{loss,n} = \frac{\sum m_s}{A} \text{ kg/m}^2 \quad (5.21)$$

where: m_s is the mass of scaled material from n cycles (kg) and A is the test surface area of the specimen.



Figure 5.27: Specimens in the chamber for freezing and thawing test.

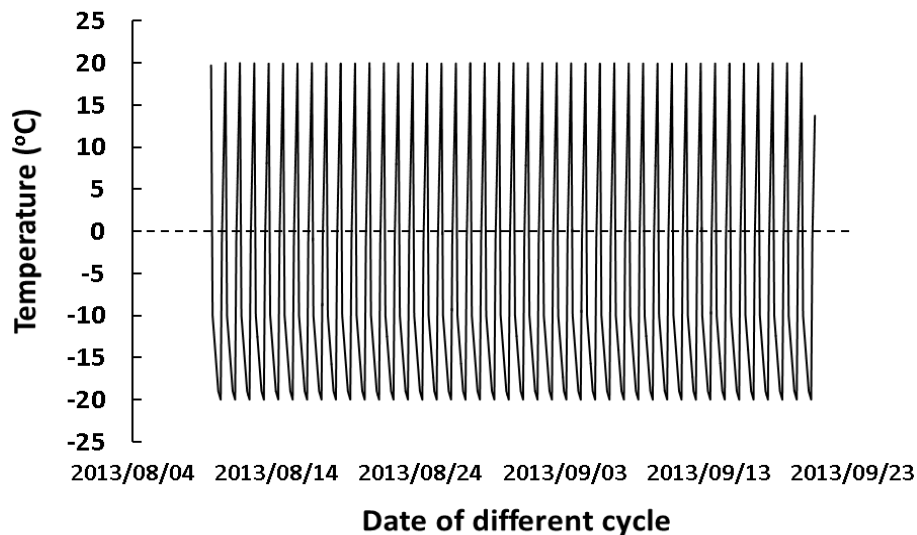


Figure 5.28: Applied temperature for freeze-thaw testing.

Experimental Methodology

5.8.4. Capillary water absorption testing

Capillary water absorption (CWA) tests according to DIN 52617 were also performed in all FS4, FM3 and HM3 types of un-cracked specimens at 33 days after casting. For this purpose 4 disc-shaped specimens of 100 mm diameter and 20 mm thickness were prepared from each material type. 48 Hours after casting, all these specimens were stored in a controlled-climate room (Temp $21 \pm 2^\circ\text{C}$ and RH $50 \pm 5\%$) until the testing date. At 30 days the surface along the 20 mm thickness was sealed so that no water could penetrate through the surface. At 33 days testing was started and one-directional water penetration (see Fig 5.29a) was allowed through the casting surfaces. Specimen mass gain readings were recorded up to 14 days. At day one, readings were collected more frequently and thereafter a minimum of one reading was taken each day. The water depth of approximately 1 mm was maintained throughout the testing duration. CWA coefficient (w) of the specimens was calculated by using Eq (5.22) below.

$$w = \frac{W}{t^{1/2}} \quad (5.22)$$

where: W is the area-based water intake (kg/m^2) and t is the time (hour).

5.8.5. Electrical resistivity testing

Concrete electrical resistivity (ER) is a material property which is independent of the geometry of concrete and denotes the resistance to the flow of a charge. It is the ratio between an applied voltage and the resulting current in a cell of defined-geometry concrete. Concrete resistivity is usually a good indication of the chloride ions transport rate and often it can be related to the likeliness of corrosion. It is depended on the concrete permeability, the number of pores and the ion concentration in the pores. When the ER of concrete is very high, it is assumed that there is less possibility of corrosion of the steel in the concrete.

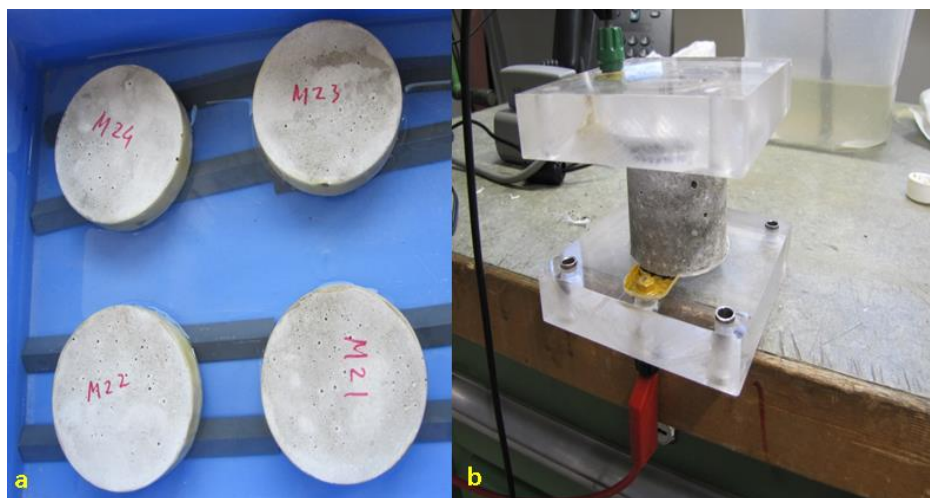


Figure 5.29: Specimens experimental set-up under (a) CWA and (b) ER testing.

Experimental Methodology

For ER of FS4, FM3 and HM3, 3 core samples (50 mm diameter and 50 mm length) were collected by drilling from the beam specimen (same as corrosion specimen) at 92 days after casting. Charges at different frequencies were applied through the specimen from both ends as shown in Fig 5.29b and the specimens resistivity was observed. Dry ER values were measured directly after collecting the specimens by drilling. All specimens were then placed in water for two days and then dried for one day before obtaining the wet ER values using Eq (5.23).

$$ER = R \frac{A}{l} \quad (5.23)$$

where: R is the electrical resistance of the specimen (it is a ratio of applied voltage and obtained current, Ω), A is the cross-sectional area of the specimen and l is the length of the specimen.

5.9. Concluding summary

This chapter provides details and graphical illustrations of how all the experiments were performed as per the requirements of the different test set-ups. In some cases especially for the mechanical properties, most experimental methodologies were followed as recommended by the appropriate different standards. For the preparation of specimens and the exposure conditions for corrosion rate and chloride testing, some new techniques were followed by the author and these techniques can be very useful for further developments and durability characterisation of this type of material.

For the purpose of this research work, quite a large number of different types of specimens were tested for both the mechanical and durability properties of materials used here. AE was used for the first time in SHCC which is a very useful tool in determining the matrix-cracking and fibre-breaking frequency. Corrosion testing was divided into four series based on the material types and an exposure and loading conditions. The influence of different exposure and loading types in the specimens from four different series of testing is discussed in the Chapter 7. In the case of chloride content and profiling in both reinforced and un-reinforced SHCC specimens, XRF and chemical testing and painting with AgNO_3 were discussed. A comparison between chloride content obtained from XRF and chemical testing are also discussed in Chapter 7. One important note is that the corrosion results reported here is from 108 weeks of testing. Within this period the application of accelerated (cyclic wetting and drying) chloride solution in the specimens by means of ponding and capillary suction was stopped for unavoidable circumstances. As a result in series one and two the accelerated exposure periods were not continuous through their total testing periods. The detailed of the exposures periods in different series is given in Fig 5.30. Another important note note is that it is known that cyclic wetting and drying exposure of NaCl solution allows for deeper penetration of chloride ions (Moukwa, 1990), and can lead to corrosion rates 20 times higher than exposure to a continuous salt fog (Yeomans, 2004). The author believes this prediction needs to be calibrated for different types of cement-based materials, including different w/b

Experimental Methodology

ratios. In this research the correlation between the 3 days wetting (with 3.5% NaCl solution) and 4 days drying exposure followed and actual field exposure was not studied. Indeed, the kinetics of cyclic wetting and drying of chloride are not fully understood, and more investigation is needed.

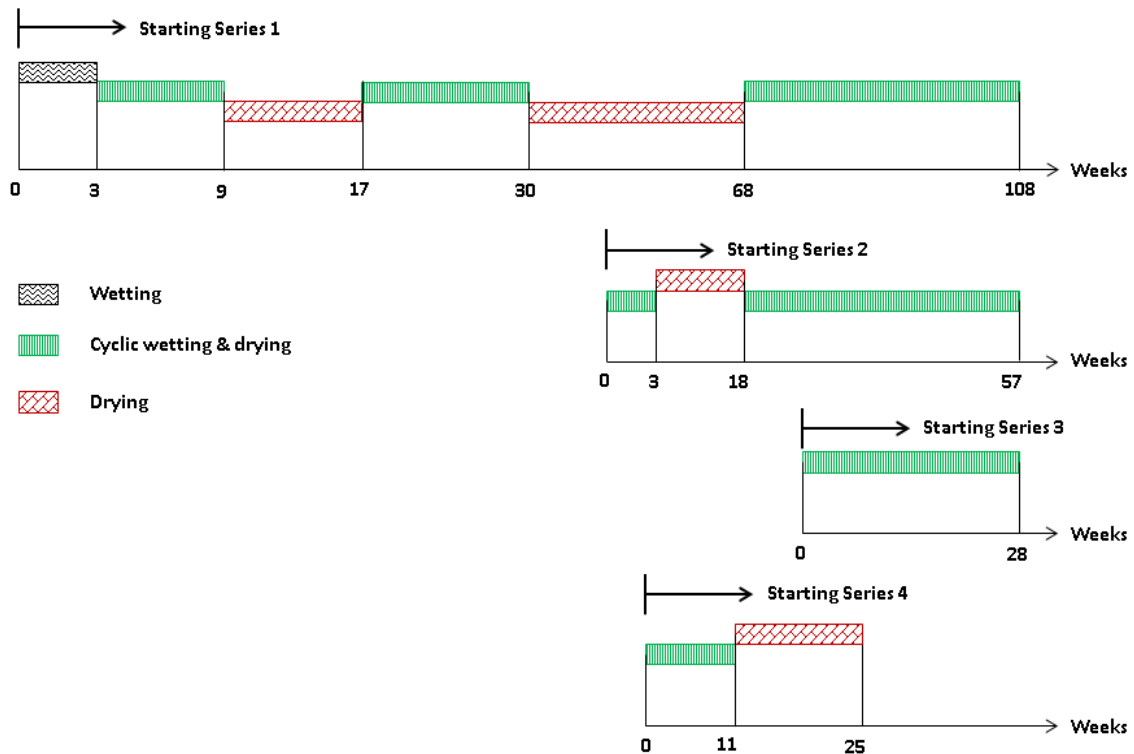


Figure 5.30: Details of the exposure periods in different series of testing.

5.10. References

- ACI Committee 226: 1987, 'Fly ash in concrete', ACI Material Journal, vol. 84, pp. 381–409.
- Adendorff, CJ, Boshoff, WP, & van Zijl, GPAG, 2009, 'Crack characterisation in SHCC: towards durability assessment', Advances in cement based materials. Advances in Cement-based Materials, CRC press, pp.215-221.
- ASTM C876-09, Standard Test Method for Corrosion Potentials of Uncoated Reinforcing Steel in Concrete.
- ASTM C 1152/C1152M-03, Standard test method for acid-soluble chloride in mortar and concrete, ASTM International, West Conshohocken, PA.
- ASTM C 1218/C1218M-90, Standard test method for water-soluble chloride in mortar and concrete, ASTM International, West Conshohocken, PA.
- ASTM E399-09, Standard test method for linear-elastic plane-strain fracture toughness K_{IC} of metallic materials.

Experimental Methodology

ASTM C1611 / C1611M-14, Standard Test Method for Slump Flow of Self-Consolidating Concrete, ASTM International, West Conshohocken, PA.

ASTM C231 / C231M-14, Standard Test Method for Air Content of Freshly Mixed Concrete by the Pressure Method, ASTM International, West Conshohocken, PA.

BAW Merkblatt (2004), Chlorideindringwiderstand von Beton (MCL)

Berry, EE 1976, 'Fly ash for use in concrete. Part 1: A critical review of the chemical, physical, and pozzolanic properties of fly ash', Energy, Mines and Resources Canada, Ottawa, ON, CANMET MSL Report 76-25.

Cabrera, JG & Hopkins, CJ 1982, 'The effect of PFA on the rheology of cement pastes', in proceedings of International Symposium on the Use of PFA in Concrete, University of Leeds, Leeds, UK, Apr 14–16, Ed.by J.G. Cabrera, A.R. Cusens, Department of Civil Engineering, University of Leeds, Leeds, UK, pp. 323–343.

Chinn, T 2013, Strain measurement validation using 3D photogrammetry techniques. MSc thesis, San Jose State University, available at http://scholarworks.sjsu.edu/etd_theses

DIN CEN/TS 12390-9 2006, Frost und Frost Tausalz Widerstand Abwitterung.

DIN 52617 1987, Bestimmung des Wasseraufnahmekoeffizienten von Baustoffen.

Song, G, 2005, Matrix Manipulation to Study ECC Behaviour. MSc thesis, Stellenbosch University, South Africa, available at <http://scholar.sun.ac.za/handle/10019.1/4647>

Kato, E, Kato, Y & Uomoto, T 2005, 'Development of simulation model of chloride ion transportation in cracked concrete' Journal of Advanced Concrete Technology, vol.3, no.1, pp. 85-95.

Kobayashi, K, Iizuka, T, Kurachi, H & Rokugo, K 2010, 'Corrosion protection of high performance fiber reinforced cement composites as a repair material', Cement and Concrete Composite, vol.32, pp. 411-420.

Kelly, A 1974, 'Microstructural parameters of an alligned fibrous composition', Conference on Composites - Standards, Testing and Design, Teddington, National Physical Laboratory, pp. 5-14.

Li, VC & Leung, CKY 1992, 'Steady state and multiple cracking of short random fiber composites', ASCE Journal Engineering Mechanics, vol. 118, no. 11, pp. 2246-2264.

Marsavina, L, Audenaert, K, De Schutter, G, Faur, N & Marsavina, D 2009, 'Experimental and numerical determination of the chloride penetration in cracked concrete', Construction and Building Materials, vol. 23, pp. 1638-1648.

Mc Kee, DC 1969, The Properties of an Expansive Cement Mortar Reinforced with Random Wire Fibres. PhD thesis, University of Illinois.

Mehta, PK 1994, 'Testing and correlation of fly ash properties with respect to pozzolanic behaviour', Electric Power Research Institute, Palo Alto, CA, Report CS3314.

Mindess, S & Young, JF 1981, Concrete. Englewood Cliffs, N. J.: Prentice-Hall, Inc.

Miyazato, S & Hiraishi, Y 2005, 'Transport properties and steel corrosion in ductile fiber reinforced cement composites', Torino, Italy: Paper 4484 of compendium of papers CD-ROM, ICF 11.

Experimental Methodology

Moukawa, M 1990, 'Deterioration of concrete in cold sea waters', *Cement and Concrete Research*, vol. 20, no. 3, pp. 439-446.

Nieuwoudt, PD 2012, Quantifying the cracking behaviour of strain hardening cement-based composites. MSc thesis, Stellenbosch University, South Africa, available at <http://scholar.sun.ac.za/handle/10019.1/20076>

NT Build 492-1999, Nordtest method: Concrete, mortar and cement-based repair materials: Chloride migration coefficient from non-steady-state migration experiments.

Ogawa, A & Hoshiro, H 2011, 'Durability of fibres', van Zijl and Wittmann (eds.), *Durability of strain-hardening fibre-reinforced cement-based composite (SHCC)*, DOI 10.1007/978-94-007-0338-4_6, pp. 81-88

Paul, SC 2011, Mechanical behaviour and durability performance of concrete containing recycled concrete aggregate. MSc thesis, Stellenbosch University, South Africa, available at <http://scholar.sun.ac.za/handle/10019.1/17962>

Paul, SC & van Zijl, GPAG 2013, 'Mechanically induced cracking behaviour in fine and coarse sand strain hardening cement based composites (SHCC) at different load levels', *Journal of Advanced Concrete Technology*, vol. 11 pp. 301-311.

Paul, SC, Pirskaewetz, S, van Zijl, GPAG & Schmidt, W 2015, 'Acoustic Emission for Characterizing the Crack Propagation in Strain Hardening Cement-Based Composites (SHCC)', *Cement and Concrete Research*, vol. 69, pp. 19-24.

RILEM TC 178-TMC 2002, Testing and modelling chloride penetration in concrete, Analysis of water soluble chloride content in concrete, *Materials and Structures*, vol. 35, pp: 586-588.

RILEM TC 178-TMC 2001, Testing and modelling chloride penetration in concrete, Analysis of total chloride content in concrete, *Materials and Structures*, Vol. 35, pp: 583-585.

Romualdi, J & Mandel J 1964, 'Tensile Strength of Concrete Affected by uniformly distributed and Closely Spaced Short Lengths of Wire Reinforcement', *Journal of the American Concrete Institute*, Vol. 61, No.6, pp. 657-671.

SANS 5863 1994, South African Standard Code of practice, First revision, Concrete tests - compressive strength of hardened concrete.

Song, G & van Zijl, GPAG 2004, 'Tailoring ECC for commercial application', proceedings 6th RILEM Symposium on fibre reinforced concrete (FRC), Varenna, Italy, pp. 1391-1400.

Thomas, MDA & Bentz, EC 2000, Life-365 computer program for predicting the service life and life-cycle costs of reinforced concrete exposed to chlorides.

Wittmann, FH, Zhao, T, Tian, L, Wang, F & Wang, L 2009, 'Aspects of durability of strain hardening cement-based composites under imposed strain', *Advances in Cement-Based Materials*, GPAG van Zijl & WP Boshoff (eds), CRC Press, p: 173-179.

Yeomans, SR 2004, *Galvanized steel reinforcement in concrete*, Elsevier Science, ISBN: 978-0-08-044511-3.

Chapter 6

We must believe that we are gifted for something, and that this thing, at whatever cost, must be attained. – Marie Curie

Fresh and Mechanical Behaviour of SHCC

6. Introduction

A number of different types of tests have been conducted to achieve the goal of this research work. This chapter describes the test results of the fresh properties such as slump flow and air content, together with the mechanical properties of strength and crack patterns of the SHCC and mortar specimens used here.

Table 6.1: Fresh properties of SHCC and mortar mixes

Id	Slump flow (mm)	% of Air	Id	Slump flow (mm)	% of Air
FS11	170-200	4.5-6.5	CS12	185	-
FS12	185	-	CS13	173	-
FS13	190	-	CS2	195-225	-
FS2	200-230	-	FM1	200	-
FS31 & FS32	180-200	5.8	FM3	195-230	0.3-0.7
FS4	185-220	1.8-2.9	CM1	220-225	-
CS11	170-200	4.5-8.9	HM3	208-220	1.3-1.6

6.1. Fresh properties of SHCC and mortar concrete

The fresh properties such as slump flow (measured with a small cone) and the percentage of air in the mixes are shown in Table 6.1. In FS and CS-SHCC the flow was within a reasonably small range of 170-230 mm and the mortar mixes had a similar flow range of 195-230 mm. Fig 6.1 shows the flow behaviour of both SHCC and mortar mixes. Typically the combination of coarse sand and fibre in CS-SHCC led to reduced flow. However, using super plasticizer in the mix any desired slump value can be obtained without any major changes in the mechanical and durability behaviour of concrete. In fibre concrete mixes, for maximum deployment of fibre properties, it is very important to have a flow-able fresh mix for good fibre dispersion. Therefore, in this research work the super plasticizer and the viscosity-modifying agent were added and adjusted in the case of CS-SHCC, leading to almost similar

Fresh and Mechanical Behaviour of SHCC

flow ranges for FS-SHCC and CS-SHCC. The air content ranges from 4.5% to 6.5 % for FS-SHCC and from 4.5% to 8.9 % for CS-SHCC. For the same mix, the variation in results was found for different batches of SHCC for different specimens (dumbbells, beams, cubes and cylinders). It is worth mentioning that in each series a minimum of 2 different batches of SHCC were required to prepare of specimens. However, dumbbell specimens were prepared and tested at 14 days for each different batch and in terms of number of cracks and crack widths no significant differences were found for the different batches of SHCC.



Figure 6.1: Slump flow measured in SHCC and mortar.

6.2. Mechanical properties of SHCC and mortar

Details of the compressive, flexural and tensile strengths together with tensile and flexural cracks in the SHCC and mortar specimens used in this research work are described here.

6.2.1. Compressive strength and E-mod

The ultimate compressive strength (f_u) range of different SHCCs was between 23 and 34 MPa and the range of E-mod was between 13 and 19 GPa. A minimum of 6 to a maximum of 20 cubes (in the case of FS11, FS3 and CS11) from each type of SHCC were tested for determining the compressive strength and a minimum of 3 to a maximum of 9 cylinders were used for E-mod testing. A maximum of 15% and 22% coefficient of variations (CoV) were observed in strength and E-mod calculations respectively as illustrated in Table 6.2. Fig 6.2 shows a typical stress-strain curve (SSC) as obtained from compressive strength testing of SHCC and mortar. After reaching the ultimate load state, mortar specimens failed suddenly because of their brittle behaviour. Note that in the case of mortar specimens when the load

Fresh and Mechanical Behaviour of SHCC

reached its peak, the resistance dropped abruptly and specimens were unloaded quickly to avoid damage to instrumentation used to obtain the load vs strain curve. Because of this sudden unloading, no strain softening can be seen in Fig 6.2 for the mortar specimens. In contrast, in SHCC specimens, the strain seems to increase even after reaching the ultimate resistance capacity but the load was reduced before testing stopped. Because of fibres in SHCC specimens, failure was not sudden as for mortar specimens.

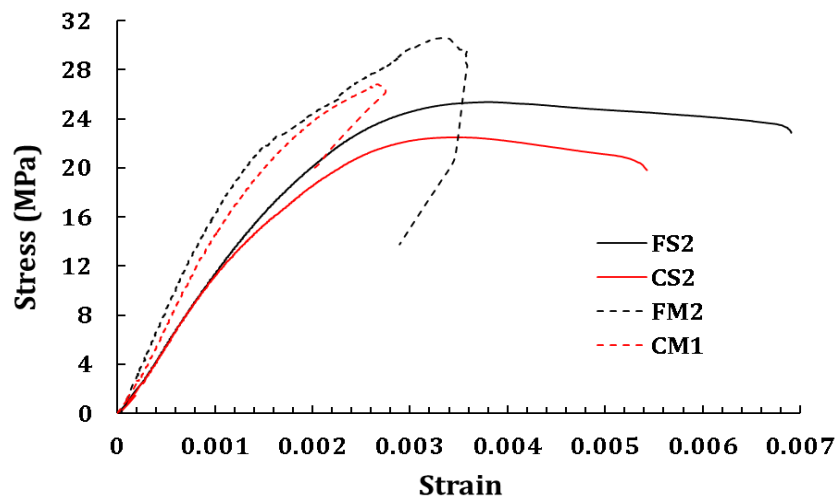


Figure 6.2: Typical stress-strain curve response of SHCC and mortar specimens under compressive strength testing.

Table 6.2: SHCC and mortar 28 days ultimate compressive strength (f_{cu}) and E-mod with their CoV (%)

Id	f_{cu} (MPa)	CoV(%)	E-mod (GPa)	CoV(%)
FS11	34	8.7	18	13.60
FS12	32	6.5	16	-
FS13	27	11.2	18	-
FS2	25	4.4	14	12.04
FS31	24	1.4	14	22.12
FS4	26	3.3	13	5.00
CS11	27	15.1	18	4.40
CS12	29	2.8	13	-
CS13	24	7.2	19	-
CS2	23	2.1	13	6.56
FM1	31	2.6	17	10.82
CM1	27	3.6	17	10.49
FM3	30	1.1	-	-
HM3	61	2.3	-	-

Table 6.2 shows the compressive strengths and E-mod for the different types of SHCC and mortar used in this research work. Not much difference was observed in the strength and E-

 Fresh and Mechanical Behaviour of SHCC

mod for the same matrix with (SHCC) and without fibre (mortar). However, a noticeable difference was observed in the failure mechanism of SHCC and mortar cubes and cylinder specimens under compressive testing. A sudden failure was observed in the mortar specimens while in SHCC, failure was gradual due to the fact that fibres bridge the matrix cracks as well as the formation of many cracks before it fails. There was no significant difference in the strength and E-mod results for FS and CS. This means that for the design compressive strength of 25 MPa to less than 40 MPa, the particle size of sand appears not to have a noticeable influence on the mechanical behaviour of SHCC.

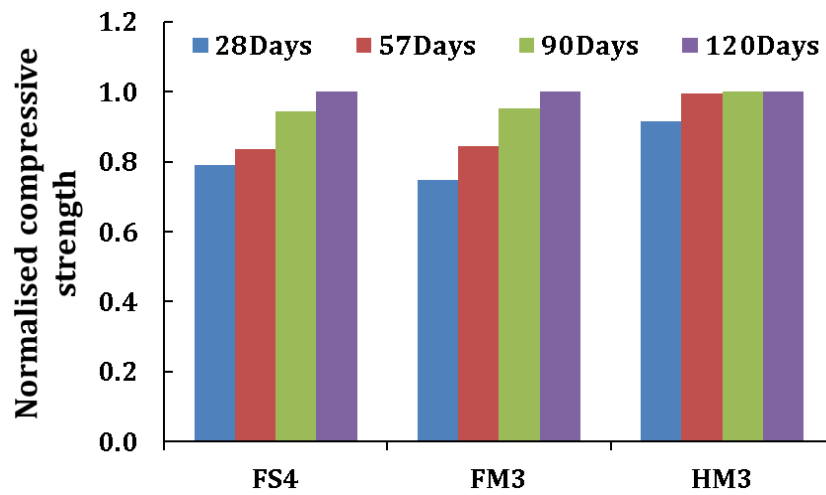


Figure 6.3: Compressive strength development in SHCC and mortar (reference strength: 120 days in each case).

Fig 6.3 shows the compressive strength development in SHCC and mortar. High strength mortar (HM3) shows little or no development of strength after 56 days while in FS4 and FM3 it shows significant development even after 90 days. The strength improvement in FS4 and FM3 can be explained by the large amount of un-hydrated binders (cement and fly-ash) which were hydrating with time in the presence of moisture. Note that all these specimens were water-cured and removed from the water just before testing. In HM3, cement was the only binder and perhaps all the cement was hydrated within 56 days and as a result no strength improvement was found in HM3. Also in concrete, slower strength development is well-known when fly ash is used, because of its pozzolanic nature. This is also the reason of strength development in FS4 and FM3.

6.2.2. Tensile stress and strain of SHCC

The typical direct tensile stress and strain responses of SHCCs containing various fibre volumes at different ages are shown in Figs 6.4- 6.6. Note that these are typical individual responses and not average or best responses. A minimum of 4 to a maximum 18 specimens from each type of FS and CS-SHCC were tested at ages of 14 and 28 days. Their average ultimate tensile strength ($f_{u,st}$), first cracking strength ($f_{cr,st}$) and strain ($\epsilon_{u,st}$) are summarised in

Fresh and Mechanical Behaviour of SHCC

as reported in Table 6.3. Note that all the tensile strength, strain and crack results reported here are from un-reinforced SHCC.

Table 6.3: SHCC tensile strength and strain at different days

Id	Days	$f_{u,st}$ (MPa)	CoV (%)	$f_{cr,st}$ (MPa)	CoV (%)	$\epsilon_{u,st}$ (%)	CoV (%)
FS11	14	3.6	7.6	2.5	25.0	3.1	17.0
	28	3.9	11.4	2.7	16.7	1.2	10.8
	56	3.8	11.4	-	-	-	-
FS12	28	3.4	18.3	2.4	33.2	1.0	40.7
FS13	28	2.5	11.6	2.1	7.7	0.8	23.2
FS2	14	2.6	11.6	2.0	6.5	2.2	46.4
	28	3.6	5.4	3.1	9.9	1.1	35.9
FS31	14	2.2	8.2	1.6	30.2	1.6	43
FS4	14	3.2	4.8	2.7	14.8	1.1	4.1
CS11	14	3.4	10.4	2.4	14.0	2.9	32.9
	28	3.6	5.8	3.0	11.6	1.0	23.5
	56	3.8	9.3	-	-	-	-
CS12	28	3.0	6.8	2.4	20.9	0.9	24.7
CS13	28	2.3	11.0	1.9	14.5	0.7	25.8
CS2	14	2.0	27.9	2.0	31.7	1.7	46.9

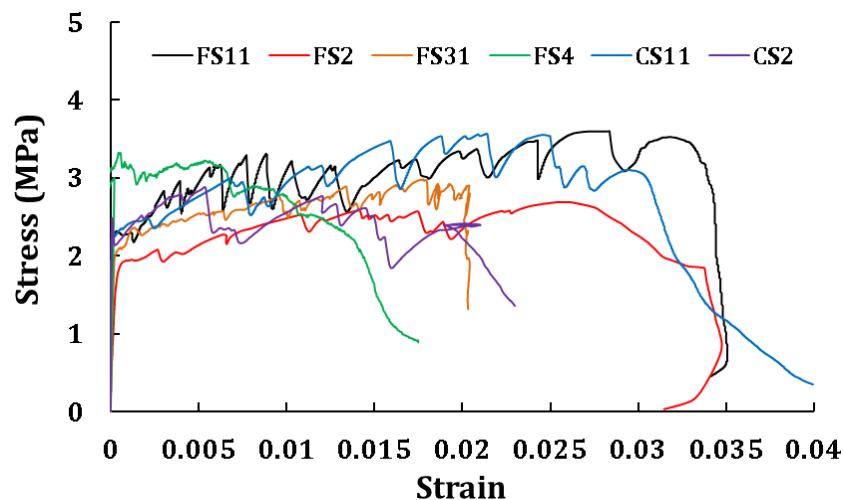


Figure 6.4: SHCC stress vs strain response in direct tensile testing at 14 days.

At the same age FS11 shows the highest tensile strength of all the SHCC types reported on here. It was discussed in the previous chapter that FS11 has slightly higher fibre content (2.2%) than the mixes with 2% fibre in FS2, FS3 and CS11 and CS2. In FS11 and CS11, the 14 day ultimate strain was significantly higher ($\leq 3\%$) than that of other SHCCs and at the age of 28 days, all SHCCs show significantly lower strain than at 14 days. However, in all cases the 28 day ultimate tensile strength increased slightly from the 14 day strength. Therefore, the experimental results show that these particular SHCCs become more brittle in

Fresh and Mechanical Behaviour of SHCC

direct tensile strength at higher ages. This trend was also found by Wang & Li (2006) and Yang *et al.* (2005) and requires further mix improvement to reduce such brittleness with aging. Also, the strain capacity of SHCC is influenced by the aggregate/binder ratio (a/b), aggregate content and the grading of aggregates (van Zijl, 2005).

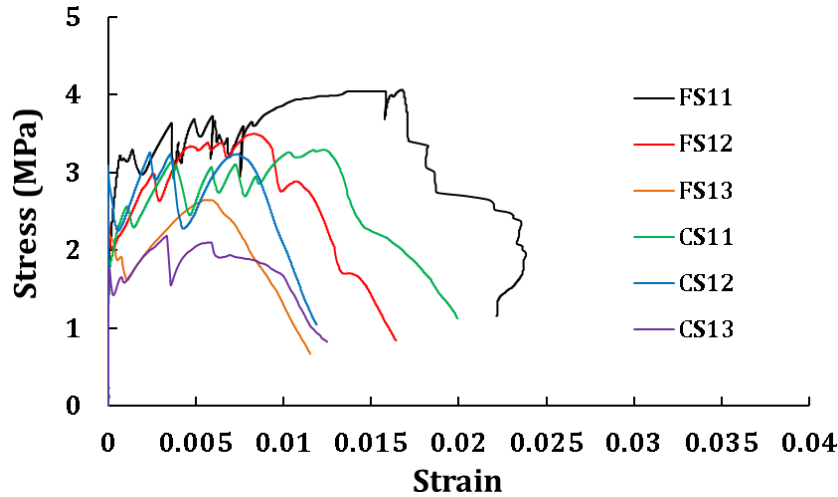


Figure 6.5: SHCC stress vs strain response in direct tensile testing at 28 days.

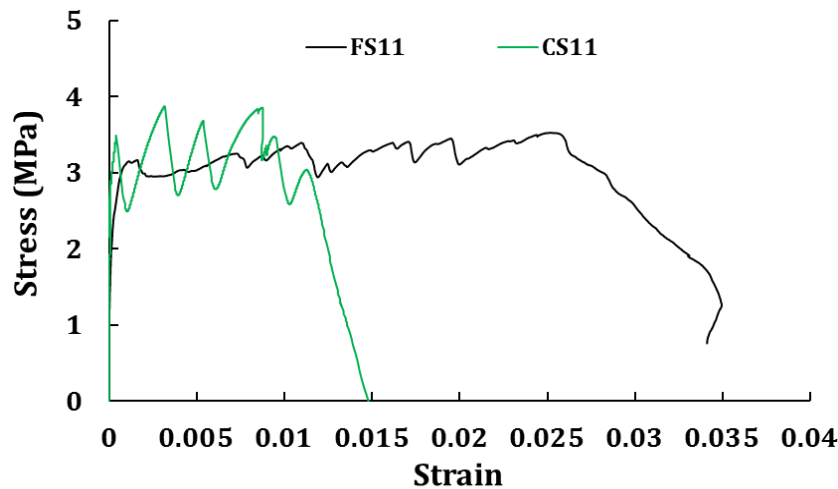


Figure 6.6: SHCC stress vs strain response in direct tensile testing at 56 days.

Table 6.3 indicates that after 28 days of testing, there is a roughly 10.6% and 35.6% lower tensile strength in FS12 and FS13 than in FS11. Similarly a 16.3% and 35.1% lower tensile strength was found in CS12 and CS13 than in CS11. Therefore higher fibre content leads to an increase in the strength as well as the ultimate strain in both FS and CS-SHCC mixes. Different results of tensile strength and strain were also observed in FS-SHCC for the same amount of fibre content (2%). It can be attributed to the difference in batches mixed as well as to the collection of the same materials but at different times. Note that the results reported

Fresh and Mechanical Behaviour of SHCC

in this research are from the years 2012 to 2014 and during this period, although the cement and fly-ash types were the same, they were collected at different times from the same companies.

The average ultimate tensile strength and first cracking strength developments (FS11 as a reference) in different SHCCs at 14 days and 28 days are shown in Figs 6.7 & 6.8. It can be seen that at both ages the difference between the first cracking strength and the ultimate tensile strength are the same in all types of SHCCs. The relationship between the ultimate tensile strength and first cracking strength to the ultimate tensile strain in FS11 were also plotted and are shown in Fig 6.9. For this particular type of FS11, there was no direct relationship found between the different strengths and the ultimate strain values.

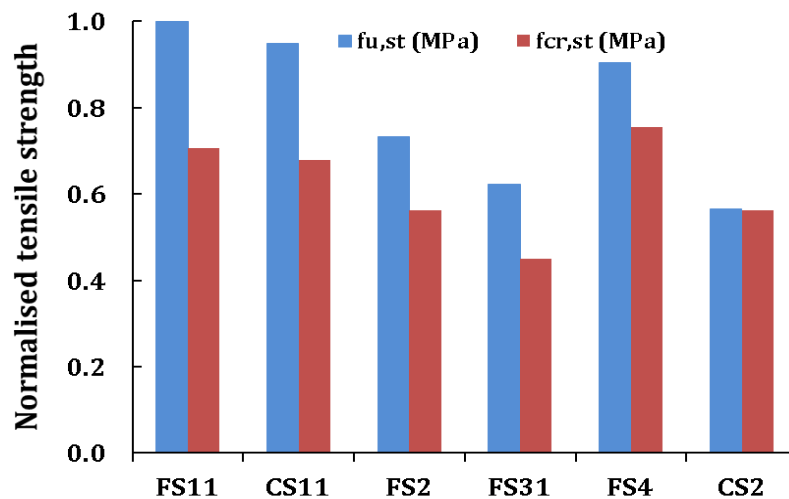


Figure 6.7: Strength development in different types of SHCCs' ultimate and cracking strength at 14 days (reference strength: FS11).

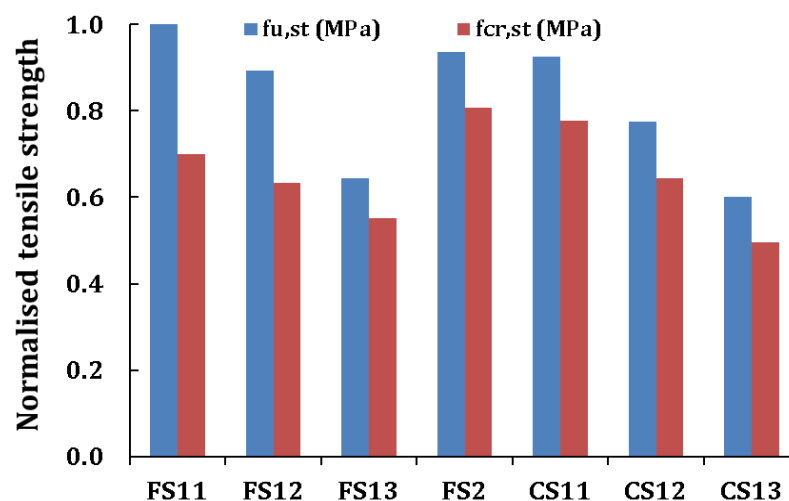


Figure 6.8: Strength development in different types of SHCCs' ultimate and cracking strength at 28 days (reference strength: FS11).

Fresh and Mechanical Behaviour of SHCC

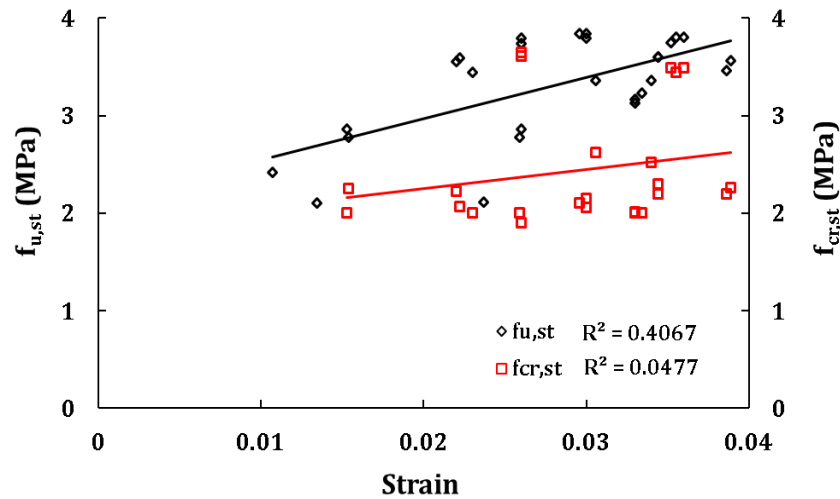


Figure 6.9: Relationship between FS11 ultimate tensile ($f_{u,st}$) and cracking strength ($f_{cr,st}$) to the ultimate strain at 14 days.

6.2.3. Number of tensile cracks and crack widths in un-reinforced SHCC

The average numbers of cracks at different strain levels of FS11 and CS11 at different test ages are shown in Figs 6.10 to 6.13. These particular mixes of FS11 and CS11 show almost the same total number of cracks at their ultimate strain levels. In both SHCCs, the average crack widths (ACW) remain below $60\ \mu\text{m}$ even at different levels of strain as shown in Figs 6.14 & 6.15. At the same strain levels (2.5%) the maximum crack widths (MCW) in both SHCCs have similar values. This implies that, if a good mix and fibre dispersion can be maintained in the SHCC with CS, similar strain hardening behaviour and crack properties as in FS-SHCC can also be obtained in CS-SHCC.

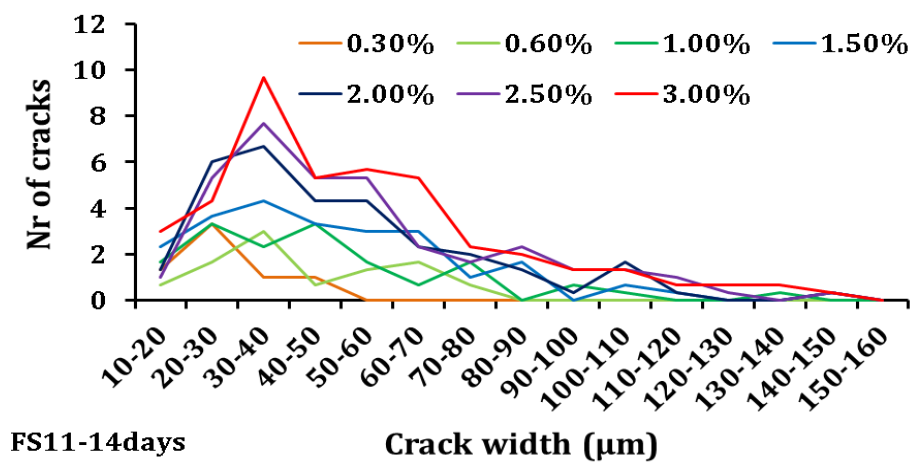


Figure 6.10: Tensile cracks at the age of 14 days of FS11 specimens at different strain (%) levels.

Fresh and Mechanical Behaviour of SHCC

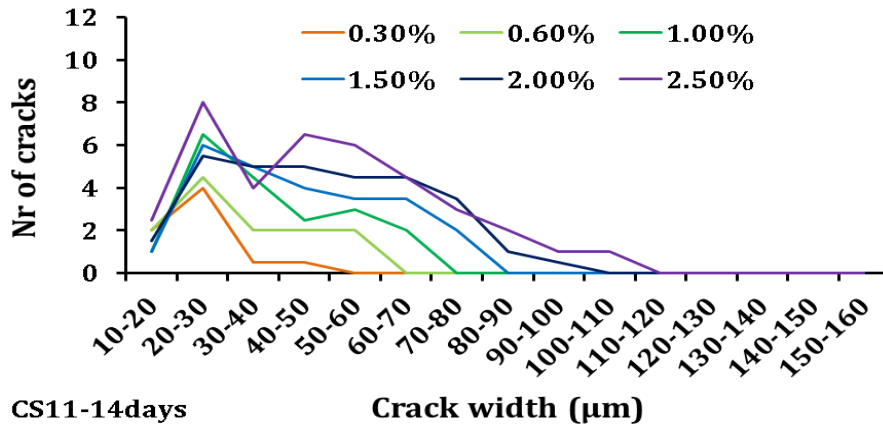


Figure 6.11: Tensile cracks in CS11 specimens at the age of 14 days at different strain (%) levels.

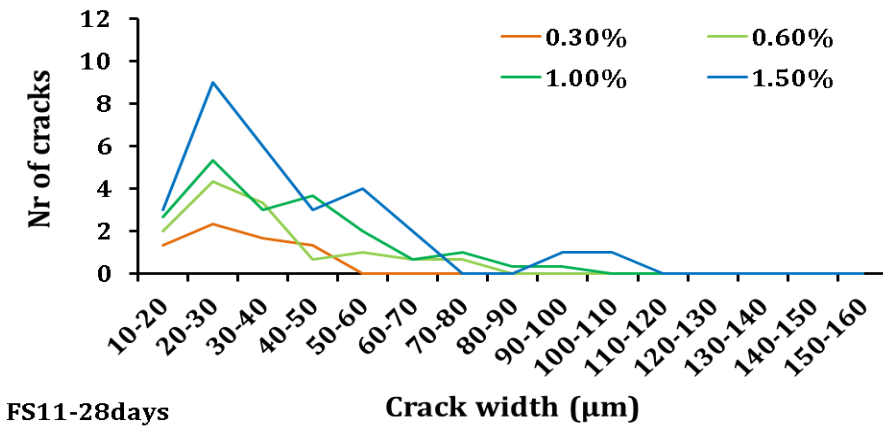


Figure 6.12: Tensile cracks in FS11 specimens at the age of 28 days at different strain (%) levels.

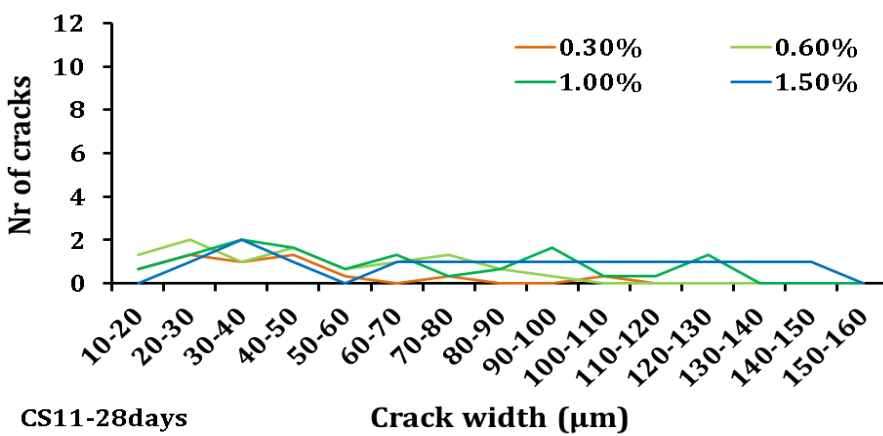


Figure 6.13: Tensile cracks in CS11 specimens at the age of 28 days at different strain (%) levels.

Fresh and Mechanical Behaviour of SHCC

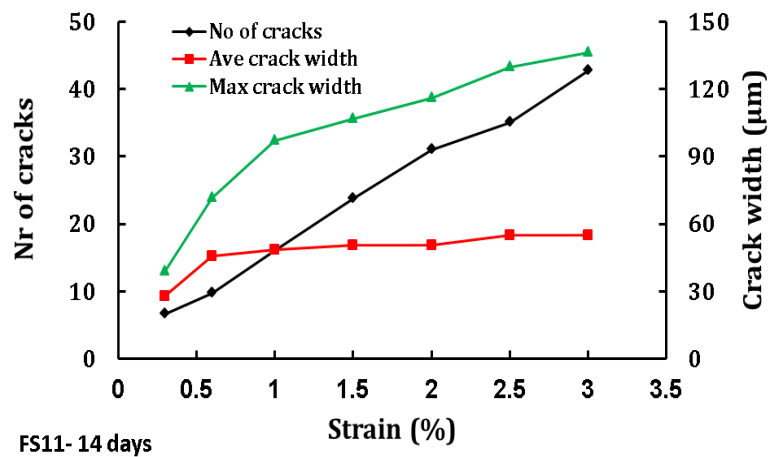


Figure 6.14: Average no of cracks and crack widths at the age of 14 days of FS11 specimens.

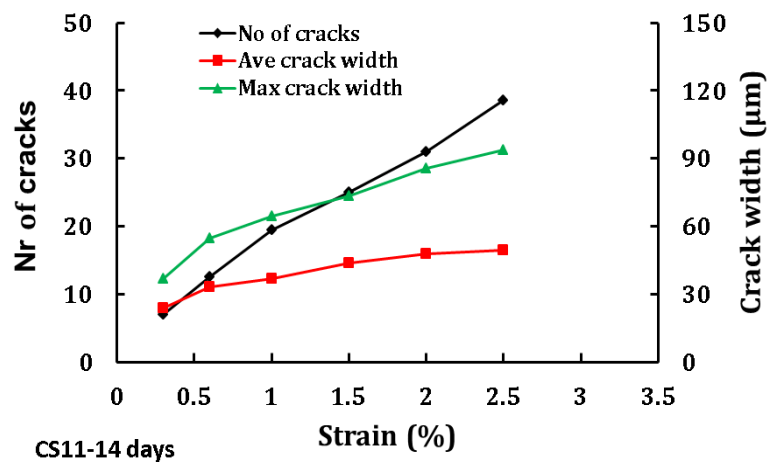


Figure 6.15: Average no of cracks and crack widths at the age of 14 days of CS11 specimens.

Figs 6.16 & 6.17 show the ACW and MCW in different FS and CS-SHCC specimens after tensile strength testing at 28 days. At the same level of deformation, the higher fibre content of FS11 shows a significantly lower ACW and MCW than FS12 and FS13. Similar trends were also found in CS-SHCC in Fig 6.17. FS11 shows better performance than CS11 while opposite trends were found in the case of lower fibre content. More research needs to be carried out to confirm this trend that lower fibre content in CS has a better performance than the FS in SHCC. Formation of tensile cracks within the gauge length of dumbbell specimens is shown in Fig 6.18. Fewer numbers of cracks were found in the specimens at 28 days which are shown in Figs 6.12 & 6.13 and the possible reasons of it were already discussed in section 6.2.2. More photos on tensile cracking in SHCC for different content can be found in Appendix C, Fig C.1.

Fresh and Mechanical Behaviour of SHCC

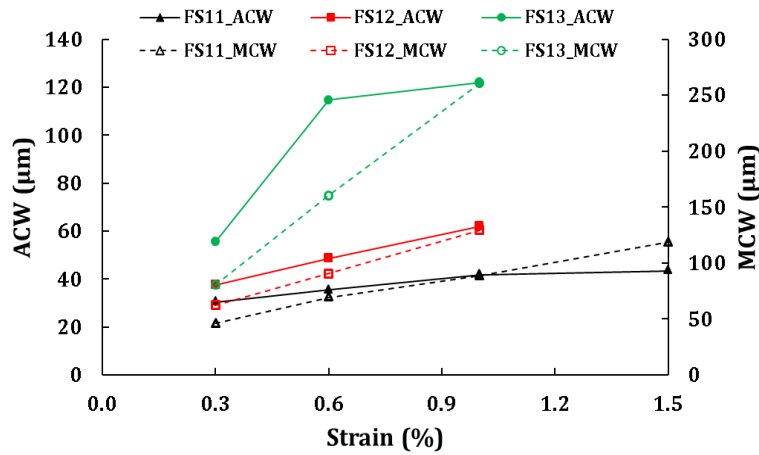


Figure 6.16: ACW and MCW at different strain levels in different FS specimens at 28 days.

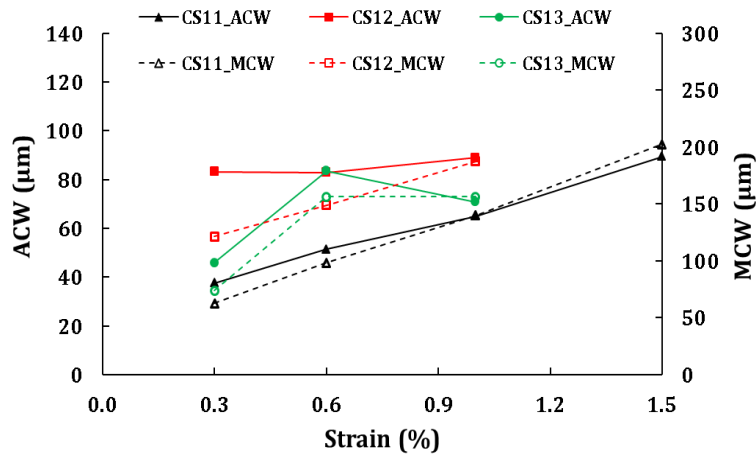


Figure 6.17: ACW and MCW at different strain levels in different CS specimens at 28 days.

The relationship between average crack spacing in FS11 and CS11 at different strain levels are shown in Fig 6.19. It can be seen that the crack spacing in un-reinforced SHCC at direct tensile testing is exponentially related to the tensile strain. A linear relationship was also found in both FS11 and CS11 for total crack widths versus different strain levels as shown in Fig 6.20. Fig 6.21 shows the average number of cracks at different strain levels of different FS-SHCC at 28 days. Once again the number of cracks linearly increases with the increased strain level in FS-SHCC.

Fresh and Mechanical Behaviour of SHCC

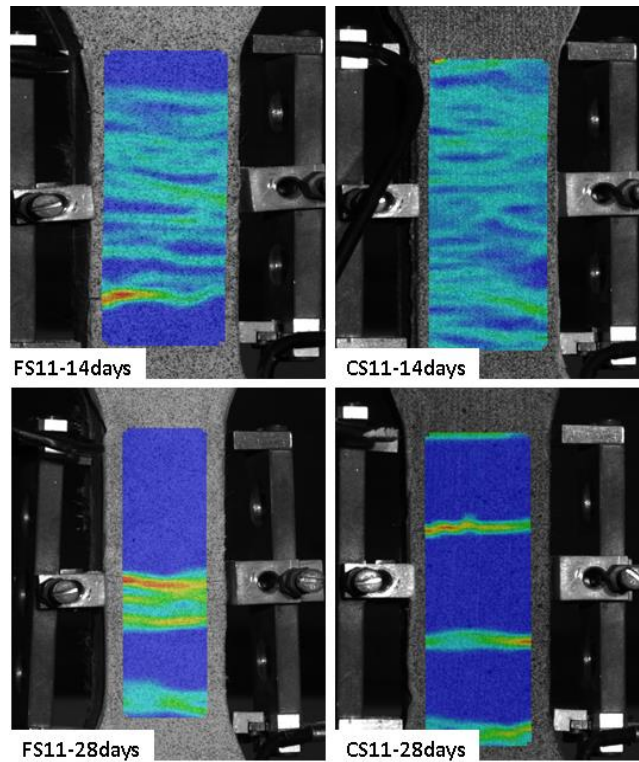


Figure 6.18: Formation of cracks in FS11 and CS11 during tensile testing.

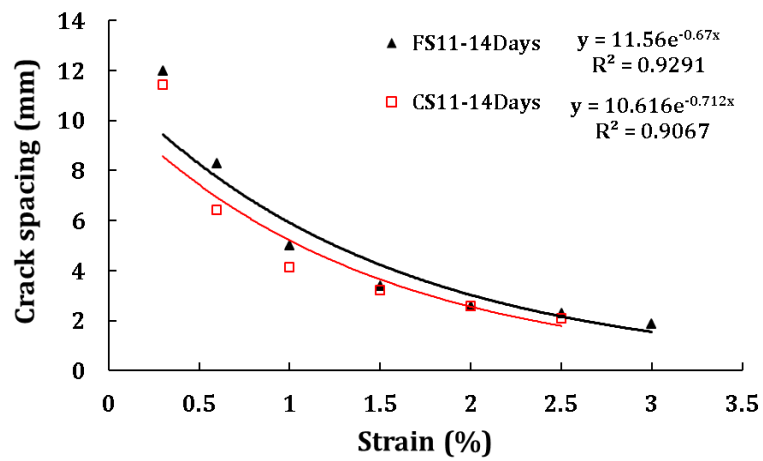


Figure 6.19: Relationship between crack spacing and strain in both FS11 and CS11.

Fresh and Mechanical Behaviour of SHCC

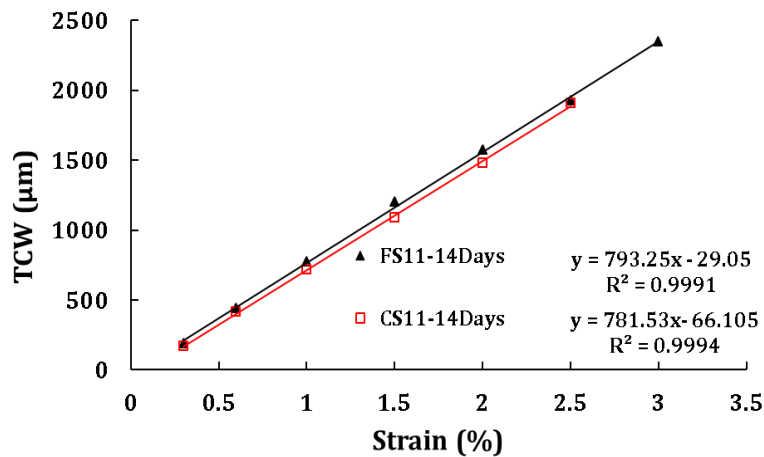


Figure 6.20: Relationship between total crack widths (TCW) vs different strain levels of FS11 and CS11 at 14 days.

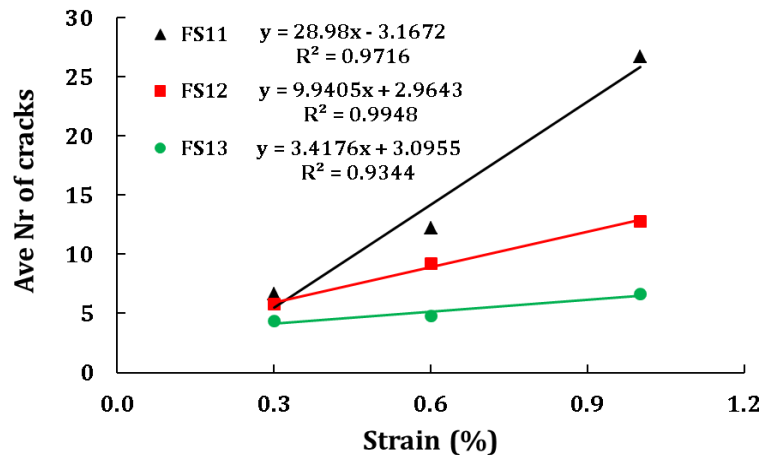


Figure 6.21: Relationship between average nr of cracks and tensile strain in FS-SHCC at 28 days.

6.2.4. Flexural strength of SHCC and mortar

Both reinforced and un-reinforced beams were used in flexural testing. It was discussed in the previous chapter that all the beams were tested under three point bending conditions. Readers must also take note that all the unreinforced SHCC and mortar specimens used for flexural strength were 100 mm x 100 mm x 500 mm in size. The reinforced FS2 (R/FS2), R/FS4, R/CS2 and R/FM3 specimens were also 100 mm x 100 mm x 500 mm in size and all R/FS31 and R/FS32 specimens were 80 mm x 100 mm x 490 mm in size. All these reinforced specimens were further used for accelerated chloride-induced corrosion testing, which is discussed in the next chapter. Table 6.4 shows ultimate-flexural and first-cracking strengths of un-reinforced SHCC and mortar specimens and their CoV (%) at the age of 28 days.

Fresh and Mechanical Behaviour of SHCC

Table 6.4: Ultimate-flexural ($f_{u,ft}$) and first-cracking ($f_{cr,ft}$) strengths at 28 days for SHCC and mortar

Id	$f_{u,ft}$ (MPa)	CoV (%)	$f_{cr,ft}$ (MPa)	CoV (%)
FS11	10.3	12.7	4.6	14.7
FS2	10.1	17.6	4.5	9.9
FS4	8.3	10.6	6.2	5.8
CS11	9.0	17.4	5.3	23.6
CS12	8.9	1.4	4.4	7.9
CS2	9.6	10.2	5.2	10.3
FS11*	13.9	8.5	-	-
CS11*	10.4	5.7	-	-
FM1	2.4	5.4	-	-
FM3	1.4	5.3	-	-
FM4	2.3	10.0	-	-
CM1	2.6	1.8	-	-
CM4	3.4	9.4	-	-
HM3	5.6	8.9	-	-

*These values are from the notched specimens

Higher fibre content in FS11 led to higher ultimate strength than other types of SHCC. All CS-SHCCs show a slightly higher first-cracking strength than the FS-SHCC used here and a similar trend was also noticed in direct tensile testing. For similar mix designs both FS11 and CS11 notched specimens show a significantly higher ultimate strength than the un-notched specimens. The reason for this difference may be explained by the different batches of mixes for notched and un-notched specimens. Also in un-notched specimens, the variation of strength was quite higher (as seen from the CoV) than in the notched specimens and this can be another reason for the lower ultimate strength.

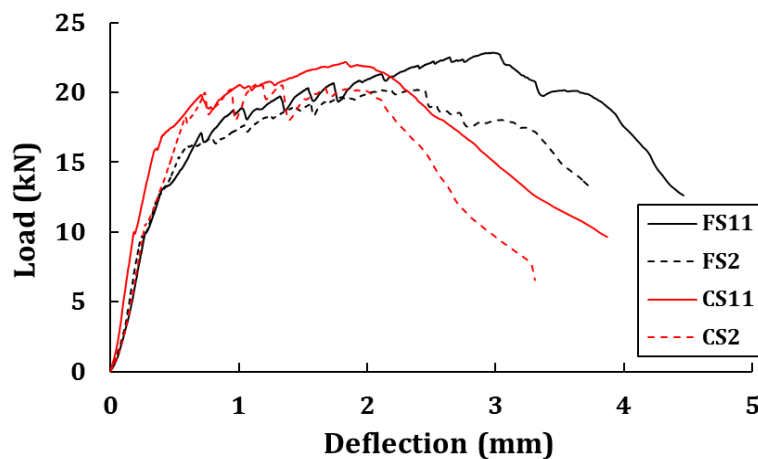
Table 6.5 shows the flexural load responses of different reinforced SHCC (R/SHCC) specimens at three different levels of deflection. The different deflection levels were based on the specimens' response at ultimate load level as well as the expected crack widths in the specimens for corrosion testing. Remember that all the R/FS2, R/CS2, R/FM1 and R/CM1 specimens' size were 100 mm x 100 mm x 500 mm and all R/FS31 specimens were 80 mm x 100 mm x 490 mm in size.

Fig 6.22 shows the different un-reinforced SHCC specimens' responses in flexural testing at 28 days where the maximum strength of FS11 is also confirmed. The average ultimate deflection in un-reinforced SHCC specimens was about 3 mm and the first crack appeared at a deflection level of about 0.5 mm. Note that in Fig 6.22, the values (load vs deflection curves) are typical individual responses and not average or best responses.

Fresh and Mechanical Behaviour of SHCC

Table 6.5: Different reinforced SHCC beam responses in three-point bending testing at 14 days

Id	Cover depth (mm)	Nr of steel bars	Level of deflection (mm)	Ave. Load (kN)	CoV (%)
FS2	C15	B1	3.5	44.4	1.7
		B2		50.2	8.7
	C25	B1		41.1	4.1
		B2		48.7	10.1
	C35	B1		39.1	0.9
		B2		45.3	8.4
CS2	C15	B1		38.1	4.7
		B2		52.7	4.7
	C25	B1		33.3	2.3
		B2		47.1	1.9
	C35	B1		29.9	3.9
		B2		41.2	1.7
FS31	C15	B1	5	14.8	11.9
		B1	7	14.1	16.4
	C25	B1	5	15.5	8.3
		B1	7	14.9	2.9
	C35	B1	5	14.0	8.9
		B1	7	12.1	22.9
FM1	C15	B1	1.2	12.0	10.0
CM1	C15	B1	1.2	12.2	8.9

**Figure 6.22:** Un-reinforced SHCC specimen response in flexural testing at 28 days.

In the case of R/FS2 and R/CS2 a total of 18 beams of each type of SHCC were tested in flexural testing and these specimens were also used for corrosion testing. All of these were pre-cracked in flexure up to a deflection level of 3.5 mm. For each cover depth of concrete, two types of reinforcement (single and double bar) were used. For each cover depth, a total of

Fresh and Mechanical Behaviour of SHCC

6 beams, 3 with a single bar (10 mm diameter, Y10) and 3 with two Y10 bars were tested for both types of SHCC. Their flexural test results are shown in Figs 6.23 & 6.24. C15, C25 and C35 denote different cover depths and B1 and B2 denote single bar and double bar specimens. Fig 6.25 shows the R/FS31 specimens' flexural responses to two levels of deflection (5 and 7 mm) with a single bar only. It is worth mentioning that a 5 mm stainless steel bar was also placed together with the Y10 steel bar in each specimen and that both bar lengths were about 500 mm each. As already mentioned in the previous chapter, the stainless steel bar was used as a counter electrode for corrosion testing. The position of this steel bar was 10 mm above the Y10 in the flexural testing condition as shown in Figs 5.15 & 5.16 in Chapter 5.

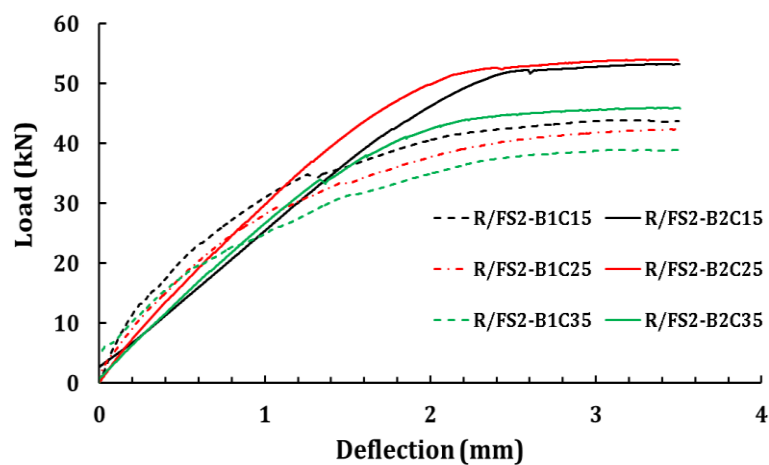


Figure 6.23: R/SHCC specimen response in flexural testing at the age of 14 days.

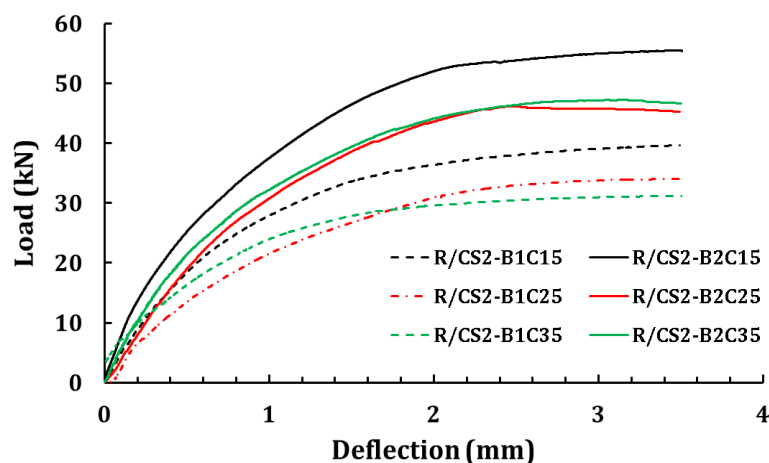


Figure 6.24: R/SHCC specimen response in flexural testing at the age of 14 days.

For R/FM1 and R/CM1 different levels of deflection were chosen as is shown in Table 6.5. The reasons for choosing different deflection levels for SHCC and mortar specimens are that (i) the deflection level at ultimate resistance of SHCC and mortar are different and (ii) for the same level of deflection in SHCC and mortar specimens, the crack widths are significantly

Fresh and Mechanical Behaviour of SHCC

different. In this research the expected average crack widths in both SHCC and mortar were below 0.10 mm and the deflection levels of SHCC and mortar specimens were chosen so that cracks would not cross this limit.

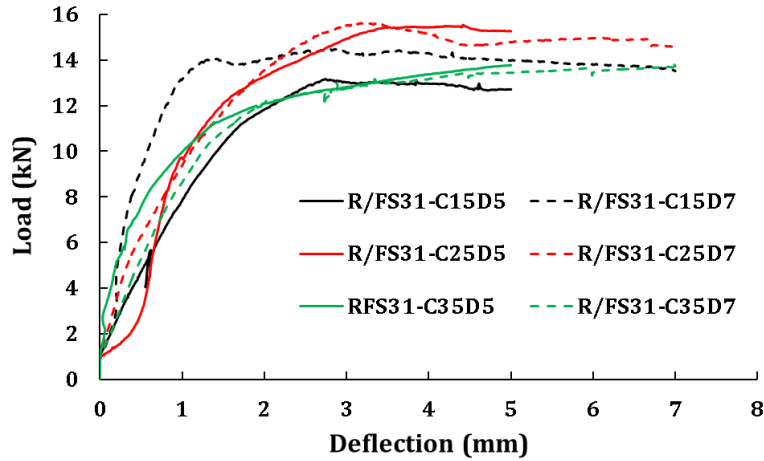


Figure 6.25: R/FS3 specimen response in flexural testing at the age of 14 days.

Fig 6.26 shows the difference between the first cracking strength and the ultimate flexural strength of different un-reinforced SHCC specimens used in the research. The average first cracking strength is about 50% of the ultimate flexural strength. Flexural strength development with time was also investigated in un-reinforced SHCC and mortar specimens as shown in Fig 6.27. It is worth mentioning that the results shown in Fig 6.27 are from the small prism specimens' response as mentioned in the previous Chapter 5, Table 5.4. Up to 90 days both FS4 and FM3 had shown significant improvement in the strength development from their early age and after 90 days no major changes were found. In the case of HM3 after 57 days, strength development was not so significant and the reason is already discussed in the previous section 6.2.1. In future more studies need to be done to prove this issue.

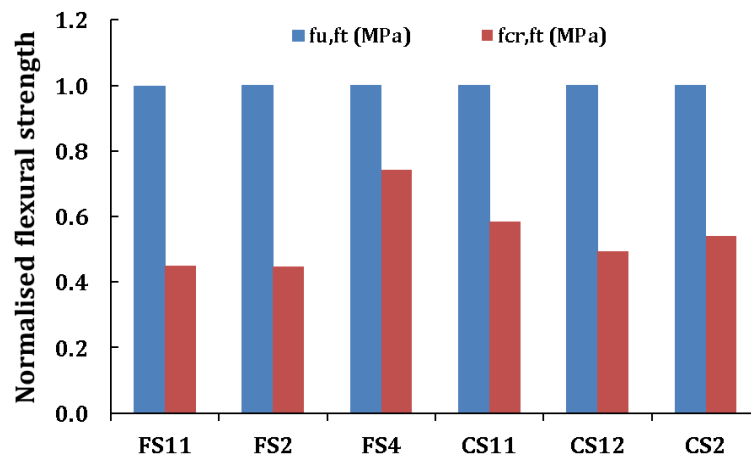


Figure 6.26: Different un-reinforced SHCCs ultimate-flexural and first-crack strengths at the age of 28 days.

Fresh and Mechanical Behaviour of SHCC

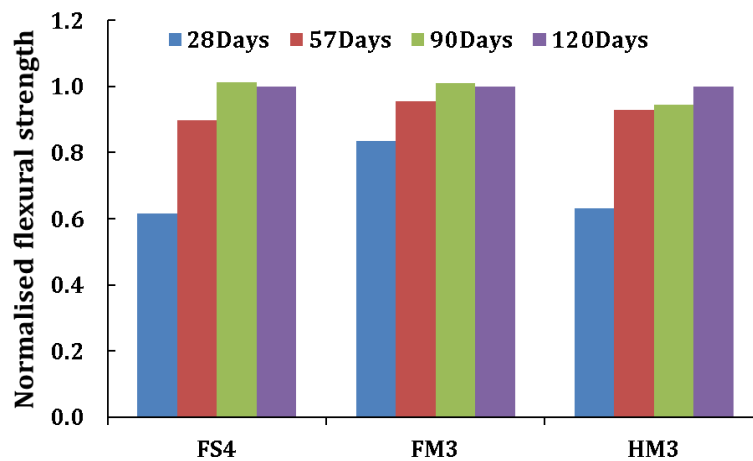


Figure 6.27: Flexural strength development of un-reinforced SHCC and mortar.

6.2.5. Flexural cracks

The total number of cracks and crack widths were also examined in the flexural specimens. However the cracks were counted only along the central 200 mm length of the bottom, tensile faces of the specimens as this limited surface was exposed to chloride penetration for the corrosion test and so the number of cracks and crack widths are from that specific region only. The crack widths were measured with the aid of a digi-portable handheld mobi-camera, specially designed for crack-width measurements as described in section 5.7.5. Cracks were counted on both un-reinforced and reinforced SHCC and mortar specimens. In the case of notched mortar specimens, a single crack was noticed in the notch vicinity at ultimate load state and after that the specimen failed abruptly. On the other hand, in SHCC specimens multiple cracks were observed in the vicinity of the notches and beyond.

6.2.5.1. Flexural cracks in un-reinforced specimens

At ultimate load level of un-reinforced SHCC, except for a wider crack in the middle (as shown in Figs 6.28a&b), more than 8 others cracks of between 50 to 100 μm wide were found in both FS11 and CS11 specimens. In the case of notch specimens of FS32 and FS5, cracks were localized at the notches and therefore equal in number to these notches in the specimens as shown in Figs 6.28c&d. The details of FS32 and FS5 specimens and their exposure periods for chloride testing are also discussed in Chapter 5, sections 5.8.2.2 and 5.8.2.3 and Table 5.7. For the different notch spacings (here they were 20 mm and 40 mm) in the specimens, the measured crack widths on the side of specimens (see Figs 6.28c&d) at ultimate and at 30% of ultimate deflection capacity (it was 1 mm) are shown in Figs 6.29a&b. The 30% load level was chosen based on the specimens' ultimate deflection level (about 3 mm) and their crack pattern at different deflection levels. It was found that at 30% load level the average crack widths in the un-reinforced SHCC specimens are within the range of 50 to 100 μm . Note that the names on horizontal axis in Figs 6.29a&b are described in Table 5.7 in Chapter 5. More details are discussed in Chapter 7 on chloride penetration testing of these

Fresh and Mechanical Behaviour of SHCC

specimens. Note that in Fig 6.28 there are some odd colours and textures which can be explained as follows; the darker stains on (a) and (b) are water, the green-yellow stains on (c) are from the algae in the curing tank and on (d), the micro-scope image shows some honeycomb on the matrix. Also note that in Fig 6.29 1hr, 1d and 7d define the testing period of 1 hour, 1 day and 7 days.

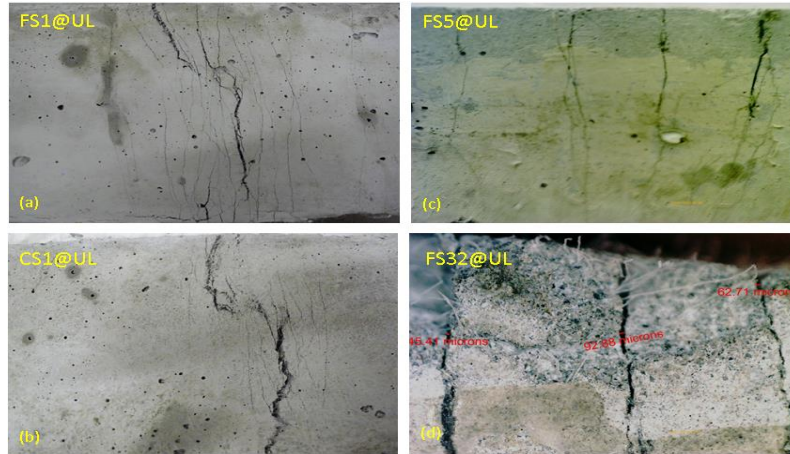


Figure 6.28: Flexural cracks in un-reinforced SHCC at ultimate deflection level.

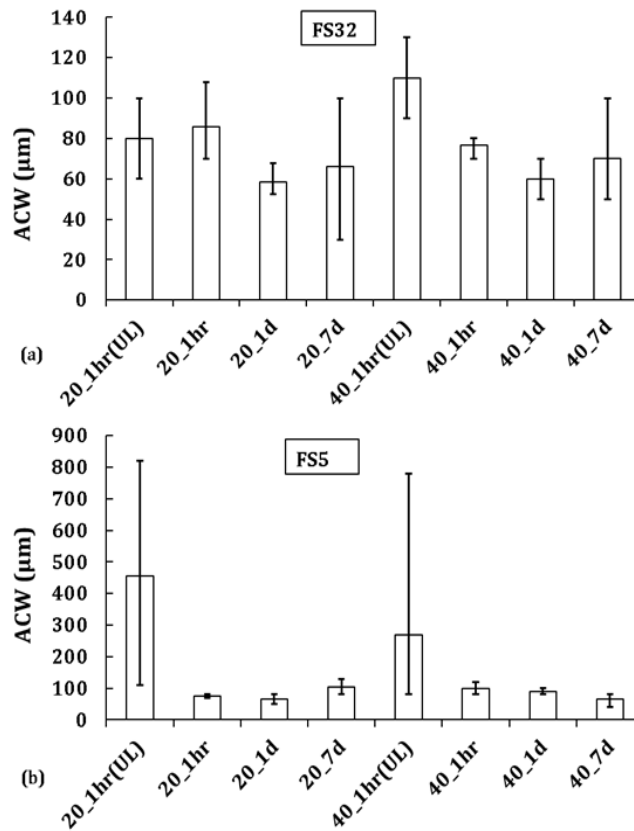


Figure 6.29: Average flexural crack widths (ACW) in un-reinforced notched specimens of (a) FS32 and (b) FS5 at ultimate and 1 mm deflection levels.

Fresh and Mechanical Behaviour of SHCC

6.2.5.2. Flexural cracks in reinforced specimens

In Chapter 5, section 5.7.5 it was already discussed how the number of cracks, crack widths and cracks spacing were measured after the flexural testing of both reinforced and unreinforced SHCC and mortar specimens. The average number of flexural cracks and their widths in different SHCC and mortar specimens are shown in Figs 6.30 to 6.33. In R/FS2 and R/CS2 specimens, most crack widths were in the range of 50 to 100 μm , but a few crack widths were found to be in the range of 100 to 200 μm . In the case of B2, most cracks were at right angles to the steel bar and no parallel cracks were found while in the case of B1, apart from multiple at right angles cracks, some cracks parallel to the steel bar were also observed in most specimens. In both SHCC types, maximum crack widths were found in those specimens with B1. In R/FM1 and R/CM1 specimens, a limited numbers of cracks (minimum 1 to maximum 4) were found at the specified 1.2 mm deflection level.

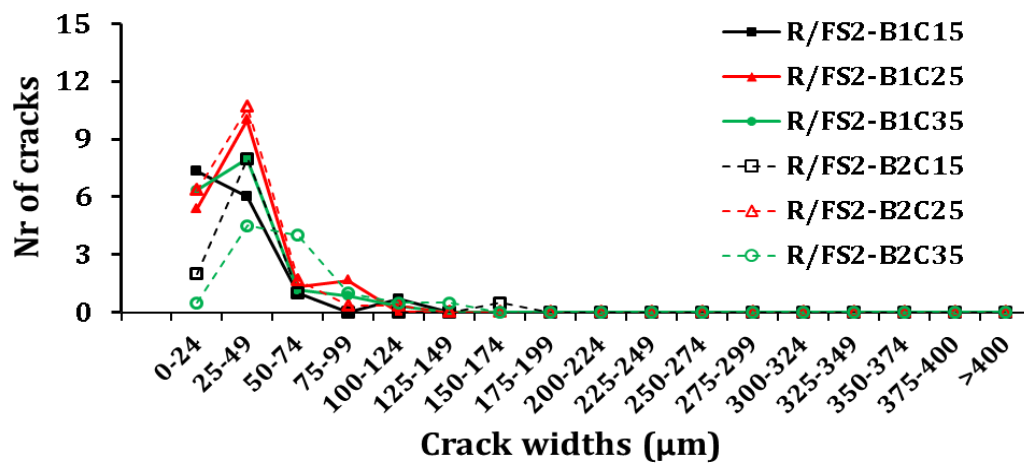


Figure 6.30: Average nr of cracks vs crack widths in R/FS2 specimens with single and double bars at different cover depths in Series One.

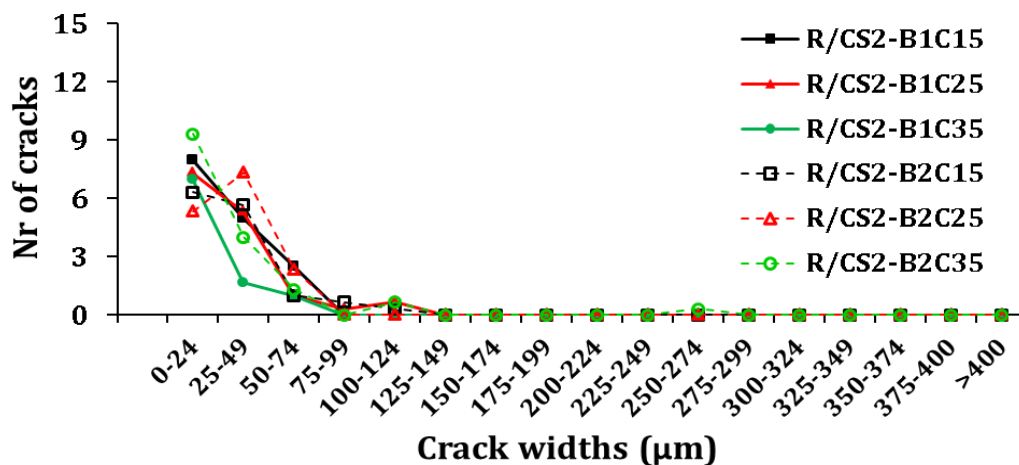


Figure 6.31: Average nr of cracks vs crack widths in R/CS2 specimens with single and double bars at different cover depths in Series One.

Fresh and Mechanical Behaviour of SHCC

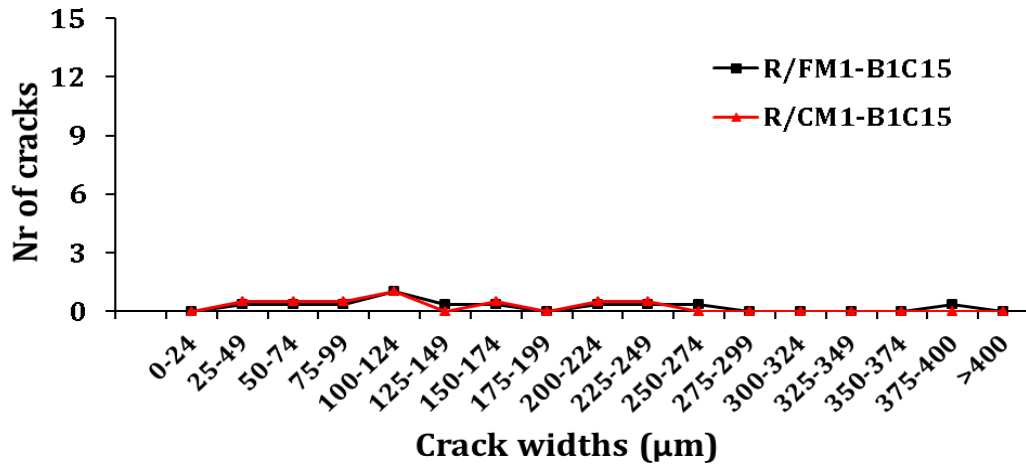


Figure 6.32: Average nr of cracks vs crack widths in R/Mortar specimens at 15 mm cover depth with single steel bar in Series One.

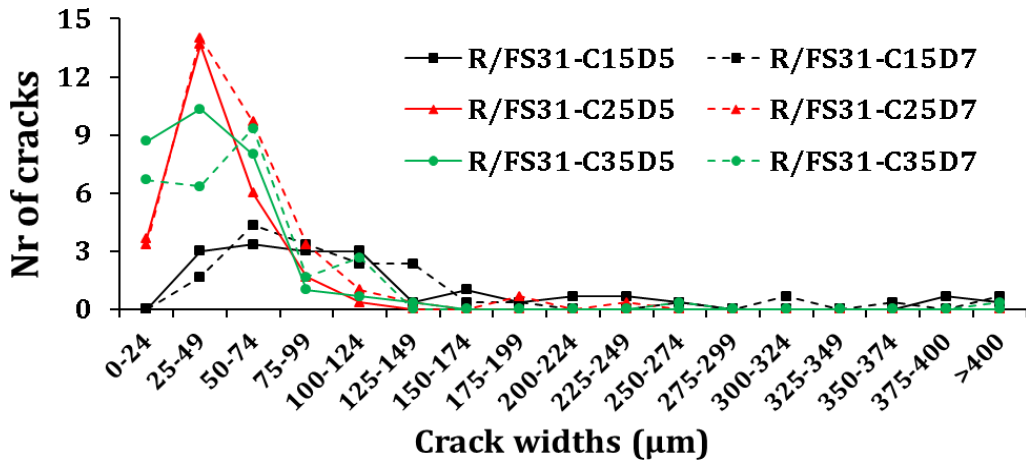


Figure 6.33: Average nr of cracks vs crack widths of R/FS31 specimens with different cover at two levels of deflection in Series Two.

Compared to R/FS2 and R/CS2, a higher number of cracks were observed in R/FS31. Remember that the specimen depth of R/FS31 was 80 mm and so deflection levels were also different from the 100 mm deep R/FS2 and R/CS2 specimens. However in all cases the ACW remained in the range of 0.025 to 0.075 mm. An insignificant difference in the number of cracks was found in R/FS31 due to the increased deflection from 5 mm to 7 mm but different crack widths were noticed in the specimens at different deflection levels, which are discussed in the next section. In some B2 specimens, shear cracks were also noticed near the supports because the double-tensile bar reinforcement led to an approaching shear-dominance and no shear reinforcements were used in the specimens. A smaller number of cracks and finer crack widths were also observed in the B2 specimens than in the B1 specimens.

 Fresh and Mechanical Behaviour of SHCC

Fig 6.34 shows the typical crack pattern that was found in the R/FS2 and R/CS2 specimens with B1 and B2 at 15 mm cover depth. More detailed crack patterns in different specimens with B1 and B2 and for different cover depths are also shown in Appendix C, Fig C.2. As mentioned before, in B2 specimens some of the cracks were found parallel to the steel bar on the bottom face, which is also clear from Fig 6.34. More crack photos can also be found in Appendix C. Fig C.3 shows the crack pattern observed in R/FM1 & R/CM1 and Fig C.4 shows observed crack pattern in unreinforced FS11 & CS11 specimens.

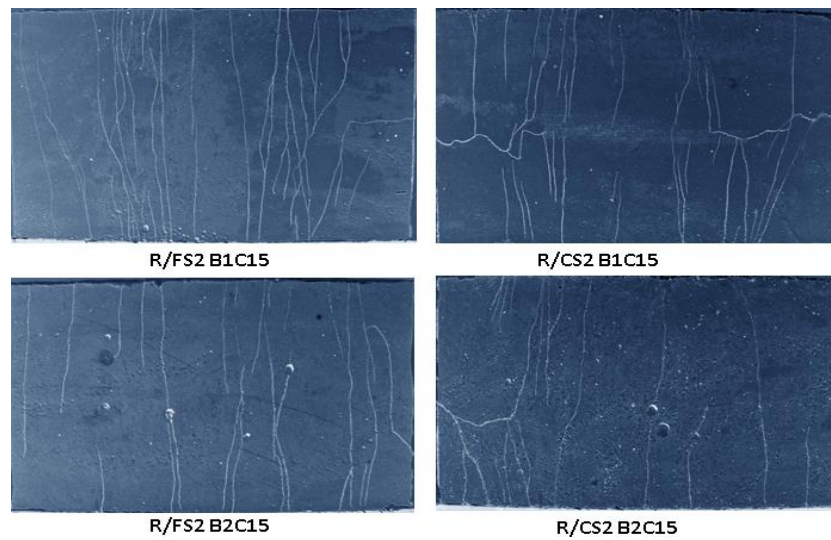


Figure 6.34: Crack pattern in 15 mm cover of R/FS2 and CS2 specimens with single and double bars in Series One.

6.2.5.3. Relationship between cracks and cover depths

Crack spacing was calculated in the central, cracked region of about 200 mm in length by dividing this length by the total number of cracks for each R/SHCC specimen for different cover depths as shown in Figs 6.35 & 6.36. Crack spacing was generally larger in the specimens with B1 and C15. In B2 specimens this difference was not that significant for different cover depths. Except in Fig 6.35 it was noticed in the scattered results with C35, that typically with an increase of cover depth, a lower crack spacing was found.

The relationships between ACW, MCW and cover depth were also determined for different R/SHCC and they are shown in Figs 6.37-6.39. Similar to the crack spacing vs cover depth, scattered results were also observed in the C35 specimens compared with C15 and C25. Nevertheless, higher ACW and MCW were generally observed in all the C15 R/SHCC specimens. Significantly higher ACW and MCW were found in R/FS31 specimens because of the specimen size change as well as the higher levels of deflection in the flexural testing. For C25 of R/FS2 and R/CS2 specimens, no significant differences were noticed for B1 and B2, where as in C15 and C35, relatively higher crack widths were found in the specimens

Fresh and Mechanical Behaviour of SHCC

with B2. In case of R/FS31 both ACW and MCW were higher in the specimens tested at 7 mm deflection level.

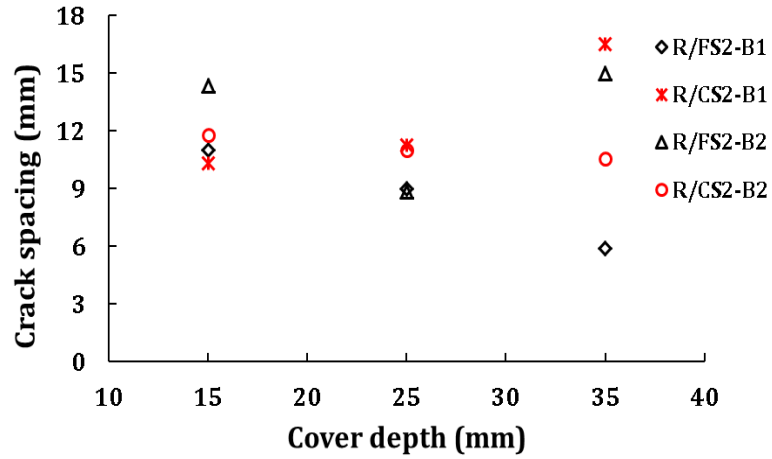


Figure 6.35: Average crack spacing vs cover depth in R/FS2 and R/CS2 at 3.5 mm levels of deflection with single and double bars in Series One.

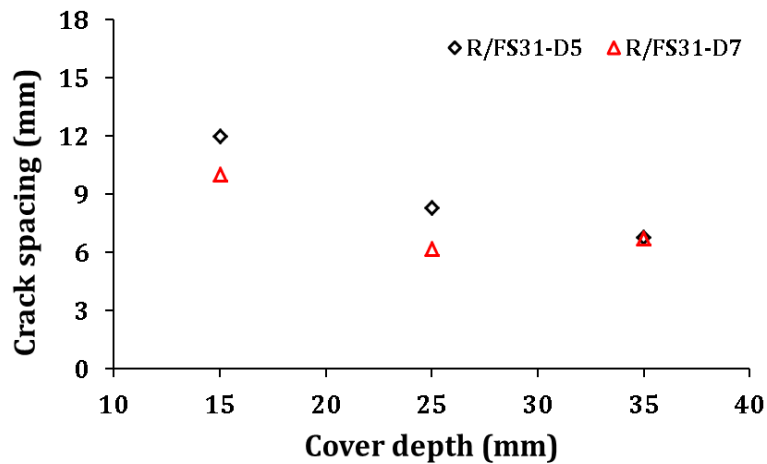


Figure 6.36: Average crack spacing vs cover depth in R/FS31 at different level of deflection in Series Two.

Fresh and Mechanical Behaviour of SHCC

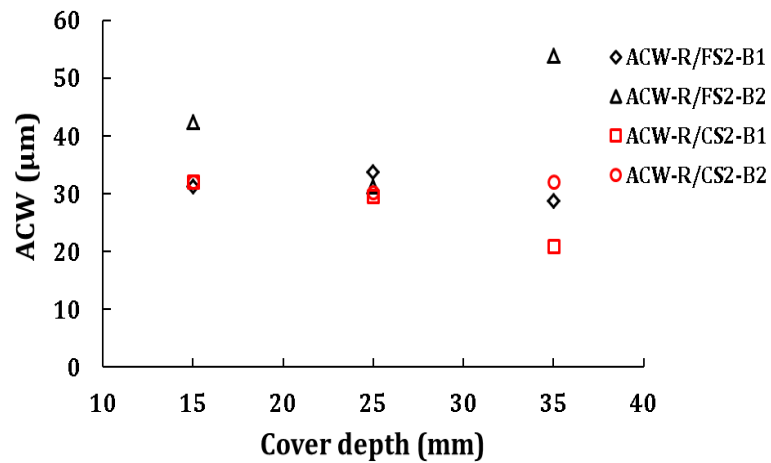


Figure 6.37: Average crack widths vs cover depth in R/FS2 and R/CS2 at 3.5 mm level of deflection in Series One.

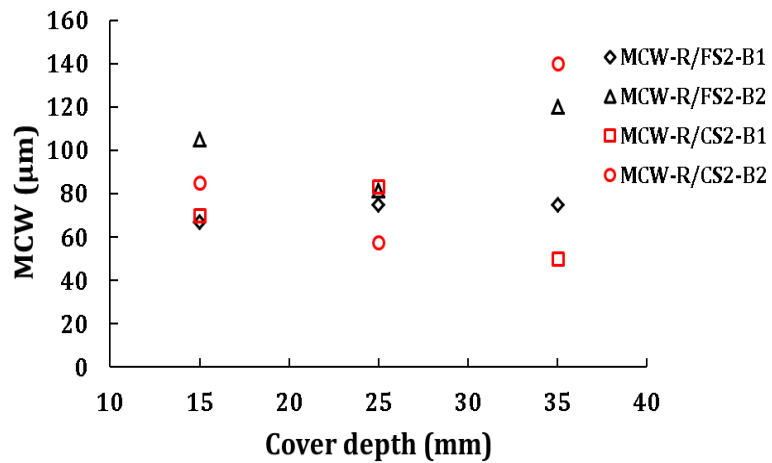


Figure 6.38: Maximum crack widths vs cover depth in R/FS2 and R/CS2 at 3.5 mm level of deflection in Series One.

Fresh and Mechanical Behaviour of SHCC

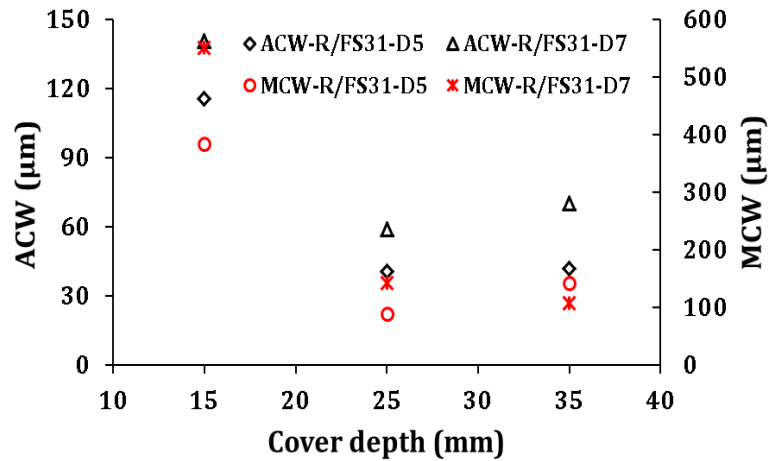


Figure 6.39: Average crack widths (ACW) and maximum crack widths (MCW) vs cover depth in R/FS31 at different levels of deflection in Series Two.

6.2.5.4. Relationship between cracks and deflection level

A relationship was determined between cracks and different deflection levels of all types of R/SHCC specimens used in the research as shown in Figs 6.40a-d. Although the specimen sizes for the 3 mm deflection level were different from those of the specimens for the 5 mm and 7 mm deflection levels, trends of increased numbers of cracks and crack widths were observed from the experimental results. A better relationship was established between total crack widths (TCW) vs deflection as shown in Fig 6.40d. Future experiments need to prove this trend in similar specimen sizes.

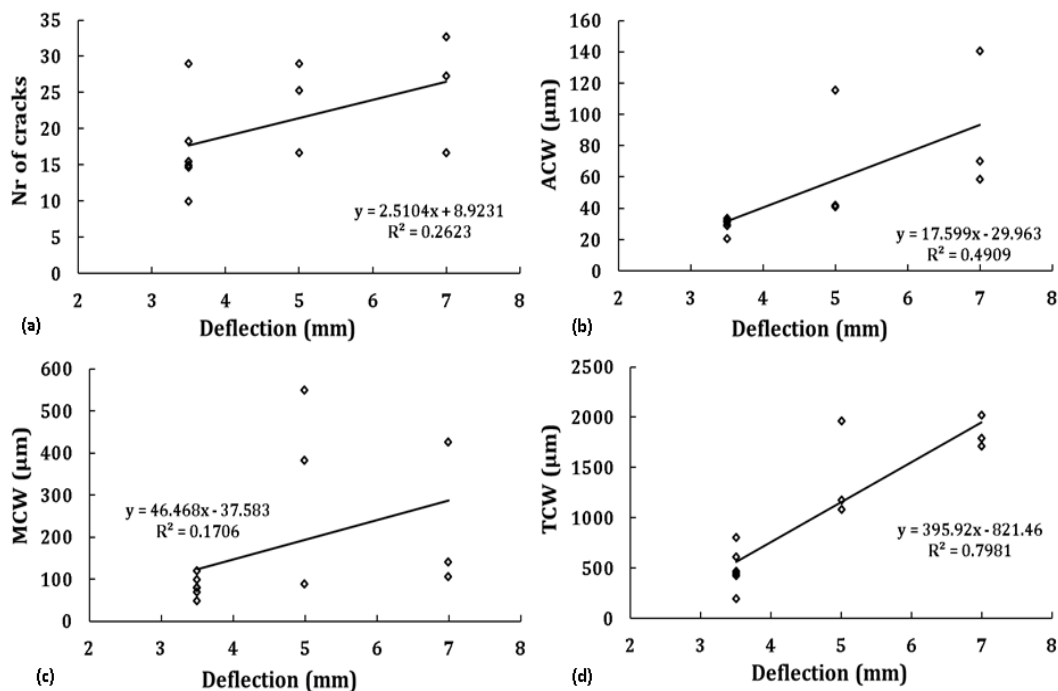


Figure 6.40: Relationship between cracks and deflections in R/SHCC specimens.

6.2.6. AE response in SHCC and mortar cracking behaviour

The brittleness behaviour of mortar can only be observed from matrix cracking while in fibre concrete like SHCC. The cracking behaviour can be observed in three ways: matrix cracking, fibre pull-out and fibre rupture. It is well known for NC that matrix cracking will be visible only after it reaches its peak strength although micro cracking does occur before that. On the other hand in fibre concrete after matrix cracking, two other phases of strain-hardening and strain-softening may occur before the concrete fails completely. This whole scenario can be observed and characterized by acoustic emission (AE) sensors. Fig 6.41 shows a typical AE response which was observed in FS4 dumbbell specimens under direct tensile testing. In the linear elastic part, a low number of AE signals were observed while the signals increased at the first cracking (matrix cracking). In the strain-softening part, as some of the fibres rupture rather than pull-out, AE signals reached a maximum level.

To identify the crack mechanism which triggers the AE, a frequency analysis of the recorded signals was carried out. First, the frequency centre of gravity (f_{COG}) and the peak frequency (f_{MXA}) in the frequency domain were calculated using the program VALLEN FFT Feature Extractor. For this analysis the frequency range 25 kHz to 400 kHz of the signals were used. The weighted peak frequency (WPF) was then calculated according to equation (6.1) suggested by Sause & Horn (2010).

$$WPF = \sqrt{f_{COG} \cdot f_{MXA}} \quad (6.1)$$

AE signals can also be classified as Cluster 1 with WPF < 90 kHz and Cluster 2 with WPF > 120 kHz which can be used to distinguish between matrix cracking and fibre rupture. It was found that matrix cracking generates signals with $f_{WP} > 120$ kHz, whereas signals with f_{WP} below 90 kHz are related to fibre pull-out as shown in Fig 6.42 for FM3 specimen in a direct tensile test.

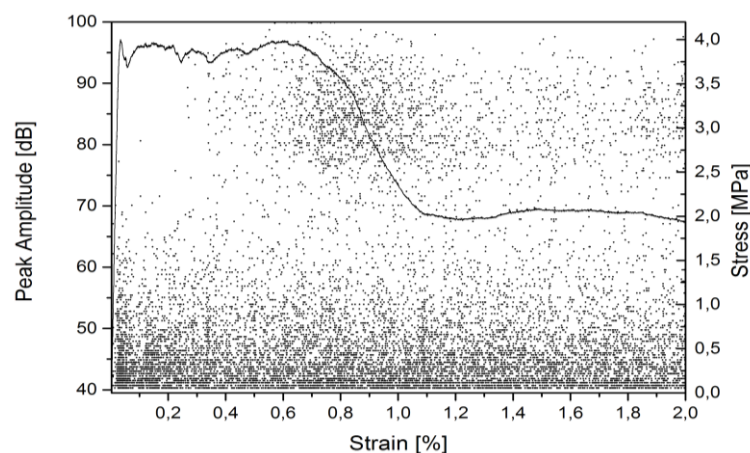


Figure 6.41: Amplitude of AE signals (dots) at different stress-strain level.

Fresh and Mechanical Behaviour of SHCC

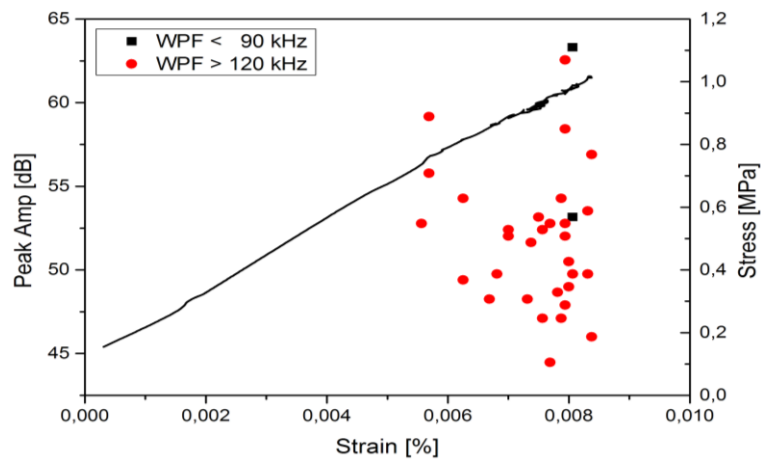


Figure 6.42: Amplitude of AE Signals with different frequencies versus strain of FM3 dumbbell specimens in direct tensile testing.

The analysis of the AE in the flexural test shows comparable results to those of direct tensile testing. As shown in Figs 6.43 & 6.44, the AE activity of FS4 and FM3 beams is low during the linear elastic stage. The final fracture of the FM3 beam generates acoustic emissions with high frequencies (Fig 6.41). The end of the linear stage of the FS4 beam is characterised by an increasing number of hits with WPF above 120 kHz, indicating the beginning of matrix cracking and an activation of the fibres at 4 MPa bending stress and at a deflection of 0.6 mm. The subsequent strain-hardening phase is dominated by AE with high frequencies and a continuous decrease of the flexural force-deflection slope. The details of the AE results on these FS4 and FM3 beams were also discussed in Paul *et al.* (2015).

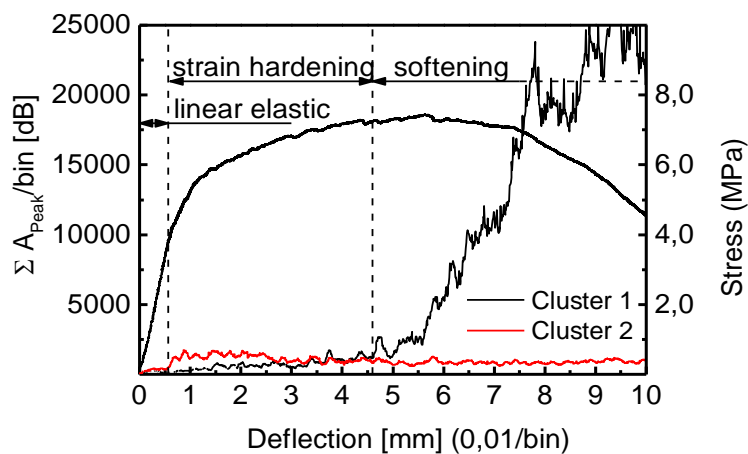


Figure 6.43: AE response of FS4 beam specimen in flexural test.

Fresh and Mechanical Behaviour of SHCC

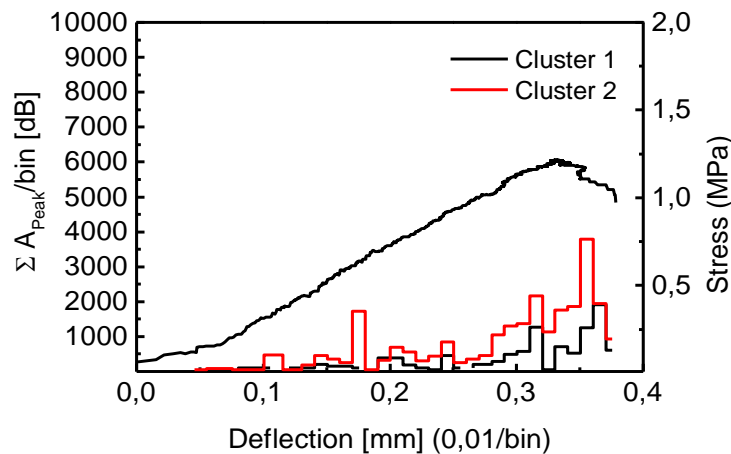


Figure 6.44: AE response of FM3 beam specimen in flexural test.

6.3. Fracture energy of SHCC and mortar

In SHCC, whether strain hardening is achieved or not depends strongly on the matrix toughness, as expressed by the crack tip toughness J_{tip} , and on the bond τ between the matrix and fibres. No direct measurement of J_{tip} has been attempted in this study. Eqs. 5.4 to 5.6 together with E-mod obtained for different matrices were used to calculate fracture and crack tip toughness. Matrix fracture toughness, crack tip toughness and fracture energy of the matrices are shown in Table 6.6.

Table 6.6: Matrix fracture toughness (K_{IC}), crack tip toughness (J_{tip}) and fracture energy (G_f)

Id	K_{IC} (MPa.m ^{1/2})	CoV (%)	J_{tip} (J.m ²)	CoV (%)	G_f (N/m)	CoV (%)
FM1	0.95	10.9	0.05	1.2	26	24.6
FM4	0.82	19.2	0.04	38.9	59	8.6
CM1	1.02	29.6	0.07	66.1	40	7.8
CM4	1.12	31.4	0.08	53.3	133	21.2
FS11	1.87	21.2	0.18	43.1	-	-
FS2	2.48	16.8	0.48	32.3	-	-
CS11	1.61	27.9	0.15	54.7	-	-
CS2	2.15	8.8	0.33	17.6	-	-

To determine the J_{tip} values for FS and CS-Mortar, the matrix toughness K_Q is required. For this purpose notched beams were prepared as described earlier in chapter 5. The responses of notched SHCC beams to three point bending are shown in Fig 6.45. However, K_Q reflects the matrix toughness, without fibres, for which the mortar beams were prepared. Fig 6.46 shows the results of notched mortar beam specimens. Fig 6.47 illustrates the variations of fracture energy for two different matrix types for both FM and CM. In both matrices, mix 1 has lower

Fresh and Mechanical Behaviour of SHCC

fracture energy than mix 4. Higher variations of fracture energy were also observed in both mix 4 matrices. Also, CM causes higher fracture energy of the matrix. Typically the fracture energy of concrete depends on the type of concrete, aggregate size and tensile strength. As a result quite a large variation (18-130 N/m) in the fracture value was reported by the different researchers (Shah & Swartz, 2012; Rahman *et al.* 2014).

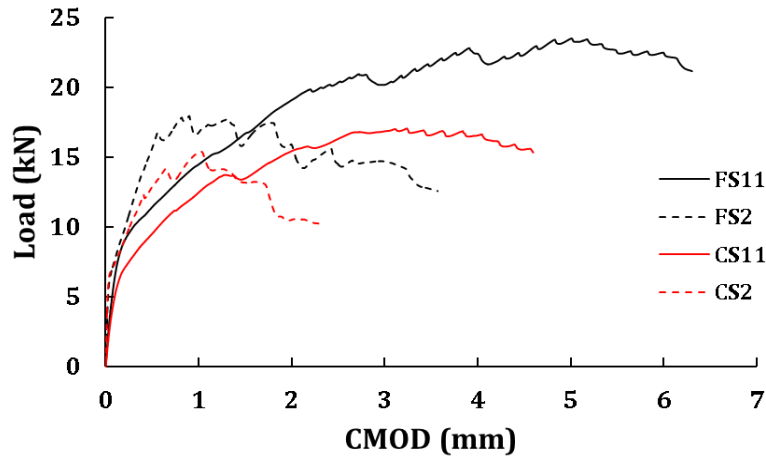


Figure 6.45: Un-reinforced FS and CS-SHCC notch specimen responses in flexural testing.

From Table 6.6 it is clear that the fibres in the matrix lead to higher apparent K_{IC} and J_{tip} values. Since the K_{IC} value is related to the P_{max} (in Eq 5.4), lower P_{max} values of FM correspond to lower K_{IC} values than for the CM. However in SHCC higher P_{max} values of FS-SHCC cause higher values of K_{IC} and J_{tip} than in CS-SHCC. Note that in the test validity check, a total of 10 out of 11 specimens of FM and 7 out of 11 specimens of CM satisfied the conditions mentioned in section 5.7.6. The CoV was also higher in the case of CM. In SHCC, almost all the FS-SHCC and CS-SHCC specimens satisfied the conditions.

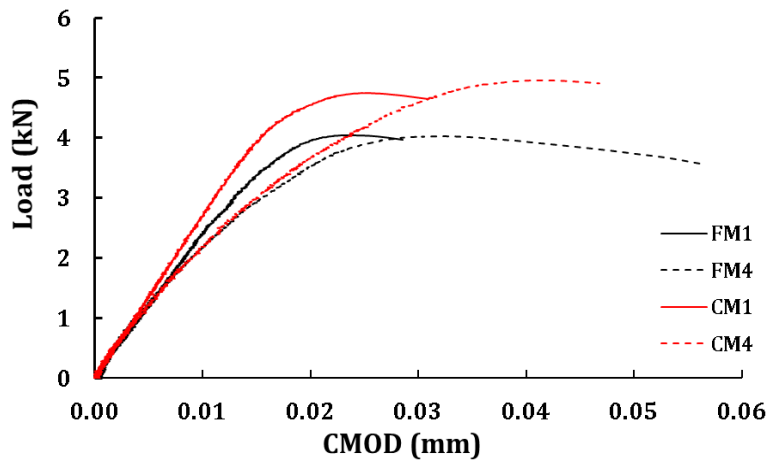


Figure 6.46: Un-reinforced FS and CS-mortar notch specimen responses in flexural testing.

Fresh and Mechanical Behaviour of SHCC

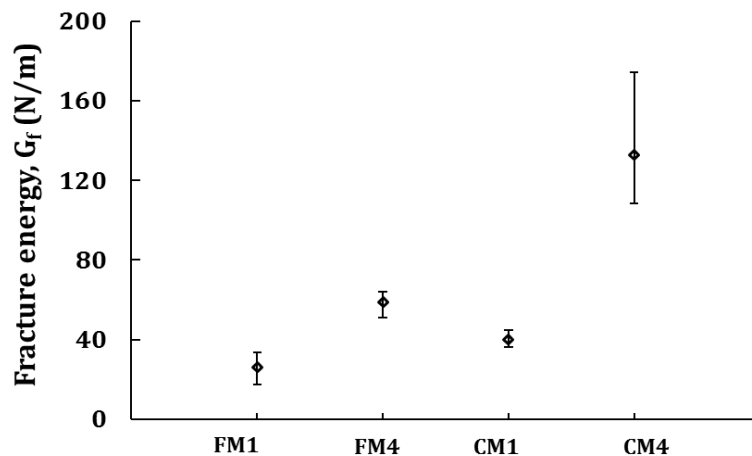


Figure 6.47: Fracture-energy (G_f) variations in different mortar types.

As shown in Eq 5.4 the K_{IC} is also related to the crack length a_c formed in the specimen during flexural testing. Fig 6.48 shows the relationship between these two parameters. Relatively higher a_c values were found in the FM specimens than in the CM specimens and it implies that finer sand in the matrix leads to higher a_c values than coarse sand. The details of the fracture energy results were also discussed in Paul & van Zijl (2013).

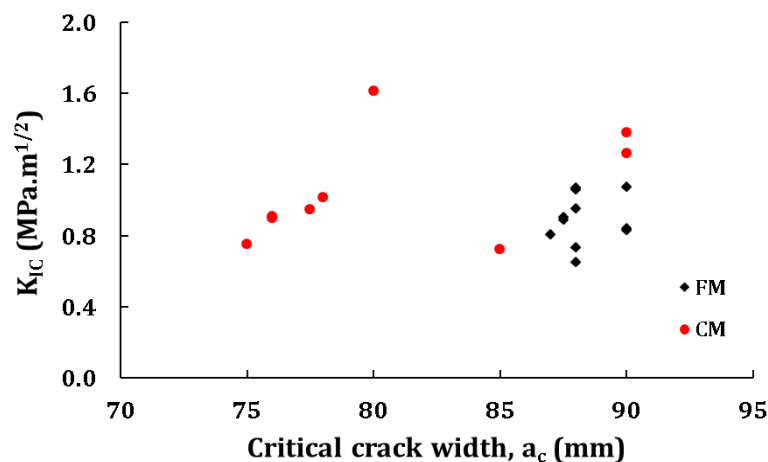


Figure 6.48: Fracture toughness (K_{IC}) vs critical crack length (a_c) in different mortar types.

6.4. Fibre distribution in SHCC matrix

The distribution of the 12 mm long and 0.04 mm diameter PVA fibres in the hardened SHCC specimens was observed by microscopic image as shown in Fig 6.49. Typically for microscopic image analysis, a polished surface is necessary to visualize any micro objects such as PVA fibre sections. In this case, a 5 mm thick SHCC slice of 30 mm x 16 mm cross-section was collected from the middle part of a dumbbell specimen. The number of fibres in that cross-section was counted manually with adequate care. In the case of FS4, about 10 fibres were found per 1 mm² area of the dumbbell cross-section. It implies that the fibre

Fresh and Mechanical Behaviour of SHCC

spacing in the actual mix was about 0.33 mm.

The fibre spacing in this research was also determined for different mixes of FS-SHCC and CS-SHCC by using Eqs (5.7) to (5.10). It was found that the range of fibre spacing in SHCC is 0.24 to 0.25 mm (using Eqs 5.7 & 5.8) and 0.89 to 0.95 mm (using Eqs 5.9 & 5.10), as shown in Fig 6.50. The values obtained from Eqs (5.7) & (5.8) are considered to be the lower limits of fibre spacing, as they in fact represent the spacing of dispersed continuous fibres. Short, randomly-oriented fibres have a larger spacing which can be seen in the values obtained from Eqs (5.9) & (5.10). It can be said that in FS-SHCC and CS-SHCC, a particle size larger than roughly 0.9 mm will disturb the regular distribution pattern of fibres. Since almost 98% of FS particles of both mixes 1 and 4 by weight pass through a sieve opening of 0.3 mm, it can be assumed that the fibre distribution in FS-SHCC will create a regular pattern, if good dispersion is ensured in the mix design and process. On the other hand about 45% of the CS particles by weight are retained on the 0.6 mm sieve, representing 0.5% of the total number of particles in the CS. In total about 19% of the CS particles by weight, or 0.04% of the total number of particles are larger than 1.18 mm (see the grading in Fig 5.1). Although the number of particles exceeding the even particle spacing of roughly 0.9 mm is relatively low, it will disturb the regular fibre dispersion and may lead to lower ultimate tensile strain.



Figure 6.49: Fibre distribution (as black dots) in the dumbbell cross-section.

Fresh and Mechanical Behaviour of SHCC

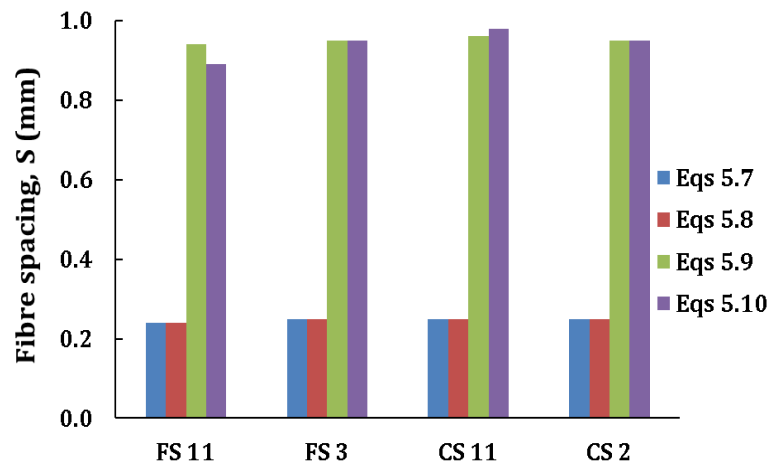


Figure 6.50: Fibre spacing in SHCC using different equations.

6.5. General discussion

This chapter has covered the most important parts of the mechanical properties of the SHCC and mortar used in this research work. Concrete durability is typically related to its compositions' physical and chemical properties. However, also the curing process, mechanical strength, low moisture permeability, volumetric stability (shrinkage and creep), etc. of concrete are related to its durability. Therefore, the experimental results obtained in this chapter will provide valuable information about the durability performance of the specific type of SHCC used in this research work.

Inclusion of fibre in the SHCC matrix leads to the increase of air content in the mix, as discussed in Chapter 3. For the large amount of cement in FS11 and CS11, the compressive strength, E-mod, tensile strength and flexural strength were found to be higher than the specimens with low amounts of cement in (FS2, FS31 and CS2). At higher tensile strain (about 3%) and higher flexural deformation (at ultimate level), the average crack widths of SHCC were found to be below 0.08 mm and this might be the key parameters of the durability design of RCS using SHCC. Introducing CS in SHCC leads to lower tensile strain, however in terms of the number of cracks and crack widths the difference between CS-SHCC and FS-SHCC was insignificant. The number of cracks and crack widths were increased in both FS-SHCC and CS-SHCC as the tensile strain and flexural deformation were increased. No noticeable difference was found in the strength properties due to inclusion of fibres in SHCC when compared to the mortar specimens. Although tensile strength of SHCC increases with time, the strain reduces significantly (Wang & Li, 2006; Yang *et al.* 2005). However, through proper materials design this problem may be overcome. In flexural testing of R/SHCC specimens a lower number of cracks and higher crack spacing were found with cover depth of 15 mm than with cover depths of 25 mm and 35 mm. For the latter cover depths, no significant difference in crack spacing was found. Some relationships were also drawn from both tensile and flexural testing response such as crack spacing and crack width at different tensile strain levels of SHCC. The number of cracks, average and maximum crack

Fresh and Mechanical Behaviour of SHCC

widths at different cover depths of the steel bar in flexural testing can be used for the prediction of cracking behaviour of R/SHCC under both tensile and flexural testing, and for interpretation of durability behaviour in the chloride-induced corrosion tests performed in this research.

Application of AE was found to present a way of distinguishing matrix cracking from fibre rupture and/or slip in SHCC specimens under both tensile and flexural testing. A slightly higher fracture toughness was found in CS-mortar than in FS-mortar and by adding fibre to the matrix leads to significantly higher apparent fracture toughness in both FS and CS-SHCC. For a fibre content of about 1.85%, a maximum of 10 fibres per one millimetre square of a dumbbell section were counted from the microscopic images. This was done to understand the influence of larger sand particles in cracking and ultimately, in tensile ductility.

6.6. References

- Paul, SC & van Zijl, GPAG 2013, 'Assessment of fracture toughness in strain hardening cement-based composite (SHCC) made from fine and coarse sand', proceeding of the fifth SEMC conference, Cape Town, South Africa, Zingoni (eds) © 2013 Taylor & Francis Group, London, ISBN:978-1-138-00061-2, p:619-624.
- Paul, SC, Pirskawetz, S, van Zijl, GPAG & Schmidt, W 2015, 'Acoustic Emission for Characterizing the Crack Propagation in Strain Hardening Cement-Based Composites (SHCC)', *Cement and Concrete Research*, vol. 69, pp. 19-24.
- Rahman, N, Jaini, ZM, Rahim, NA & Razak, SA 2014, 'An experimental study on the fracture energy of foamed concrete using V-notched beams', in proceeding of the international civil and infrastructure engineering conference, (Eds) Hassan *et al.* ISBN 978-981-287-290-6.
- Sause, MGR & Horn, S 2010, 'Simulation of Acoustic Emission in Planar Carbon Fibre Reinforced Plastic Specimen', *Journal of Nondestructive Evaluation*, vol. 29 pp. 123-142.
- Shah, SP & Swartz, SE 1987, 'Fracture of concrete and rock', in proceeding for SEM-RILEM international conference, June 17-19, Houston, Texas, USA.
- Van Zijl, GPAG 2005, 'The role of aggregate in HPRFCC', *Concrete Beton*, vol. 110, pp. 7-13.
- Wang, S & Li, VC 2006, 'High early strength engineered cementitious composites', *ACI Materials Journal*, vol. 103, no. 2, pp. 97-105.
- Yang, Y, Lepech, M & Li, VC 2005, 'Self-healing of engineered cementitious composites under cyclic wetting and drying', proceeding of international Workshop on Durability of Reinforced Concrete under Combined Mechanical and Climatic Loads (CMCL), pp. 231-242. Qingdao, China.

Chapter 7

*I have been impressed with the urgency of doing. Knowing is not enough; we must apply.
Being willing is not enough; we must do. – Leonardo da Vinci*

Chloride Ingress and Reinforcement Corrosion in SHCC

7. Introduction

At present in the construction industry, one of the major reasons for using SHCC can be to increase the structural durability performance. During its life cycle, a structure may experience many durability problems from various sources including chloride and carbonation attack. However, in this research, the work is limited to SHCC durability in a chloride-laden environment only, because it is believed that chloride-induced corrosion contributes most significantly to the maintenance and repair costs world-wide. Note that the corrosion results reported on in this chapter are described in accordance with the four different series of experiments introduced in Chapter 5. For ease of reference, the different series are summarised in Table 7.1.

Table 7.1: Specimen details in different series of corrosion testing in this research

Series	Id No	Nr of specimens	Specimen conditions	Exposure types	Duration of testing
1	R/FS2, R/CS2, R/FM1 and R/CM1	18 + 18 + 3 + 3 = 42	All pre-cracked	Capillary (unloaded)	754 days / 108 weeks
2	R/FS31	18	All pre-cracked	Ponding (loaded)	399 days / 57 weeks
3	R/FS32, R/FM2 and R/CM2	18 + 2 + 2 = 22	All pre-cracked	Ponding (loaded)	193 days / 28 weeks
4	R/FS4, R/FM3 and R/HM3	8 + 4 + 4 = 16	Cracked and un-cracked	Ponding (loaded and unloaded)	172 days / 25 weeks

7.1. Corrosion potential of R/SHCC and R/mortar specimens

The corrosion potential in the modified matrix of SHCC is believed to be different from that of the matrix in NC and therefore the typical half-cell corrosion potential (HCP) range for NC in the assessment of the corrosion status by ASTM C876 appears not to be applicable for SHCC. As per ASTM recommendation, an HCP value of less than -350 mV indicates a high

Chloride Ingress and Reinforcement Corrosion in SHCC

possibility of steel corrosion (as already shown in Table 4.3). The presence of cracks in the specimens leads to a significantly higher potential value (a higher negative reading than -350 mV) just after the exposure to chloride. These higher potential values were observed in all the reinforced cracked SHCC and mortar specimens tested in the four different series as shown in Table 7.1. Unless noted otherwise, the higher potential value reported in this research means more negative potential value than -350 mV.

Figs 7.1a-f show the average corrosion potential (E_{corr}) values recorded in both cracked and un-cracked R/SHCC and R/Mortar specimens in different series. It is worth mentioning that, during the whole research period (more than 3 years) different series of experiments were started at different times resulting in different starting and ending times of the recorded data as shown in all figures.

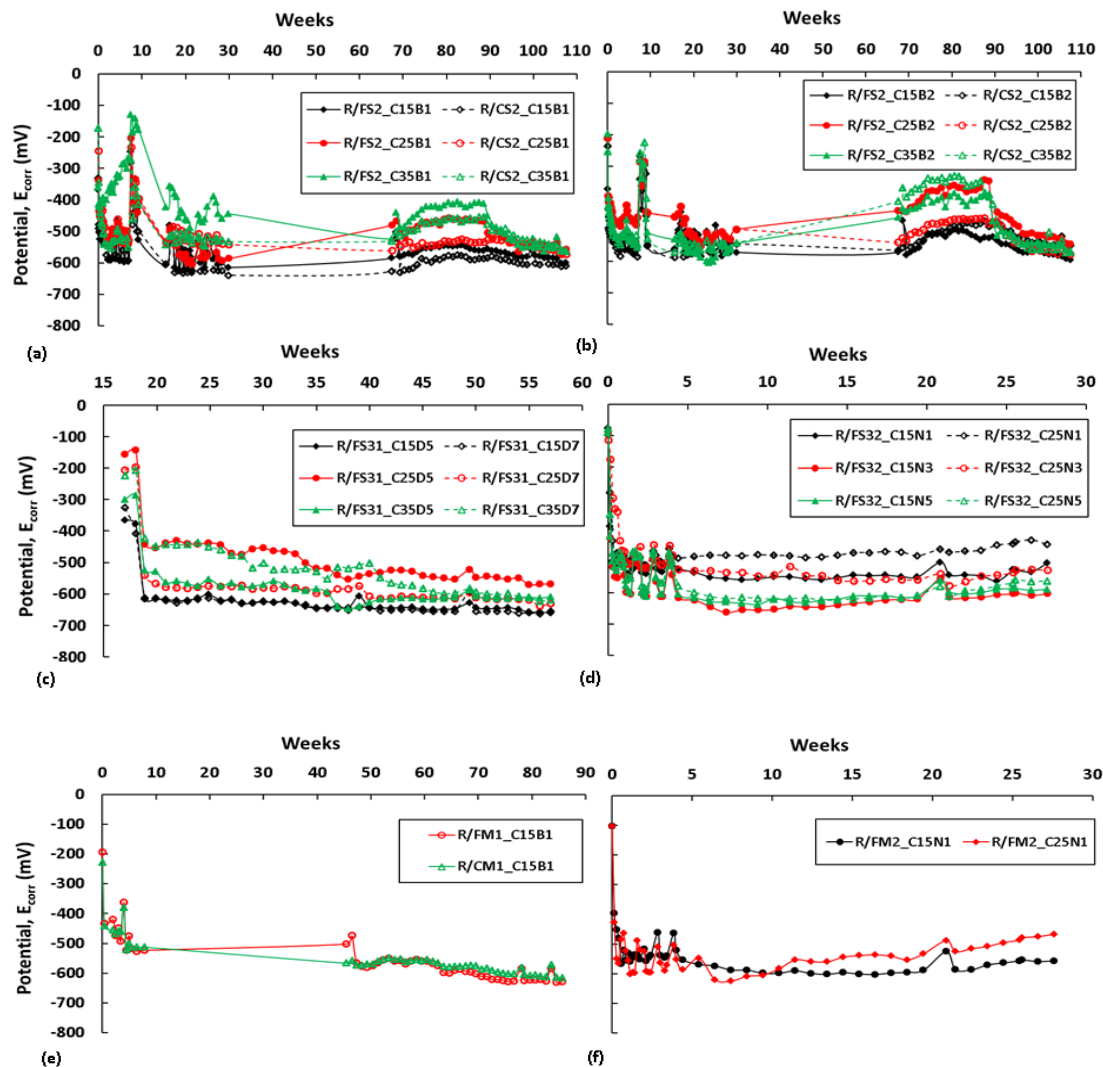


Figure 7.1: Corrosion potential in different R/SHCC and R/mortar specimens for different cover depths in different series.

Chloride Ingress and Reinforcement Corrosion in SHCC

The time is expressed in weeks with the zero point at the time of commencing of the test, i.e. at a specimen age of 14 days. Corrosion measurements started after 30 minutes from the application of chloride by means of capillary or ponding exposure. Higher potential readings were observed even within the first day of chloride exposure, especially in the cracked specimens and the possible reasons are discussed below.

To understand the higher potential readings, it must be borne in mind that the potential indicates a likelihood of corrosion, or corrosion probability and not necessarily an actual corrosion process. Also it can be seen from the figures that the potential value in all specimens did not increase (in some specimens the value was lower) from the potential value found at the day of starting corrosion testing. Except for specimens with lower cover depth of steel, there is no noticeable difference in the potential reading due to different crack properties in the specimen in Series One and Two. However, in Series Three it can be seen that potential value was lower for single notch specimen than for others. The presence of water and chloride in the vicinity of the steel, influences the electro-chemical process, and therefore the higher potential reading can be seen even without an active corrosion process occurring. These phenomena are considered next.

Firstly, it is investigated whether corrosion occurs and possibly causes the more negative potential readings. Some specimens were destructed for visual observation of the corrosion status of reinforcing steel bars at an early stage of corrosion testing. The first, a R/CS2_C15B1 specimen was destructed after 17 days, but no evidence of active corrosion was observed at this stage. After 52 days two specimens (R/FS2_C35B1 and R/FS2_C15B2) were destructed and the corrosion status was inspected visually. In all specimens, the only indication of corrosion activities was discolouration, with no sign of pitting or steel volume reduction. The positions of discolouration coincided with concentrations of cracks. Of course visually it is not possible to quantify the exact corrosion status in steel bars. That is why the Coulostatic method was also used to monitor the corrosion rate in steel bars as introduced in Chapter 4, and of which the results are discussed in Section 7.2.

Next, the influence of moisture content on the potential reading is investigated. In each drying exposure a higher potential rate was observed than during a wetting cycle. To demonstrate this clearly, the author performed another experimental series on R/FS4 specimens and two types of R/mortar (R/FM3 and R/HM3) specimens, in the cracked and un-cracked state subjected to the same cyclic chloride exposure (3.5% NaCl solution) in series four. In total 8 specimens (6 cracked and 2 un-cracked) of R/FS4 and 4 specimens (2 cracked and 2 un-cracked) of each mortar type were used in this series. As already discussed in Chapter 5, an ERE20 reference electrode (which has a fixed potential value) was placed inside the concrete near the steel bar and connected to the data logger to record the potential difference of the steel bar and reference electrode. The average potential reading at the end of the wetting cycle, and again at the end of the drying cycle for each specimen type is reported in Figs 7.2 & 7.3. It is clear from both figures that the potential value depends on the presence of cracks and water in the specimen. At the end of 25 weeks of corrosion testing of the specimens in Series Four, it was found that the potential value was higher in cracked

Chloride Ingress and Reinforcement Corrosion in SHCC

specimens than in the uncracked specimens. As will be shown in a next section, no significant corrosion other than local colour changes on the steel bar surface was found after several weeks, despite evidence of chloride presence at the steel bar location within hours after the first exposure to chloride solution.

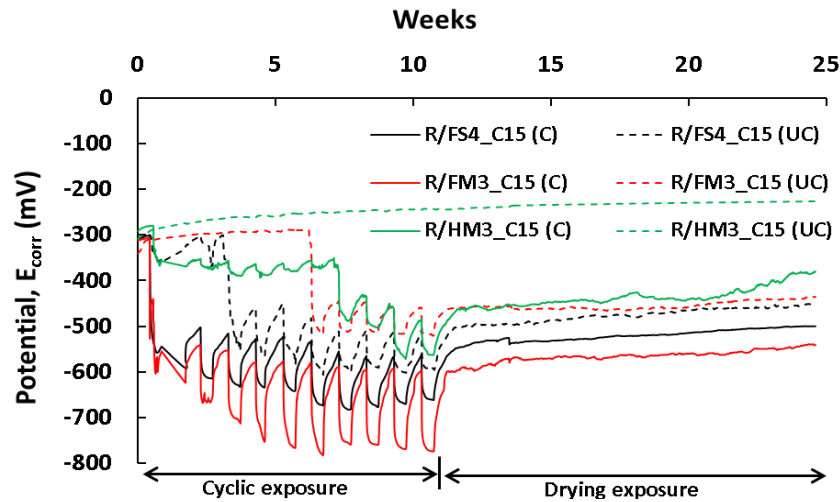


Figure 7.2: Corrosion potential in cracked and un-cracked R/FS4, R/FM3 and R/HM3 with B1 and C15 in Series Four.

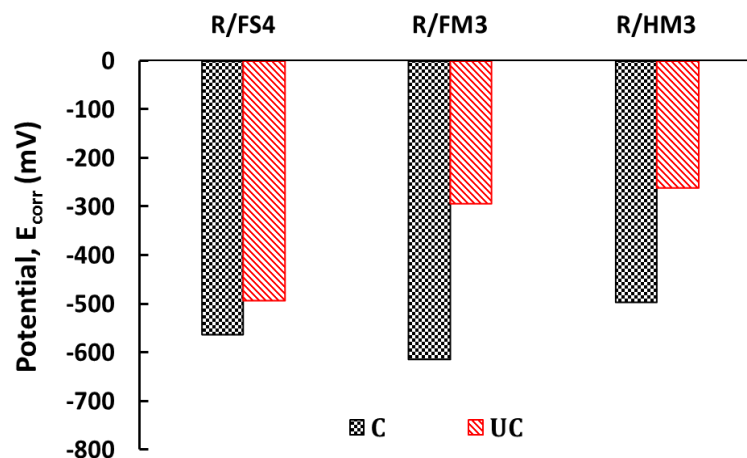


Figure 7.3: Corrosion potential in cracked (C) and un-cracked (UC) specimens at the end of 25 weeks in Series Four.

Note that the results in these Figs 7.1a-f are the average results of at least 2 to 3 specimens for each cover depth from each series. So, each data point is the average of 3 and 6 readings for B1 and B2 respectively. These readings were taken by placing the half-cell in the middle of each specimen on the top surface, i.e. at the opposite side of the exposed, cracked surface. Fig 7.4 shows the influence of taking E_{corr} readings in the middle part of the specimens (shown in Fig 5.15 point B) as compared with those taken at the side (shown in Fig 5.15 points A & C). There appears to be an influence on the potential reading associated with the distance

Chloride Ingress and Reinforcement Corrosion in SHCC

between the half cell and the steel bar, although it is not of major significance. For lower cover depth (C15) the distance between steel bar and half-cell in Series One was 75 mm.

However, for a smaller distance (55 mm for C35) between the steel bar and half-cell, slight difference in the result was noticed. Therefore, the position of half-cell may have some influence in the potential reading. This issue is further discussed in Section 7.1.2.

No major difference is found between R/FS-SHCC and R/CS-SHCC corrosion potential values in Series One. This is attributed to similar crack patterns in these specimens (van Zijl & Paul, 2013), which may cause similar chloride solution penetration rates. For both types of sand, a smaller cover depth of steel in SHCC shows a higher corrosion potential than the others. This is attributed to the shorter distance the chloride solution has to penetrate.

Inconsistent readings were observed in some specimens for larger cover depths and the reason is not clear yet, other than the inconsistent crack spacing results reported in Chapter 6 for C35 specimens. Perhaps for these specimens and at this larger cover depth (35 mm), crack widths and the number of cracks near the steel bar are not the same as seen at the surface, leading to reduced levels of water and chloride close to the steel bar. In Series Four, after 60 days of cyclic NaCl application, a corrosion stain was observed on top of both cracked R/HM3 specimens as shown in Fig 7.5. On the other hand no corrosion was observed in R/FM3 and R/FS4 specimens. However, the same R/HM3 specimens show a lower corrosion potential value than the R/FS4 and R/FM3 specimens. Therefore it can be said that the corrosion potential does not really show the actual corrosion status in the specimen. Also in this type of corrosion test, it is only possible to check the time until the rebar de-passivates. In case of R/HM3 the author suspects that there might be a higher value of bound chloride inside the structure and this issue will be discussed in Section 7.3.

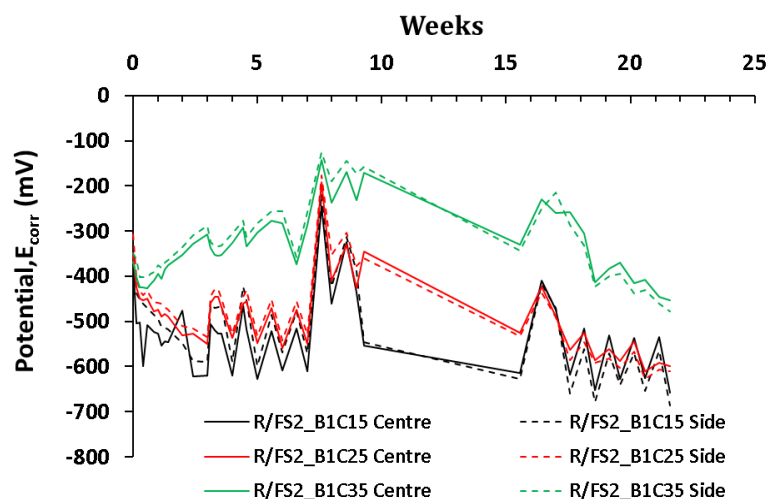


Figure 7.4: Centre versus side corrosion potential reading in Series One.

Chloride Ingress and Reinforcement Corrosion in SHCC

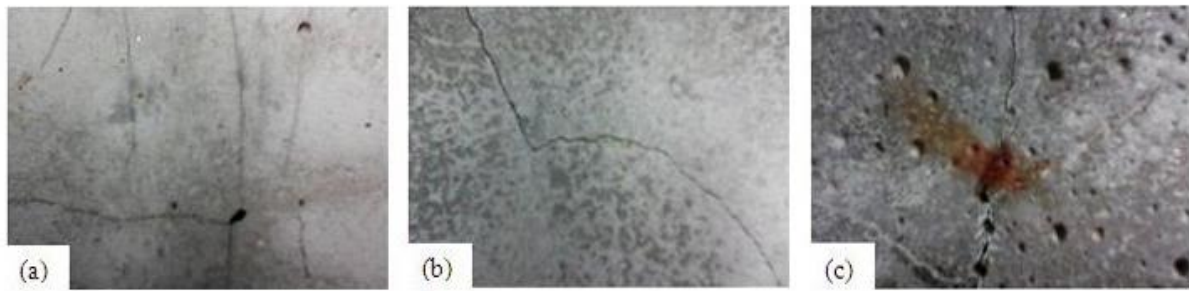


Figure 7.5: Corrosion status in the cracked (a) R/FS4 (b) R/FM3 and (c) R/HM3 specimens after 60 days of accelerated chloride exposure of the Series Four specimens.

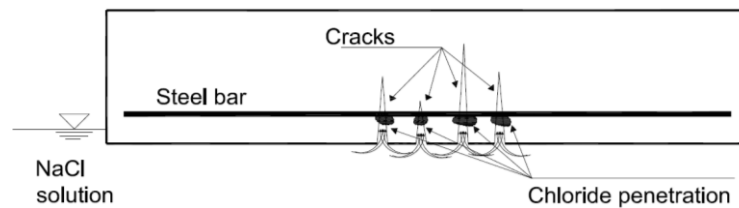


Figure 7.6: Capillary chloride penetration in cracked SHCC beam.

One of the important findings from the corrosion potential readings is that there is no apparent difference between the potential reading in R/SHCC and R/mortar (except R/HM3). Also the influence of crack characteristics on potential readings is not clear from different types of SHCC and mortar specimens. The reason might be the fact that the SHCC and mortar (except HM3 in Series Four) have the same materials compositions which dominate the potential readings here. The aforementioned statement can be verified from the potential reading of R/HM3 where the materials compositions were completely different from the SHCC and mortar specimens made from SHCC composition. In both cracked and uncracked state of R/HM3, the potential value was significantly lower than for R/FS4 and R/FM3. However, in the same exposure condition of corrosion testing, stains were observed in the cracked R/HM3 specimens after just 60 days, while there was no sign of stains on the surface of cracked R/FS4 and R/FM3 specimens. Another important matter is that high volume of binder in R/FM3 and R/FS4 may create an extra protective layer above the passive film of the steel bar which gives more protection against the aggressive substances and ultimately delay the corrosion process in the steel bar. More studies will be helpful to increase the depth of knowledge in this regard.

7.1.1. Reason for higher/more negative half-cell potential values

The potential value is influenced by several factors, including the moisture content in the specimen, the presence of oxygen and temperature. In addition to moisture, it is postulated that the presence of chloride at the steel surface, as illustrated in Fig 7.6, influences the

Chloride Ingress and Reinforcement Corrosion in SHCC

corrosion potential reading. Therefore, without any significant corrosion of steel, more negative values can also be found in concrete.

A reason for the more negative potential readings may of course be corrosion starting already at an early stage, due to quick ingress of water and chlorides in the cracks. Without the presence of a sufficient amount of oxygen in concrete, steel becomes more active, but corrosion does not proceed and the obtained potential value may be achieved due to the saturated half-cell electrode used in the potential measurement (Arup, 1983). As a result, when a concrete specimen is fully submersed, a more negative potential value can be obtained than when a specimen is drying after exposure since it allows faster penetration of free oxygen in concrete. Also, a higher resistivity of the concrete layer can influence the potential reading because of difficulties for oxygen and water to penetrate into concrete (Markeset & Myrdal, 2008). So due to the different cover depths in concrete, a different corrosion potential value can be obtained since the cathodic area of concrete affects the potential reading and it has a lower negative value than the adjacent steel. According to Browne *et al.* (1983) this potential reading difference can be 200-300 mV. The age of concrete, the placement of the reference electrode, cracks in concrete, temperature and cement type can also influence the potential reading of concrete (Montemor *et al.* 2003).

In summary, the recommended corrosion potential values by ASTM are for normal concrete in the un-cracked state. In un-cracked specimens, water and chlorides take longer to reach the steel surface. Therefore a more negative potential reading, indicating a higher corrosion potential is found in the specimen at a much later stage of exposure to water and chloride. Cracks in R/SHCC and R/mortar allow quick penetration of water and chloride. However, this indicates a potential for corrosion, but not necessarily active corrosion, as shown for cracked R/SHCC tested here.

7.1.2. Corrosion potential mapping

Corrosion mapping is an effective way of finding, revealing and measuring corrosion, erosion, pitting, doubling, and delamination or of mapping the whole thickness. Corrosion mapping positioned on the area to be inspected and it allows the corrosion speed of the materials to be calculated efficiently. The location of repair of RCS due to corrosion damage can also be decided based on the corrosion mapping. Fig 7.7 shows the positions of taking corrosion mapping in the specimens in accelerated corrosion tests. As shown in Fig 7.8, corrosion mapping was drawn below 50 mm and 75 mm from the exposed surface and at 50 mm intervals along the specimen length. It means that in one specimen a total of 18 readings (9 at 50 mm depth and 9 at 75 mm depth) were taken to draw the mapping graph as shown in Fig 7.8. Only R/FS4 cracked and un-cracked specimen mapping is shown here and more photos can be found in Appendix C, Figs C.11 & C.11. Potential values were higher in the middle portion of all specimens because chloride solution was applied in that specific area. The region of higher and lower potential area is quite clear from the figure. Note that, in this case the distance between the steel bar and half-cell was 45 mm. Therefore from the Figs 7.4

Chloride Ingress and Reinforcement Corrosion in SHCC

& 7.7, it can be said that the potential reading is influenced by the steel bar and half-cell position and. For smaller distance potential reading becomes clearer than for longer distance.

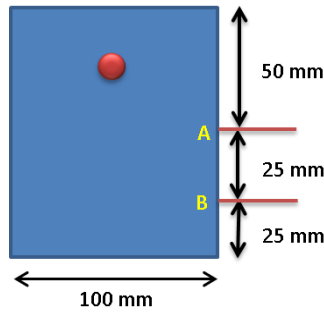


Figure 7.7: Positions of taking corrosion mapping data in the specimen cross section.

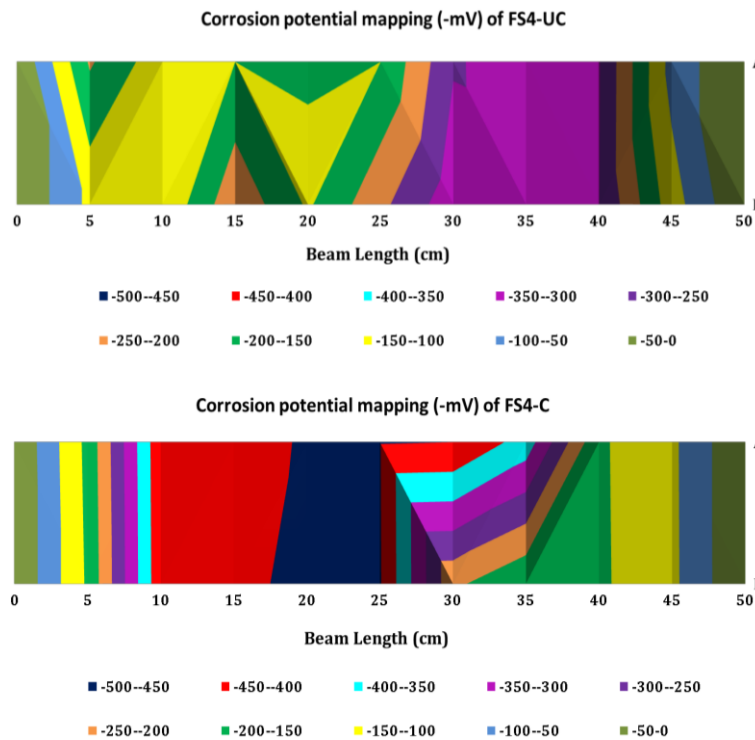


Figure 7.8: Corrosion potential mapping in un-cracked and cracked FS4 specimen at 65 days.

7.1.3. Relationship between corrosion potential and cracks

Figs 7.9 & 7.10 show the relationship between the number of cracks, ACW, MCW, TCW and the corrosion potential in the cracked R/SHCC and R/mortar specimens. The corrosion potentials mentioned here are related to the cracks in the specimens. It is interesting to see that there may be a relationship between these afore-mentioned parameters in cracked R/SHCC specimens. Very good correlations were found for potential in terms of the number of cracks and crack widths. From all the R/SHCC cracked specimens, it was noticed that larger crack widths but a smaller number of cracks in R/SHCC specimens led to a lower corrosion potential whereas, when there are smaller crack widths and a higher number of

Chloride Ingress and Reinforcement Corrosion in SHCC

cracks the potential is higher. In the R/mortar specimens the above relationship was not found, as shown in Fig 7.10 and the reason may be the presence of wider cracks in these specimens. Perhaps the aforementioned relationship is valid only for the finer crack widths in the SHCC specimens and in future more work in this regard will be beneficial to verify this phenomenon.

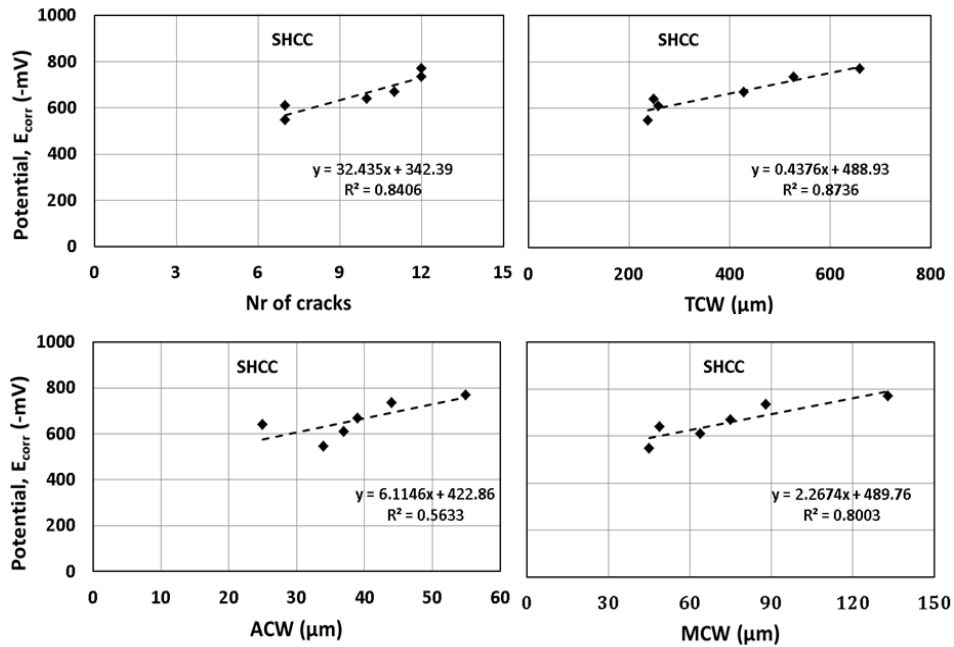


Figure 7.9: Relationship between cracks and corrosion potential in SHCC specimens.

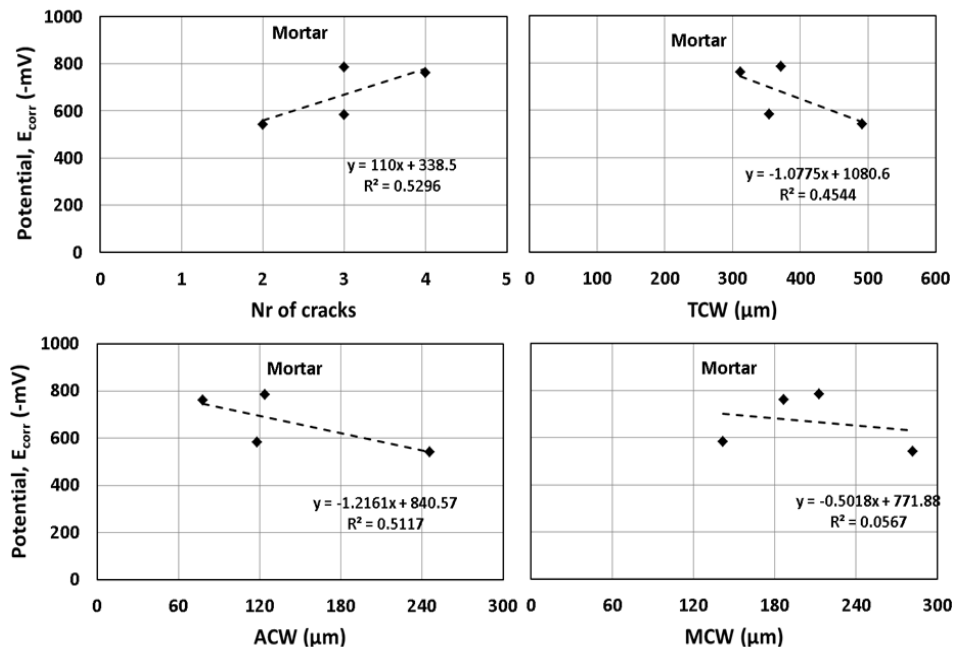


Figure 7.10: Relationship between cracks and corrosion potential in mortar specimens.

Chloride Ingress and Reinforcement Corrosion in SHCC

7.2. Corrosion performance of R/SHCC and R/mortar specimens

Corrosion rate (V_{corr}) results offer a non-destructive way of presenting the reinforcement condition inside a concrete or SHCC. As mentioned in section 4.3 in Chapter 4, different methods can be used to determine the corrosion rate values of the specimens but in this research only the Coulostatic method was followed. As for corrosion potential values, corrosion rate is influenced by various parameters such as temperature, humidity and the presence of moisture and oxygen in the specimens. As a result a corrosion rate value shows the specimens' condition during the specific time of taking the reading and so it cannot be expected that the corrosion rate value will be consistent since all those aforementioned parameters may vary from one day to another.

7.2.1. Corrosion rate in R/SHCC and R/mortar specimens

Figs 7.11 to 7.16 show the corrosion rate in mm/year and the estimated corrosion/corroded depth (d_c) in all R/SHCC and R/mortar specimens. Wiggles in the corrosion rate readings are evident in each figure (a). It is ascribed to sensitivity to variations in factors such as temperature, humidity and moisture content of the specimens. However, upon integration according to Eq. (4.11), d_c values shown in each figure (b), are relatively smooth, allowing improved interpretation of steel bar corrosion in the various specimens. Note that the recording of corrosion rate readings was started sometime after the start of chloride exposure of R/SHCC and R/mortar specimens as it is explained in Section 5.8.1.2. In Eq (4.11) provision is made to add the corrosion depth at the start of time integration, but no attempt was made to estimate the corrosion up to that point and the d_{c0} value in Eq. (4.11) was set to zero.

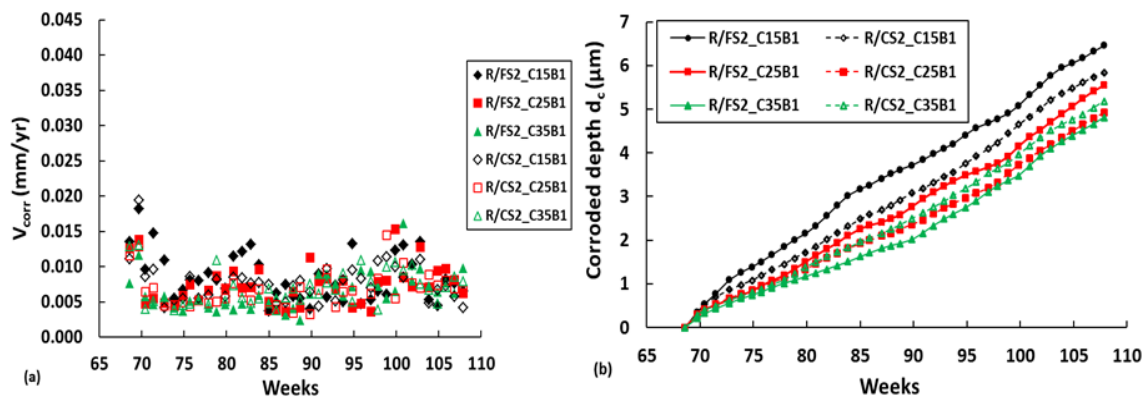


Figure 7.11: R/SHCC with B1 specimens (a) corrosion rate and (b) estimated corroded depth in Series One.

Chloride Ingress and Reinforcement Corrosion in SHCC

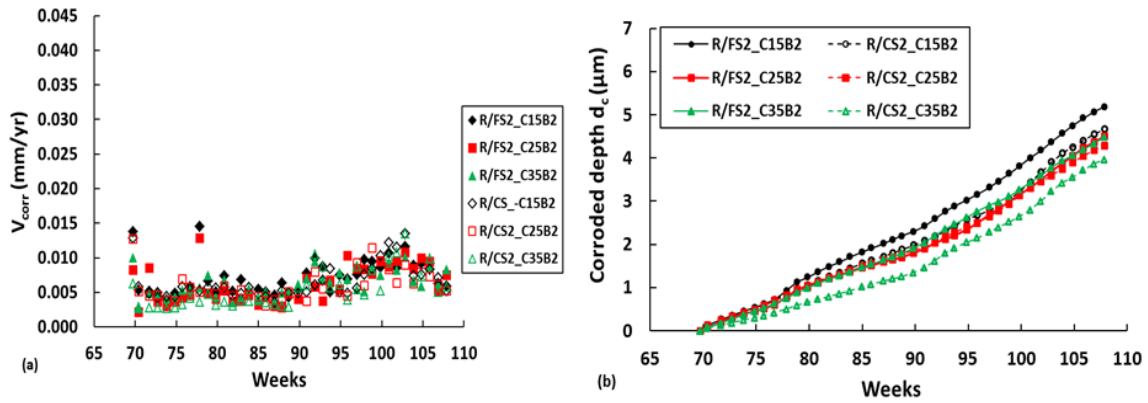


Figure 7.12: R/SHCC with B2 specimens (a) corrosion rate and (b) estimated corroded depth in Series One.

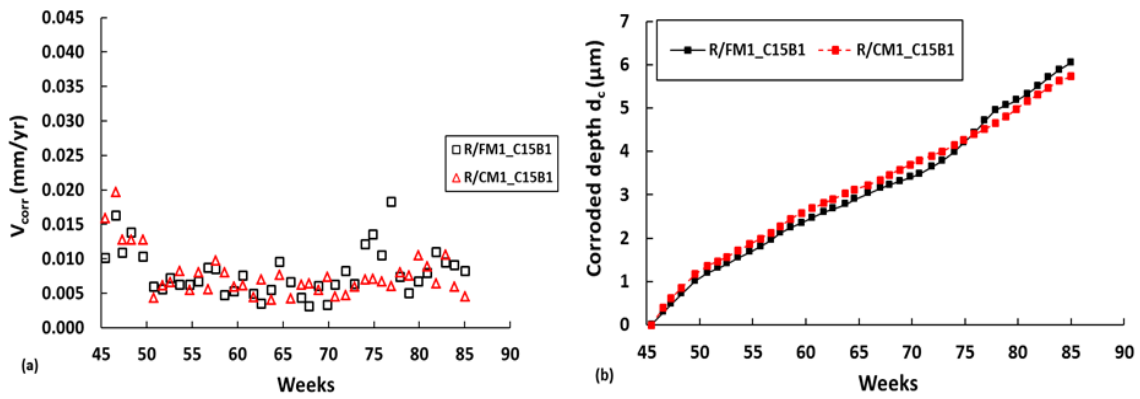


Figure 7.13: R/mortar with B1 specimens (a) corrosion rate and (b) estimated corroded depth in Series One.

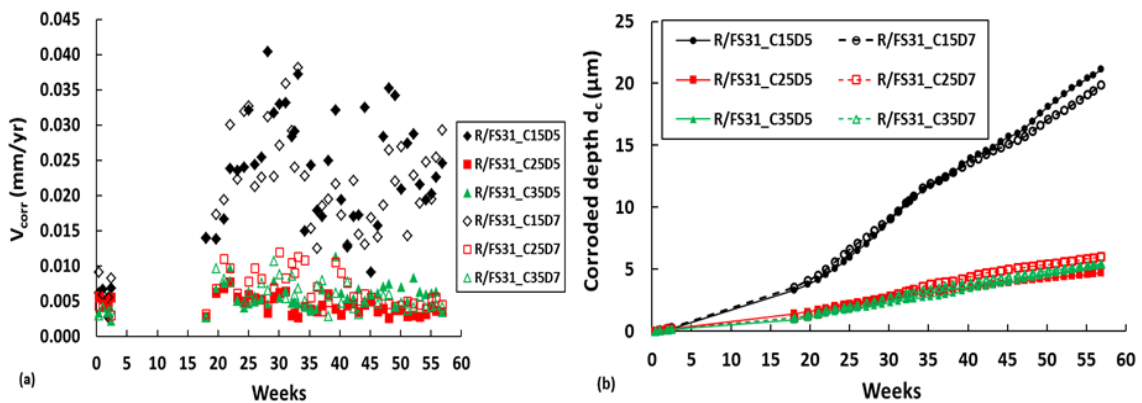


Figure 7.14: R/SHCC specimens (a) corrosion rate and (b) estimated corroded depth in Series Two.

Chloride Ingress and Reinforcement Corrosion in SHCC

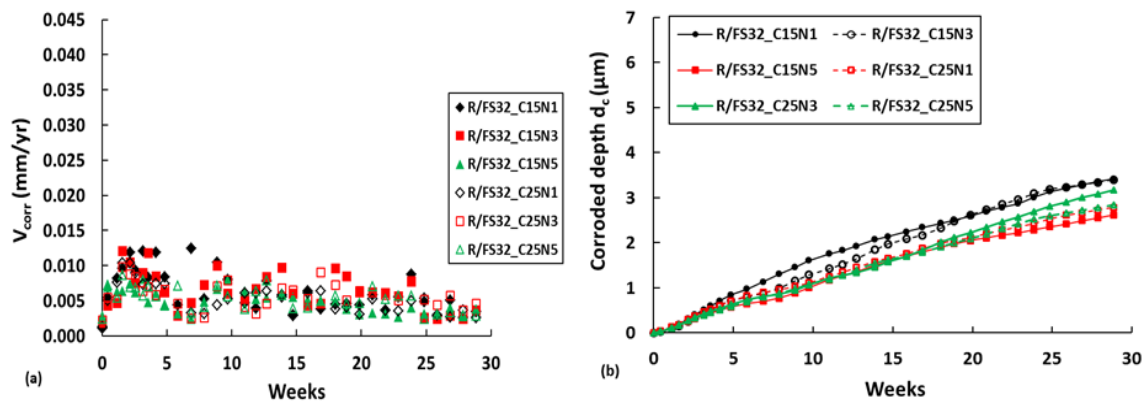


Figure 7.15: R/SHCC specimens (a) corrosion rate and (b) estimated corroded depth in Series Three.

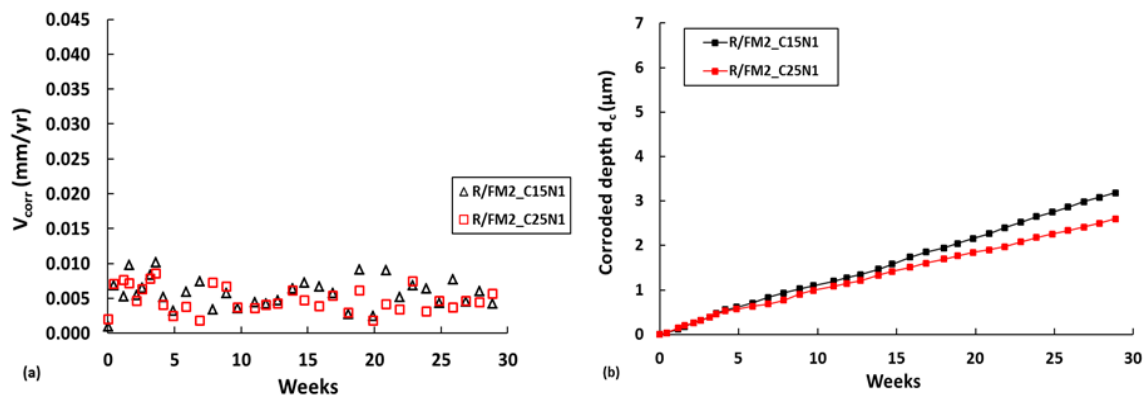


Figure 7.16: R/mortar specimens (a) corrosion rate and (b) estimated corroded depth in Series Three.

It appears from the figures of all three series that the higher corrosion rate values are dominant in specimens with C15, with relatively similar values in C25 and C35 specimens. In terms of the type of sand in SHCC in series one, no clear difference is observed in the results of R/FS2 and R/CS2. A slightly lower corrosion rate was observed in the specimens with double steel bars than in those with a single bar and this can be explained by the difficulty of chloride penetration through the lower number of cracks and finer crack widths in the double bar specimens. Evidence of the higher corrosion rate values in C15 specimens was provided by the corrosion stains on only these specimens' surfaces at cracks just after 6 months of testing, as shown in Fig 7.17. Corrosion rate values in mortar specimens are also similar to those in R/SHCC, in spite of them containing fewer cracks.

Chloride Ingress and Reinforcement Corrosion in SHCC

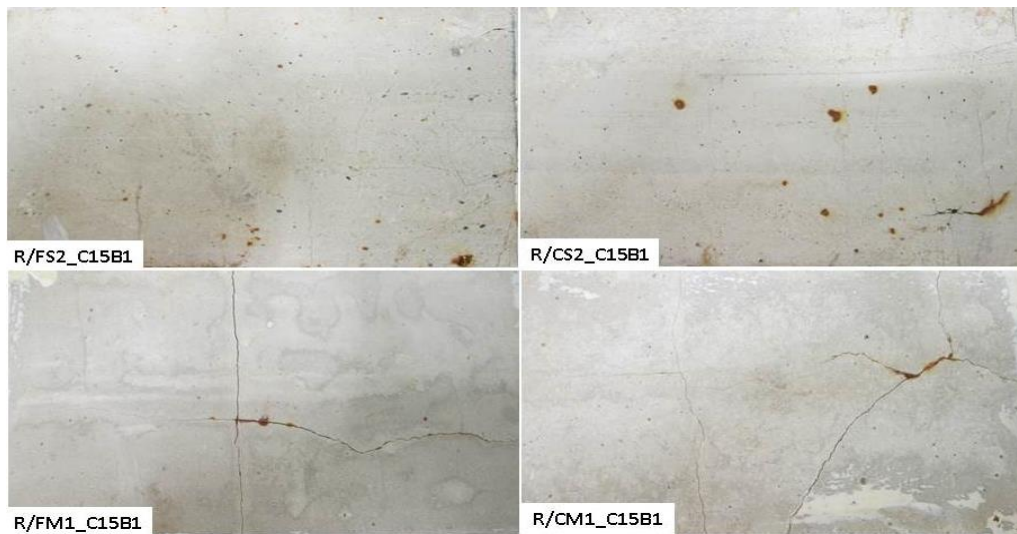


Figure 7.17: Observed corrosion stains in C15B1 specimens after 6 months of exposure.

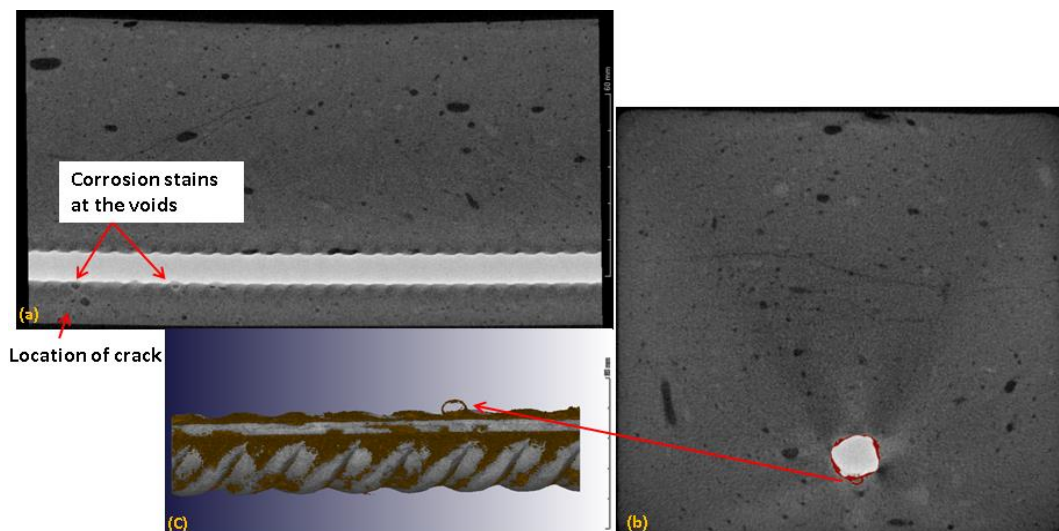


Figure 7.18: XCT images showing corrosion status inside the R/SHCC specimen.

In series two, the corrosion rate in C15 specimens is significantly higher. This might be explained by the higher applied current during the corrosion testing and the reason for this has already been explained in chapter 4. But despite this reason, it is still not clear why such higher corrosion rate did actually occur. The answer was sought by means of the non-destructive method of X-ray computer tomography (XCT) as shown in Fig 7.18. However, by this method the images were not considered to be of sufficient resolution to distinguish clearly an evidence of higher corrosion activity in the respective specimen types. On the other hand, lower corrosion activities were measured by the Coulostatic method in C25 and C35 specimens and from the destruction method to extract the bars, there was evidence of a lower corrosion rate in the specimens as well. No major difference of corrosion rate was noticed

Chloride Ingress and Reinforcement Corrosion in SHCC

because of different cover depths (C25 and C35). More photos of corrosion status in the different steel bars are shown in the Appendix C, Figs C.13-C.15.

Higher corrosion rate values were observed in the C15 specimens in series three as shown in Figs 7.15 & 7.16. However, due to the presence of cracks in the specimens and also due to the exposure conditions of applied chloride (in this case ponding exposure where the water pressure supplements to gravity), the difference of C15 and C25 cover depth in the corrosion rate readings are not that significant as is also confirmed in the previous series. Interesting results were found in the specimens with five notches (N5) for both cover depths and during most days of taking corrosion readings, mostly lower corrosion rate readings were recorded in these specimens. This shows that the corrosion rate in smaller crack spacing (here 20 mm) is lower than in the higher crack spacing (here 40 mm) in specimens with three notches (N3). Future studies on cracked R/SHCC specimens with different crack spacings and cover depths will be helpful to reach a definite conclusion in this regard.

7.2.2. Verification of corrosion activities in the R/SHCC and R/mortar specimens

To verify the corrosion potential and corrosion rate measurements, almost all the specimens were broken to extract the steel bars, after different exposure periods. At an early stage of testing in series one, three specimens were destructed at 17 and 52 days respectively for visual observation of the corrosion status of reinforcing steel bars. First, a R/CS2_C15B1 specimen was destructed after 17 days and after 52 days, two more specimens (RFS2_C35B1 and R/FS2_C15B2) were destructed and the rebar corrosion status inspected visually. In all three these specimens, the only indication of corrosion activities was discolouration, with no sign of pitting or steel volume reduction. The positions of discolouration coincided with concentrations of cracks in the specimen as was also proven in non-destructive testing using XCT scanning as shown in Fig 7.18. After 590 days of accelerated corrosion testing, a R/FS2_C15B1 specimen was taken for XCT scanning to observe the corrosion activities in the steel bar in this non-destructive way. From the XCT images of the specimens it was found that the corrosion stains coincided with the corrosion damage positions. Although it was not used extensively in this research work, XCT scanning might be useful to observe the voids in the matrix, the depth of cracks and the corrosion affected area in the steel bar.

After longer accelerated exposure periods, more rebars were removed from specimens for inspection and corrosion damage detection. In these specimens, evidence of corrosion was found in the form of pitting. It is worth noting that before breaking the specimens, drilling was used to collect powder samples from each specimen for chloride testing, details of which are discussed in section 7.3. After collecting the required powder samples, specimens were broken and photographs of corrosion discolouration of the steel bars were taken (see Fig 7.19b. Fig 7.19a is the virgin non-corroded steel bar). Subsequently, HCl acid was used to remove the corrosion stains from the steel bars and photographs were taken again. Fig 7.19c shows the corroded steel bar after cleaning with HCl acid. It is interesting to note that after cleaning the steel bar, what appeared to be widely-spread corrosion, turned out to have only

 Chloride Ingress and Reinforcement Corrosion in SHCC

been mere discolouration and that the steel bar appears to be without damage and again resembles the virgin steel bar shown in Fig 7.19a.



Figure 7.19: Corrosion inspection by destruction method (a) virgin steel (b) R/FS31_C15D5 steel before cleaning and (c) R/FS31_C15D5 steel after cleaning with HCl.

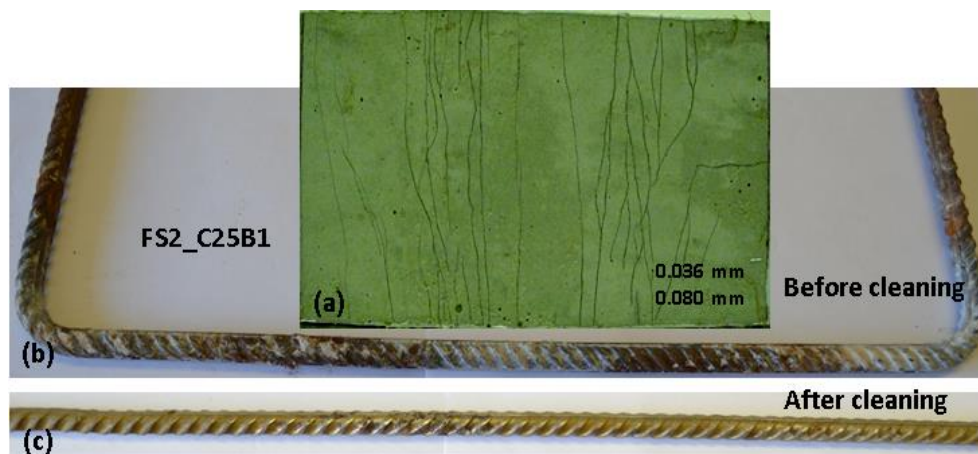


Figure 7.20: Inspection of corrosion in the reinforcing bars by destruction of R/SHCC specimens.

Once cleaned, steel section loss could be seen to be distributed over a significant rebar length in the case of longer exposure periods (over 500 days), but more localised in the case of shorter exposure periods (below 500 days). This creates the impression that the assumption of a uniform diameter loss as expressed in Eq. (4.11) may underestimate the loss in diameter in localised regions on a rebar. Figs 7.20 & 7.21 show the corrosion inspection in the steel bars taken from R/SHCC and R/mortar specimens after cleaning them with HCl. In most R/SHCC specimens, it was found that the corrosion stain was distributed over the whole length of the steel bar. More corrosion activities were seen clearly outside the cracked region of R/SHCC specimens while in R/mortar specimens, the corrosion was more localized around the wider crack widths. The reason for the distributed corrosion in R/SHCC outside the cracked region

Chloride Ingress and Reinforcement Corrosion in SHCC

can be explained as follows. (i) The levels of deformations (3.5 mm, 5 mm and 7 mm) in the R/SHCC specimens in flexural testing were higher and so the delamination which happened between the matrix and the steel surface, created a path for chloride to travel through that weaker path through the steel bar length (ii) parallel cracking was also observed in some of the R/SHCC specimens which was also caused by chloride penetration parallel to the steel bars. Several cases of pitting of corrosion areas were observed in the steel bars especially in the cracked region of R/mortar specimens. In R/SHCC specimens, pitting was also observed in the cracked region as shown in Fig 7.18. However, some pitting was also found outside the cracked region because of the presence of chloride.

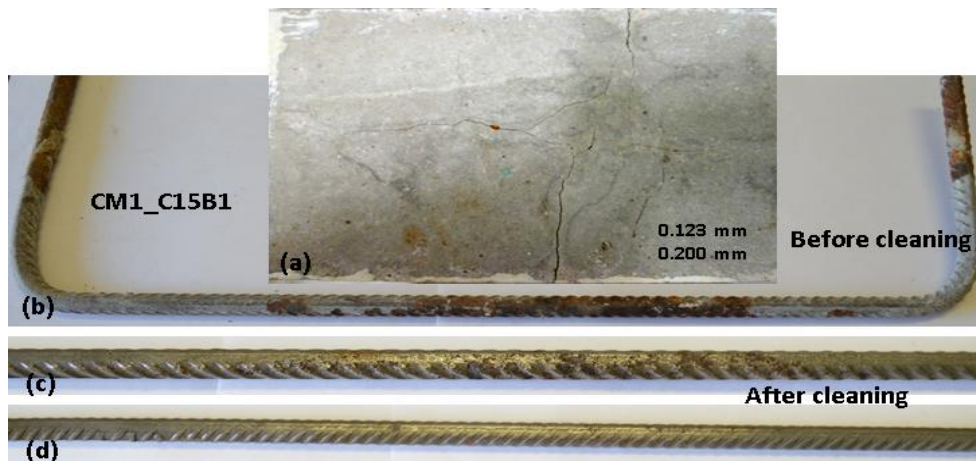


Figure 7.21: Inspection of corrosion in the reinforcing bars by destruction of R/mortar specimens.

7.2.3. Steel mass loss due to corrosion

Estimated mass loss due to the corrosion of a steel bar was calculated by using Eq (4.12) and it was then compared with the actual mass loss of the steel bar by taking the weight difference before casting them in the moulds and after destruction of the specimen and cleaning the steel bar using HCl acid before using it for corrosion testing. Note that the actual mass loss was considered only in the specimens of R/FS32 and R/FM2 in series three. Fig 7.22 shows the estimated mass loss and the actual mass loss of the average of three R/FS32 specimens and two R/FM2 specimens. There is a noticeable variation between the estimated and actual mass loss. The possible reasons may be (i) considering a lower B value (26 mV) in the corrosion Eq (4.9) since the range of B values varies from 26 to 52 mV depending on the corrosion status (active or passive), (ii) a wrong assumption of d_{co} values in Eqs (4.11 and 4.13) and (iii) some mass loss of steel caused by using HCl acid. If the aforementioned parameters are corrected to within a reasonable range, the difference in estimated and actual mass loss may also be reduced. Therefore, in future work these issues should be considered carefully for the improved prediction of the actual mass loss from corrosion rate readings.

Chloride Ingress and Reinforcement Corrosion in SHCC

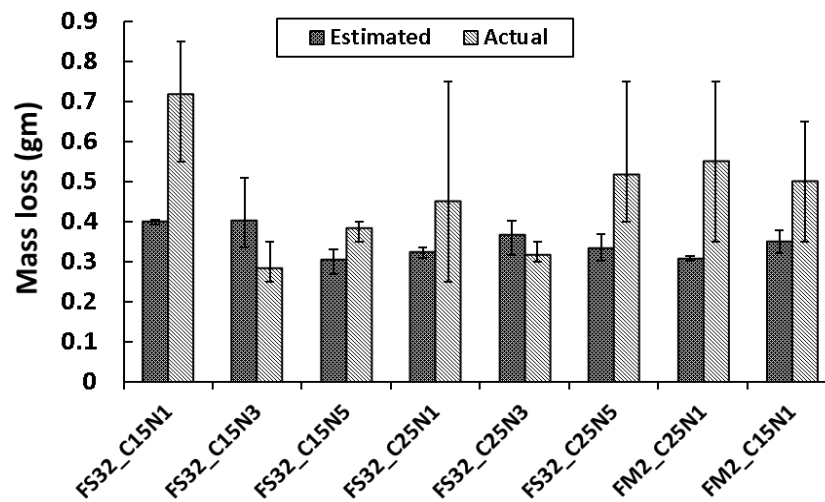


Figure 7.22: Estimated and actual mass loss of steel in R/FS32 and R/FM2 specimens in Series Three.

7.2.4. Loss of steel yield resistance due to corrosion

After cleaning all the corroded steel bars, they were used for tensile testing in a Zwick Z250 Materials Testing Machine. For the reference yield forces, four undamaged Y10 bars were also tested to determine the average, reference Y10 rebar yield resistance. From the corroded depths calculated by using Eq. (4.11), the yield force ($F_y (Cal)$) was calculated by using Eq. (4.13) by the assumption of a retained 510 MPa yield stress and the residual cross section. These values are compared with the actual measured yield forces ($F_y (Exp)$) in Fig 7.23, clearly showing a significant divergence due to the assumption of uniformly-smearred damage as opposed to localised corrosion. In addition to the localised vs smearred nature of corrosion damage, the negligence of corrosion depth development up to the time of commencement with corrosion rate measurements (d_{c0} in Eq. 4.11), i.e. after 320 and 480 or more days of cyclic chloride solution exposure respectively for R/FM1, R/CM1, R/FS2 and R/CS2 specimens, contributes to the discrepancy. Although the C15 mm SHCC specimens clearly show the highest corrosion rates and visual damage, they do not, in this limited data set of corroded rebar tensile tests, lead to the largest drop in resistance. Because of lowest exposure times, R/FS31, R/FS32 and R/FM2 show minimum differences in the calculated and experimental value of yield forces. While the yield resistance in R/FS31_C15 specimens appears to be marginally lower than in C25 and C35 specimens in Fig 7.23b, and C25 specimens in Fig 7.23c, it is not as pronounced as the significantly higher measured corrosion rates shown in Fig 7.14b.

With the exception of R/FS31_C35D7 specimens, a lower yield resistance was found in the steel bars of specimens that were deflected up to a 7 mm (D7) vertical deflection level, than in those deflected to 5 mm. Interesting results were found in R/FS32 specimens (see Fig 7.23c). Higher retained resistances were observed in the specimens with five notches than in specimens with one notch. It also agrees with the lowest corrosion rates measured in the

Chloride Ingress and Reinforcement Corrosion in SHCC

specimens with five notches. It is also important to note that the steel bars used in series one (R/FS2, R/CS2, R/FM1 and R/CM1) specimens were bent to have U shape as shown in Figs 7.20 & 7.21 while in other cases steel bars were straight. The purpose of this was to connect the necessary cable connection during the corrosion rate testing of these specimens. However, for the tensile testing the bent portions of these bars were straightened again. It is reported by the Choi *et al.* (2003) that this procedure (bent and straighten) can cause significant loss of yield force (20-25%) of the steel bar. This may also explain the higher loss of yield force in the steel bars of R/FS2 and R/CS2 specimens as shown in Fig. 11.

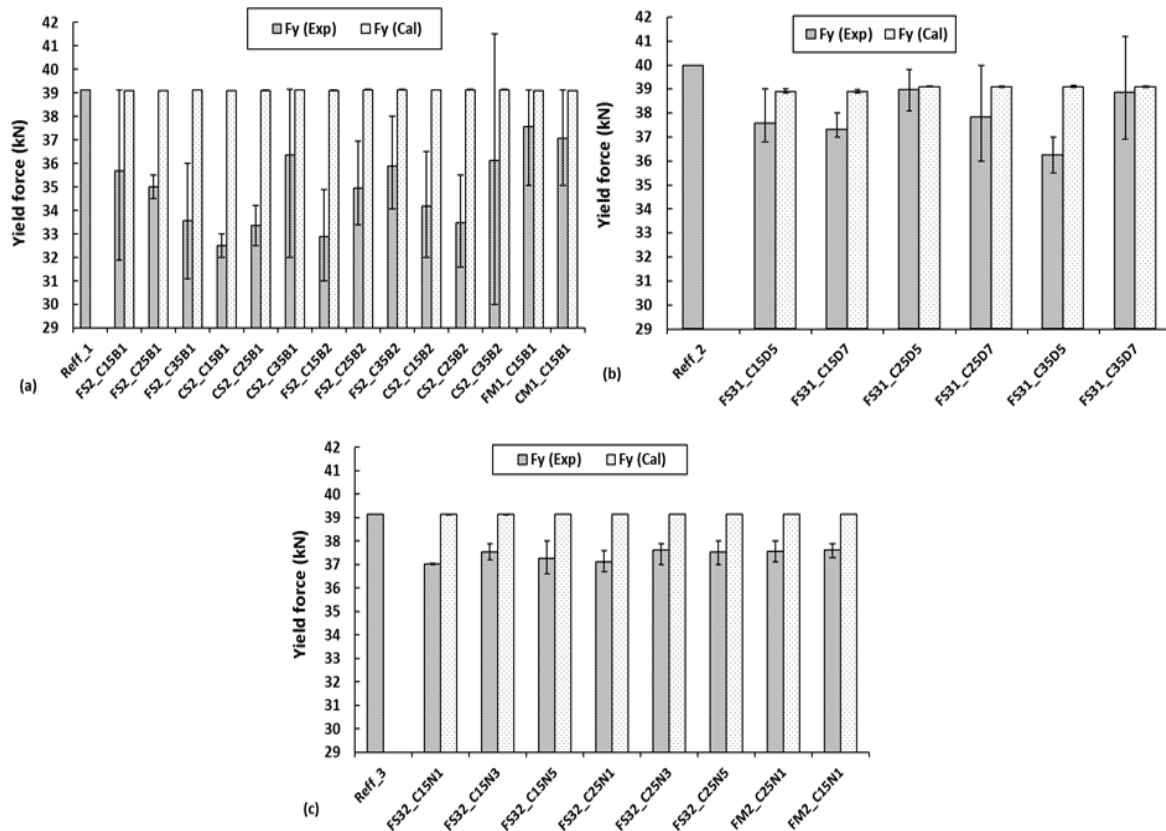


Figure 7.23: Difference of analytical and experimental yield forces in different R/SHCC and R/mortar specimens due to loss of section in corrosion.

7.2.5. Pitting depths in steel due to corrosion

Measured actual pitting depths (d_p) in the steel bars are shown in Figs. 7.24a-d. As the corrosion rates of the specimens were low, the pitting depths were also low. A dial gauge with a resolution of 10 μm was used to measure the pitting depths as described in Section 5.8.1.2. The accurate measurement of these depths is complicated by pitting shape and size. Because of the difficulty of measuring these small pitting depths (most of them were less than 10 μm which were difficult to measure with the current set up of dial gauge), not all pitting depths were measured, but the deeper pitting depths in the steel bars were chosen by visual inspection. A minimum of three to a maximum of six pitting depths on each steel bar were

Chloride Ingress and Reinforcement Corrosion in SHCC

measured and their average value is reported in Table 7.2 and in Fig 7.24, while the minimum and maximum values of these 3 – 6 largest pitting depths are indicated by error bars. It is quite clear that the average pitting depths in the older FS2 and CS2 specimens (series 1) are higher compared to those of the newer specimens FS31 (series 2) and FS32 (series 3). In SHCC, lower pitting depths were observed for larger cover depth of the steel bar as well as for a higher level of pre-deflection (D7 vs D5) in the specimens. In FS31, at 5 mm deflection level, almost 35% and 43% lower pitting depths and at 7 mm deflection level, almost 66% and 5% lower pitting depths were observed in C25 and C35 specimens than in C15 specimens. However, because of the relatively low corrosion damage in the steel bars, no strong correlations were found for different sand types and the number of notches in the R/SHCC specimens tested here.

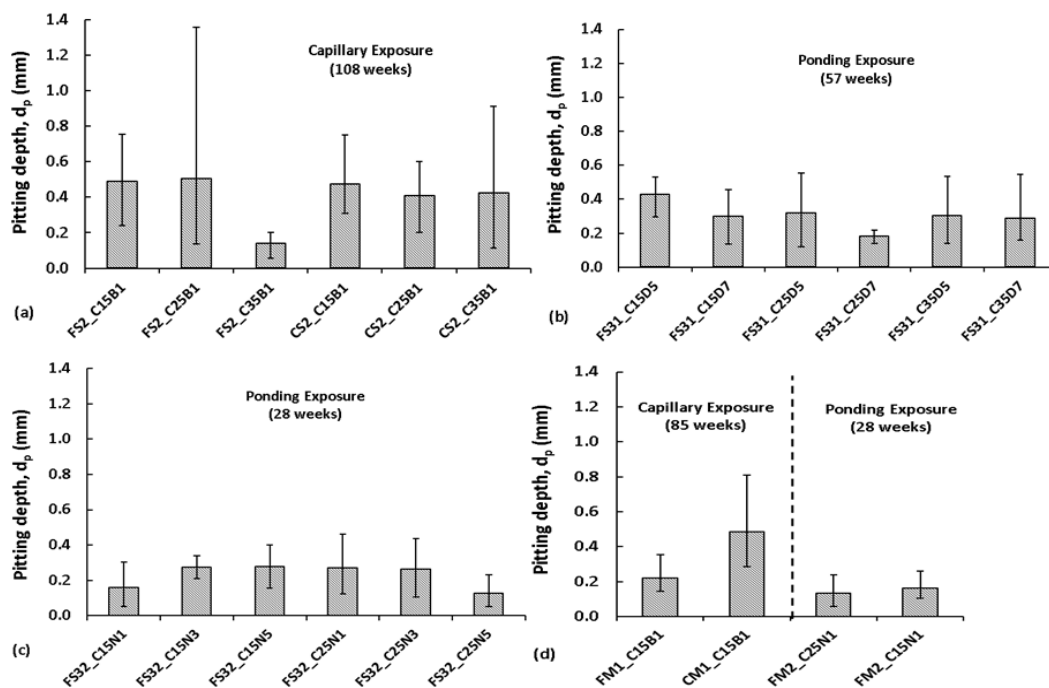


Figure 7.24: Average pitting depths in the single steel bars (B1) at different series.

Fig 7.25 shows a relationship between pitting depths and corrosion –induced loss of tensile yield resistance. An upward trend in loss of yield resistance with increased pitting depth is seen. Of importance in rebar resistance is the reduction in its cross-sectional area, which is clearly not represented by the pitting depth only, in the light of the rather poor correlations shown in the figure. More accurate representation of loss of cross-sectional area is required to improve correlation with and estimation of corrosion damage to steel reinforcement, which is the subject of further research.

Chloride Ingress and Reinforcement Corrosion in SHCC

Table 7.2: Average and maximum pitting depths in the steel bars in different series at the end of testing period as reported in Table 7.1

Type	Ave pitting depth (mm)			Max pitting depth (mm)		
	C15	C25	C35	C15	C25	C35
R/FS2_B1D3.5	0.49	0.50	0.14	0.76	1.36	0.2
R/CS2_B1D3.5	0.47	0.41	0.42	0.75	0.60	0.91
R/FS2_B2D3.5	0.41	0.29	0.43	0.79	0.35	0.73
R/CS2_B2D3.5	0.53	0.36	0.27	0.77	0.52	0.45
R/FS31_B1D5	0.39	0.33	0.45	0.53	0.56	0.54
R/FS31_B1D7	0.33	0.17	0.22	0.46	0.22	0.55
R/FS32_B1N1	0.25	0.27	-	0.42	0.41	-
R/FS32_B1N3	0.30	0.26	-	0.39	0.41	-
R/FS32_B1N5	0.34	0.22	-	0.54	0.33	-
R/FM1_B1D1.5	0.28	-	-	0.36	-	-
R/CM1_D1.5	0.49	-	-	0.81	-	-
R/FM2_B1N1	0.22	0.20	-	0.26	0.24	-

Note: B, D and N represent nr of bar, level of deflection (mm) and nr of notches in the specimen.

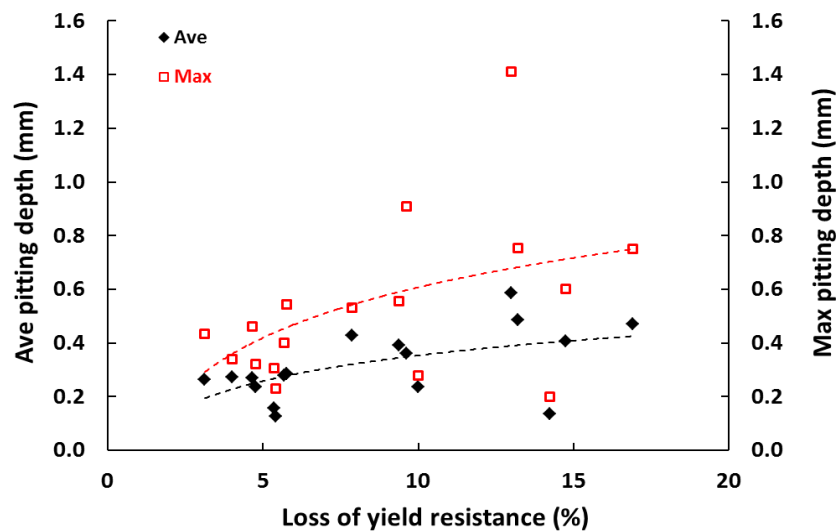


Figure 7.25: Pitting depths versus loss of yield resistance of steel bars.

The detailed influence of crack properties such as the number of cracks, crack widths and spacing in the corrosion rate of R/SHCC is discussed in Chapter 8. The steel pitting depths and mass loss in R/SHCC specimens and their influence on the yield force loss of steel bars will also be discussed broadly in that chapter. Finally a corrosion model will be proposed from the obtained results which can ultimately give an indication of the remaining design life of a SHCC structure after being affected by corrosion.

Chloride Ingress and Reinforcement Corrosion in SHCC

7.2.6. Relationship between corrosion potential, corrosion rate and moisture content in the specimen

Fig 7.26 shows the relationship between corrosion potential (E_{corr}) and corrosion rate (V_{corr}) in R/FS2 and R/CS2 specimens after two different numbers of days (500 and 600 days). It is worth mentioning that these corrosion potential and rate values were taken from the same specimens on the same day. No direct relationship was found between them. As already discussed in Chapter 4 and in the Section 7.1, the corrosion potential value does not really represent the real corrosion activities in the steel bar. It is merely an indication of probability of corrosion of a steel bar. While the corrosion rate of a steel bar specifies the loss of steel due to the attack of chloride and carbonation on concrete, it depends on many factors such as temperature, RH, available moisture content, exposure types, etc.

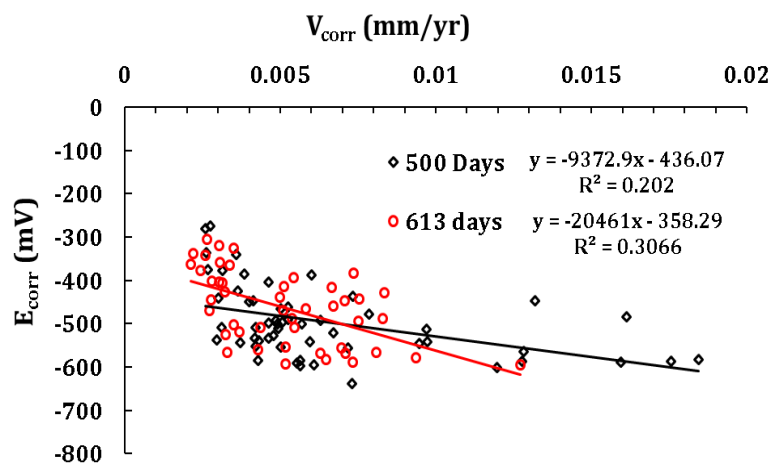


Figure 7.26: Relationship between corrosion potential (E_{corr}) and rate (V_{corr}) in the cracked R/SHCC specimens at different days.

A moisture meter, also known as hygrometer (Type DM4A) was used to measure the moisture content in the R/SHCC specimens and the moisture reading was compared with the corrosion rate reading on the same specimen at the same time. Note that with the specific type of moisture meter used here, a maximum moisture content of 20% (% by weight of SHCC matrix) can be measured. The detailed methodology of how the moisture meter works is not discussed here since this is beyond the scope of this research. Methods for measuring moisture content in concrete can be found in Rode & Wendler (1996). Fig 7.27 shows the relationship between moisture content and the corrosion rate of specimens. Although there appears to be an indication that higher corrosion rates occur at higher moisture content in the specimens, between corrosion potential and corrosion rate, no significant correlation was found. Note that the moisture content was measured with a moisture meter which gives the percentage of moisture by weight of concrete.

Chloride Ingress and Reinforcement Corrosion in SHCC

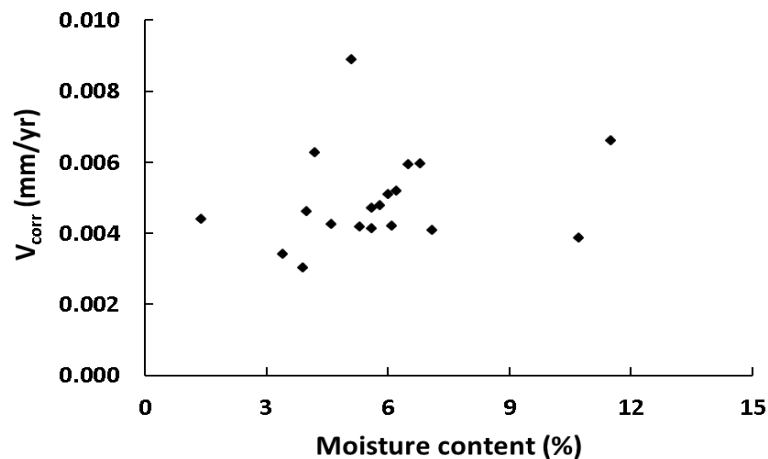


Figure 7.27: Relationship between corrosion rate (V_{corr}) and moisture content in the specimens.

7.3. Chloride profile in SHCC and mortar specimens

Chloride profiles in both SHCC and mortar specimens were determined in various ways namely by visual observation after spraying AgNO_3 solution on the specimen surfaces, by testing for chloride content the powder samples obtained from drilling at different depths of the specimens as well as by RCM testing. Outcomes from these different types of tests are discussed in this section.

7.3.1. Influence of cracks on penetration of chloride profile in SHCC

Cracks were found to be the fastest way for the chloride to penetrate into the specimens. However, the amount of chloride is mostly depended on the crack widths and the exposure time. It was found that chloride reaches a maximum crack depth within one hour of testing in both capillary absorption and ponding exposure conditions. Depending on the type of matrix, chloride penetration subsequently becomes wider, penetrating into the matrix from the cracks. Detailed results are discussed below.

7.3.2. Chloride penetration in un-reinforced SHCC

A total of 25 different un-reinforced types of SHCC specimens were used for determining the chloride profile. Chloride profiles in the specimens were determined by using the common methods of spraying AgNO_3 solution, XRF and chemical testing. Details of the outcomes are discussed in this section.

7.3.2.1. Chloride penetration in un-reinforced SHCC using AgNO_3

Figs 7.28-7.30 show the chloride penetration depths obtained by spraying the AgNO_3 solution on different cracked SHCC specimen surfaces at different time periods. Chloride penetration

Chloride Ingress and Reinforcement Corrosion in SHCC

depths through cracked specimens FS1 and CS1 were observed at the three different durations of cyclic wetting (3 days), drying (4 days) and exposure (4, 8, 12 cycles) as shown in Fig 7.28. A total of 5 specimens (3 from FS1 and 2 from CS1) were used in this case. Similarly, a total of 4 specimens (3 from FS2 and 1 from CS2) and 18 specimens (9 from FS5 and 9 from FS32) were also tested. The white-grey colour represents the chloride penetration in the specimens. It is clear from the figures that the waterproofing repellent used here did not work at all. As a result penetration through the sealed faces was also observed as well. In these specimens the average crack widths were below 50 μm and it is interesting to see that the chloride reaches to the whole depth of the cracks after a short exposure period while with time the penetrations were found to be widening and expanding horizontally from the cracks.

In the case of FS32 and FS5 (as shown in Fig 7.30) the chloride penetration was monitored for different exposures of 1 hour, 1 day and 7 days in two different notched spacings (20 mm and 40 mm) in the specimens. High strength FS5 shows better penetration resistance than the lower strength FS32. However, again the chlorides reach to the entire depth of cracks in both the types of SHCC. In all the above cracked specimens (except FS5_20mm @ 1 hr (UL) where the specimen was loaded to ultimate deflection level) the applied load was up to a deflection level of 1 mm and the average crack width range was between 50 to 100 μm . So it can be said that the crack width range of 50 to 100 μm provides a quick path for chloride penetration into the SHCC. It is also worth mentioning that the exposure type in FS32 and FS5 was ponding (NaCl solution was kept on top of each specimen) while in other cases it was capillary sorption i.e. bottom face of the each specimen was in contact with the NaCl solution as is also shown in Figs 7.28 & 7.29.

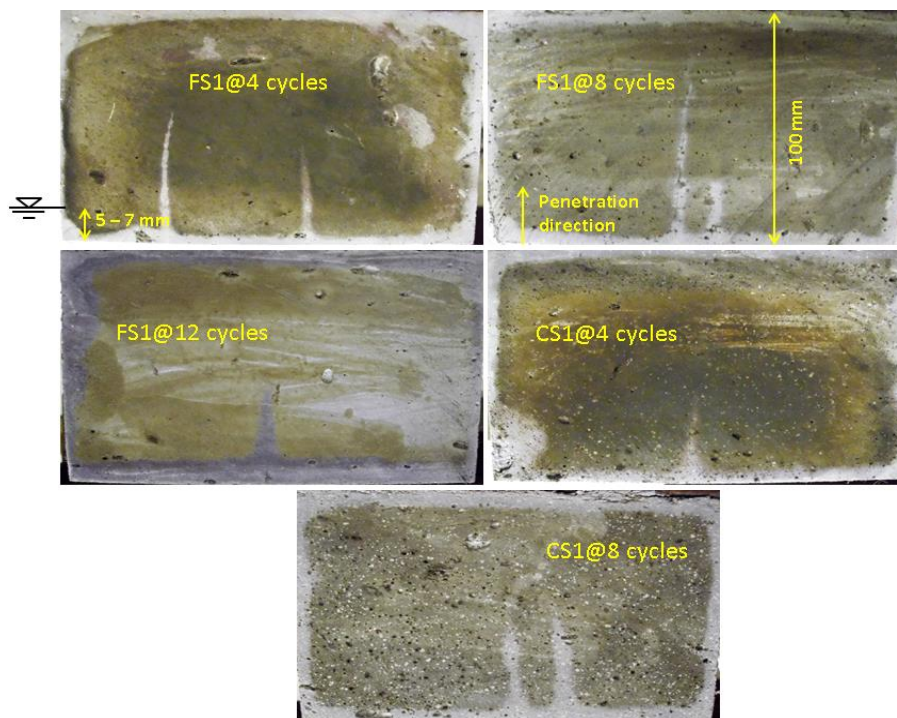


Figure 7.28: Chloride penetration in R/FS1 and R/CS1 at different exposure cycles.

 Chloride Ingress and Reinforcement Corrosion in SHCC

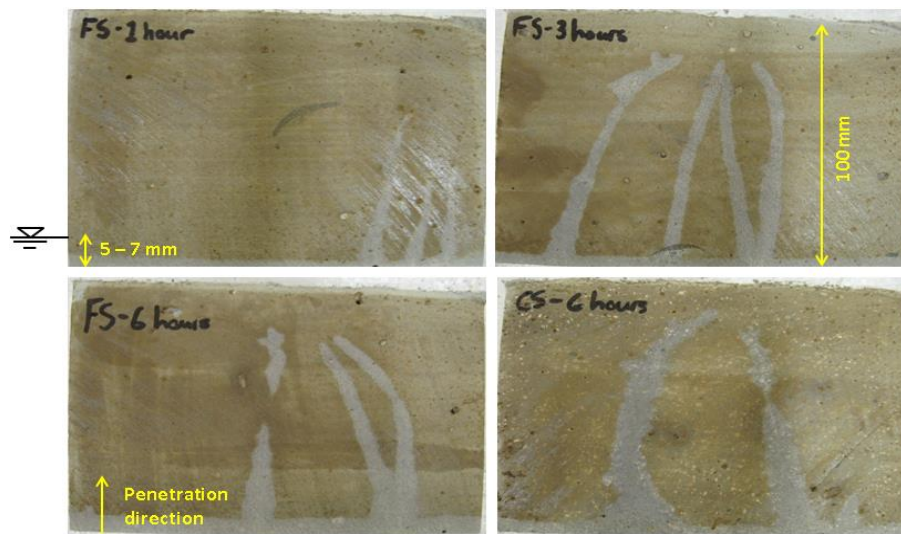


Figure 7.29: Chloride penetration in R/FS2 and R/CS2 at different time periods.

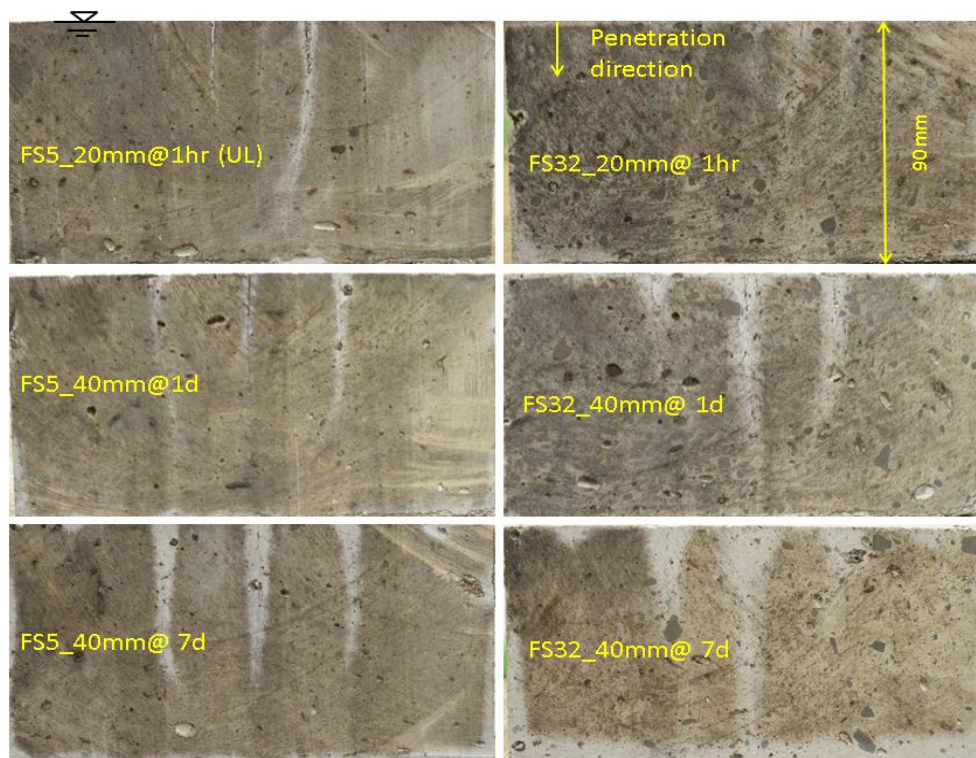


Figure 7.30: Chloride penetration in R/FS5 and R/FS32 after different exposure periods.

7.3.2.2. Chloride profile in un-reinforced SHCC using XRF

The chloride determination method shown in the previous section does not provide information about the actual chloride level in the specimen and because of that, it is not possible to determine the risk of steel corrosion inside the concrete from the above method. Therefore, to determine the actual concentration of chloride in the specimen, two layers of

Chloride Ingress and Reinforcement Corrosion in SHCC

SHCC were sliced from one specimen of FS1 and tested after 12 cycles with the XRF method. In layer one (4 mm from the contact face with NaCl solution) and layer two (at the crack height, i.e. roughly 60 mm from the NaCl solution surface) the concentration of chloride was about 0.1% and 0.004% respectively by weight of cement. It was noted that for the discolouration, a chloride content level of about 0.1% – 0.15% was present at the lower end of the crack, but because of the large portion of material away from the crack tip included in this particular chloride concentration test, a low overall concentration of 0.004% was found.

To obtain more detailed chloride profile, drilling was done as described in Section 5.8.2.3. Chloride profiles in un-reinforced SHCC specimens were drawn for FS32 and FS5 as shown in Figs 7.31a-c. Recall that except for one specimen from the each case which was loaded at the ultimate deflection level, all the FS32 and FS5 specimens were loaded up to a 1 mm level of deflection. In both these SHCCs, a slightly higher chloride content was found in the specimens with notch spacing of 40 mm. In these specimens the drillings were started at the tip of the notches (about 10 mm below the specimen's surface), and so the starting chloride profile shown here is at a depth of 13 mm except for one un-cracked specimen in Fig 7.31c. In this case the drillings were performed on top of the specimen surface but at a sufficient distance from the notch position. The influence of crack spacing was clearer in Fig 7.31c for the ultimate load levels of specimens. Significantly less chloride was found in the un-cracked portion of specimen after 7 days of continuous NaCl ponding testing. Note that in Fig 7.31, UC stands for un-cracked specimen, UL stands for ultimate loaded state and 1hr, 1d and 7d stands for the exposure periods of the specimens which were loaded up to 30% of ultimate load (1 mm) capacity.

7.3.2.3. Chloride profile in un-reinforced SHCC using chemical testing

Chemical chloride testing (for both free and total) was also performed on the same powder samples which were used in XRF tests. Only limited samples were chosen for chemical testing as shown in Fig 7.32 and these results were also compared with XRF results. Some deviations in results from these tests were found for the total chloride contents but a good consistency was noted for free chloride. The total chloride content in high strength FS5 was slightly lower than in FS32. However, the free chloride content in high volume of fly-ash in FS32 was found to be lower than in the low volume of fly-ash in FS5.

Chloride Ingress and Reinforcement Corrosion in SHCC

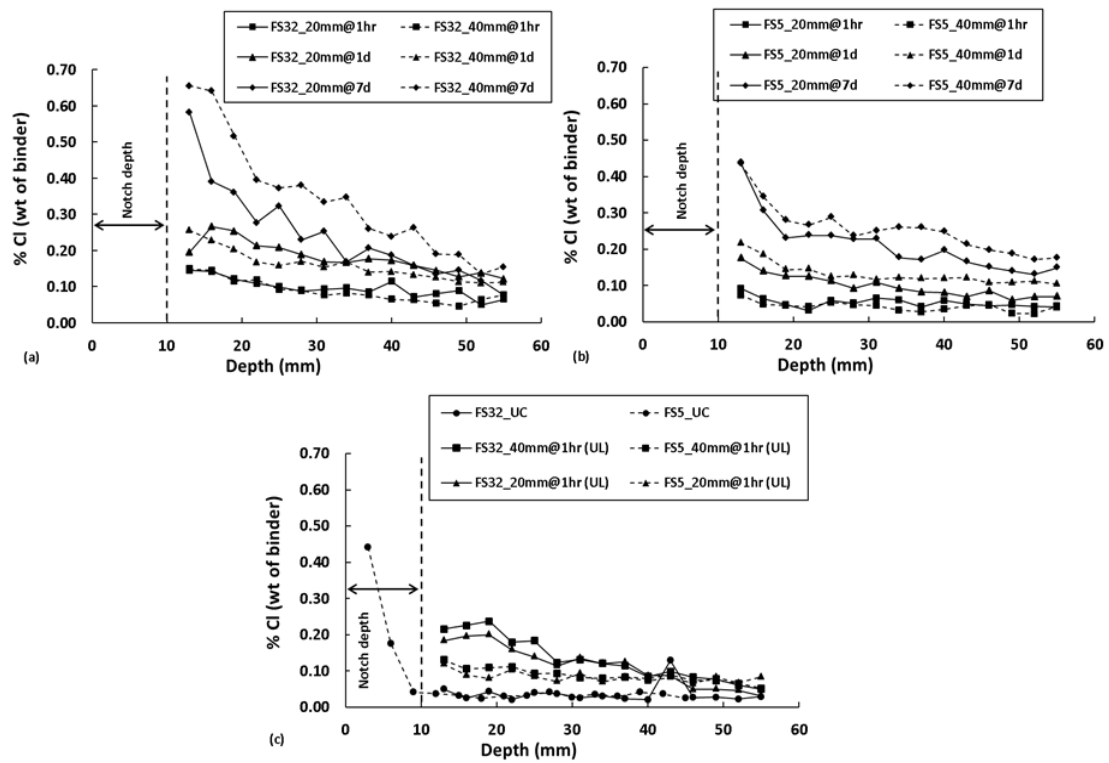


Figure 7.31: Chloride profiles in FS32 and FS5 specimens for different notch spacings for different exposure periods.

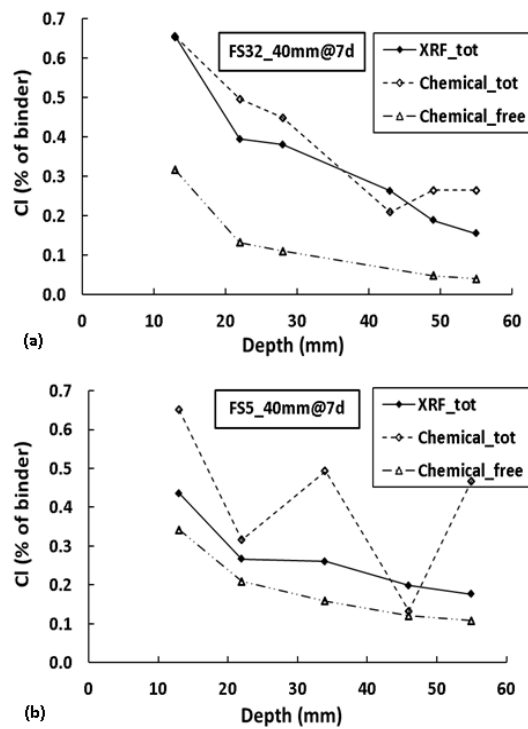


Figure 7.32: Comparison of XRF and chemical chloride profile in (a) FS32 and (b) FS5 specimens.

Chloride Ingress and Reinforcement Corrosion in SHCC

7.3.3. XRF chloride profile in R/SHCC and R/mortar specimens

A total of 30 different R/SHCC and R/mortar specimens were used at different days to determine the chloride profile using XRF as shown in Fig 7.33. Similar procedures as discussed for the un-reinforced SHCC were also followed for determining the XRF total chloride content of reinforced SHCC. The specimens exhibited different corrosion rates before they were used for chloride profiling. Recall that test samples were taken by drilling in the cracked region. The 16 mm drill diameter exceeds the crack spacing, resulting in more than one crack being represented by the chloride profiles. It is presumed that the geometry of the cracks, which may vary with depth, contributes to the local high internal Cl concentrations (% by wt of binder) seen in all figures. From the figures it is clear that a significant amount of chloride penetrates the cracked R/SHCC and R/mortar specimens right up to and beyond the steel bar. As mentioned before, the XRF data reflects the total chloride content and chemical testing for total and free chloride is discussed in the next section.

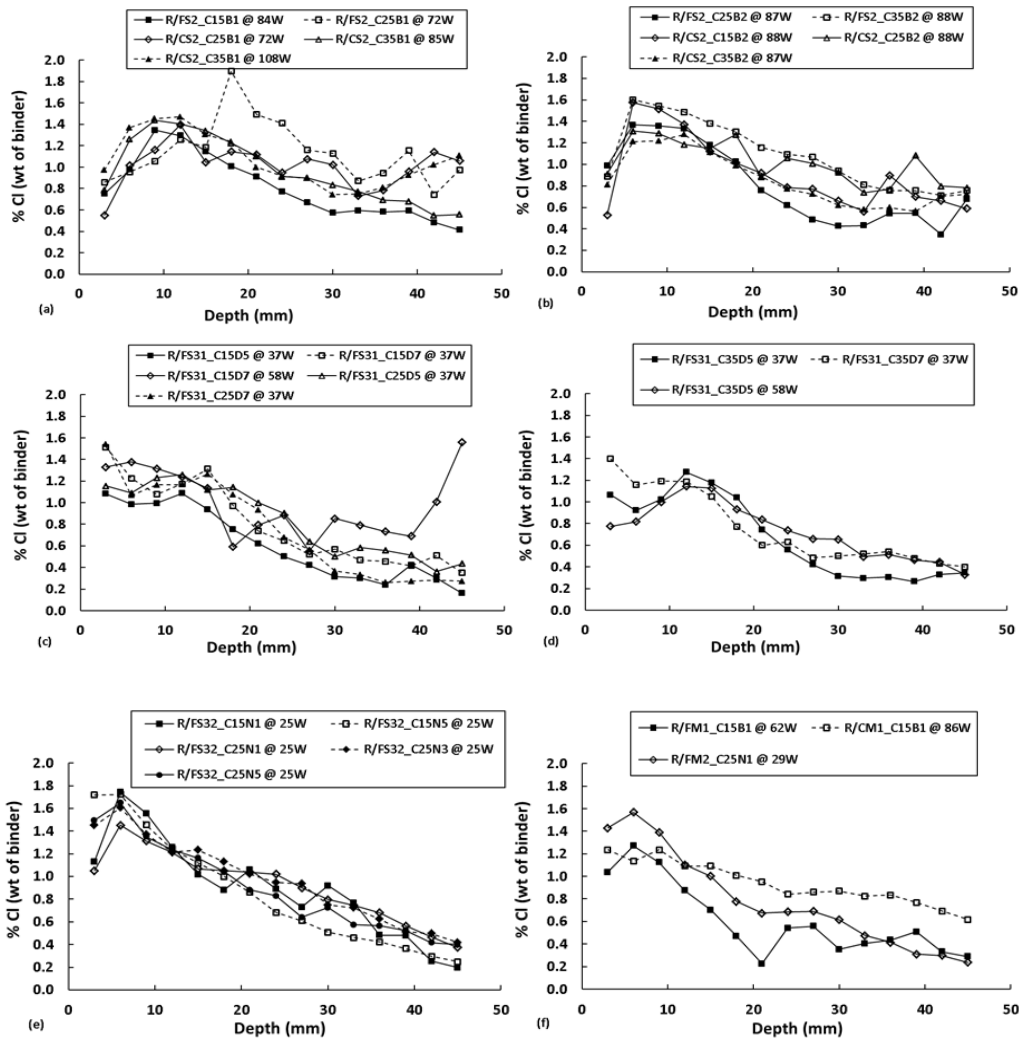


Figure 7.33: XRF chloride profile in different (a-e) R/SHCC and (f) R/mortar specimens after different weeks (W).

Chloride Ingress and Reinforcement Corrosion in SHCC

Note that the lower chloride value at the surface (starting point in the figure) of the most specimens in Fig 7.33 can be explained by the different crack geometry in both surface and perhaps through the depth of each the different specimen. Also the surface of the specimen dry out quicker which may also diminish some of the chloride. However, this issue was not investigated in this research which needs future studies.

Fig 7.34 shows the chloride profile through the entire depth (100 mm and 80 mm) of specimens including one for un-cracked specimens. Higher chloride content was found at the deeper face of specimens (90-100 mm depth) than at the surface where the NaCl solution was applied. A similar trend was also found by Wittmann *et al.* (2011) and Maruya *et al.* (2007) in SHCC and NC materials and the reason of this is not quite clear yet. Maruya *et al.* (2007) was drawn the contours of distribution chloride ions in the specimen from the half-cell potential and the direction of current by solving the Laplace's equation. In uncracked NC, at the anodic region of steel the authors found the higher chloride concentration and the corrosion potential values due to the higher current flow towards the outer surface of concrete specimen. However, in this research by visual inspection it was noticed that salts (by means of efflorescence) formed on all the sides of specimens which can be a reason for a higher chloride-content on the opposite face of specimens.

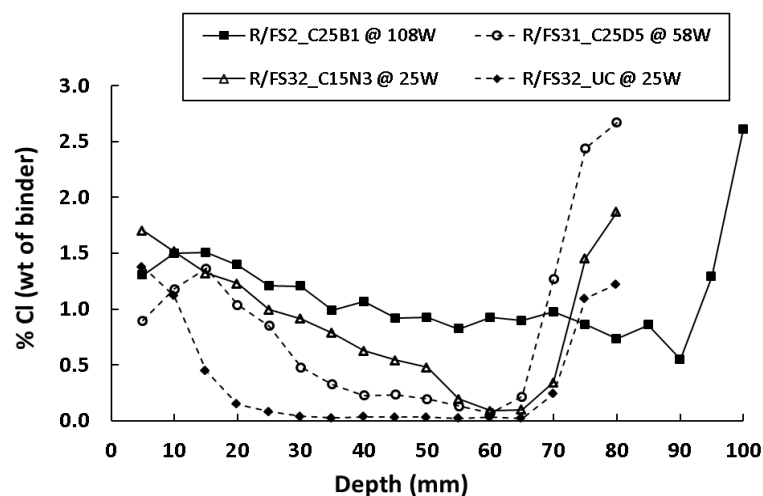


Figure 7.34: Chloride profile for the entire depth of different cracked and un-cracked (UC) R/SHCC specimens after different exposure weeks (W).

7.3.4. Chemical total and free chloride profile in R/SHCC and R/mortar specimens

Chemical analyses for determining the total and free chloride content in SHCC and mortar specimens as recommended by the RILEM TC178 were also performed. For this purpose a total of 30 samples from 6 different types of specimens were chosen for total chloride content testing. In the case of free chloride testing, a total of 42 samples from 8 different specimens were chosen. The outcomes on total and free chloride content are shown in Fig 7.35. It is also worth mentioning that all the samples which were used for chemical analysis were also first used for XRF as well. In all specimens the free chloride content was found to be lower than

Chloride Ingress and Reinforcement Corrosion in SHCC

the total chloride content. In Fig 7.36, a noticeably lower amount of free chloride was found in mortar specimens than SHCC. So it can be said that the presence of fibres in SHCC may cause a higher amount of free chloride in the matrix.

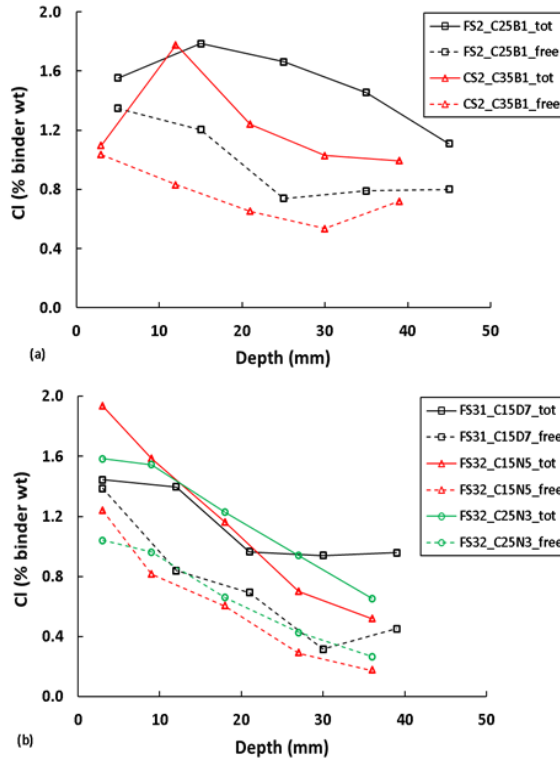


Figure 7.35: Chemical total and free chloride profile in different R/SHCC specimens.

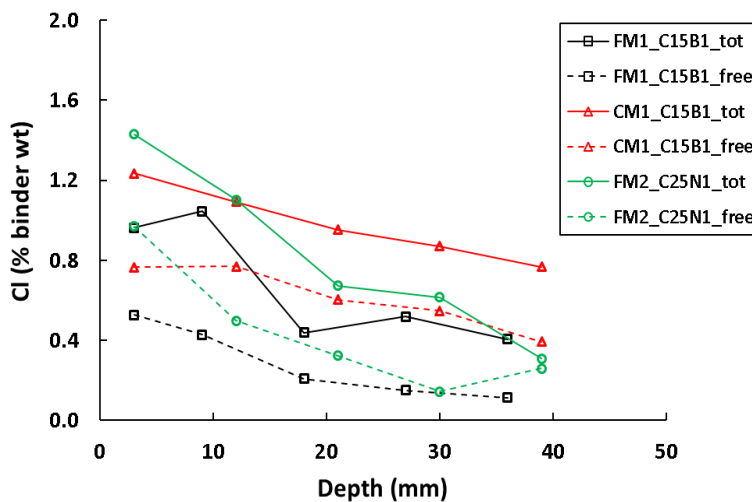


Figure 7.36: XRF total and chemical free chloride content in different R/mortar specimens.

7.3.5. Relationship among XRF and chemical total, free chloride and corrosion

In Chapter 5 the use of XRF for chloride analysis was discussed as it is the easiest way of determining the total chloride content in concrete and it is also less time consuming than

Chloride Ingress and Reinforcement Corrosion in SHCC

chemical analysis. However, the results obtained from XRF were also compared with the results obtained in chemical analysis. Fig 7.37 shows the relationship between total chloride obtained from both chemical and XRF analysis. A linear relationship was found between XRF and chemical total chloride content in the R/SHCC specimens. Linear relationships were also found amongst free chloride with the total chloride obtained from both XRF and chemical testing, as shown in Fig 7.38. From both Figs 7.37 & 7.38 it can be seen that the XRF analysis is a good alternative to chemical analysis for determining the chloride content in concrete.

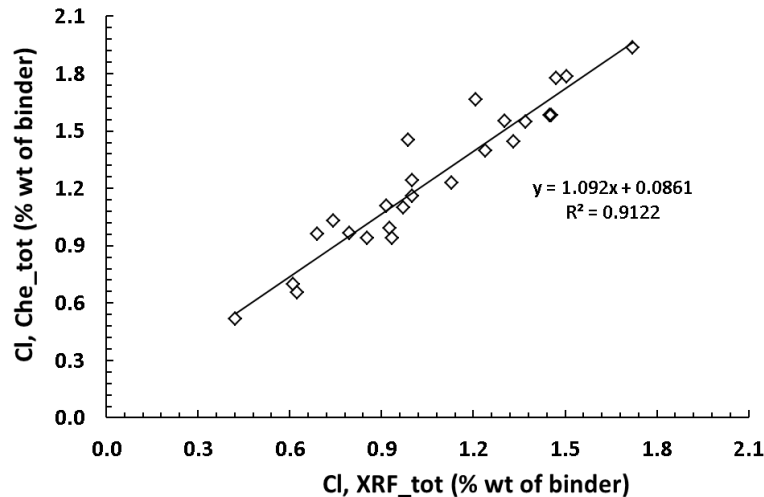


Figure 7.37: Chemical versus XRF total chloride content profile in R/SHCC specimens.

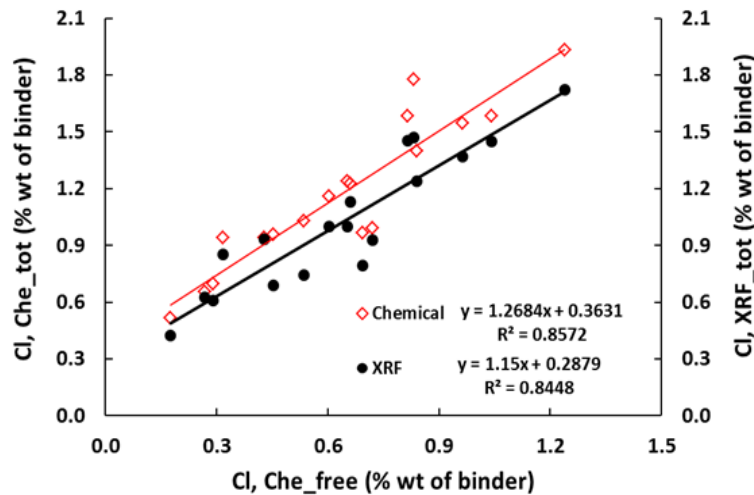


Figure 7.38: Total versus free chloride relationship in R/SHCC specimens.

Figs 7.39a-c show the different chloride profiles of R/SHCC specimens tested in this research. XRF and free chloride content analyses show a better consistency of reduced chloride content with respect to depth. Fig 7.39d shows the difference between the chemical total and free chloride analyses at different depths. It can be seen that the difference gets

Chloride Ingress and Reinforcement Corrosion in SHCC

larger deeper in the specimens, varying from about 40% at the surface to 70% at a depth of 30 mm - 35 mm.

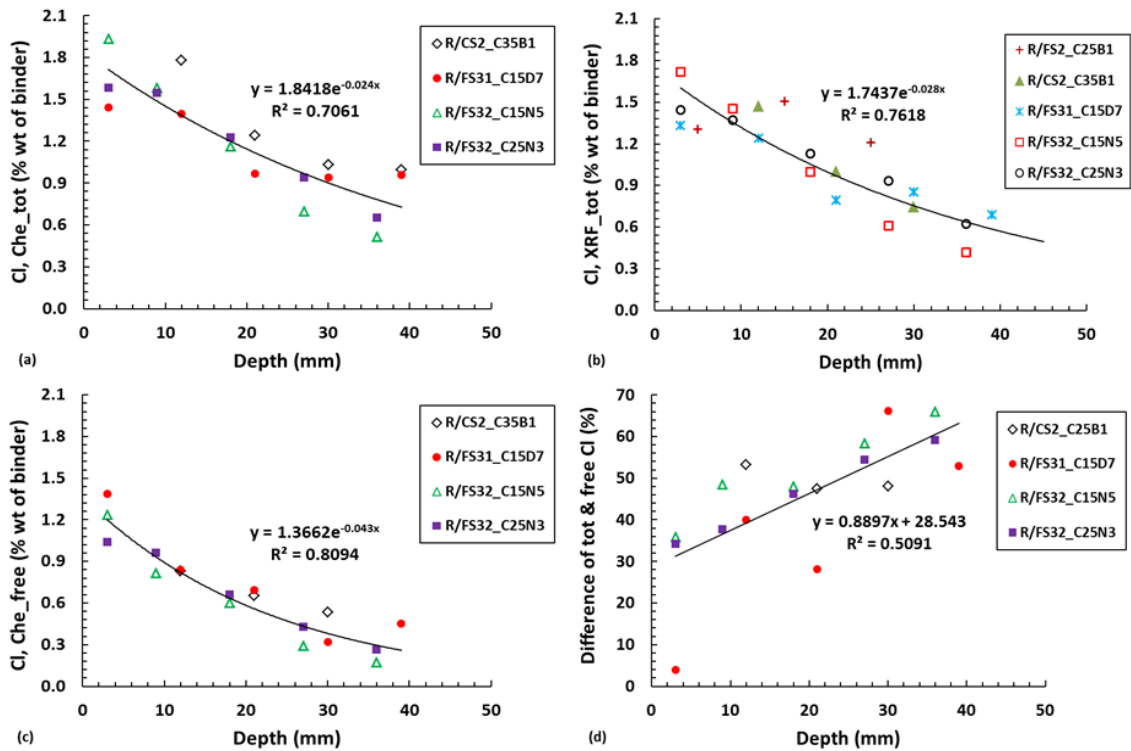


Figure 7.39: (a to c) Different chloride content profiles with respect to the cover depth and (d) the difference between total and free chloride at different depths.

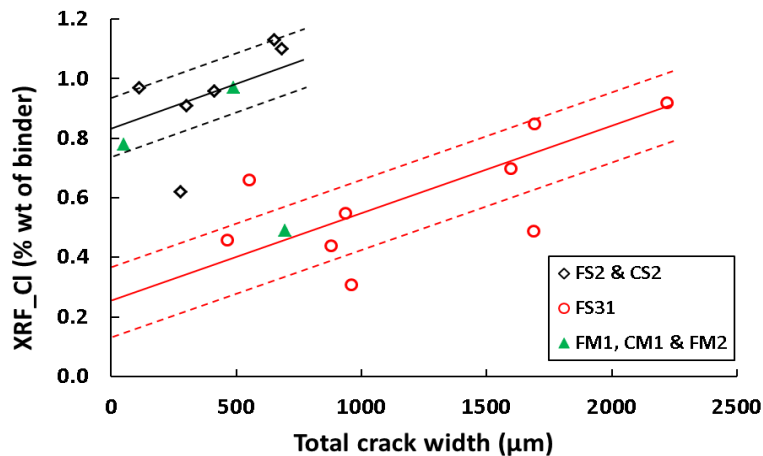


Figure 7.40: XRF chloride content versus total crack width relationship in different specimens.

Fig 7.40 shows the relationship between the total chloride content (obtained by XRF) and total crack widths in the different R/SHCC and R/mortar specimens. Higher chloride content was found as the total crack widths increased. Smaller total crack widths but longer

Chloride Ingress and Reinforcement Corrosion in SHCC

accelerated cycles of R/FS2 and R/CS2 specimens show a higher chloride content. A better correlation with the chloride content and crack width was found in FS31 specimens. Therefore it can be said that the chloride content in the cracked specimens is related to the total crack width. It is also clear that the chloride level is higher for a larger number of chloride exposure cycles (see Fig 7.41).

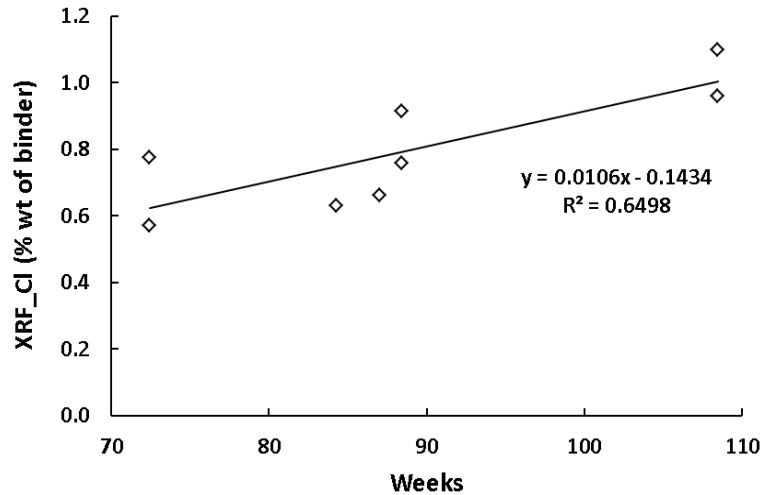


Figure 7.41: Influence of exposure period on the chloride content at the steel bar surface in the specimens in Series One.

Fig 7.42 shows a relationship existing between the corroded depths calculated with Eq (4.23) (which also represents the corrosion rate of the specimen) which is due to different total and free chloride contents at the surface of steel bars in the different R/SHCC specimens. Free chloride content was found to be the stronger feature correlated to the corrosion of the steel bars.

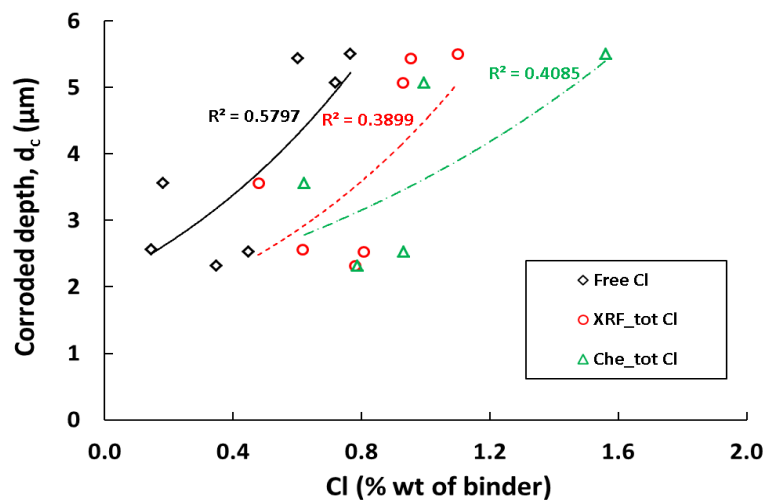


Figure 7.42: Corroded depths versus different chloride content relationship in R/SHCC specimens.

Chloride Ingress and Reinforcement Corrosion in SHCC

The difference between the total and free chloride in SHCC and mortar specimens for C15 is shown in Fig. 7.43. Note that the chloride contents shown here are the average chloride content in the specimens from the top surface to the bottom surface of each individual steel bar. For instance the chloride content in a C15 specimen steel bar was determined by taking the average XRF chloride value from a depth of 15 to 25 mm as reported in Figs. 7.33-7.35. A lower chloride content (both total and free) was found in the mortar specimens. The reason may be the larger total crack widths in SHCC. Multiple fine cracks were found in the SHCC specimens and the total crack width in SHCC specimens was higher than in the mortar specimens. Another reason is that when drillings were performed to collect the powder samples of the mortar specimen, only one crack was covered by the drill diameter (16 mm) while in SHCC 2 to 4 cracks were included. Also, the presence of fibre in the SHCC matrix forms, may provide paths for chloride ions.

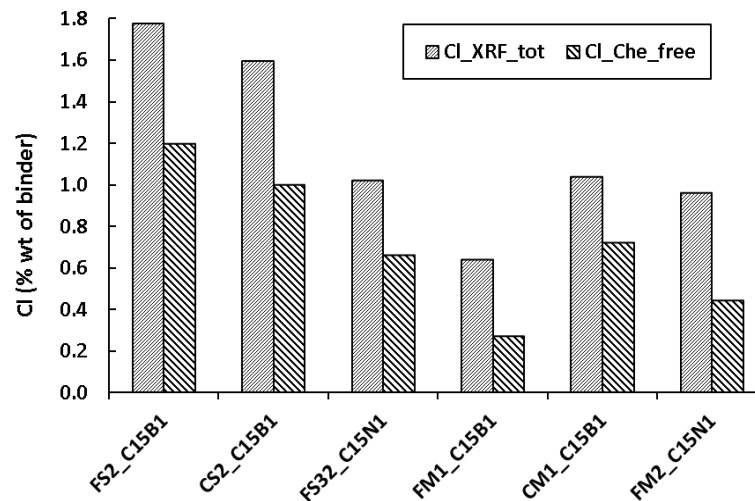


Figure 7.43: Comparison of chloride content at the level of the steel bar in the R/SHCC and R/mortar specimens.

7.3.6. RCM coefficient of SHCC and mortar

RCM testing was performed only in series four of FS4, FM3 and HM3. Fig 7.44 shows the chloride penetration depths in different specimens after RCM testing. Chloride penetration depths were calculated using AgNO_3 solution as described in Section 7.3.2.1. RCM coefficient (D_{cl}) and chloride penetration depth (X_d) in both FS4 and mortar are shown in Fig 7.45. The chloride penetration depth of each specimen reported on here is the average of 10 readings along the 100 mm width of the cylinder diameter as already described in chapter 5. HM3 was found to be much more prone in the RCM test than the two others materials used here. Therefore, in RCM tests, the higher strength of HM3 has no impact in lowering the chloride penetration depth. Even in SHCC, a little higher D_{cl} and X_d values were found than in FM3. It can be explained that the RCM test is a kind of accelerated test and it may depend on so many factors. For the same mix of concrete the presence of fibre may play an important role in chloride penetration which needs to be investigated in future research. More photos on

Chloride Ingress and Reinforcement Corrosion in SHCC

chloride penetration in the FS4, FM3 and HM3 specimens in Series Four are shown in the Appendix Fig C.16-C.17.

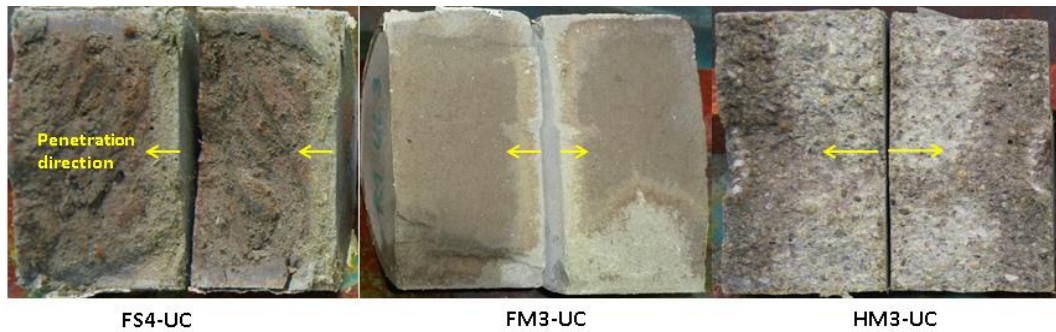


Figure 7.44: Chloride penetration during RCM test in un-cracked FS4, FM3 and HM3 specimens in Series Four.

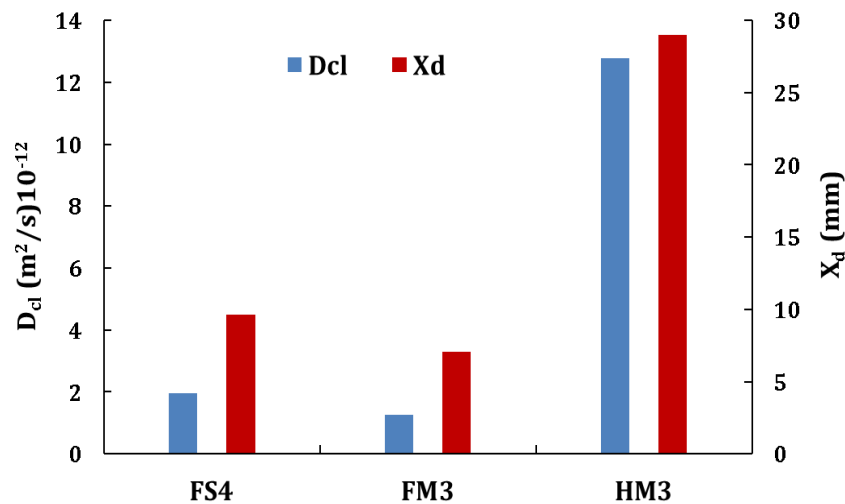


Figure 7.45: Diffusion coefficient (D_{cl}) and penetration depth (X_d) in un-cracked FS4, FM3 and HM3 specimens in Series Four.

7.4. Performance of SHCC against freeze and thaw attack

It is quite clear from Fig 7.46 that FS4 has a better performance against freeze-thaw attack than the two types of mortar concretes used in series four. After 42 cycles of freeze-thaw attacks, less than 0.35 kg/m^2 mass loss were found in FS4. On the other hand just after 7 cycles, significant mass losses were found in both mortar specimens and the loss in HM3 was very high compared to that of FM3. Scaled materials were evident at more than 5 mm depth from the surface of HM3 specimens. Therefore, the results indicate that the high strength of HM3 concrete does not mean that it is resistant enough against freeze-thaw attack. From RCM tests it was found that HM3 has a higher chloride penetration depth, which means it has higher permeability than other concretes and this high permeability means a very poor resistance against freeze-thaw cycles. On the other hand SHCC, with a slightly higher permeability than FM3, is still more stable due to the fact that fibres bridge the matrix and

Chloride Ingress and Reinforcement Corrosion in SHCC

increase the tensile force. Therefore, the tensile force generated by freezing of de-icing salt in concrete pores is not sufficient to create any damage in the specimen. Fig 7.47 shows the specimen's surface after 28 and 42 cycles of freeze-thaw attack and the excessively higher mass loss of HM3 specimens can also be observed from the figure.

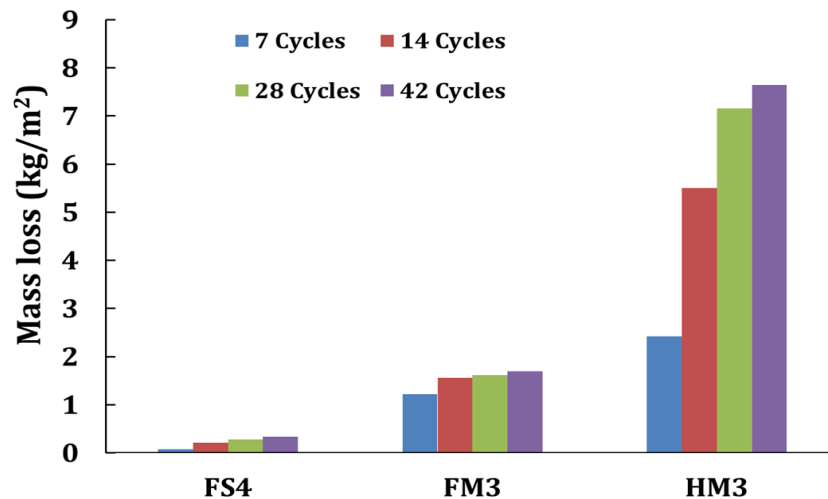


Figure 7.46: Mass loss of un-cracked FS4, FM3 and HM3 specimens in freeze-thaw test in Series Four.

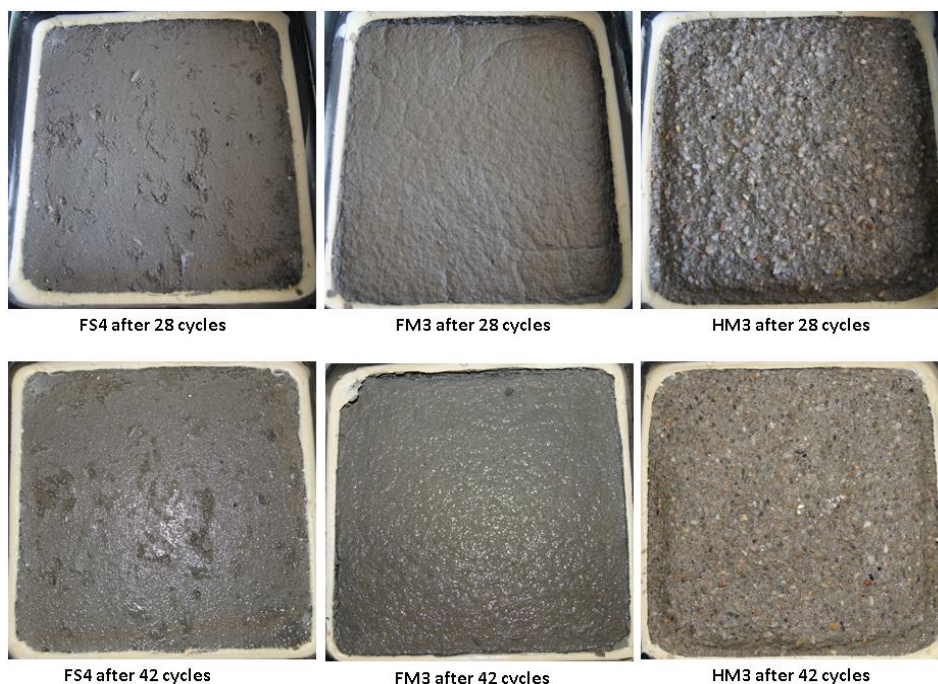


Figure 7.47: Mass loss from the freeze-thaw testing in the different specimens after 28 and 42 cycles in Series Four.

Chloride Ingress and Reinforcement Corrosion in SHCC

7.5. Capillary water absorption (CWA) in SHCC and mortar specimens

Much lower capillary water absorption (CWA) was found in HM3 than in FS4 and FM3 in series four as shown in Fig 7.48. The higher CWA values of FS4 and FM3 can be explained by the presence of a large amount of un-hydrated binder particles which may start hydration and reduce the water content much faster than HM3. It is also clear from Fig 7.49 that within 1 hour all FS4 and FM3 specimens were saturated by the water but no water was observed on the surface even after 14 days of CWA testing. On the other hand, after 11 days it was noted that all the HM3 specimens were saturated and water was also seen on the surface of one specimen. Although all the specimens were absorbing water for 14 days it can be seen from Fig 7.49 that after 1 day the rate of water absorption is not that significant. More photos on CWA are shown in the Appendix C, Fig C.18.

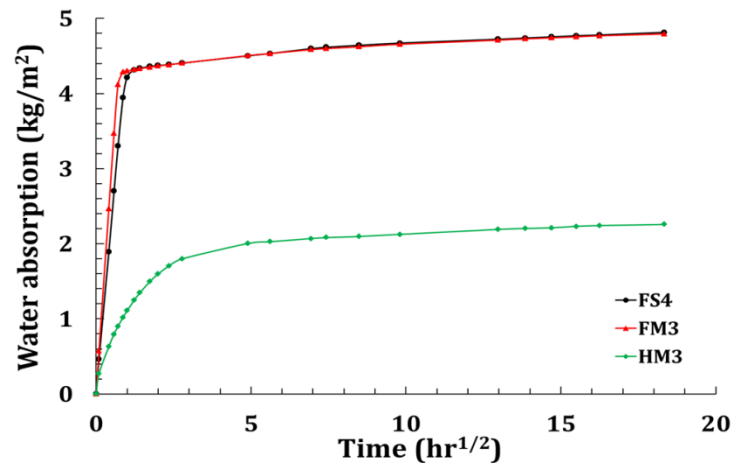


Figure 7.48: Capillary water absorption in un-cracked FS4, FM3 and HM3 specimens in Series Four.

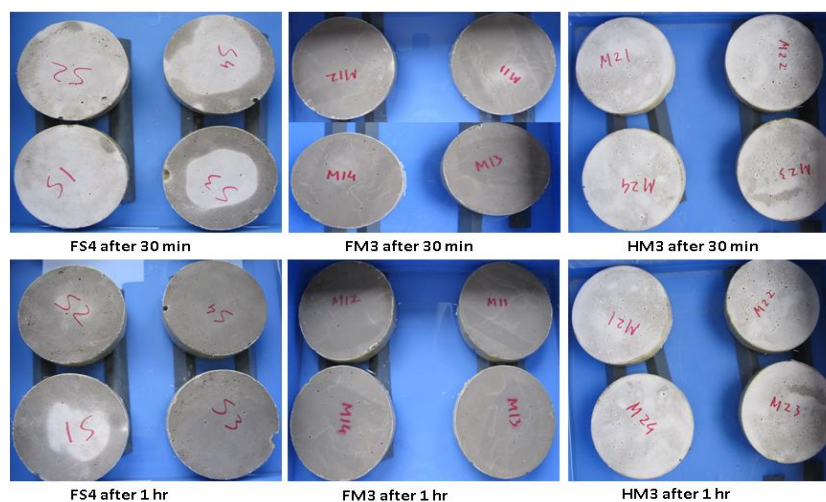


Figure 7.49: Water gains by different specimens during capillary absorption testing in Series Four.

7.6. Electrical resistivity (ER) in SHCC and mortar concrete

Fig 7.50 shows the electrical resistivity (ER) values of FS4 and two mortar types concretes used in the series four of this research. A higher ER value was found in FS4 and FM3 in both dry and wet conditions than in HM3. Very fine aggregate and more binder in FS4 and FM3 lead to fewer pores inside the matrix which may be the reason for a higher ER value than in HM3. Also the dense microstructure of concrete has higher resistance against current passing through it and this dense microstructure is often related to the materials composition, particles grading, compaction and curing, etc. Therefore, the ER value can be found different in different materials. The concrete resistivity is also related to the presence of moisture in concrete specimens which is quite clear from Fig 7.49. Lower ER values were found in all types of concrete in the wet stage. Due to the changes in the applied frequency from 100 Hz to 100 kHz, FS4 and FM3 show a significant reduction in resistance. On the other hand, this change was not that significant in the case of HM3 the specimens were nearly 100 day old and the influence of the high fly-ash content is significant for the higher resistances of FS4 and FM3.

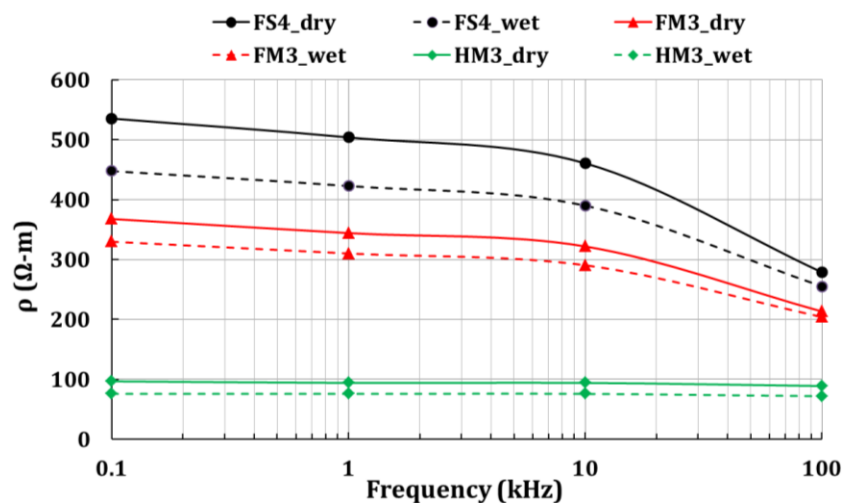


Figure 7.50: Electrical resistivity of un-cracked FS4, FM3 and HM3 specimens at different frequency in Series Four.

7.7. Concluding remarks

Improved mechanical behaviour of SHCC has already been proven by the researchers (Li *et al.* 2001, RILEM state of the art reports, van Zijl & Wittmann (*eds.*) 2011 and Paul & van Zijl, 2013, 2014) mentioned in this research work as has already been discussed in Chapter 6. In this chapter some of the major SHCC durability properties such as corrosion rate and chloride penetration are discussed. This research has focused on some important durability issues which can be very beneficial in designing RC structures using SHCC.

As was also reported by many researchers, there is no doubt about the difficulty of measuring the real corrosion rate of steel bars inside concrete because the actual active corroding area of

Chloride Ingress and Reinforcement Corrosion in SHCC

steel bars is mostly unknown. Potential measurement gives a mixed potential of active and passive areas as well as the possibility of checking whether depassivation has likely occurred. The results obtained in this research work on SHCC durability are also good incentives for using this material in a concrete structure in order to improve its durability. An example is the high strength of HM3, a typical preferred repair mortar material, but where a corrosion stain was found just after 60 days of accelerated chloride exposure, while the corrosion potential was low compared to that of FM3 and FS4. On the other hand there was no sign of a corrosion stain in FS4 and FM3 for the same exposure period but the corrosion potential was higher in these specimens. It was also observed that the corrosion potential values in the cracked reinforced specimens increased as the number of cracks and crack widths increased. Better correlation was found between the potential values with TCW than ACW and MCW in the specimens.

Corrosion rate measurements for cracked R/SHCC and R/mortar specimens were found to vary with time, most likely due to variations in the moisture content and temperature. However, when integrated to obtain corrosion depth, smooth corrosion curves were obtained which clearly indicate the different corrosion rates in different specimens. Corrosion damage was also confirmed by the removal of the steel bars from specimens after extended periods of accelerated exposure periods. In most cases discolorations in the steel bars do not really represent the true corrosion damage. After cleaning the steel bars with HCl, in most cases no major damage was noticed in the discoloration area. After 2 years of testing, the average pitting depths in the steel of R/FS2 and R/CS2 specimens were below 0.60 mm. A trend of an increase in the yield force loss of steel was found with average pitting depths of the steel bars.

For determining the total chloride content in concrete, XRF can be an alternative to doing chemical analyses as recommended by the RILEM TC, as XRF shows a very good correlation with the chemical analysis for total chloride content. However, a calibration should be done to compare the total chloride content obtained from XRF and relate it to the chemical analyses, in order to estimate the free chloride content, which is believed to be more relevant for actual corrosion. Chloride concentration in cracked specimens may be influenced by the crack geometry and the presence of pores adjacent to the crack. As a result a scattered chloride profile with respect to the depth can be found in the cracked specimen. Total chloride contents in the R/SHCC specimen are also influenced by the exposure periods. Longer exposure periods have been found to be the cause of a higher chloride content in the specimens.

Almost similar chloride diffusion coefficients were found in FS4 and FM3 and significantly higher in HM3, in the RCM testing. FS4 has significant resistance against freeze-thaw attack and electrical resistivity over FM3 and HM3. At the early stage of capillary water testing (within 6 hours) much higher water absorption was observed in FS4 and FM3 than in HM3 specimens. The water mass gain from 1 hour to 14 days in the different specimens of FS4, FM3 and HM3 was about 14%, 11% and 104% respectively.

7.8. References

- Arup, H 1983, Corrosion of reinforcement in concrete construction, Page et al (eds), The royal society of chemistry, London, UK, p: 151.
- Browne, RD, Geoghegan, MP & Baker, AF 1983, 'Analysis of structural condition from durability tests', Corrosion of Reinforcement in Concrete Construction, A.P. Crane, ed., Society of Chemical Industry, London, pp. 193-222.
- Choi, H, Kim, H, Seo, D & Kang, K 2003, 'The study on the capacity transform and alternative plan of reinforcing bar with straightening after bending', Journal of the Architectural Institute of Structural Systems , vol. 19, no. 9, pp. 181-188.
- Li, VC, Wang, S & Wu, C 2001, 'Tensile strain-hardening behaviour of polyvinyl alcohol engineered cementitious composite (PVA-ECC)', ACI Materials Journal, vol. 98, No. 6, pp. 483-492.
- Markeset, G & Myrdal, R 2008, 'Modelling of reinforcement corrosion in concrete', State of the art, COIN Project report no7, SINTEF Building and Infrastructure, ISBN 1891-1978.
- Maruya, T, Takeda, H, Horiguchi, K, Koyama, S & Hsu, KL, 2007, 'Simulation of steel corrosion in concrete based on the model of macro-cell corrosion circuit', Journal of Advanced Concrete Technology, vol. 5, no. 3, pp. 343-362.
- Montemor, MF, Simoes, AMP & Ferreira, MGS 2003, 'Chloride-induced corrosion on reinforcing steel: from the fundamental to the monitoring techniques', Cement & Concrete Composite, vol: 25, pp. 491-502.
- Paul, SC & van Zijl, GPAG 2013, 'Mechanically induced cracking behaviour in fine and coarse sand strain hardening cement based composites (SHCC) at different load levels', Journal of Advanced Concrete Technology, vol. 11 pp. 301-311.
- Rode, M & Wendler, D 1996, 'Methods for measuring moisture content in concrete', Concrete Repair Bulletin, March-April.
- van Zijl, GPAG & Paul, SC 2013, 'Crack spacing in steel bar reinforced strain hardening cement-based composites (R/SHCC), towards corrosion modelling', in proceeding of International Conference on Sustainable Construction Materials & Technologies (SCMT3), Kyoto, Japan.
- van Zijl, GPAG & Wittmann, FH 2011, 'Durability of strain-hardening fibre-reinforced cement-based composites (SHCC)', RILEM state of the art report, Springer Publications, ISBN-13: 978-94-007-0333-7.
- Wittmann, FH, Wang, P, Zhang, P, Zhao, Tie-Jun & Betzung, F 2011, 'Capillary absorption and chloride penetration in neat and water repellent SHCC under imposed strain', proceeding 2nd International RILEM Conference on Strain Hardening Cementitious Composites, pp.165-172. Brazil.

Chapter 8

I didn't fail the test. I just found 100 ways to do it wrong.

– Benjamin Franklin

Towards Corrosion Modelling of R/SHCC

8. Introduction

The modes of attack in RCS can be described by the adjacent environment, physical attack and chemical attack as shown in Fig 8.1. RCS through its whole service life experiences all these modes to some degree which ultimately leads to the durability problem. Therefore, it is necessary to take a step (or several steps) back from the detail of corrosion measurement in previous chapters, in order to give perspective for a design model. In fact, most durability problems occur in RCS due to their combined effects, and it is imperative that designers identify the particular deterioration mode or modes to which a particular structure will mostly be exposed during its life span, as designing for all possible modes may not be economical. Another important aspect is that all these attacks may not come at the same time in the structure's life. In this regard, a durability modelling approach is a helpful tool to minimise the influence of the different modes during the design life of RCS.

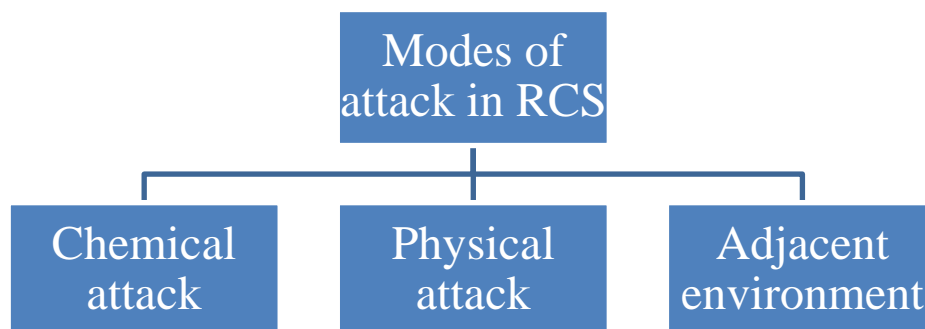


Figure 8.1: Typical modes of attack in reinforced concrete structures.

Long term experimental and field data are required to develop reliable models. Until now the data on SHCC is limited to both field and laboratory experimental testing. Currently there is no corrosion model for this new type of material and the existing corrosion models for NC are also criticized by researchers as designers sometimes overestimate or underestimate the actual corrosion in steel bars (Otieno *et al.* 2010). Corrosion indeed is a very complex mechanism and there is no direct way to determine the actual corrosion rate. As a result there are always some differences between experimental findings and the actual corrosion in a

Towards Corrosion Modelling of R/SHCC

structure. Since no information on corrosion status was found from real applications where SHCC was used, the experimental results obtained in this research were not validated against actual field performance. Also the accelerated exposure condition decided on needs to be compared with the real exposure conditions in different countries. Although EN 206 already classifies the estimated corrosion rate from various types of exposure conditions in RCS as shown in Table 8.1, it is still unknown how one cyclic wetting and drying exposure to 3.5% NaCl solution relates to real RCS exposure for service life design. Based on the results obtained in this research, some relationships have been developed which can be used to predict the strength loss of a steel bar after the corrosion starts. The author believes that this extensive research on the corrosion of SHCC is a first step towards future extensive corrosion modelling.

Table 8.1: Proposed estimated corrosion rate (V_{corr}) in steel bars at different exposure classes (EN 206)

Exposure name	Defined exposure conditions	Exposure conditions	Mean V_{corr} (mm/yr)
Carbonation	XC1	Dry	0
	XC2	Wet rarely dry (unsheltered)	0.004
	XC3	Moderate humidity (sheltered)	0.002
	XC4	Cyclic wet and dry (unsheltered)	0.005
Chloride	XD1	Wet rarely dry	0.004
	XD2	Cyclic wet and dry	0.03
	XS1	Airborne sea water	0.03
	XS2	Submerged	Not expected*
	XS3	Tidal zone	0.07

* Unless concrete is bad or cover depth is very low.

8.1. Background of the Study

Prediction models for chloride-induced corrosion generally assume uncracked concrete, while design standards generally limit crack widths. Cracks act as pathways for the ingress of chlorides, which de-passivate the protective local environment of steel in concrete, causing dissolution of iron into the pore water. Ingress of water and oxygen either in the crack, or through the cover concrete, forms the cathode of the chemo-electrical corrosion cell by the formation of hydroxyls in close vicinity of the anode in the crack zone or at passive steel further away in uncracked regions.

A vast pool of research data on RC corrosion has been developed over the past several decades, including the reduced density or increased volume of various corrosion products (FeO , Fe_3O_4 , $\text{Fe}(\text{OH})_3 \cdot 3\text{H}_2\text{O}$, etc.) (Liu & Weyers 1998), the time to corrosion cracking due to pressure build-up once the porous interfacial zone surrounding the steel is exceeded and also the role of crack width and spacing. It is generally agreed that the probability of corrosion is increased with increased crack width. This is strengthened by the results of Arya

Towards Corrosion Modelling of R/SHCC

& Ofori-Darko (1996) where artificially induced cracks (0, 1, 2, 4, 8, 12 and 20) were formed in the specimens but of equal total width (2.5 mm) over the same length of about 1300 mm. This means that the crack width (W_{cr}) and spacing (S_{cr}) varied from $W_{cr} = 0.125$ mm and $S_{cr} = 67$ mm in the case of 20 cracks, to a single crack with $W_{cr} = 2.5$ mm. The significant change in corrosion rate trend from the fast corroding specimens containing 16 cracks ($W_{cr} = 0.156$ mm, $S_{cr} = 84$ mm) to the low corroding rate in specimens with 20 cracks, is believed to indicate the importance of crack spacing, and the coinciding corrosion cell size. This motivates the investigation of crack width and spacing in R/SHCC in the next sections.

8.2. Existing modelling on corrosion

To date no corrosion modelling has been proposed or written about cracked SHCC specimens. The existing corrosion modelling on NC mainly focuses on the time to cracking due to corrosion in steel bars (Liu, 1996; Bazant, 1979) in uncracked concrete. Some empirical formulas were proposed to calculate the corrosion rate in steel bars (Alonso *et al.* 1988; Liu & Weyer, 1998; Scott, 2004). A study by Liu (1996) proposed a model for the time to first cracking in NC due to steel corrosion. His model is based on concrete cover depth, interface properties of steel/concrete, type of corrosion product, steel bar diameter, critical weight of rust product and corrosion rate. However, there is no information about the expected crack width which will cause the failure of the structure. Some of the existing corrosion modelling on NC is reported here.

In chloride-induced corrosion, Liu & Weyer (1998) proposed an empirical formula based on chloride-content, temperature, concrete resistivity and time of corrosion to calculate corrosion rate (i_{corr}) ($\mu\text{A}/\text{cm}^2$) in a steel bar as shown in Eq (8.1).

$$i_{corr} = 102.47 + 10.09 \ln(1.67Cl) - 39038.96(T^{-1}) - 0.0015R_c + 290.91t^{-0.215} \quad (8.1)$$

where, Cl is the chloride-content at the steel bar level (kg/m^3), T is the temperature at the steel bar surface (K), R_c is the concrete cover resistivity (Ω) and t is the period of measuring corrosion (yrs).

In carbonated concrete, based on concrete resistivity Alonso *et al.* (1988) proposed an empirical formula for predicting the corrosion rate (i_{corr}) in steel bars. The authors have considered many factors to calculate the corrosion rate as shown in Eqs (8.2) and (8.3). The main deficiency in this proposed modelling is that there is no consideration of cover depth, temperature, humidity and pH level in concrete. Even in Liu & Weyer formula Eq (8.1), the authors did not consider cover depth, humidity and pH in concrete.

$$i_{corr} = \frac{k_{cpr}}{\rho_t} F_{cl} F_{Galv} F_{Oxide} F_{Oxy} \quad (8.2)$$

Towards Corrosion Modelling of R/SHCC

$$\rho(t) = \rho_o f_e f_t \left(\frac{t}{t_o} \right)^n \quad (8.3)$$

where, k_{cpr} is a constant regression parameter (10^4). F_{cl} , F_{Galv} , F_{oxide} and F_{Oxy} are factors due to chloride content in concrete, galvanic effects, ageing and formation of oxides during the corrosion process and oxygen availability in concrete, $\rho(t)$ and ρ_o are the concrete resistivity ($\Omega\text{-m}$) at times t and t_o respectively. n is an ageing factor on resistivity of concrete. f_e is an environmental factor which also influences resistivity of concrete. f_t is a factor which depends on the type of concrete resistivity test.

In a recent study by Scott (2004) on corrosion in different binder contents and cracked concrete the author proposes an empirical formula to predict the corrosion rate (i_{corr}) in steel bars. The NC specimens made with various percentages of binder were cracked up to 0.2 and 0.7 mm wide in two different cover depths of concrete. The proposed corrosion rate formula is shown in Eq (8.4).

$$i_{corr} = \left(1.43 \frac{C_c}{f} + 0.02 \right) e^{\left[\left(\frac{40-x}{20} \right) 1.2 \left(\frac{C_c}{f} \right)^3 \right]} \quad (8.4)$$

where, f is a factor dependent on slag content, C_c is the chloride conductivity index value (mS/cm) at 90 days and x is the concrete cover depth (mm).

The main problem with Scott's model is that there is no consideration of concrete crack widths, temperature and resistivity as being important service life prediction model parameters. None of the corrosion models (Eqs 8.1 – 8.4) consider the chloride conductivity of concrete. This is considered to be because it does not really give any indication of corrosion. The amount of total and/or free chloride and availability of oxygen are most probably the dominating parameters for corrosion.

It is clear from the above proposed models that different parameters are considered in the corrosion models proposed thus far. As a result, the results obtained from these corrosion models vary significantly. Also, in most corrosion models it is assumed that the rate of corrosion is consistent with time. However in reality corrosion may not increase constantly with time since the adjacent exposure condition of a concrete structure varies and as a result the corrosion rate can also drop from a higher to lower value as was shown in Figs 7.11-7.16 in Chapter 7. The corrosion rate in high and low humidity is not the same, which is often neglected in corrosion modelling. It is a difficult task to establish how the exposure level influences the rate of corrosion in steel bar with time and no research was found on this issue to date.

8.3. Factors involved in the error of corrosion prediction

Corrosion in a steel bar reduces the cross-sectional area and thereby the strength and introduces pressure in the concrete adjacent to the steel bar, since the volume of the corrosion products is higher than that of the corroding iron (Papadakis, 2005). Typically, corrosion current is caused by the potential difference between the anode and cathode areas, causing movement of electrons from one area to the other. Many factors such as temperature, pH, availability of oxygen in the cathodic area and chloride in the anodic area can influence this corrosion current. Although in this research work the influence of these factors is not investigated directly due to the vast amount of research already carried out to quantify the influence of each variable, it is important to keep these factors in mind in the interpretation of the current results and the improvement of current corrosion modelling in future. Some of these factors are briefly discussed below:

Temperature: The chemical corrosion process in steel is directly related to the temperature. It is believed that with an increase of 10°C in the temperature of concrete, the chemical reaction in the corrosion rate doubles. However, when the temperature reaches beyond 40°C, the solubility of oxygen decreases and as a result the corrosion rate also reduces (Mareset & Myrdal, 2008). Therefore, if the temperature at the steel surface is not measured simultaneously with that of concrete, an error might arise in the reported corrosion rate.

pH: The pH of concrete is very important in carbonation induced corrosion. Typically a lower pH in concrete increases the corrosion cell potential and increases the rate of the current passing between the anode and the cathode area, causing an increased corrosion rate. In chloride-induced corrosion, a higher corrosion rate can be caused by increased dissolution of bound chloride in the concrete matrix due to a decrease in the pH of the concrete (Mareset & Myrdal, 2008).

Oxygen: Sufficient oxygen and water must always be present at the cathode to ensure that the reaction (shown in Fig. 4.4) continues. In dry concrete, the electrolytic process is blocked and no corrosion can occur. Similarly, in wet concrete, the corrosion process will be insignificant due to lack of oxygen even in the presence of a high chloride content at the steel surface. The highest corrosion rate will take place in the concrete surface layers exposed to greatly altering drying and wetting states (Papadakis, 2005). In concrete, a relative humidity (RH) of up to 95% does not confine the oxygen supply that much, while at 100% RH the starvation of oxygen is significant (Mareset & Myrdal, 2008).

C₃A: Depending on the types of cement, the amount of C₃A may vary significantly. Chloride ions in reaction with C₃A (in concrete) form Friedel's salt (also called bound chloride). Depending on the cementitious materials' composition and content, the bound chloride percentage varies in the range 30%-60% (by cement wt). It is believed that if the pH of concrete remains high (above 12.5), the bound chloride will remain bound or harmless and

Towards Corrosion Modelling of R/SHCC

does not participate in the corrosion process. So the percentage of C_3A content in the cement is also an important parameter and should be considered in the prediction of corrosion rate modelling.

Resistivity: In lower resistivity concrete the transport of moisture, oxygen, CO_2 , etc. becomes easier and the possibility of corrosion or the corrosion rate may be increased. This concrete also favours the migration of ions between the anode and cathode parts of the corroded steel. As a result, in a large cathode/anode area of steel, lower resistivity also helps in developing the corrosion pits. More ions from the large cathodic area will easily migrate to the anodic area and create large pitting depths in a small anode area (Broomfield, 2007). The moisture content in the concrete pores reduces the concrete resistivity and therefore in corrosion modelling, concrete resistivity should be considered.

The aforementioned parameters are inter-dependent. For example, the resistivity of concrete changes as the moisture content in the concrete changes (see Fig 7.50) which moisture content is also depended on temperature and humidity. Similarly, pH and oxygen levels in concrete are also related to the moisture and temperature. Therefore, it is indeed a complex task to consider all these effects and as a result, they are often neglected by researchers in their proposed corrosion modelling. Apart from these factors some others such as cover depth, water binder ratio, aggregate binder ratio, types of steel bars, bar diameter, cracks in the concrete, volume of pores in the concrete, etc. also have significant influence on the corrosion rate.

8.4. Towards the modelling of corrosion in R/SHCC

Due to limited corrosion data on SHCC, the validation of the results is indeed a difficult task and more research is needed in this regard. Long term laboratory and field data are necessary to validate any corrosion model for this new material. The data sets generated during this research project are used to develop a model, which is compared with the existing chloride-induced corrosion data obtained from the numerical analysis in NC as discussed in section 8.4.5. Further research towards increasing the pool of data on these materials, especially field performance data for validation, is clearly required and will enable improvement of corrosion models. One important note is that all the crack widths reported on in this research are the surface crack widths of reinforced and unreinforced specimens. Having reported on full chloride profiles in Chapter 7, where the chloride content at the surface level of the steel bars is considered towards developing a corrosion model.

8.4.1. Influence of cracks in R/SHCC

The influence of cracks on chloride penetration and corrosion in SHCC and mortar is reported on in Chapter 7, where correlations in the reported results are studied to form a corrosion modelling approach.

Towards Corrosion Modelling of R/SHCC

8.4.1.1. Cracks and corrosion in R/SHCC

The influence of average crack widths (ACW) and crack spacing on the corroded depths of R/FS31 specimens after 57 weeks of accelerated testing is shown in Figs 8.2a&b. For the ACW it appears that crack width has an influence on corroded depth as calculated from Eq (4.23) and as shown in Fig 8.2a. Similarly, higher spacing differences in the corroded depths were also noticed in these specimens. It must be kept in mind that the results reported on in Figs 8.2a&b are for the different cover depths of R/FS31 specimens. Therefore the influence of cover depths on the corroded depths is not considered here and as a result the influence of crack widths and crack spacing on corroded depth may not be clear. The influence of cover depth combined with crack width and spacing is discussed later in this chapter.

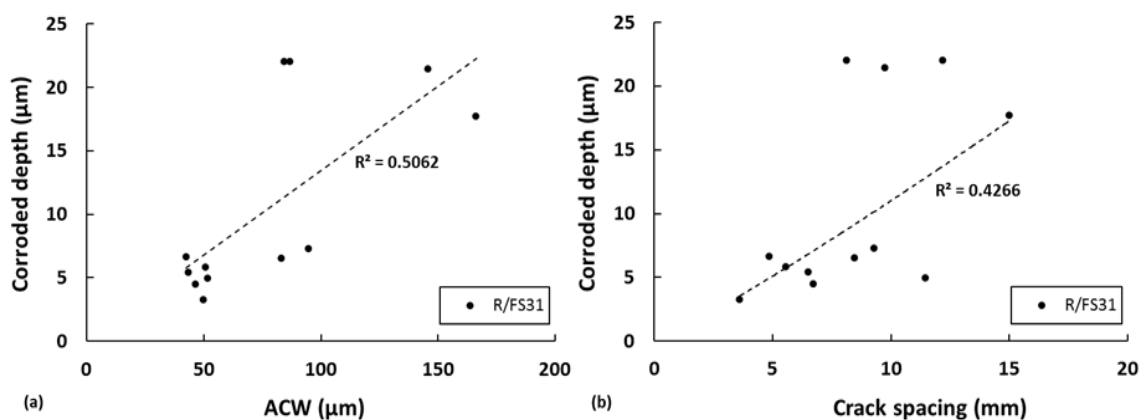


Figure 8.2: Influence of crack widths and spacing on corroded depths in R/FS31 specimens after 57 weeks of exposure.

The corrosion pitting depths in the individual steel bars were found to be lower for a larger number of cracks in the R/SHCC specimens, as shown in Fig 8.3a&b. It can be explained by the fact that when the number of cracks increases in the specimen over a given length, the crack spacing and thus the cathodic area reduces relative to the anodic area. Thereby less OH^- ions are available from the smaller cathodic area to react with the Fe^+ in the anodic area. In this case corrosion is also distributed over the lengths of steel bars and it is expected to have distributed pitting (see in Figs 7.19 & 7.20) rather than concentrated corrosion (see Fig 7.21).

The influence of TCW and crack spacing on the corrosion pitting depths in steel bars was also studied. It was found that TCW below 1 mm shows a trend of reduced pitting depths as the crack widths increase as shown in Fig 8.4a. In larger TCW (> 1 mm) of R/FS31 specimens this trend is not significant as seen in Fig 8.4b. It might be explained by the formation of micro-cell corrosion in the steel bar due to a higher number of cracks and thus closer crack spacing which led to distributed corrosion. Note that for pitting depth as a function of TCW, it appears that it may actually be the number (or spacing) of cracks that are important. A larger number of cracks seem to have a higher TCW and thus lead to lower pitting depth (Figs 8.3a & 8.4a). A trend of increased pitting depths was also found for larger

Towards Corrosion Modelling of R/SHCC

crack spacing in the R/SHCC specimens as shown in Fig 8.5a&b. Typically in the steel bars, more severe pitting depths can be found due to macro-cell corrosion than due to micro-cell corrosion (Broomfield, 2007). This postulation was also verified by measuring the pitting area in the steel bars as shown in Fig 8.6. After cleaning the steel bars with HCL the pitting area was also calculated. In this case pitting areas were marked on the steel surface as circular, rectangular and trapezoidal shapes. A Vernier scale was then used to accurately measure the marked areas in order to calculate the total pitting area on the surface of each steel bar. It is quite clear from Fig 8.6 that a higher number of cracks in the specimens causes a lower pitting area.

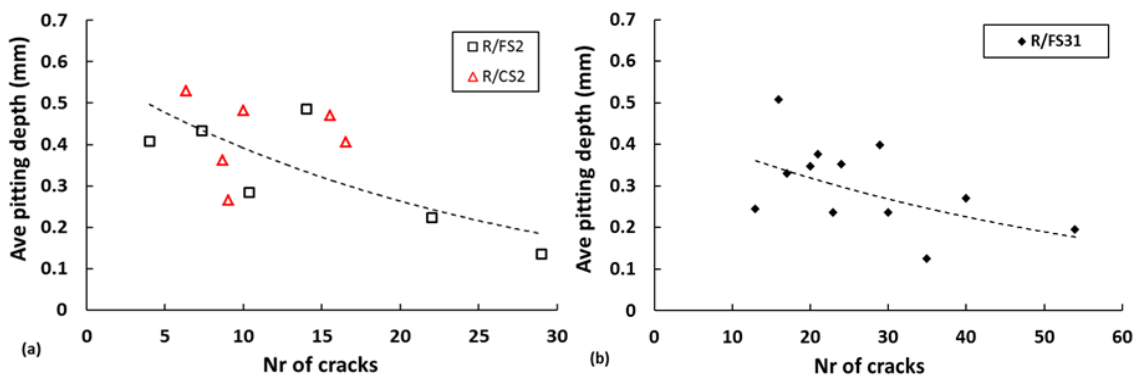


Figure 8.3: Pitting depths with different numbers of cracks in R/SHCC specimens at the end of their exposure period.

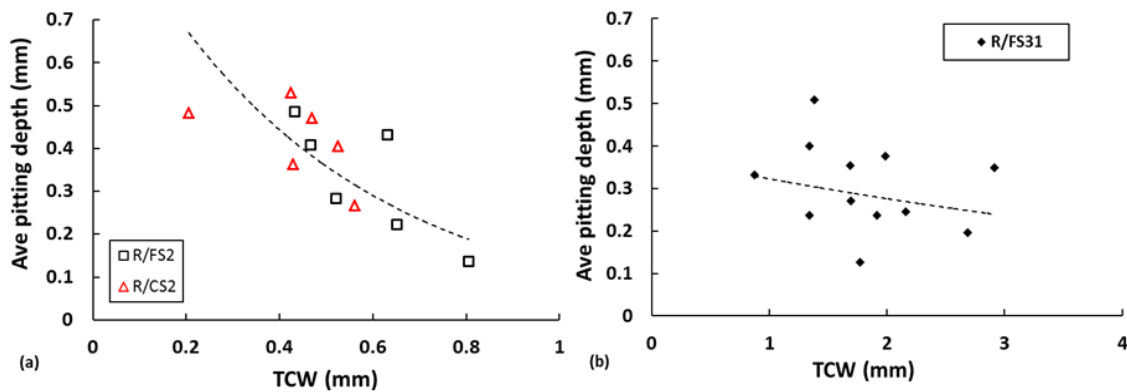


Figure 8.4: Pitting depths versus total crack widths (TCW) in R/SHCC specimens at the end of their exposures period.

The influence of TCW on the steel pitting diameter at the crack locations of the corroded steel bars in NC was also examined by Mohammed *et al.* (2001) as shown in Fig 8.7. The details of NC specimens are discussed in the section 8.5. After breaking the NC specimen the pitting diameter in the corroded steel bars was measured by a microscope at the location of known crack widths. A trend of lower pitting diameters was found in the steel bars for larger

Towards Corrosion Modelling of R/SHCC

crack widths as shown in Fig 8.7. Therefore, it can be said that in the corrosion damage of steel bars, the number of cracks, TCW and crack spacing are related.

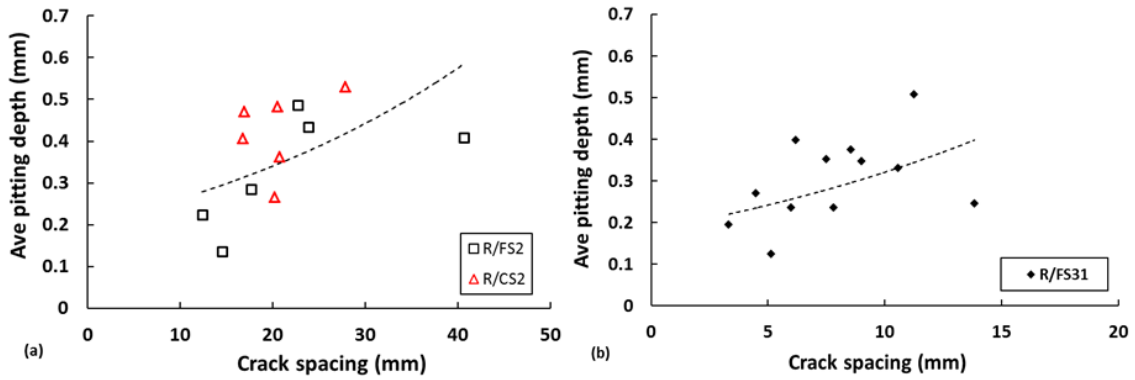


Figure 8.5: Relationship between pitting depths and crack spacing in R/SHCC specimens at the end of their exposures period.

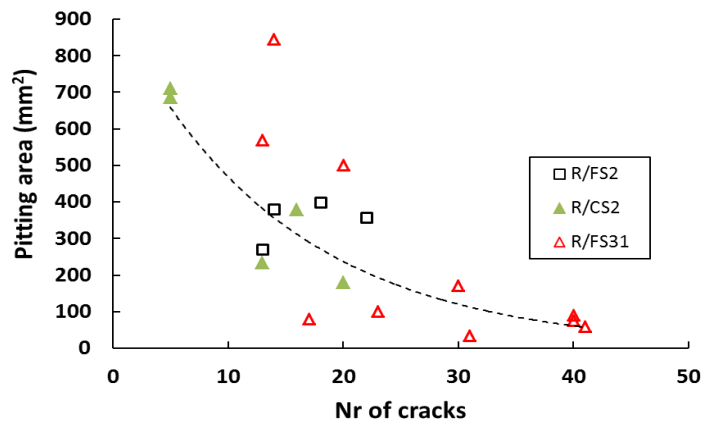


Figure 8.6: Pitting area in steel due to different number of cracks in the R/SHCC specimens.

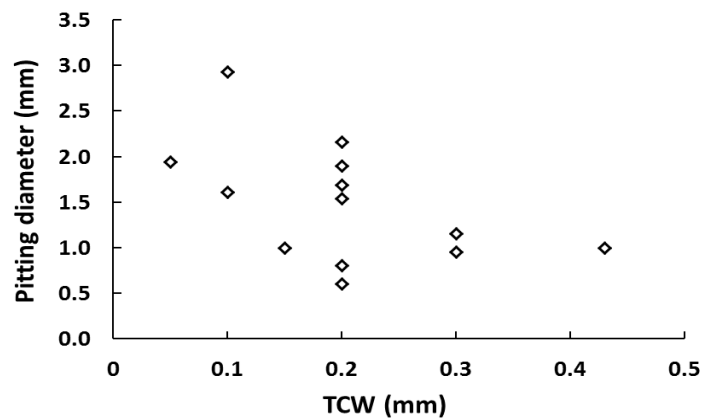


Figure 8.7: Pitting diameter in steel due to different crack widths in NC (reproduced from Mohammed *et al.* 2001).

Towards Corrosion Modelling of R/SHCC

8.4.1.2. Cracks and chloride in R/SHCC

The influence of crack widths (both ACW and TCW) on chloride penetration was also observed in R/SHCC, as shown in Figs 8.8 & 8.9. No relationship was found between crack and chloride for ACW below 0.05 mm in Fig 8.8a. In Fig 8.8b, it appears that the total chloride increases as ACW increases from 0.03 - 0.16 mm. It must be added that the total exposure time of the specimens in Figs 8.8a & 8.9a was 108 weeks, i.e. near double the exposure time of those specimens shown in Figs 8.8b & 8.9b. Therefore, the influence of crack widths in the figures (a) might diminish through gradual chloride ingress into the matrix from the crack faces subsequent to quick ingress into the cracks. From Fig 8.8b it appears as if a threshold crack width exists (0.03 – 0.05 mm), below which the chloride content is low and relatively constant, but above which width the total chloride penetration becomes more significant in the cracked R/SHCC specimens. Water permeability testing in SHCC and steel mesh mortar conducted by Lepech & Li (2005) found a similar trend at a crack width in the range 0.05 – 0.1 mm, beyond which water permeability increased rapidly. Therefore, it appears that the number of cracks and crack widths play an important role in the penetration of chloride and water in cracked SHCC. In the case of TCW, a linear upward trend is apparent between the TCW and chloride content when the TCW is more than 0.80 mm. However, it must be kept in mind that the chloride content shown represents that in a few cracks only, keeping in mind the drilling method to collect powder samples for chloride content testing.

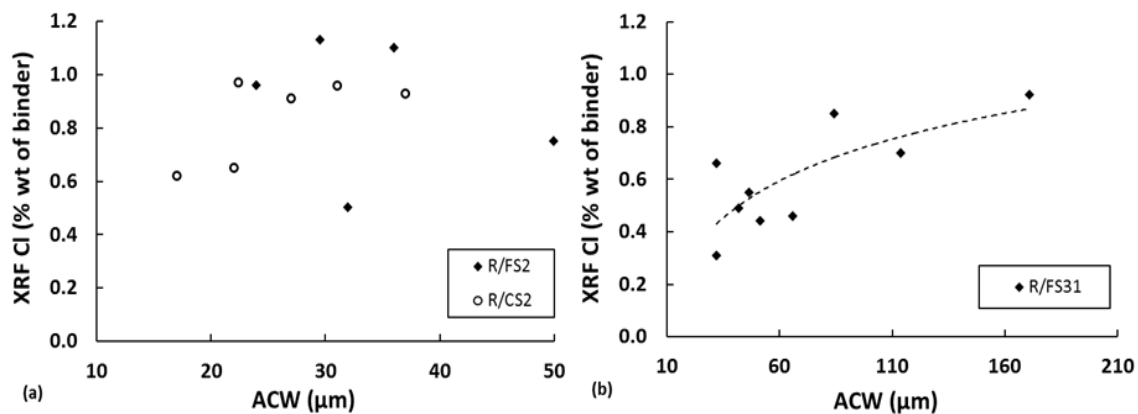


Figure 8.8: XRF total chloride (Cl) and average crack widths (ACW) relationship in R/SHCC specimens after (a) 108 weeks and (b) 57 weeks of chloride exposure.

8.4.2. Influence of cover depths in corrosion of R/SHCC

The cover depths of steel bars inside concrete play an important role in RCS durability since the possibilities of corrosion in steel near the exposed surface is higher. Depending on the importance of the structure (residential, commercial, public, etc.), the location of the structure and the types of structural elements such as columns, beams, slabs, etc. the cover depths are typically defined by design codes such as ACI: 318-11, EN 1992 (EC2), BS: 8110.

Towards Corrosion Modelling of R/SHCC

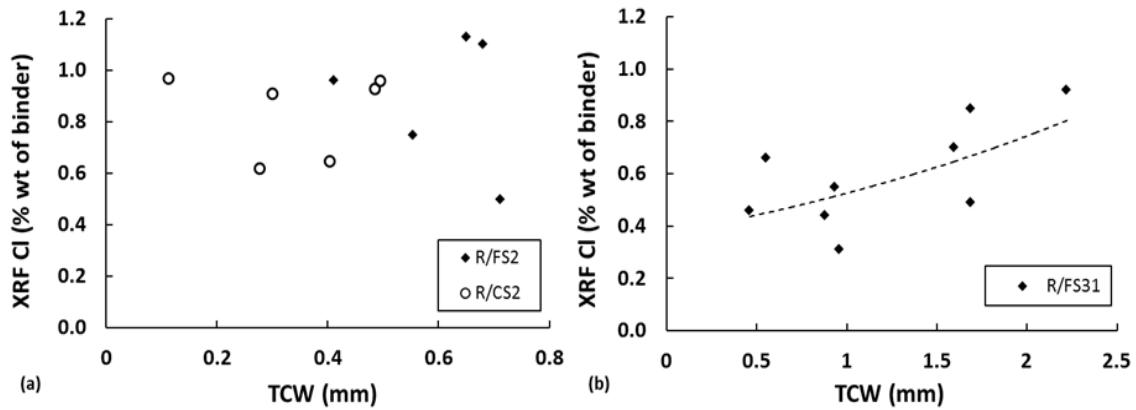


Figure 8.9: XRF total chloride (Cl) and total crack widths (TCW) relationship in R/SHCC specimens after (a) 108 weeks and (b) 57 weeks of chloride exposure.

Fig 8.10 gives further information on total (XRF) chloride content at different cover depths of the R/SHCC specimens in series one and two. Shorter exposure periods of R/FS31 specimens showed a lower total chloride content at different cover depths. For the same exposure period but a lower level of deformation (5 mm, as opposed to those deflected to 7 mm) in the R/FS31 specimens, they were found to have a lower amount of chloride.

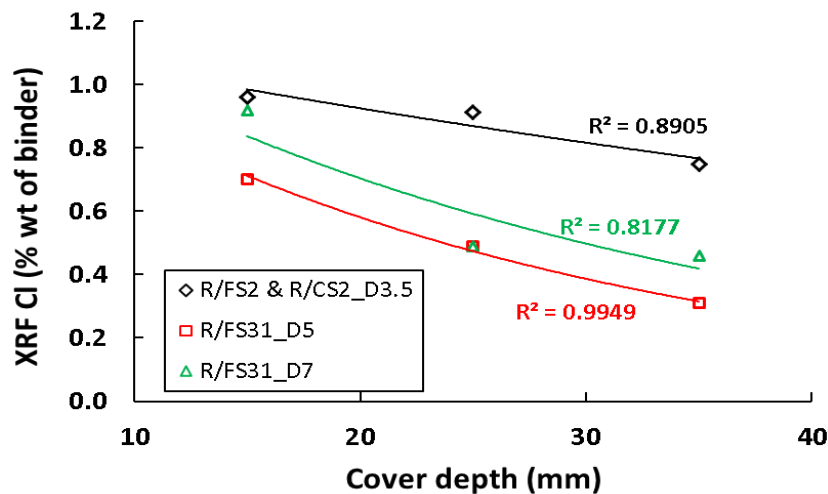


Figure 8.10: XRF total chloride (Cl) at the cover depths on R/SHCC specimens.

The corrosion is also influenced by the cover depths of the specimens. Typically, higher corrosion rate/corrosion depth can be found for lower cover depths of specimens. It is because the shorter distance between the exposed concrete surface and the steel bar allows chloride, oxygen and water to reach the steel sooner. The phenomenon was also shown in this research for chloride penetration in Fig 8.10. Otieno *et al.* (2010) suggested that in cracked concrete it is preferable to consider the cover depths' effect rather than reporting the surface crack widths alone. In Fig 8.11a-c, a threshold cover depth of about 25 mm is apparent and

Towards Corrosion Modelling of R/SHCC

below this the corroded depths increased as the ACW / cover depths ($W_{cr,ave} / C$), TCW / cover depths ($W_{cr,tot} / C$) and the cracks spacing / cover depths (S_{cr} / C) of the specimens increased. Recall that in the same specimens the trend was different and clear in Figs 8.2a&b without considering the cover depths. Therefore, for the interpretation of corrosion rate and cracks the influence of cover depth must also be considered. Also note that the trend lines shown in Fig 8.11 were drawn manually. Similar trends were also observed in R/FS2, R/CS2 and R/FS32 which are not shown here since they represent different exposure periods and exposure conditions (ponding, versus capillary absorption).

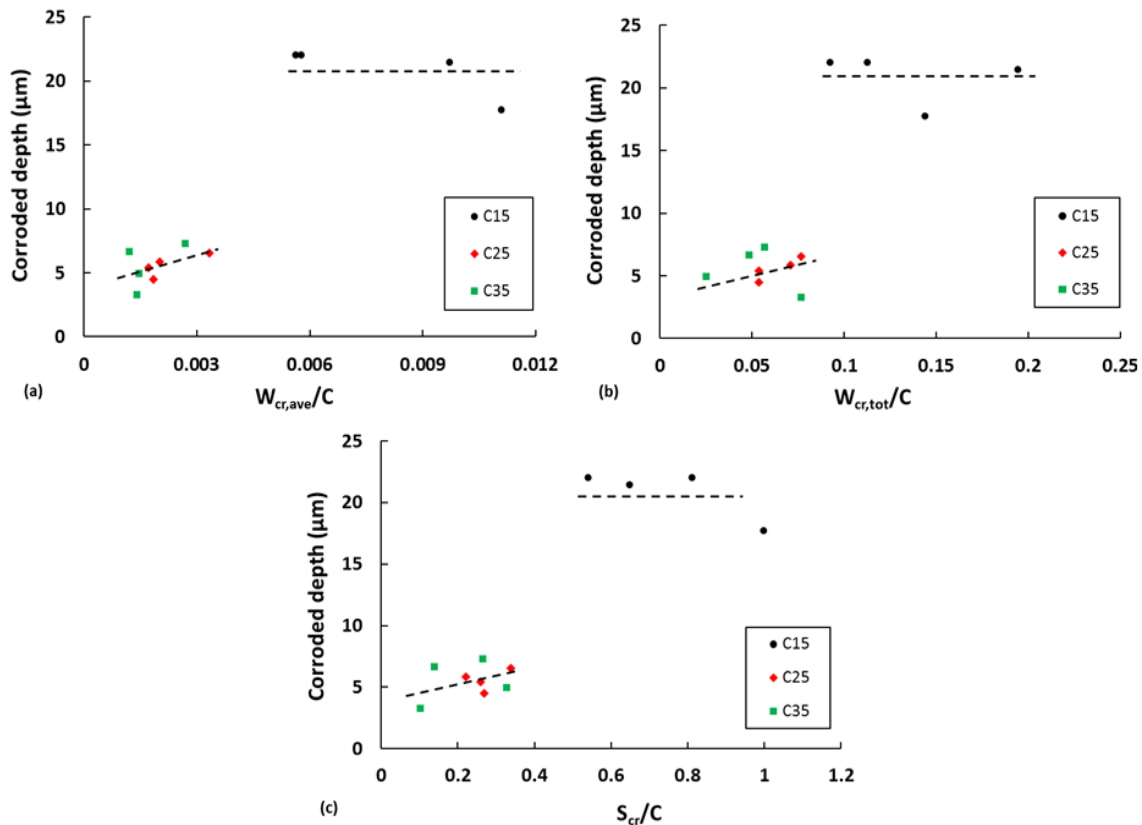


Figure 8.11: Relationship between the corroded depths calculated from corrosion rate readings by Eqs. (4.22 & 4.23) and cover depths (a) average crack widths/cover depth ($W_{cr,ave} / C$) (b) total crack widths/cover depth ($W_{cr,tot} / C$) and (c) crack spacing/cover depth (S_{cr} / C) in R/FS31 specimens at 57 weeks of exposures periods.

8.4.3. Consequences of chloride and corrosion of steel bars in R/SHCC

Because of corrosion, the mechanical behaviours such as strength and ductility of a steel bar changes due to the change in cross section, and ultimately the steel bar loses its design properties. So in designing the RCS, the designer must take into consideration the influence of corrosion in steel bars and its consequences on the structure's service life design period. Some of the parameters that influence the steel bar properties when corrosion takes place are discussed here.

Towards Corrosion Modelling of R/SHCC

The actual mass loss (after 28 weeks of exposure) of steel due to corrosion is also compared with the corroded depths and actual loss of yield forces in the steel bars of R/FS32 & R/FM2 specimens as shown in Figs 8.12 & 8.13. The values reported in these figures are the average values of three R/FS32 and two R/FM2 specimens respectively. The corroded depths and the loss of yield force are higher for higher mass loss in the steel bars. The measured corroded depths by the Coulostatic method and actual mass in the steel bars due to corrosion were found to be related to each other as shown in Fig 8.12. This phenomenon is to be expected, as corrosion-induced loss of steel bar cross section must lead directly to mass loss. Therefore, it can be said that the corrosion results obtained in this research using the Coulostatic method is relevant to the real corrosion in the steel bar.

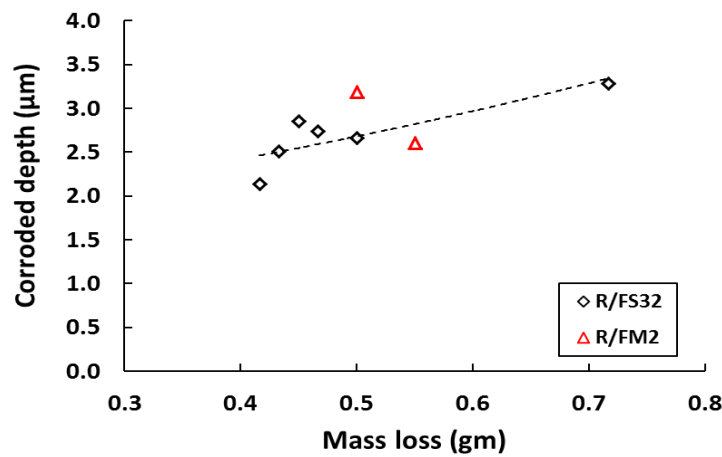


Figure 8.12: Corroded depths and actual mass loss of steel in the specimens in Series Three.

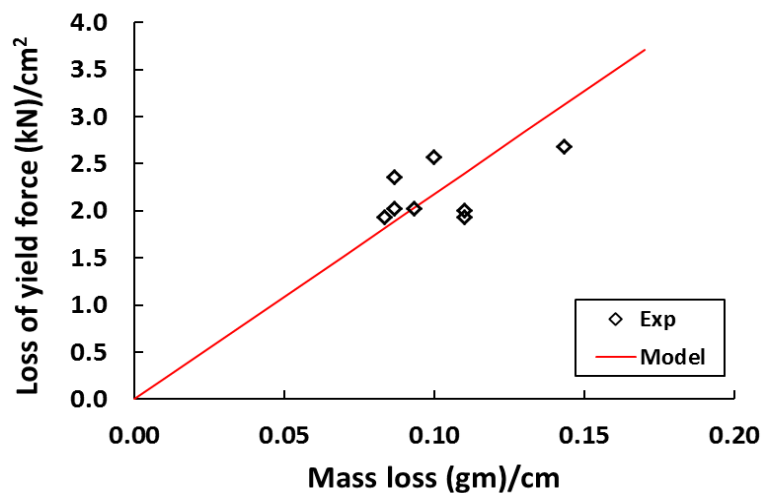


Figure 8.13: Relationship between loss of yield force and actual mass loss in the specimens in Series Three.

Eqs (8.5) & (8.6) were used to derive an empirical equation (Eq 8.7) for predicting the loss of yield force per unit area due to the mass loss per unit length of steel bar. The results obtained

Towards Corrosion Modelling of R/SHCC

from the empirical equation (model) are plotted in Fig 8.13 using the experimental data. It was found that the loss of yield force is linearly increased as the mass loss of steel bar increases.

Proposed equations for yield force loss due to mass loss in a steel bar

$$m_1 = \rho_s A_s \quad (8.5)$$

$$A_r = \frac{A_s m_2}{m_1} \quad (8.6)$$

$$Y_{loss} = \frac{1}{k} \sigma_y A_r \quad (8.7)$$

where, m_1 is the mass of steel per unit length (gm/cm), ρ_s is the density of steel (gm/cm³), A_s is the cross section area of steel (cm²), g is gravitational acceleration (9.81), A_r is the steel reduced area due to corrosion (cm²), m_2 is the corrosion mass loss per unit length (gm/cm), Y_{loss} is the loss of yield force per unit area (kN/cm²), σ_y is the yield strength of steel (MPa) and k is a factor which depends on the specimens' testing age, specimen types, etc. In this case a value of k equal to be 2.8 produces the shown agreement with the experimental data points, but this value may need to be calibrated for other specimen types, ages and loading rate of tensile testing of steel bar.

Corrosion mass loss per unit length (m_2) was calculated from the total mass loss of steel divided by the pitting length in the steel bars. In this particular type of R/FS32 the average pitting length in the steel bars was found to be about 50 mm after 28 weeks of accelerated testing.

The author believes that the mass loss of steel is related to its section loss which influences the resisting force of a steel bar directly. It was assumed that the mass loss of a steel bar is linearly proportional to the loss of yield force of steel and based on this consideration the author developed the Eqs. 8.5-8.7. These Eqs. cannot be justified fully with the limited experimental results shown in Fig 8.13. More data set is required in this regard which is also subjected to the further research. Also, in the proposed equation Eq (8.7), it is not important to know the cover depth, cracks, and chloride-content at the surface of steel bars. It is assumed that the aforementioned parameters are more important for calculating the corrosion rate or corroded depth of corrosion in a steel bar. Therefore, this equation is only valid when the mass loss of steel per unit length is known.

8.4.4. Proposed corrosion modelling of R/SHCC

A corrosion modelling was attempted from the results obtained in series three of R/FS32 specimens. The reason for choosing this series is because the readings were taken from the

Towards Corrosion Modelling of R/SHCC

start of testing and because continuous cyclic chloride exposure was also carried out until the end of testing. In Chapter 7 as well as in this current chapter, correlations have been observed between corrosion, cracks, cover depth and chloride content as shown in Table 8.2. Based on these correlations two empirical Eqs (8.8) & (8.9) were developed by trial and error to predict the corroded depths in the steel bars due to chloride-induced corrosion based on the results obtained in Series One to Three. Eq (8.8) is valid for a single crack while Eq (8.9) is for multiple cracks in the R/SHCC specimen. Also note that the corrosion rate measured in this research was from the Coulostatic method and so these equations may need to be adjusted before using them for another corrosion rate measurement method. The proposed Eqs (8.8) & (8.9) were validated with the results obtained in series three. Fig 8.14 shows the experimental and model data for single crack specimens with different cover depths. Multiple cracks and the influence of crack spacing were also considered in the modelling of R/SHCC specimens and are shown in Figs 8.15a&b.

For single crack specimens:

$$d_c = \frac{\delta_T \delta_{RH} W_{cr,ave} t^{\alpha_t} Cl_{free}^{\alpha_{cl}}}{C^{\alpha_C}} \quad (8.8)$$

For multiple cracks specimens:

$$d_c = \frac{0.35 \delta_T \delta_{RH} W_{cr,ave} t^{\alpha_t} Cl_{free}^{\alpha_{cl}} S_{cr}^{\alpha_S}}{C^{\alpha_C}} \quad (8.9)$$

where d_c is the corroded depth (μm), t is the corrosion time (year), $W_{cr,ave}$ is the average crack width in the specimens (μm), Cl_{free} is the % of free chloride at the steel surface level (% wt of binder), S_{cr} is the average crack spacing in the specimens (mm) and C is the cover depth of the steel bar. δ_T and δ_{RH} are the factors that depend on the temperature and relative humidity (RH) at the steel bar level. At the specimen surface temperature of $20 \pm 3^\circ\text{C}$, δ_T can be considered to be 1. And similarly for $55 \pm 5\%$ RH, δ_{RH} can be considered to be 1. α_t , α_{cl} , α_S and α_C are the factors that depend on the ratio of wetting and drying periods, types of binder, range of maximum crack spacing and quality of cover concrete, i.e. micro-structure and tensile strength of concrete. In this research work, the value of α_t , α_{cl} , α_S and α_C were considered to be 0.68, 0.5, 0.27 and 0.3 respectively. With these values, Eqs. (8.8) & (8.9) show reasonable agreement with the experimental data points, but these values may need to be re-calibrated for other material types, exposure conditions, age and different corrosion rate measurement techniques.

Towards Corrosion Modelling of R/SHCC

Table 8.2: Observed corroded depth relationships with time, cracks, cover depths and chloride

Corroded depths, d_c (μm) vs	Observed relationship	Regression factor (R)
Average crack widths, $W_{cr,ave}$ (μm)	$d_c = 0.134W_{cr,ave}$	0.51
Crack spacing, S_{cr} (mm)	$d_c = 0.853S_{cr}^{1.11}$	0.43
Cover depths, C (mm)	$d_c = 13.2C^{-0.284}$	0.97
Free chloride, Cl_{free} (% binder wt)	$d_c = 2.55Cl_{free}^{0.39}$	0.58
Time, t (year)	$d_c = 5.73t^{0.98}$	0.97

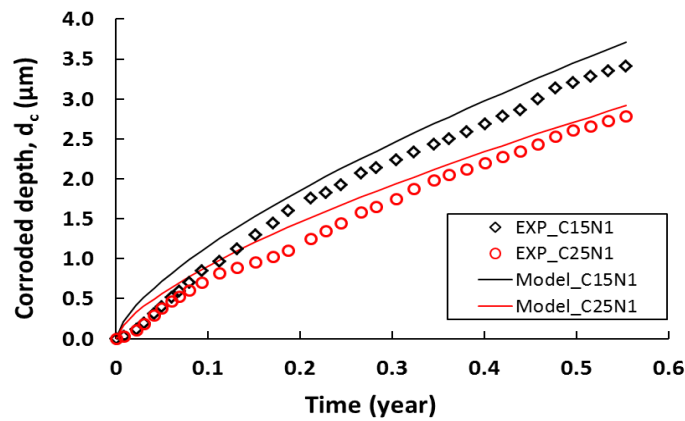


Figure 8.14: Corrosion modelling using Eq (8.8) of cracked R/SHCC specimens with a single crack.

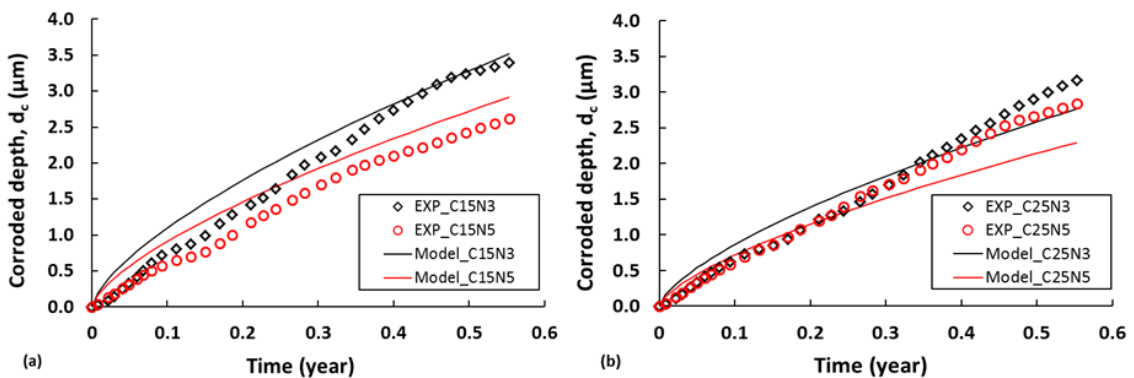


Figure 8.15: Corrosion modelling using Eq (8.9) of cracked R/SHCC specimens with multiple cracks.

Fig 8.15a shows the 15 mm cover of R/FS32 specimens with three notches (N3) and five notches (N5) which correspond to the crack spacing of 40 mm and 20 mm. The larger crack spacing of N3 specimens was found to cause higher corroded depths in the steel bar. Fig

Towards Corrosion Modelling of R/SHCC

8.15b shows a similar trend as Fig 8.15a, but now for 25 mm cover depth. The proposed corrosion modelling is valid for the laboratory experiments where the temperature ($21 \pm 2^\circ\text{C}$) and RH ($60 \pm 5\%$) were a constant throughout the whole testing period. So the influence of different temperatures and RH was not considered in the proposed modelling.

8.4.5. Model validation

The current research on corrosion modelling in R/SHCC is limited and as far as the author could establish no corrosion model exists to predict the corrosion rate in cracked R/SHCC specimens. Another important observation from the existing corrosion models for NC is that the parameters considered in the models vary. Therefore, validation of the proposed models (Eqs 8.8 & 8.9) remains to be done in future studies. However, an attempt was made by the author to compare the proposed models with existing data found in a numerical corrosion modelling approach by Chen & Leung (2013) in NC specimen. The authors performed finite element analysis for cover cracking in NC due to non-uniform and uniform corrosion in the steel bars. By considering different corroded depths in the steel bars, the ACW on the reinforced NC surface for two different cover depths (20 mm & 40 mm) were predicted from the finite element analyses. In the finite element analyses the material constants such as concrete, rust and steel E-mod, Poisson's ratio, steel yield strength, diameter, concrete tensile strength, fracture energy, friction coefficient of concrete/rust, etc. were considered. The corrosion initiation period of 0.8 years was calculated by solving the diffusion equation for critical chloride content of 0.71 kg/m^3 . Eq (8.8) was used to calculate the ACW in the NC surface and to compare them with the results predicted from the numerical modelling data of Chen & Leung (2013) in Fig 8.16. It was found that the proposed modelling in this research for corroded depth in a steel bar in a single cracked specimen is in agreement with the numerical results found by Chen & Leung (2013).

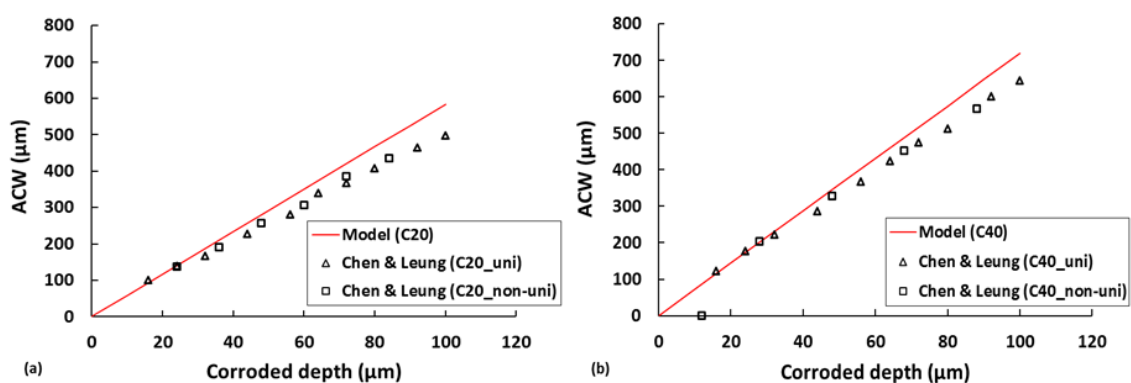


Figure 8.16: Validation of proposed corrosion modelling for single crack specimens using Eq. (8.8) (a) for 20 mm cover depths (C20) (b) for 40 mm cover depths (C40) of steel.

Note that to calculate the corroded depth or crack widths using Eq. (8.8), the amount of free chloride and time of corrosion testing are required. Therefore, the initiation corrosion period t

Towards Corrosion Modelling of R/SHCC

= 0.8 year and the critical chloride content 0.71 kg/m^3 as reported by Chen & Leung (2013) were used to calculate the ACW for any assumed corroded depths in the steel bar. The free chloride content was calculated from the critical chloride content. In this case a minimum amount of binder (300 kg/m^3) in the mix was assumed and from that the percentage of free chloride (by wt of binder) was calculated. The time of corrosion testing was considered as being the same as the corrosion initiation period.

8.5. Important observations and comparison of results

It is quite clear that cracks play an important role in chloride attack and corrosion in R/SHCC specimens tested in this research. Although no final relationships are proposed because of the variations in specimens' age, exposure period, level of deflections, etc. in the research results trends have been found that were also observed by other researchers (Mohammed *et al.* 2001; Busba, 2013; Kojima *et al.* 2014) in NC and SHCC (Kojima *et al.* 2014). In Fig 8.17 a relationship was drawn between the actual corrosion mass losses of similar types of galvanized steel and TCW in pre-cracked (by bending) NC specimens. After 13 weeks (105 days) of cyclic 3.5% NaCl chloride exposure (wetting 24 hrs and drying 60 hrs) in single crack RC specimens (100 mm x 100 mm x 400 mm in size) with three different crack widths Mohammed *et al.* (2001) found a slight increment in steel mass loss as the crack widths increased. Mass loss of steel was determined by immersing corroded steel bars in 10% (by wt) di-Ammonium hydrogen citrate solution for 24 hrs and then removing the rust. Similarly, Busba (2013) observed increased mass loss in steel bars in the pre-cracked NC pipe specimens for larger crack widths after up to 39 weeks (274 days). In this case specimens were exposed to different regimes such as the first 5 weeks in de-ionised water, then 5 to 21 weeks in continuous chloride exposure (ponding) and the last 21 to 39 weeks in cyclic chloride exposure (ponding). From the figure it is apparent that there is a threshold TCW of 0.7 mm in NC specimens and below this crack width the rate of mass loss of steel is not significant.

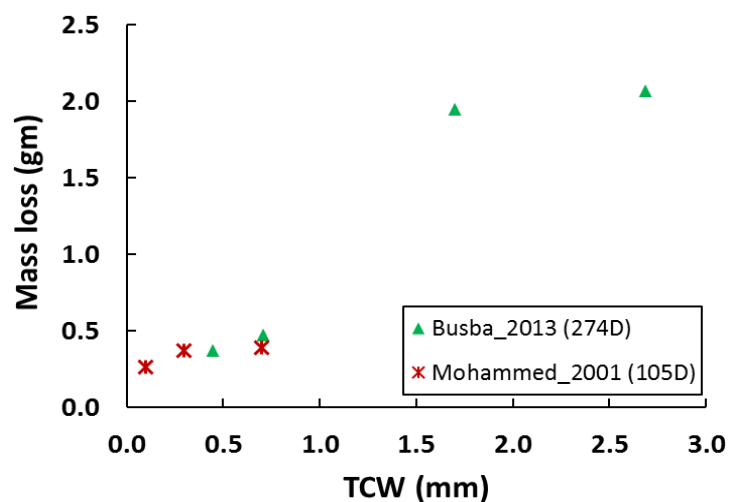


Figure 8.17: Observed mass loss due to different crack widths in NC.

Towards Corrosion Modelling of R/SHCC

Regarding the chloride penetration in cracked unreinforced SHCC specimens, Kojima *et al.* (2014) found that the penetration of chloride increased as the total crack width increased as shown in Fig 8.18. In this case the dumbbell specimens with a cross-section of 30 mm x 30 mm were made with different fibre contents. Cracks in the specimens were then created by tensile testing. After pre-cracking, all the specimens were kept in 10% NaCl solution for a minimum period of 2 months to a maximum period of 11 months. XRF was used to determine the average chloride-content measured at three points (top, middle and bottom) along the specimens' cross-sectional depth. The results shown in Fig 8.18 are for the average chloride content at different TCW of specimens after 11 months or about 47 weeks of testing. Almost for the same exposure duration of R/FS31 specimens (57 weeks), a similar trend of increased chloride content was found as the crack widths increased as shown in Fig 8.9b. However, for the longer period of testing, the influence of crack widths in chloride penetration may become insignificant.

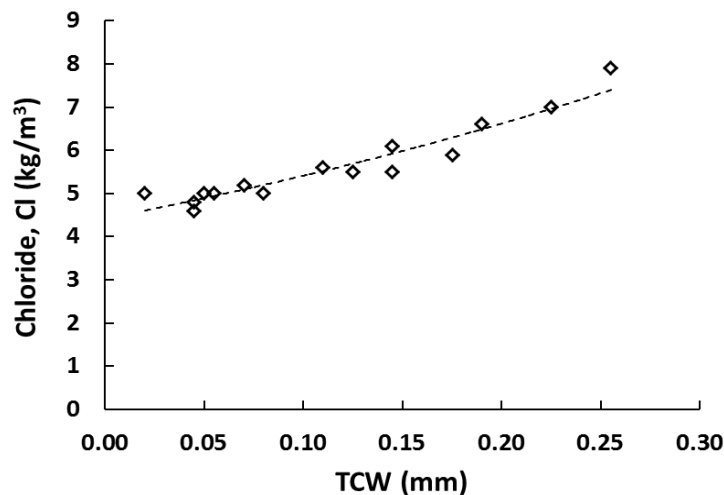


Figure 8.18: Relationship between XRF total chloride (Cl) content and total crack widths (TCW) in unreinforced SHCC specimens (reproduced from Kojima *et al.* 2014).

The relationship between the chloride, corrosion area and cracks in NC was also examined by Mohammed *et al.* (2001) and it is shown in Fig 8.19. In NC beams of size 150 mm x 150 mm x 1250 mm, multiple cracks (number of cracks not given) were formed in flexure by placing and anchoring the specimens with nuts and bolts to a steel frame. 3.5% NaCl solution was sprayed on the specimens once a week in the open air environment for 16 months. The total chloride content (by means of water soluble chloride testing on powder sample) at the various crack locations and corrosion areas over the whole length (methods of measuring not reported) was compared for different crack widths in the specimens. It is quite clear that no relationship was found between the chloride and corrosion area for the TCW range 0.1-0.4 mm. This result also confirms the trend shown in Fig 8.9a where no relationship was found because of smaller TCW in the R/SHCC specimens tested here. Similar results were found by Huang (2006) in NC as shown in Fig 8.20. In this case the specimens were 100 mm x 150

Towards Corrosion Modelling of R/SHCC

mm x 800 mm in size and cracks were formed by applying sustained flexural load in loading frames. A maximum of 3 cracks were formed in each specimen and the ACW were measured. For the chloride exposure condition the cracked face to the half of the beam height was continuously submersed in a 10% NaCl solution for 49 days. Corrosion rate in the specimens was then measured by means of a linear polarization technique. In Fig 8.20 it can be seen that no correlation was found between crack widths and corrosion rate in NC (Huang, 2006). This can be explained by the finer crack widths in NC as well as in SHCC specimens with a single steel bar as tested in this research, where the relationship between crack widths, corrosion and chloride penetration are not clear. The others factors such as the amount of oxygen, temperature and moisture content may be more important than the presence of finer cracks in both NC and SHCC specimens.

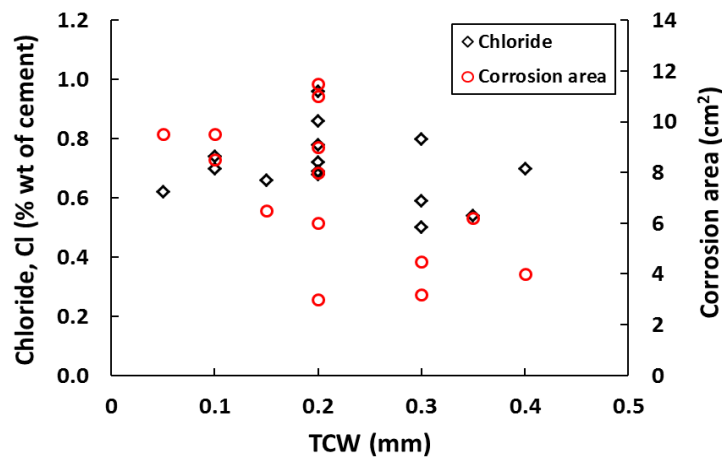


Figure 8.19: Chloride content and corrosion area at different total crack widths (TCW) in NC (reproduced from Mohammed *et al.* 2001).

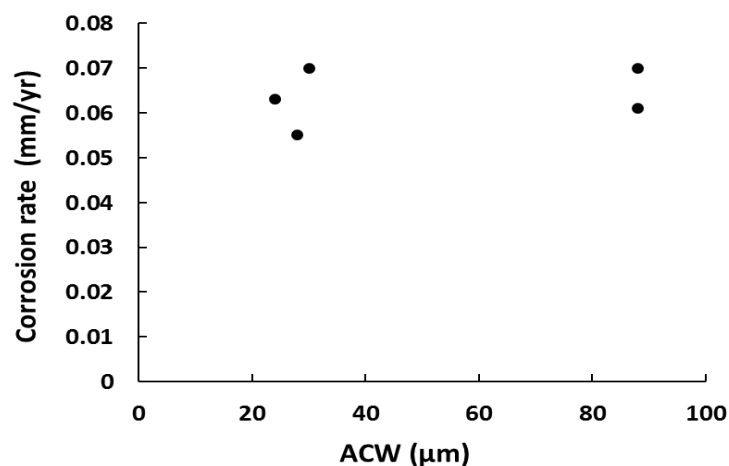


Figure 8.20: Corrosion in steel due to different average crack widths (ACW) in NC specimen (Huang, 2006).

Towards Corrosion Modelling of R/SHCC

One of the major concerns of existing different corrosion rate measuring techniques is that in the same specimens they may give different readings. Liu & Weyers (1998) performed different corrosion measuring techniques on the same specimens and observed significantly different corrosion currents as shown in Fig 8.21a. However, using calibration factors (in this case the lowest values of each corrosion measuring method) the normalised corrosion current was determined for each test series as shown in Fig 8.21b. It is clear that although different corrosion measuring techniques give different results, the results can be improved by using the calibration factors. It must be born in mind that, without calibration against a large pool of actual, observed corrosion data, the corrosion rate of steel bars measured by one of the techniques is just an illustration of the corrosion status; and just give an indication of the different ranges of low, moderate and high rates of corrosion in the steel bars. So, when comparing the results of this research obtained from the Coulostatic method with other research results, a calibration factor may need to be used for better comparison. Nevertheless, Fig 8.12 shows a reasonable correlation of the real corrosion status of steel bars measured with the Coulostatic method.

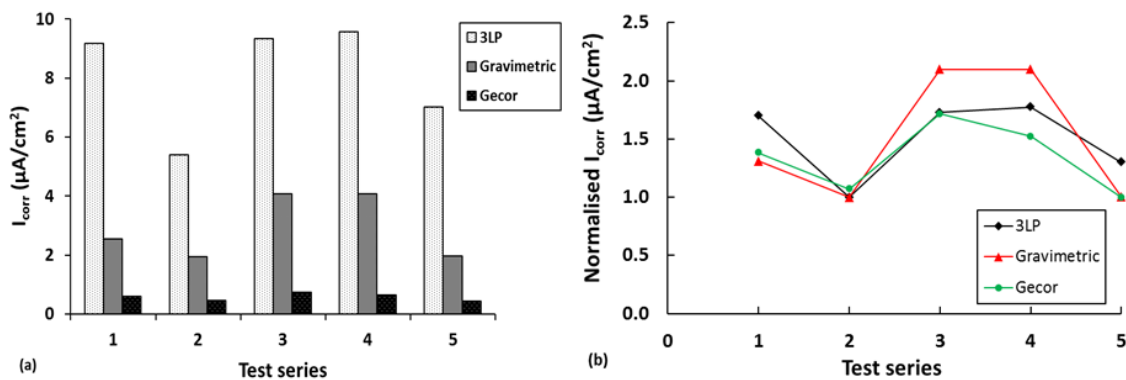


Figure 8.21: (a) Measured corrosion current (I_{corr}) in steel using different measuring techniques by Liu & Weyers, (1998) (b) normalised corrosion current after multiplying with the calibration factors.

8.6. Concluding remarks

The corrosion rate in the steel bar is related to many parameters of the specimen such as crack width and spacing, cover depth, chloride-content, temperature and moisture content. Therefore, in the corrosion modelling all the parameters should be considered carefully. In this research, the crack properties of SHCC such as the number of cracks, crack widths and crack spacing have been found to be important parameters in limiting the corrosion damage in the steel reinforcing bars in SHCC and therefore should be considered in corrosion modelling in R/SHCC for durability design. The corrosion pitting depths in the steel bars are influenced by the aforementioned crack properties. The area of bond fracture or delamination between the matrix and the steel surface is regarded to be smaller in SHCC than in NC because of the tighter microstructure and crack-bridging effect by fibre in SHCC. As a result,

Towards Corrosion Modelling of R/SHCC

SHCC can be considered to offer superior resistance to steel corrosion than NC, for instance due to this resistance to separation and creation of space for deleterious materials and corrosion products.

The XRF total chloride-content in the cracked specimens at rebar depth is higher when the ACW and TCW are above 0.05 mm and 0.5 mm respectively. Exposure period and cover depth also influence the chloride-content in the specimens. Higher chloride-content is found for longer exposure periods and smaller cover depths of specimens. Similarly, the corroded depth in the steel bars is higher for smaller cover depths. However, no clear relationship has been found between the corroded depths assuming uniformly-distributed corrosion and the actual, average pitting depths in the steel bars. This may be because of the formation of general corrosion (also known as micro-cell corrosion) in the steel bars and also due to possible damage caused to the steel bars in the process of extracting them.

The threat of chloride exposure increases the risk of a reduced structural service life. However, it is still not predictable what the real loss of service life may be due to the actual exposure types experienced by structures from the cyclic wetting and drying experiments performed here. However, a relationship has been found between the loss of yield force, pitting depth and mass loss in the steel bars in series three and empirical formulas were also proposed from the obtained results. Finally, results obtained in this research work have been compared with the results in the literature on NC. Based on smaller crack widths, chloride-content and corrosion rate/corroded depth similar trends were found between SHCC and NC.

8.7. References

- ACI 318-11: 2011, Building code requirements for structural concrete and commentary.
- Alonso, C, Andrade, C & Gonzalez, JA 1988, 'Relation between resistivity and corrosion rate of reinforcements in carbonated mortar made with several cement types', *Cement and Concrete Research*, vol. 8, no. 5, pp. 687-698.
- Arya, C & Ofori-darko, FK 1996, 'Influence of crack frequency on reinforcement corrosion in concrete', *Cement and Concrete Research*, vol. 26, no. 3, pp. 345-353.
- Bazant, ZP 1979, 'Physical model for steel corrosion in concrete sea structures – Theory', *Journal of the Structural Division of the ASCE*, vol. 105, pp. 1137-1153.
- Broomfield, JP 2007, 'Corrosion of steel in concrete: Understanding, investigations and repair', Publisher Taylor & Francis, New York, NY, ISBN 0-203-41460-8.
- BS 8110-1: 1997, Structural use of concrete: Code of practice for design and construction.
- Busba, ER 2013, Effect of localized corrosion of steel on chloride-induced concrete cover cracking in reinforced concrete structures. Graduate Theses and Dissertations, available at <http://scholarcommons.usf.edu/etd/4872>
- Chen, E & Leung, CKY 2013, 'Numerical modelling of non-uniform steel corrosion development and its mechanical influences on reinforced concrete structures', proceeding for

Towards Corrosion Modelling of R/SHCC

VIII International Conference on Fracture Mechanics of Concrete and Concrete Structure, van Mier et al. (eds), Spain.

EN 1992-1-1: 2004, Design of concrete structures- part 1-1: General rules and rules for buildings.

EN 206-1: 2000, Concrete – Part 1: Specification, performance, production and conformity.

Florida method of test for determining low-levels of chloride in concrete and raw materials, FM 5-516, Florida Department of Transportation (FDT), September 1994.

Huang, Q 2006, Influence of cracks on chloride-induced corrosion in reinforced concrete structures. MSc thesis, Chalmers University of Technology, Sweden.

Kojima, Y, Dung, LA, Rokugo, K & Kobayashi, K 2014, ‘Chloride proofing and rebar corrosion proofing performances of SHCC having cracks’, proceeding for third RILEM conference on SHCC, Netherland.

Lepech, M & Li, VC 2005, ‘Water permeability of cracked cementitious composites’, proceedings of ICF11, Turin, Italy, pp. 113-130.

Liu, Y 1996, Modelling the time-to-corrosion cracking of the cover concrete in chloride contaminated reinforced concrete structures, PhD thesis, Virginia Polytechnic Institute and State University, USA.

Liu, T & Weyers, RW 1998, ‘Modelling the dynamic corrosion process in chloride contaminated concrete structures’, Cement and Concrete Research, vol. 28, no. 3, pp. 365-379.

Markeset, G & Myrdal, R 2008, Modelling of reinforcement corrosion in concrete- State of the art, COIN Project Report No 7, SINTEF Building and Infrastructure, ISBN 1891-1978.

Mohammed, TU, Otsuki, N, Hisada, M & Shibata, T 2001, ‘Effect of crack width and bar types on corrosion of steel in concrete’, Journal of Materials Civil Engineering, vol.13, pp: 194-201.

Morinaga, S 1988, Prediction of service lives of reinforced concrete buildings based on rate of corrosion of reinforcing steel, Report No. 23, Published by the Institute of Technology of Shimizu Corporation, Japan.

Otieno, MB, Alexander, MG & Beushausen, HD 2010, ‘Corrosion in cracked and uncracked concrete –influence of crack width, concrete quality and crack reopening’, Magazine of Concrete Research, vol. 62, no. 6, pp. 393–404.

Papadakis, VG 2005, Estimation of concrete service life- the theoretical background, Building Technology and Durability, V.G. Papadakis & Associates, 1st Edition, Patras, Greece.

Scott, AN 2004, The influence of binder type and cracking on reinforcing steel corrosion in concrete. PhD Thesis, Department of Civil Engineering, University of Cape Town.

Shetty, MS 2009, Concrete Technology, Theory and Practice, S. Chand & Company Ltd., New Delhi, ISBN: 81-219-0003-4.

Towards Corrosion Modelling of R/SHCC

Tuutti, K 1982, Corrosion of steel in concrete, Swedish Cement and Concrete Research Institute, CRI research, No. Fo 4:82.

van Zijl, GPAG & Paul, SC 2013, 'Crack spacing in steel bar reinforced strain hardening cement-based composites (R/SHCC), towards corrosion modelling', proceeding for International Conference on Sustainable Construction Materials & Technologies (SCMT3), Kyoto, Japan.

Chapter 9

A person who never made a mistake never tried anything new.
– Albert Einstein

Conclusions and Recommendations

9. Introduction

This research was aimed at creating a better understanding of SHCC's behaviour relating to its durability. It addressed the corrosion rate and chloride-content in finely-cracked SHCC specimens at different deformation levels and it also introduced coarse sand in SHCC. Durability issues, especially the deterioration process in NC have already been broadly explained by researchers during the last 30-40 years. As a new material, there are still some gaps in the knowledge of SHCC. The initial cost of SHCC is higher than that of NC but its potentially better resistance to long term deterioration processes is of importance. If an increased life span and/or reduced repair frequency can be assured by SHCC, it will be possible to save the money otherwise needed for the repair and rehabilitation of structures. The insight gained from both the mechanical and the durability tests can be summarised as follows:

9.1. Role of slump flow and air in SHCC

To achieve strain-hardening, it is important to assure that the ingredients including fibres are evenly distributed in the matrix. In this regard, the slump flow of the matrix is an important indicator. A slump flow range from 170 mm – 210 mm was found to be suitable for SHCC made with both fine and coarse sand. Slump flow below 170 mm leads to the formation of voids as observed in trial mixes in this research. In higher slump flow (more than 250 mm), there is a possibility of segregation.

A range of 4.5% - 9% air content was measured in the SHCC used in this research. However, the influence of air content in the SHCC results such as stress-strain, cracks, etc. was not investigated. It is believed that a certain amount of air is necessary in the matrix for SHCC to form multiple cracks. It is also advisable to use admixtures, a viscosity-modifying agent and an air-entraining agent in the matrix to obtain the desired fresh properties of SHCC.

9.2. Role of aggregate size and binder content in SHCC

Generally specially-graded fine sand is used in SHCC because larger aggregate sizes influence the distribution of micro fibres such as PVA and PE. In this research more than 2%

Conclusions and Recommendations

ultimate tensile strain was observed in SHCC (CS11) with a maximum of 2.36 mm local coarse sand. No noticeable difference was found in terms of the number of cracks and crack widths. Therefore if the well-graded particle size can be confirmed, the coarse sand with a particle size of more than 2 mm can be used as an alternative source of sand in SHCC. The prominent behaviour typical of fine sand SHCC can be reproduced. The multiple cracks in SHCC are fully dependent on its overall mix design.

9.3. Mechanical performances of SHCC and mortar

Materials in structures are exposed to varying loads such as compression, tension, shear, bending and torsional loads and they may be subjected to a combination of loads. The conditions to which materials are exposed are also diverse in terms of the environment, the rate of applying loads and changes in nature over time. Accordingly, there are many factors influencing the materials' mechanical properties and many ways of performing mechanical tests. In concrete, tests of compression, tension, flexure/bending and shear are the most widely-used mechanical tests with which to evaluate its properties for structural design purposes. The results obtained in this research of SHCC's mechanical properties by various tests such as compression, tension, flexure/bending, etc. are discussed here.

9.3.1. Compressive strength and E-mod

The average compressive strength and E-mod of SHCC were found within a range of 24-33 MPa and 12-19 GPa respectively. No significant reduction in the results was noticed due to the inclusion of fibre in SHCC when compared with the mortar specimens made from the same matrix without fibre. It was found that the compressive strength of FS-SHCC and mortar (same matrix of SHCC without fibre) increased gradually from 28-120 days. However, in the high strength mortar HM3, after 57 days the compressive strength development was negligible.

9.3.2. Tensile strength and cracks

At the age of 14 days, an almost equal number of cracks and average crack widths were noticed in high-fibre content FS-SHCC (2.2%) and CS-SHCC (2%) (max size of CS = 2.36 mm) specimens at the strain level of 2.5%. However, at the same strain level as a particular mix of CS-SHCC, the maximum crack widths were found to be 44% lower than those of FS-SHCC. It may be that the optimum fibre content of CS-SHCC matrix is 2% while 2.2% fibre in FS-SHCC may not be reached with the matrix as its optimum fibre limit. In the same matrix of FS-SHCC and CS-SHCC at the age of 28 days, the ultimate tensile resistance was higher than at 14 days. However, a significant reduction in the strain capacity was observed in both SHCC at 28 days and the average and maximum crack widths were also higher. Both the ultimate stress and strain in a lower fibre content (1% and 1.5%) of FS-SHCC and CS-SHCC specimens were significantly lower than FS-SHCC with 2.2% fibre and CS-SHCC with 2% fibre. With a higher fibre content in both SHCC, the average crack widths remained

Conclusions and Recommendations

the same as the strain increased. However, the number of cracks and maximum crack widths increased.

9.3.3. Flexural strength and cracks

In all unreinforced FS and CS matrices, a slightly higher load and vertical deflection/deformation capacity was found in FS-SHCC than in CS-SHCC specimens under flexural testing. The flexural strength development with age was in agreement with their compressive strength development, increasing gradually from the age of 28 to 120 days but with a negligible increase for the high strength mortar HM3 after 28 days.

In unreinforced SHCC specimens, the surface crack distribution was found to be limited to the 100-120 mm (of the 300 mm span) length in the middle of the specimens in the region of the central load application in three point bending.

In reinforced SHCC specimens R/FS2 and R/CS2, for the same level of deflection (in this case 3.5 mm), specimens with higher reinforcement level, i.e. those with two steel bars had a higher flexural resistance than the specimens with a single steel bar. The load capacity of specimens was reduced due to reduced leverage arm as the cover depths were increased from 15 to 35 mm.

At 3.5 mm vertical deflection level, the average crack widths in R/FS2 and R/CS2 specimens with three different cover depths and two levels of steel bars were found to be in a range of 24-74 μm . In R/FS31 specimens with three different cover depths and a single steel bar at 5 and 7 mm vertical deflection levels, the average crack width was in a range of 49-99 μm .

The crack spacing in all R/FS2, R/CS2 and R/FS31 specimens with C15 was higher and there was no significant difference in crack spacing in the specimens with C25 and C35. However, a scattered result was found in all R/SHCC specimens with C35 and the average crack widths of specimens were smaller for larger cover depths. The total crack widths of R/SHCC specimens were found to be best correlated with the level of vertical deflection in flexural testing.

9.3.4. AE responses in SHCC

The SHCC specimens' failure characteristics under tensile and flexural tests were investigated by means of the AE technique only in series four. From the time of the start of matrix cracking to the fibre rupture in SHCC, AE was found to be a better way of visualizing the whole scenario in the specimen under load. In AE testing, weighted peak frequencies of <90 kHz and >120 kHz were found to distinguish between the matrix cracking and the fibre rupture in the SHCC specimens. A clear picture of the linear elastic region and the strain-hardening and strain-softening in SHCC specimens can also be visualized from the AE responses.

Conclusions and Recommendations

9.3.5. Fracture energy of SHCC

The large particle size of CS was found to cause higher fracture toughness in CS-mortar than in FS-mortar. However, in the same matrix when fibres were added, increased fracture toughness was found in the SHCC when compared with that in the mortar specimen, since the crack growth rate in the SHCC specimen is much lower than in the mortar specimen. Also in FS-SHCC the fracture toughness was higher than in CS-SHCC. CS-SHCC has a higher crack tip toughness value than FS-SHCC, which may explain the lower ductility in SHCC containing coarse sand. It is postulated that, in addition to the matrix crack tip toughness, the distribution of flaw size, here in the form voids formed by entrained air, may influence the tensile ductility and the number of cracks.

9.4. Corrosion and chloride attack in SHCC and mortar

The chloride penetration and the deterioration of steel bars accelerate when there are cracks in concrete. So it was the aim to observe the chloride-induced corrosion performance of SHCC in the cracked stage. Corrosion potential was observed by using the half-cell potential measurement method, and corrosion rate was observed by using a Coulostatic method. Through integration of the corrosion rate (i_{corr}) a uniform corroded depth (d_c) was determined in the steel bars. The following conclusions can be drawn from the corrosion potential and corrosion rate of steel bars.

9.4.1. Corrosion potential values of R/SHCC and R/mortar specimens

From the corrosion potential readings using a Cu/CuSO₄ half-cell, the following conclusions can be made:

The half-cell potential readings ranges recommended by the ASTM indicate a high probability of corrosion for all cover depths of R/SHCC used here.

The presence of cracks in the specimens appears to cause a significantly higher corrosion potential reading directly after the application of chloride solution. In uncracked specimens, a longer period is necessary for the half-cell potential to increase as the penetration of chloride and depassivation of a steel bar is slower in uncracked specimens. Corrosion potential values in the cracked reinforced specimens increased as the number of cracks and crack widths increased. Better correlation was found between the potential values and the total crack widths than the average and maximum crack widths in the specimens. The position of the half-cell on the specimens (top or sides) during the taking of corrosion potential readings was found to have influence on the reading.

Corrosion potential readings are strongly affected by the level of absorbed chloride solution, with higher potential (more negative potential value) being indicated after a three day period of wetting than after a subsequent four day period of drying of cracked and uncracked

Conclusions and Recommendations

R/SHCC and R/mortar in series four. This is particularly significant in cracked specimens with 51% to 99% increase in potential from the end of the dry cycle to the end of the wet cycle, as opposed to up to 26 % increase in uncracked R/FS4 specimens in series four. After 60 days of corrosion testing, corrosion stains were observed in the cracked R/HM3 specimens. Therefore the higher corrosion potential values of R/FM3 and R/FS4 may not mean higher corrosion activities in the specimens. It is, however, acknowledged that a rust stain does not prove significant corrosion activity, or more significant corrosion than in specimens not showing such stains. This remains to be tested in future work.

The severity of corrosion in the reinforced specimens can be observed by corrosion potential mapping. In series four, higher corrosion activities were found in the middle of the each specimen since the NaCl solution was applied in that location.

9.4.2. Corrosion rate in R/SHCC and R/mortar specimens

The corrosion rates of the specimens were measured only in series one to three. Due to the process of developing the corrosion rate measurement setup, readings were not possible from the beginning of the exposure period of the specimens in series one. From the corrosion rates that were measured in both R/SHCC and R/mortar by a Coulostatic method, the following conclusions could be made:

Influence of cover depth in corrosion

In chloride-induced corrosion performed here, higher corroded depths both calculated from measured corrosion rates and actual measured pitting depths, a higher loss of yield resistance in the steel was found in the specimens with cover depth of 15 mm than in 25 mm and 35 mm cover depths. No significant difference was observed in the specimens with 25 mm and 35 mm cover depths.

Destructive and non-destructive testing of corrosion

The removal of the steel bars from specimens after extended periods of accelerated corrosion confirmed corrosion damage to steel bars in R/mortar as well as in R/SHCC specimens. However, discolourations in the steel bars do not represent the true corrosion damage. After cleaning the steel bars with HCl, in most cases no major damages were noticed in the discolouration area. From the limited data set, distributed corrosion damage was found in R/SHCC specimens, as opposed to localised damage in R/mortar specimens. Also from the CT images it was found that the corrosion activity in the steel bar is higher at the location of the cracks in the specimen. Non-destructive methods like CT scanning can be used to analyse the corroded area of the steel bar, the crack depth and the number of voids in the specimen.

Conclusions and Recommendations

Influence of cracks in corrosion damage of steel bars

The corroded depths were found to be higher for wider average crack widths in the R/SHCC specimens. Increased crack spacing also leads to higher corroded depths in the specimens.

In R/FS32 with 15 mm cover depth specimens, the average mass loss in single notch specimens was 60% and 67% higher than in the specimens with three and five notches. Similarly a 14% and 25% higher yield force loss was found in single notch specimen than in three and five notch specimens. Therefore a large number of cracks in R/SHCC specimens leads to a lower mass and yield force loss in the steel bars.

The average and maximum pitting depths in the steel bars decreased as the number of cracks, the total crack widths and the crack spacing in the R/SHCC specimens increased. The pitting depths in the steel bars also depend on the exposure periods. Higher average pitting depths were found in FS2 and CS2 specimens than in other types of SHCC used but were tested over significantly shorter periods. A good correlation was found between the average pitting depths and the loss of yield force capacity of the steel bars.

9.4.3. Chloride profile in the SHCC and mortar specimens

Chloride presence in SHCC and mortar specimens were visualised by spraying AgNO_3 on the specimens' cracked surface, by the XRF method for determining total chloride content as well as by chemical analysis for both total and free chloride content.

9.4.3.1. Chloride profile in un-reinforced SHCC specimens

Chloride profiling using AgNO_3

In un-reinforced SHCC specimens with a crack width range of 20 to 50 μm , the chloride penetration reaches to the full depth of the crack (50-80 mm) within 1 to 3 hrs. Even in high strength of FS5, chloride reaches the full depth of the crack within a short period of exposure. Depending on the matrix properties (mainly strength in this research) chloride penetration widens along the crack width as time increased. However, the higher density associated with the higher strength of FS5 is postulated to restrict chloride penetration widening more than the low strength of FS32 (as shown in Fig 7.30).

Chloride profiling using XRF

For a total chloride analysis, XRF can be an alternative to doing chemical analysis as recommended by the RILEM, as XRF shows a very good correlation with the chemical analysis results. However, the free chloride is considered to be more relevant for corrosion. It would be useful if a unique relationship between fixed and free chloride could be found by calibration. Here, it was found that the portion of free to total chloride varied with depth in the SHCC specimen.

Conclusions and Recommendations

XRF analyses of FS32 and FS5 notch specimens show a trend towards an increased chloride content in the specimens as the exposure periods increased from 1 hour to 7 days. In most cases at the same depths of specimens a slightly higher chloride content (as shown in Fig 7.31) was found in the larger notch spacing (40 mm) of FS32 and FS5 than in the smaller notch spacing (20 mm) specimens. After the notch depth, only 0.05% chloride penetration was observed in the un-cracked portion of FS32 and FS5 specimens after 7 days of continuous NaCl exposure.

9.4.3.2. Chloride profile in the R/SHCC and R/mortar specimens

Both the total and free chloride contents reduce with depth and in R/SHCC specimens a minimum 4% to maximum 66% total chloride can be found as free chloride. The difference between the XRF total chloride content and the chemical free chloride content in R/SHCC specimens was about 13% to 63% while in R/mortar it was about 2% to 77%. Chloride concentration in cracked specimens may be influenced by the crack geometry and the presence of pores adjacent to the crack. Therefore, in cracked specimens higher concentrations of chloride may be found deeper than at the surface of specimens. In this research, for a specific matrix of SHCC the maximum total chloride content was found to be 1.8% (by binder weight). For specific thicknesses of a specimen (here it was 80 mm and 100 mm), a significantly higher chloride content can be found at the opposite face of the cracked and un-cracked specimens' than their exposure surface. The higher chloride content may be explained by the storage of chloride at the opposite face of exposure for longer accelerated wetting and drying cycles.

The XRF total chloride-content in the cracked specimens at the rebar depth is increased when the average and total crack widths are above 0.05 mm and 0.5 mm respectively. The total chloride content in the cracked specimens is higher for higher total crack width in the specimens. Total chloride content in R/SHCC specimens also influenced by the exposure periods. Longer exposure periods are found to be the cause of higher chloride content in the specimens. The corroded depths of steel bars are more representative of the level of free chloride content in the specimens. The presence of a higher amount of free chloride also increased the corroded depths of steel bars.

9.4.3.3. Chloride diffusion coefficient

The chloride diffusion coefficient (D_{cl}) value obtained from the RCM test is not directly related to concrete strength and air content. For the same water binder ratio the presence of fibre in FS4 shows a slightly higher diffusion coefficient value than in FM3. Also a higher water binder ratio and the presence of large particles in HM3 show a significantly higher diffusion coefficient in the RCM tests. Recall that the RCM test was only performed for FS4, FM3 and HM3 where maximum air content and compressive strength were found in FS4 and HM3. Therefore, for the D_{cl} of concrete, there may be some other parameters such as the grading of aggregates, binder content, etc, which are more important than the strength of

Conclusions and Recommendations

concrete. A slightly higher D_{cl} value was found when FS4 specimens were loaded at different levels of deformation in flexural testing than when the specimens were unloaded. This indicates that the presence of cracks below 0.05 mm wide in FS4 has little influence on the diffusion coefficient value. Future studies with various crack widths in SHCC specimens will be helpful to find the acceptable crack width limit for D_{cl} .

9.5. Freeze-thaw attack, water absorption and electrical resistivity of SHCC and mortar specimens

FS4 has been found to have significant resistance against freeze-thaw attack over that of FM3 and HM3. After 42 cycles of freeze-thaw attack, FM3 and HM3 show a 400% and 2200% higher mass loss respectively than that of FS4.

Large amounts of binder in FS4 and FM3 result in a much higher capillary water absorption than does HM3. However, the water mass gain from 1 hr to 14 days for the different specimens of FS4, FM3 and HM3 were about 14%, 11% and 104% respectively.

FS4 has a higher electrical resistivity than FM3 and HM3 and the resistivity value reduces from the dry to wet conditions of the specimens and this depends on the specimens' age at the time of measurement. The influence of fly ash is shown in the bigger resistance compared to that of HM3. Also at a higher frequency, HM3 shows lower electrical resistivity than do FS4 and FM3. In the case of corrosion it is possible that HM3 has higher corrosion rates because of its lower electrolyte resistance.

9.6. Empirical corrosion modelling of R/SHCC

Crack properties such as the number of cracks, crack widths and crack spacing have been found to be important parameters in corrosion. It was observed from the results that the corrosion in the steel bars proportionally increases as the average crack widths, crack spacing, free chloride content at the steel surface and the time of exposure increase. In smaller cover depths (here 15 mm) the corrosion was also higher and therefore all these parameters were considered in corrosion modelling in R/SHCC for durability design. Depending on the number of cracks (single or multiple) the empirical corrosion prediction model for both single and multiple cracked specimens were developed and found to be in agreement with the experimental results obtained in control specimens of series three (R/FS32 & R/FM3). Finally the empirical model was also validated with the existing results obtained from the numerical analysis in NC. It was found that the proposed modelling in this research for corroded depth in a steel bar in a single cracked specimen is in agreement with the numerical results of corrosion in NC specimens.

Conclusions and Recommendations

9.7. Research hypothesis and findings

The corroded depths measured by the Coulostatic method and the actual mass loss in the steel bars due to corrosion were found to be related to each other in series three. As corrosion-induced cross-sectional loss of a steel bar is related to its mass loss, it can be said that the corrosion results obtained in this research using the Coulostatic method is relevant to the real corrosion in a steel bar. This outcome satisfies the first hypothesis stated in Section 1.7.

A larger number of cracks, associated with finer crack spacing, lead to significantly lower corrosion damage in R/SHCC which was the second hypothesis of this research.

Two years of accelerated chloride testing in the specimens of series one led to a maximum amount of 1.34% free chloride (by wt of binder) content, which is significantly higher than the threshold chloride values as proposed in the literature for concrete, as summarised in Chapter 3. This occurred for even the fine cracks in the R/SHCC specimens tested in the unloaded condition, i.e. with crack widths reduced after removal of the mechanical load. Therefore the third hypothesis of this research is in contradiction with the findings. Nevertheless, low corrosion rates were found.

9.8. General conclusion

From this research, it is clear that there is a relationship between the crack characteristics of crack widths and crack frequency or spacing with the corrosion of steel bar in SHCC. Therefore, in SHCC if the crack characteristic such as average crack width and crack spacing can be maintained up to 0.1 mm and 40 mm corrosion in the steel bar can also be controlled. In this sense, forming multiple finer cracks under any load and crack bridging capacity of SHCC can be considered to offer superior resistance against corrosion of steel bar than NC.

From the limited data set of uncracked R/SHCC and R/mortar specimens, it was found that the corrosion depassivation time and resistance against chloride penetration in these specimens are higher than the pre-cracked specimens. It deems that finer cracks in R/SHCC also accelerate the chloride ingress, and initiation of the corrosion process. The free chloride at the steel level was found more relevant to the corrosion and in the SHCC tested in this research, the difference between the total and free chloride can be in a range of 5-60%. Finally the first step towards corrosion modelling of R/SHCC seems to be successful as the outcome from the modelling is in an agreement with the research results. Obviously further studies are necessary to bring more factors into the model in order for the corrosion prediction to become more complete and relevant to real structures.

9.9. Recommendations for future work

In this research, an attempt was made to contribute towards enhancing the in-depth knowledge of the durability properties especially those of the corrosion of R/SHCC specimens in the cracked state. Not all parameters for mechanical and micromechanical

Conclusions and Recommendations

behaviours have been characterised by means of testing. However, this research has focused on several important parameters such as different crack properties (number, widths and spacing), the chloride-induced corrosion rate, etc. which are key parameters of a design service-life modelling of RCS. Many issues were undertaken and were resolved, while others arose or were left unresolved. So in future work, the following issues could be considered for research:

It is necessary to find the limit of using the maximum aggregate size and a particles distribution curve for coarse sand in SHCC. As the cost of fine sand is high, the introduction of local coarse sand may reduce the production cost of SHCC. A significant reduction in the tensile behaviour of CS-SHCC was observed when a different batch of local sand was used. Therefore the mix design of CS-SHCC must be improved in future research.

The Coulostatic method used here was found to be in agreement with the real corrosion damage in the steel bars such as actual mass loss and loss of yield force (see Figs 8.12 & 8.13). However, the magnitude of the corroded depth/corrosion rate results may vary when different methods are used. Therefore, it is recommended that the results obtained from the Coulostatic method should be calibrated with other methods such as 3LP and Gecor. Also the important notes made on Coulostatic methods in Chapter 4, section 4.5 must be followed before and during the taking of readings in the specimens.

HCl was not found suitable for cleaning the corroded steel bars. When a steel bar sinks into HCl, and depending on the time, an average 0.70 gm (30-41% of actual mass loss) mass loss was found in virgin steel. Therefore, it is recommended to use another method of doing mass loss experiments for corroded steel bars.

In reinforced concrete, crack properties such as the number of cracks, average crack widths, maximum crack widths and total crack widths must be considered in the corrosion activities.

Corrosion in steel bars causes the reduction of the steel cross-sectional area which ultimately reduces the yield force capacity of steel. Therefore, it is recommended that the pitting depths and the loss of yield force of steel due to corrosion are noted. Manually-measured pitting depths in the steel bars were found to be a difficult task when using a dial-gauge. Therefore, a new technique should be introduced for measuring very fine pitting depths, pitting shapes and pitting areas in corroded steel bars more accurately.

The free chloride content was found to be more relevant for corrosion than total chloride content in the specimens. Therefore, more work on the free chloride level in SHCC with different binder and fibre contents is recommended. For total chloride content, XRF can be used as an alternative to chemical chloride testing recommended by the RILEM TC 218.

Conclusions and Recommendations

The corrosion models proposed in this research may need to be improved when the temperature, RH, moisture content and oxygen level at the surface of steel bars are known. Also the long term experimental and field results are necessary to improve the proposed corrosion modelling and relate them to the actual damage in steel bars due to corrosion as well as to the remaining service of RCS. In this case, a statistical data base is required for SHCC and its various parameters such as crack properties at different strain and deformation levels, rate of corrosion of steel, amount of free chloride, pitting depths, loss of yield force, etc. must be observed carefully.

Appendix

Appendix – A

A.1. Applications of SHCC



Figure A.1: Application of HPFRCC (a type of SHCC) in Mihara Bridge in Japan (imitated from Mitamura *et al.* 2005).

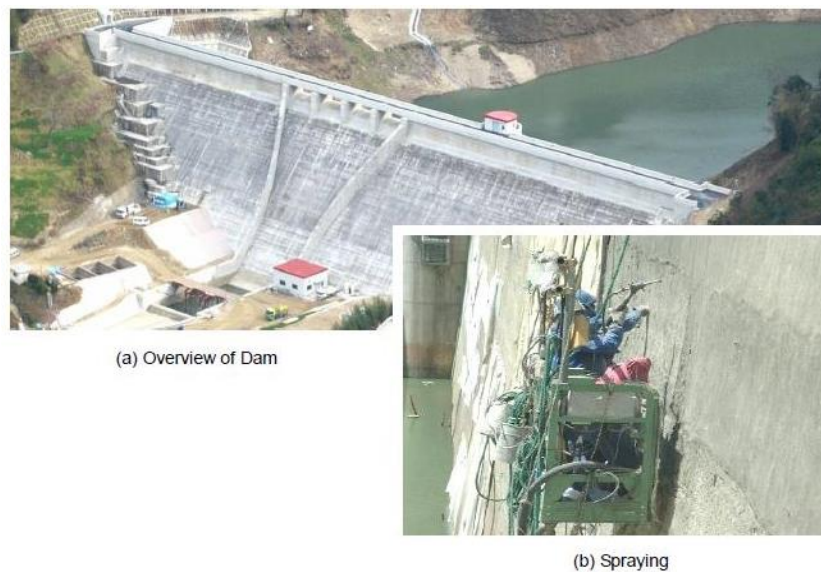


Figure A.2: Surface repair of concrete dam using sprayable SHCC in Japan (imitated from Kojima *et al.* 2004).

Appendix

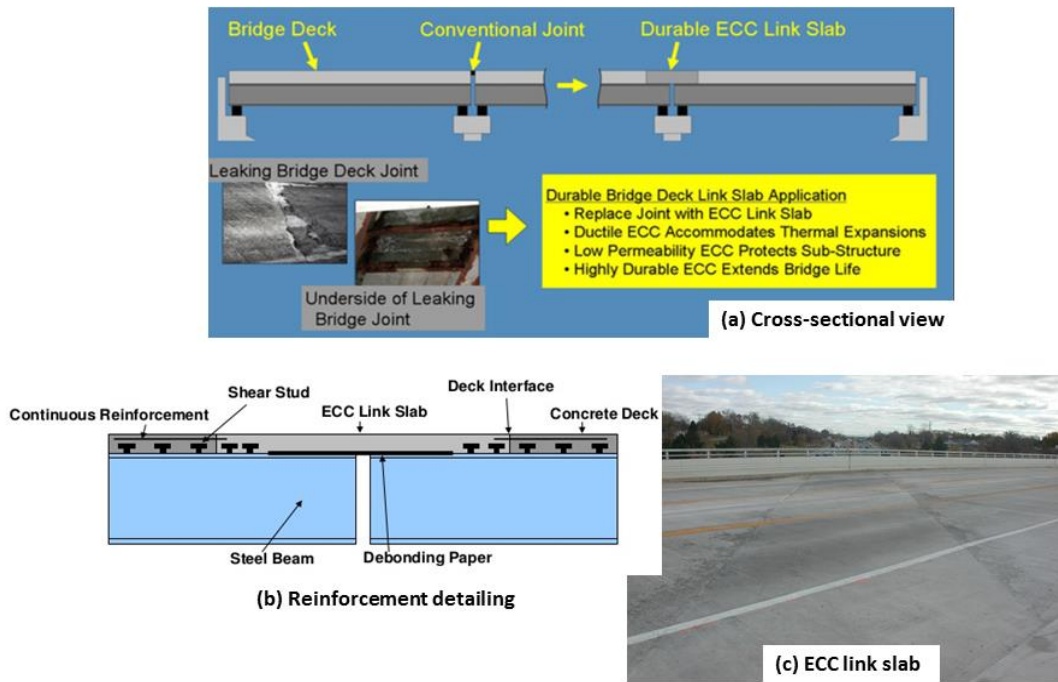


Figure A.3: Application of ECC (a type of SHCC) in bridge deck repair in Michigan, USA (imitated from Li *et al.* 2005).



Figure A.4: HPFRCC used as damper in high building in Japan (imitated from Mitamura *et al.* 2005).

Appendix

Appendix – B

B.1. Apparatus used in the research experiments



Figure B.1: Set up for corrosion pitting depths measurements in the steel bar.

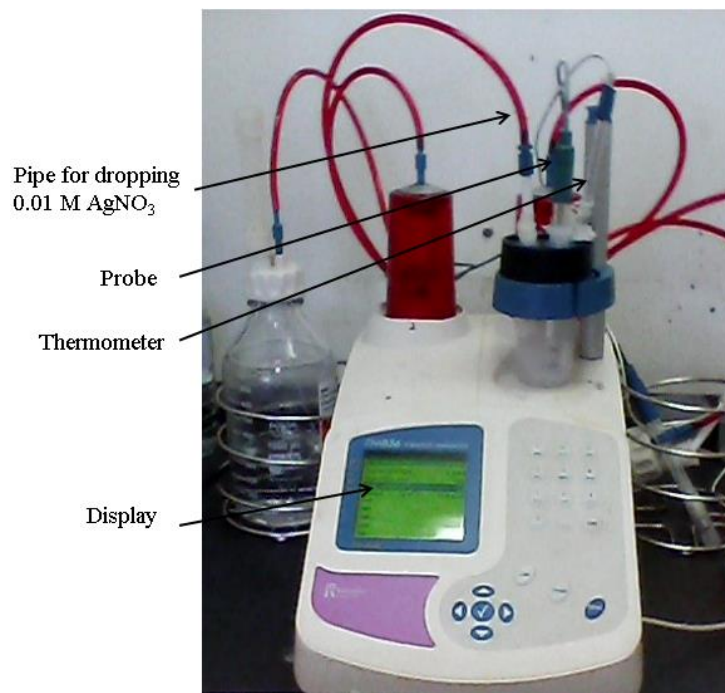


Figure B.2: Titrator used for determining the free chloride-content in SHCC and mortar powder.

Appendix

Appendix – C

C.1. Different strengths properties of FS-SHCC and CS-SHCC

Table C.1: SHCC mix 1

SHCC Mix 1		
Cement	441	kg/m ³
Water	387	kg/m ³
Fly ash	657	kg/m ³
Sand	539	kg/m ³
Fine sand maximum size 0.3 mm		
Coarse sand maximum size 2.36 mm		

Table C.2: FS-SHCC 28 days ultimate compressive strength and strain at ultimate strength for mix 1

Type of SHCC	Fibre content	f_{cu} (MPa)	Strain	Type of SHCC	Fibre content	f_{cu} (MPa)	Strain
FS-SHCC	2.20%	31.52	0.003089	CS-SHCC	2%	31.73	0.00383
		29.98	0.002237			30.95	0.002469
		35.79	0.003473			30.65	0.002374
		31.01	0.003728			24.78	0.003995
		31.95	0.004862			27.43	0.002991
		32.13	0.004621			27.21	0.003973
		34.54	0.002848			28.61	0.002393
		37.63	0.003277			29.59	0.002754
		37.85	0.002612			30.67	0.003027
	2%	24.01	0.003469		20.4	0.00479	
		29.1	0.005134		20.15	0.003295	
		27.17	0.007491		23.16	0.004469	
	1.50%	32.22	0.002393		28.41	0.002134	
		30.27	0.002295		30.06	0.004464	
		34.46	0.002991		29.32	0.002607	
	1%	31.01	0.003728		21.64	0.003616	
		25.23	0.004179		24.44	0.003138	
		26.23	0.004352		24.74	0.004321	

Appendix

Table C.3: FS-SHCC 28 days flexural resistance and deformation for mix 1

Type of SHCC	Fibre content	Days	$f_{cr,ft}$ (MPa)	Cracking deformation (mm)	$f_{u,ft}$ (MPa)	Ultimate deformation (mm)
FS-SHCC	2%	28	4.3	0.26	10.2	3.07
			4.8	0.29	10.7	3.41
			4.0	0.25	8.9	2.65
			5.3	0.81	11.7	4.68
			4.5	0.62	9.0	3.59
			5.0	1.19	10.7	5.21
			4.8	0.91	11.5	3.31
			3.4	0.39	8.1	3.81
			5.2	0.32	11.4	4.52
			4.5	0.30	9.4	3.74
			4.5	0.30	10.6	4.25

Table C.4: CS-SHCC 28 days flexural resistance and deformation for mix 1

Type of SHCC	Fibre content	Days	$f_{cr,ft}$ (MPa)	Cracking deformation (mm)	$f_{u,ft}$ (MPa)	Ultimate deformation (mm)
CS-SHCC	2%	28	4.3	0.18	9.6	1.84
			4.3	0.31	8.9	1.27
			4.0	0.26	9.1	1.56
			4.7	0.54	8.8	3.50
			4.1	0.50	9.0	3.58
			5.0	0.80	12.2	4.88
			5.5	0.68	8.7	2.37
			4.9	0.85	10.2	4.00
			4.4	0.76	9.7	3.87
			4.7	0.68	10.2	4.05
			4.8	0.66	9.4	3.74

Appendix

Table C.5: FS-SHCC tensile resistance for mix 1

Type of SHCC	Fiber content	Days	$f_{cr,st}$ (MPa)	$\epsilon_{cr,st}$ (%)	$f_{u,st}$ (MPa)	$\epsilon_{u,st}$ (%)
FS-SHCC	2.2%	14	3.7	-	3.7	2.60
			2.0	-	3.1	3.30
			2.2	-	3.6	2.20
			3.5	-	3.8	3.52
			2.2	-	3.8	3.00
			2.3	0.0325	3.6	3.89
			2.2	0.0260	3.6	3.44
			2.5	0.0255	3.4	3.40
			2.0	0.0303	3.4	2.30
			1.9	0.0195	2.9	2.60
			3.6	0.0120	3.8	2.60
			2.0	0.0095	3.2	3.30
			2.1	0.0120	3.6	2.22
			3.5	0.0094	3.8	3.60
			2.1	0.0089	3.8	2.96
			2.2	0.0325	3.5	3.86
			2.3	0.0260	3.6	3.44
			2.6	0.0260	3.4	3.06
	3.4	0.0087	3.8	3.55		
	2.1	0.0069	3.8	3.00		
	2.6	0.0120	4.3	1.20		
	2.5	0.0060	4.1	1.10		
	2.6	0.0065	4.4	1.24		
	2.2	0.0050	3.3	1.01		
	2.4	0.0030	3.5	1.10		
	2.9	0.0195	3.8	1.40		
	3.5	0.0067	4.1	1.10		
	3.3	0.0067	3.9	1.31		
	2.3	0.0260	3.2	1.32		
	3.0	0.0129	3.9	1.10		
	1.5	28	1.5	0.0065	2.7	0.54
	2.8		0.0060	3.7	0.61	
2.0	0.0010		2.1	0.96		
1%	28	2.0	0.0000	2.7	0.98	
2.1		0.0091	2.8	0.61		
2.4		0.0000	2.4	0.69		

Appendix

Table C.6: CS-SHCC tensile resistance for mix 1

Type of SHCC	Fiber content	Days	$f_{cr,st}$ (MPa)	$\epsilon_{cr,st}$ (%)	$f_{u,st}$ (MPa)	$\epsilon_{u,st}$ (%)
CS-SHCC	2%	14	1.8	-	3.0	3.10
			2.4	-	3.7	4.40
			2.7	-	2.9	1.96
			2.6	-	3.5	4.08
			2.3	-	2.9	3.00
			2.4	0.0130	3.9	3.50
			2.1	0.0257	3.5	4.28
			2.2	0.0260	3.5	1.80
			2.2	0.0260	3.6	3.20
			2.9	0.0100	3.2	1.85
			1.9	0.0290	3.1	3.05
			2.5	0.0390	3.8	4.40
			2.4	0.0220	2.9	1.00
			2.5	0.0150	3.5	4.50
			2.3	0.0160	2.9	3.67
			2.4	0.0389	3.5	3.98
			3.2	0.0256	3.8	3.19
			2.7	0.0256	3.5	4.94
	2%	28	3.0	0.0130	3.8	0.75
			2.5	0.0067	3.3	1.30
			3.1	0.0065	3.5	1.10
			3.5	0.0125	3.7	0.90
			3.0	0.0650	3.5	0.80
	1.5%	28	3.1	0.0000	3.3	0.85
			2.6	0.0065	3.0	0.61
			2.0	0.0130	2.8	0.50
			2.1	0.0065	2.8	0.55
	1%	28	2.3	0.0000	2.2	0.95
			2.0	0.0000	2.6	0.55
			1.6	0.0052	2.4	0.64
			1.8	0.0013	2.0	0.90

Table C.7: SHCC mix 2

SHCC Mix 2		
Cement	392	kg/m ³
Water	392	kg/m ³
Fly ash	674	kg/m ³
Sand	553	kg/m ³
Fine sand maximum size 0.3 mm		
Coarse sand maximum size 2.36 mm		

Appendix

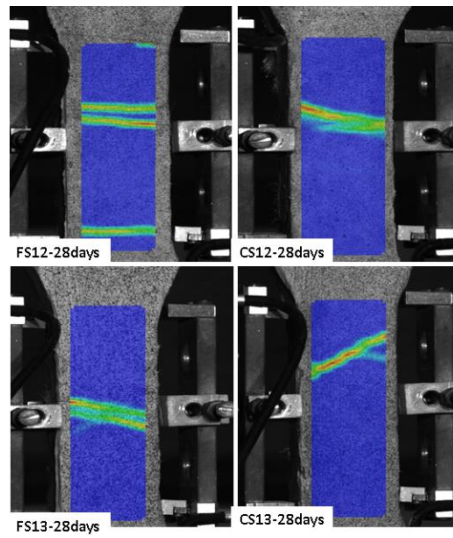
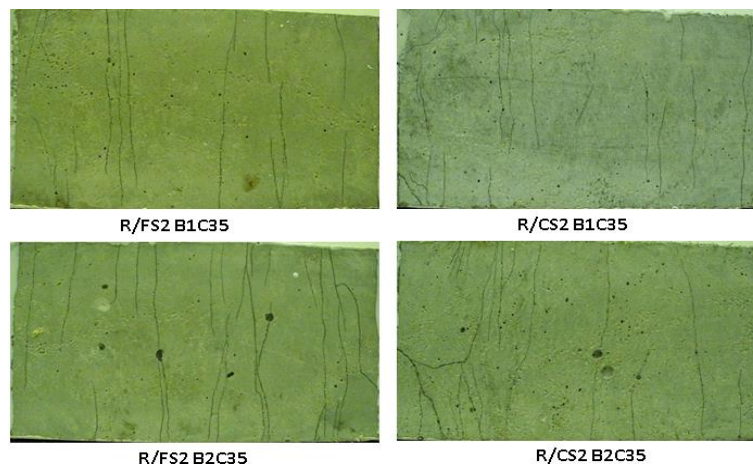
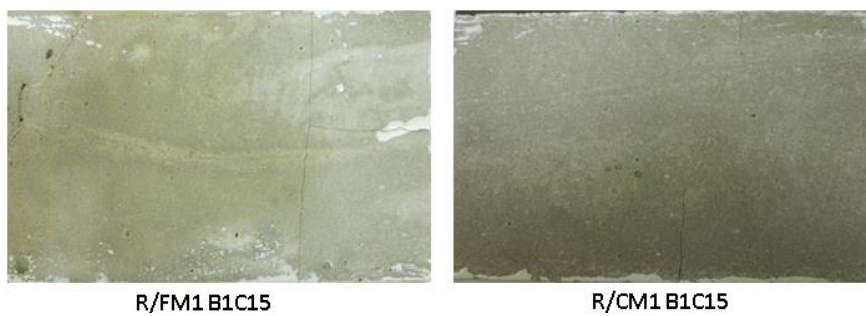
Table C.8: FS-SHCC tensile resistance for mix 2

Type of SHCC	Fiber content	Days	$f_{cr,st}$ (MPa)	$\mathcal{E}_{cr,st}$ (%)	$f_{u,st}$ (MPa)	$\mathcal{E}_{u,st}$ (%)
FS-SHCC	2%	14	-	-	2.11	-
			-	-	2.17	-
			-	-	2.19	-
			1.8	0.0220	2.48	2.89
			-	-	2.51	-
			2.1	0.0022	2.52	0.75
			1.8	0.0195	2.69	3.21
			2.0	-	2.69	1.00
			2.0	0.0246	2.71	3.35
			-	-	2.72	-
			2.0	0.0286	2.78	2.59
			2.3	-	2.78	1.54
			2.0	0.0208	2.86	1.53
			2.0	-	3.23	3.34
	2%	28	2.7	0.0013	3.51	0.91
			3.0	0.0104	3.86	0.62
			3.0	0.0052	3.57	1.12
			3.5	0.0104	3.72	1.04
			3.4	0.0026	3.35	1.67
			-	-	-	-

Table C.9: CS-SHCC tensile resistance for mix 2

Type of SHCC	Fiber content	Days	$f_{cr,st}$ (MPa)	$\mathcal{E}_{cr,st}$ (%)	$f_{u,st}$ (MPa)	$\mathcal{E}_{u,st}$ (%)
CS-SHCC	2%	14	1	-	1.27	0.0137
			-	-	1.34	-
			-	-	1.54	-
			-	-	1.57	-
			-	-	1.67	-
			-	-	1.75	-
			1.48	-	1.82	2.29
			-	-	1.91	-
			-	-	2	-
			-	-	2.27	-
			2	-	2.48	1.24
			2.5	0.0052	2.73	0.90
			2.45	0.0078	2.88	1.50
			2.52	0.0052	2.95	3.10

Appendix

C.2. Tensile and flexural cracking behaviour of SHCC specimens**Figure C.1:** Formation of tensile cracks in different FS-SHCC and CS-SHCC specimens.**Figure C.2:** Observed crack pattern in R/FS2 & R/CS2 specimens.**Figure C.3:** Observed crack pattern in R/FM1 & R/CM1 specimens.

Appendix

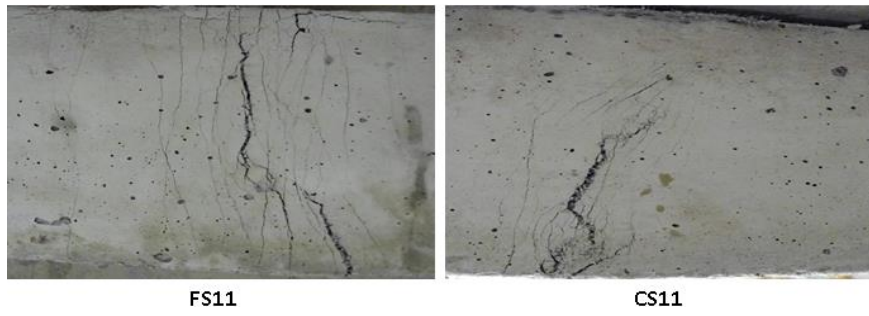


Figure C.4: Observed crack pattern in unreinforced FS11 & CS11 specimens.

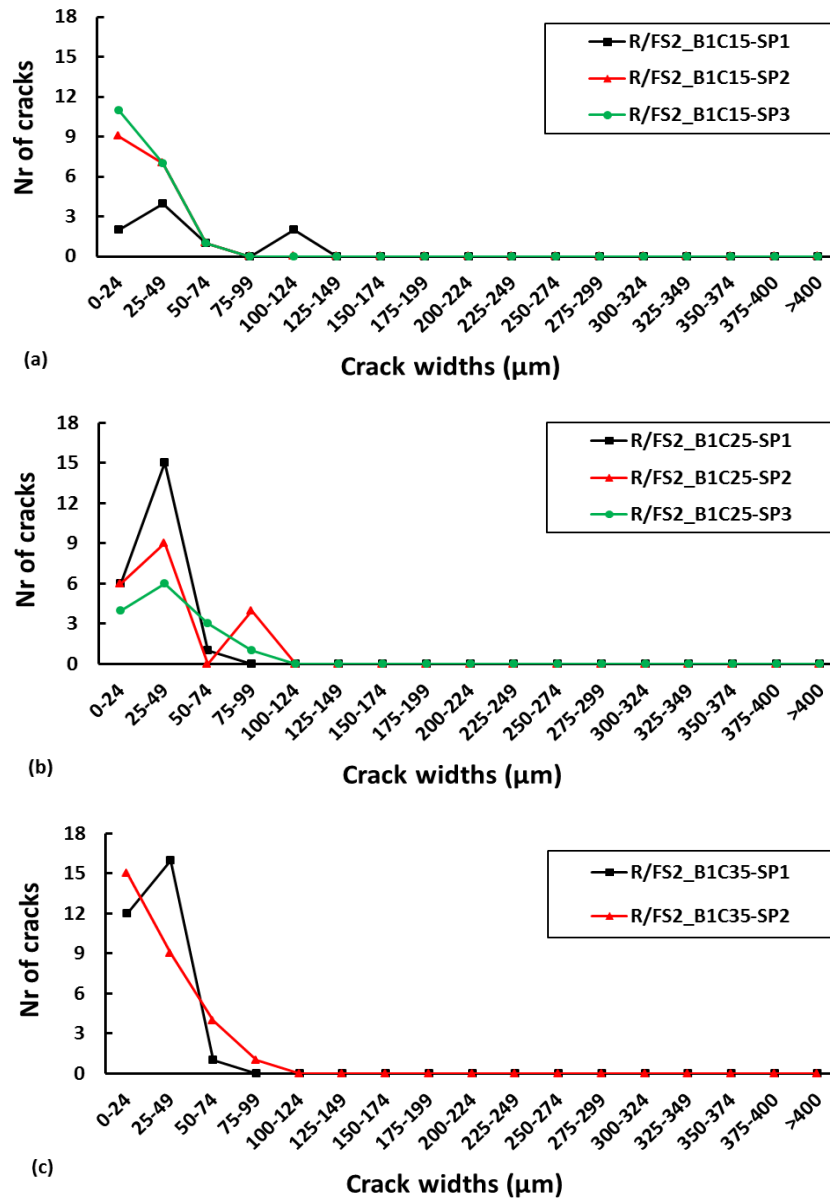


Figure C.5: Flexural cracks in individual specimens of R/FS2 with B1 at D3.5.

Appendix

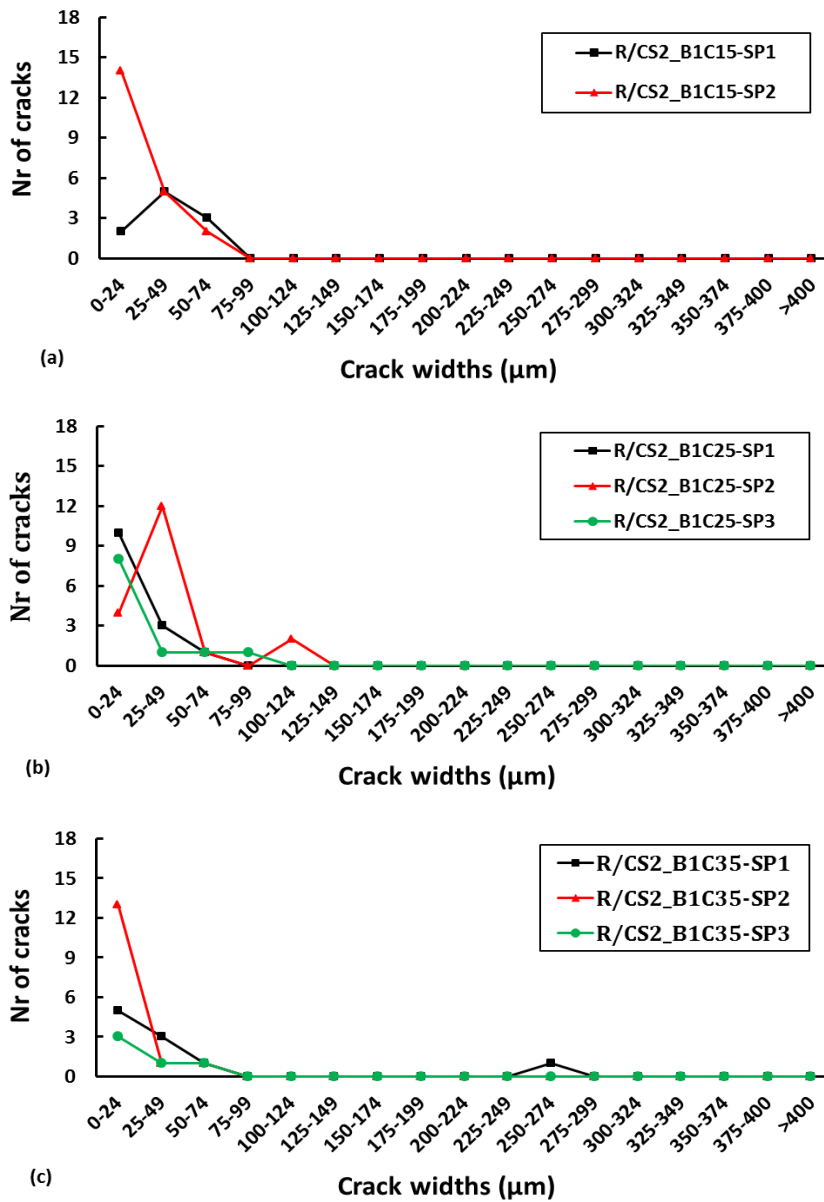
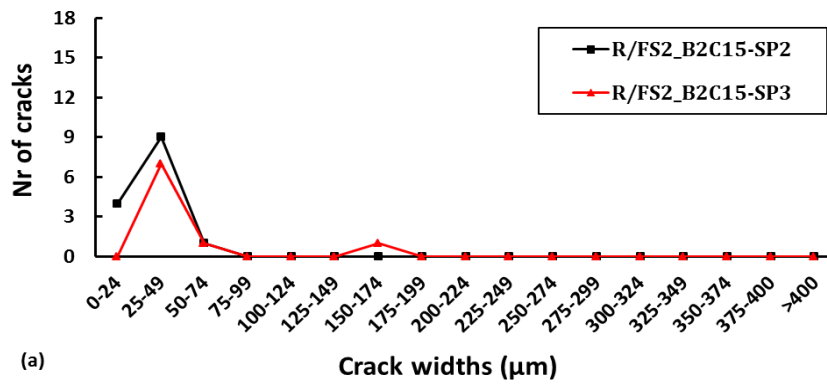
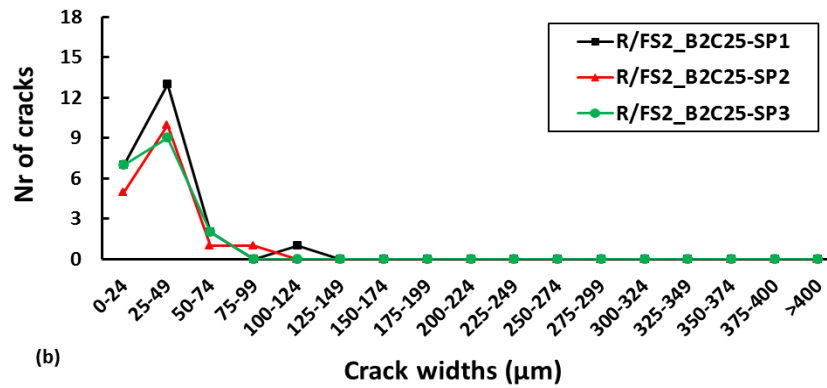


Figure C.6: Flexural cracks in individual specimens of R/CS2 with B1 at D3.5.

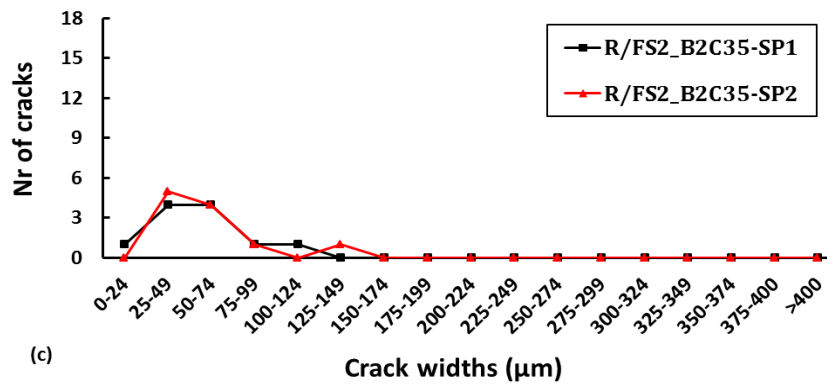
Appendix



(a)



(b)



(c)

Figure C.7: Flexural cracks in individual specimens of R/FS2 with B2 at D3.5.

Appendix

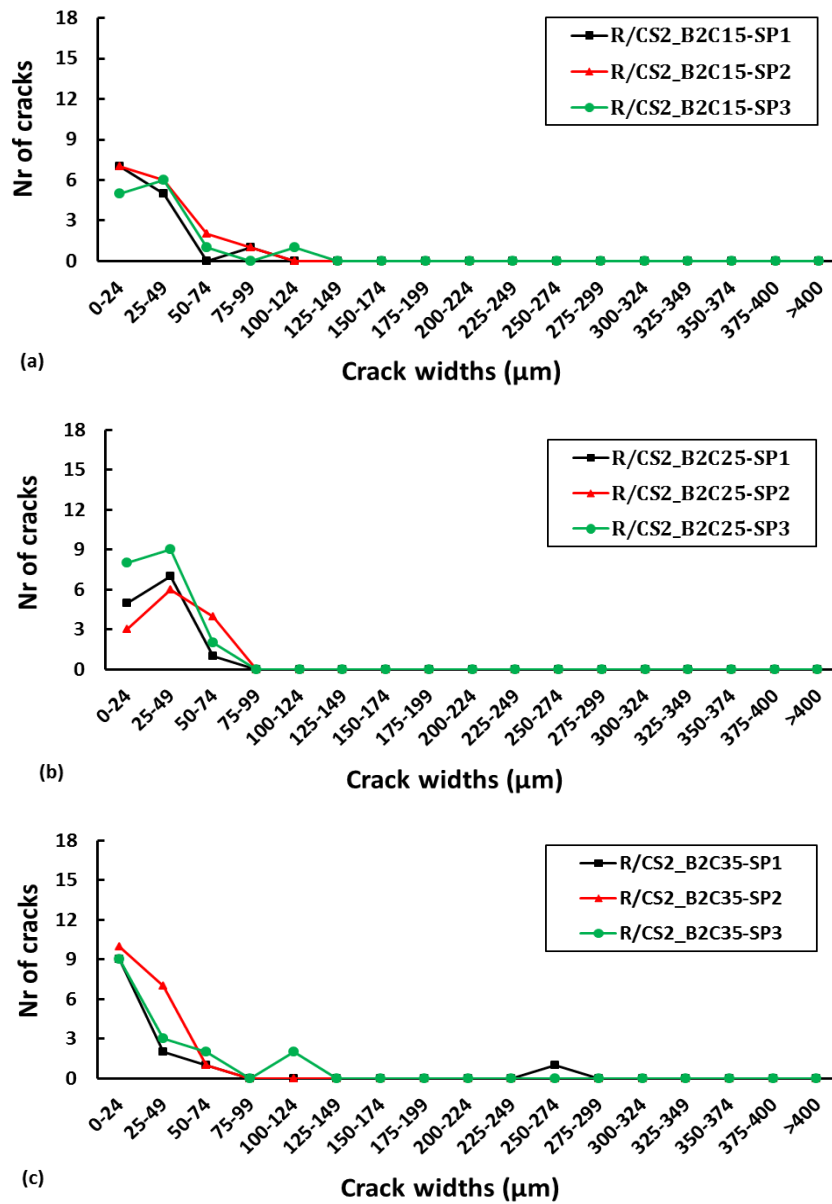


Figure C.8: Flexural cracks in individual specimens of R/CS2 with B2 at D3.5.

Appendix

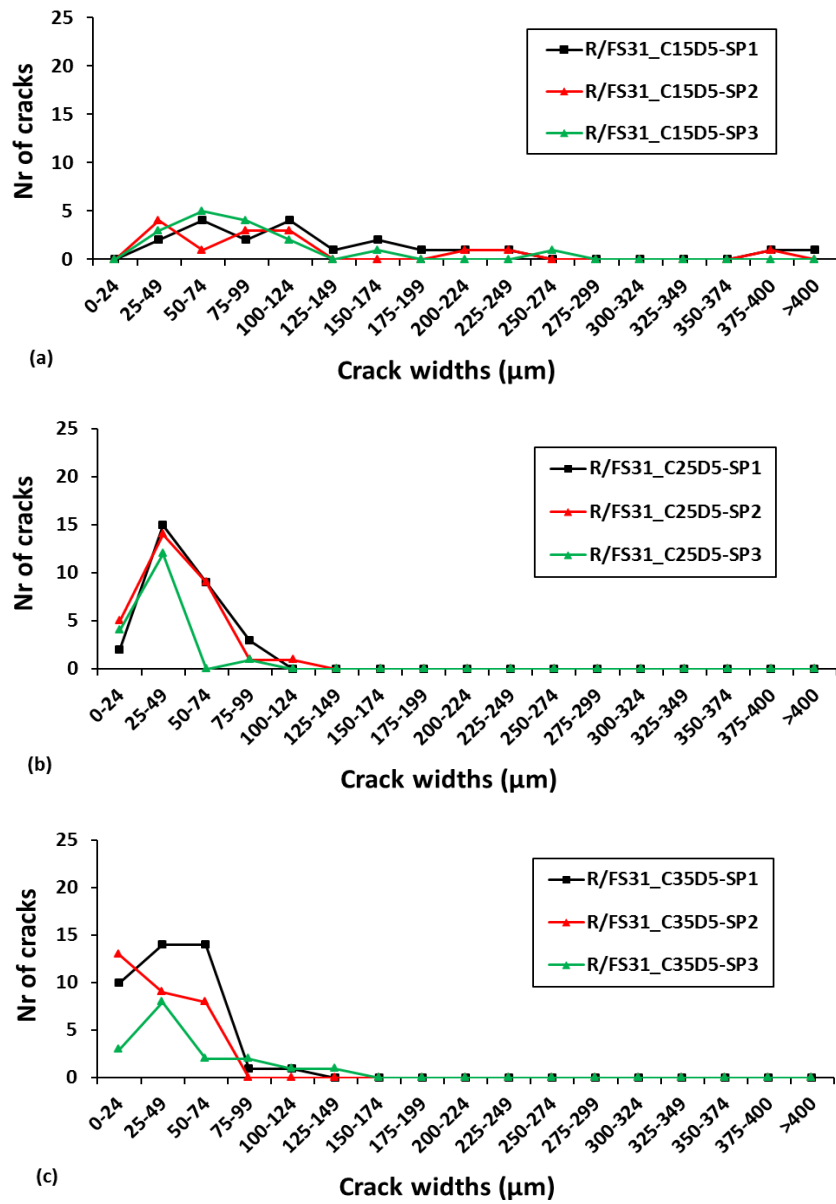


Figure C.9: Flexural cracks in individual specimens of R/FS31 with B1 at D5.

Appendix

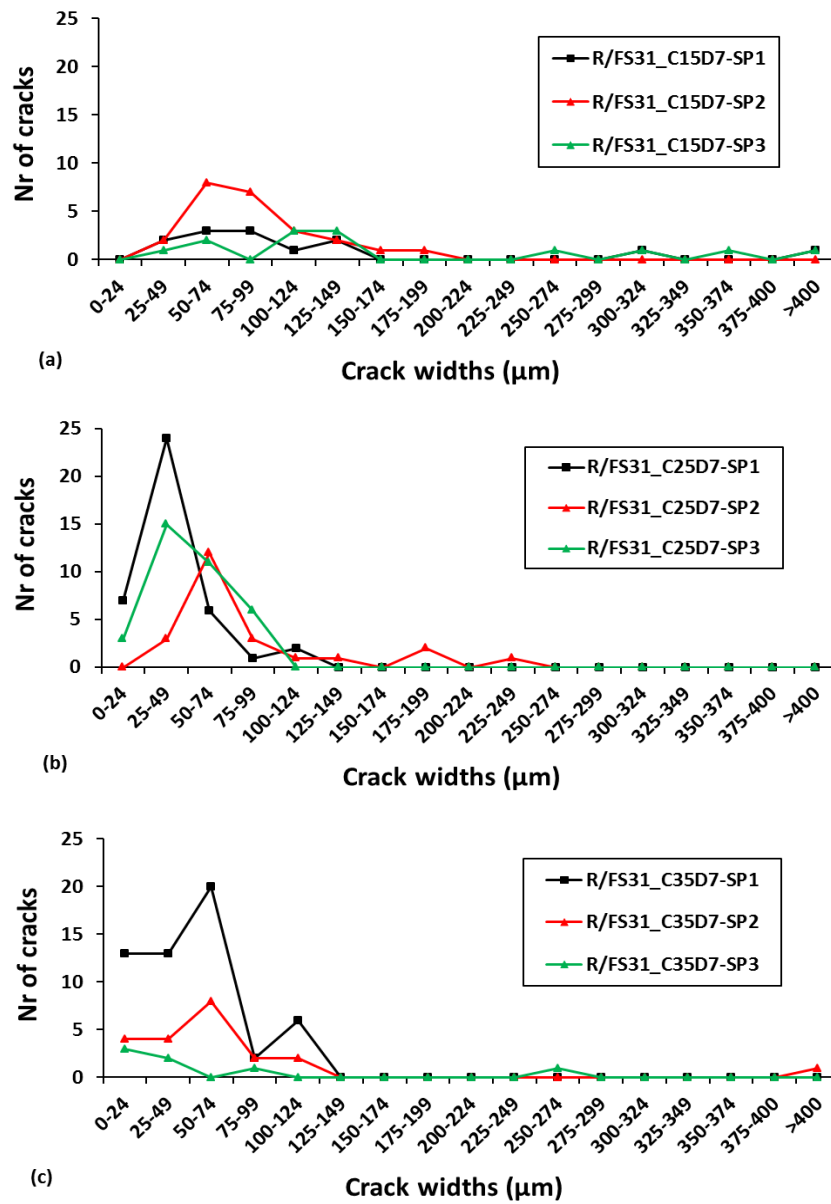


Figure C.10: Flexural cracks in individual specimens of R/FS31 with B1 at D7.

Appendix

C.3. Corrosion potential mapping in R/mortar specimens

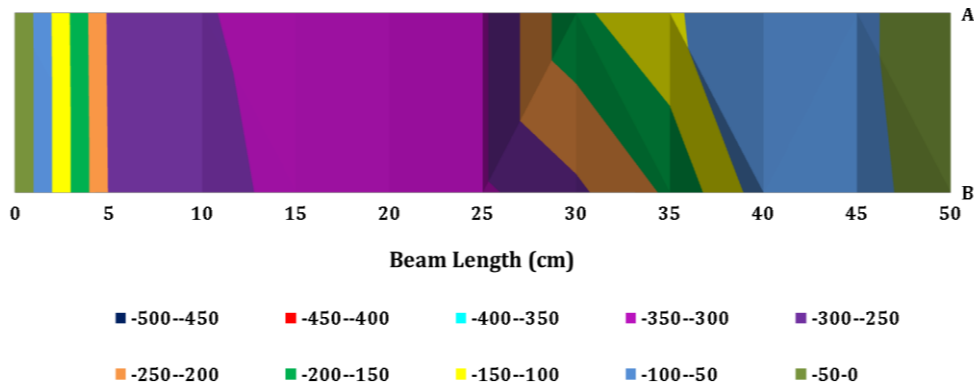


Figure C.11: Corrosion potential mapping in uncracked R/FM3 specimen in series four.

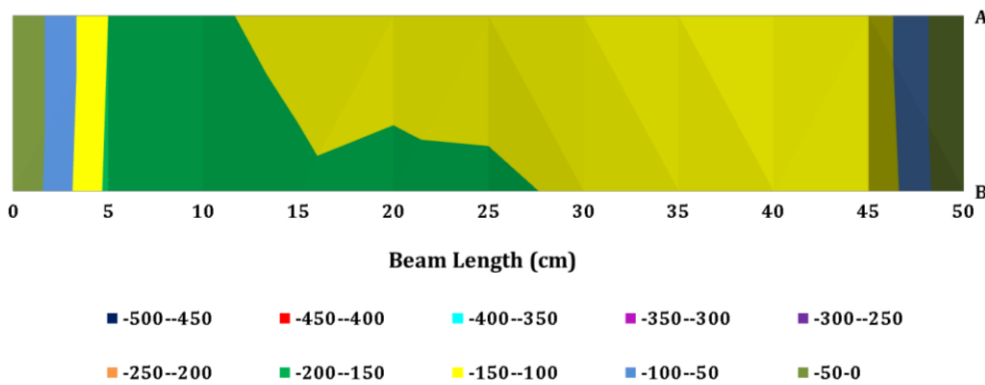


Figure C.12: Corrosion potential mapping in uncracked R/HM3 specimen in Series Four.

C.4. Corrosion damage in the steel bars



Figure C.13: Corrosion in steel bars in Series One

Appendix



Figure C.14: Corrosion in steel bars in Series Two.



Figure C.15: Corrosion in steel bars in Series Three.

Appendix

C.5. Chloride penetration in SHCC and mortar specimens in rapid chloride migration test

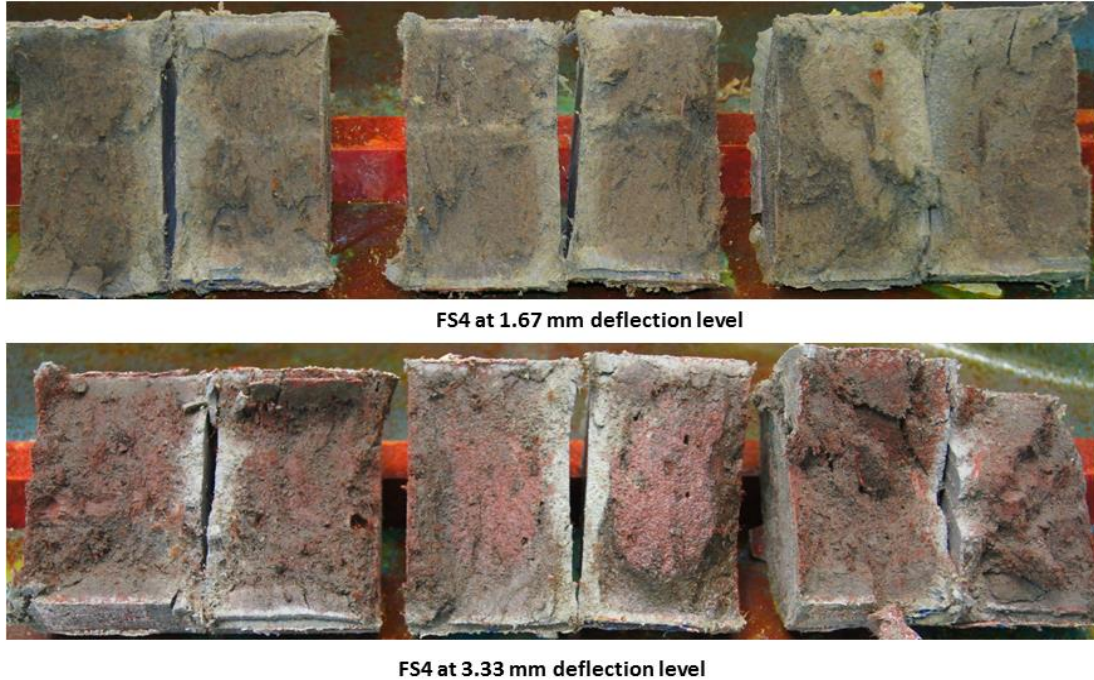


Figure C.16: Chloride penetration during RCM test in cracked FS4 specimens loaded at different levels of deformation in Series Four.

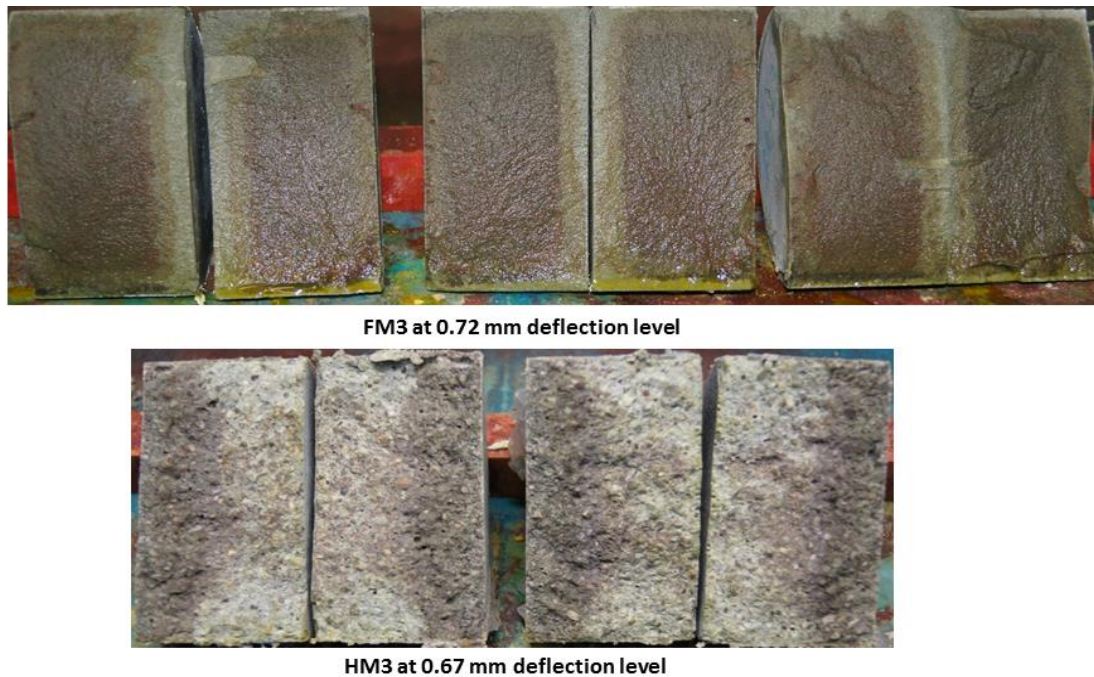


Figure C.17: Chloride penetration during RCM test in FM3 and HM3 specimens loaded at different levels of deformation in Series Four.

Appendix

C.6. Capillary water absorption in SHCC and mortar specimens in rapid chloride migration test

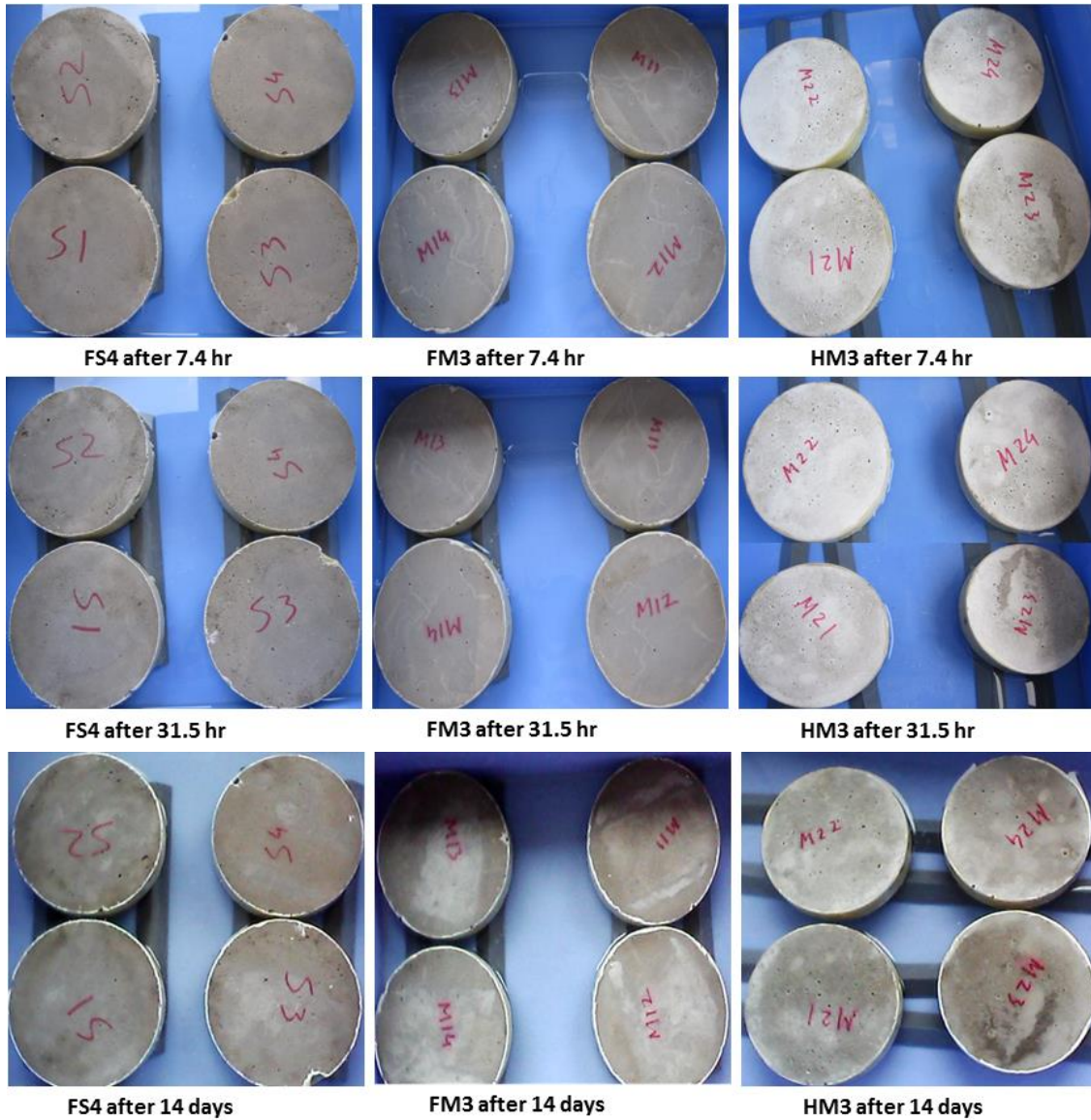


Figure C.18: Water gains by different specimens during capillary absorption testing in Series Four.